THESIS

THE VALIDATION OF EMISSION RATE ESTIMATION METHODS

Submitted by

Bradley Wells

Department of Atmospheric Science

In partial fulfillment of the requirements

For the Degree of Master of Science

Colorado State University

Fort Collins, Colorado

Spring 2015

Master's Committee:

Advisor: Jeffrey Collett, Jr.
Co-Advisor: Jeffrey Pierce

Jay Ham

ABSTRACT

THE VALIDATION OF EMISSION RATE ESTIMATION METHODS

Oil and natural gas production throughout the United States has been dramatically increasing in recent years, due in large part to hydraulic fracturing processes and horizontal drilling techniques that allow for extraction from unconventional wells. The rise in well drilling and completion activities raises concern over potential air quality impacts on nearby communities. Methane, other volatile organic compounds (VOCs), and nitrogen oxides (NO_x) may be emitted into the atmosphere during well development and production activities. Methane is a greenhouse gas, VOCs and NO_x act as ozone precursors, and some VOCs are classified as air toxics. For these reasons, there is a need to accurately quantify the rate of emissions of these gases into the atmosphere from oil and gas development and production.

One such emission rate estimation technique is the tracer ratio method (TRM). The TRM requires access to a well site and involves the release of a passive tracer gas as close to the source of emissions as possible. This known emission rate is multiplied by the ratio of the downwind concentrations of emission gas to the tracer gas (both in excess of background) to derive an estimate of the emission gas emission rate. Another technique, recently developed by the Environment Protection Agency, utilizes a simplified point source Gaussian plume (PSG) dispersion model. This approach requires only one mobile downwind measurement location for both concentration and meteorological measurements, without the need for site access; it does not require a tracer gas.

In order to evaluate the effectiveness of these techniques, a series of experiments were conducted at Christman airfield in Fort Collins, Colorado. These experiments involved releasing both acetylene, as a tracer gas, and methane (to simulate an emission source) at controlled flow rates to compare the predicted emission rate of methane to its actual emission rate. A vehicle equipped with a PICARRO methane and acetylene analyzer traversed or remained stationary within the gas plume to provide real-time concentration measurements of both gases. A 3-D sonic anemometer was used to characterize local meteorological conditions.

The TRM is evaluated using both a mobile transect and a stationary approach. There is an overall positive bias in both cases. Our best results are obtained when sources are co-located during a stationary analysis and changes in background methane concentrations are determined and corrected. In these cases the mean bias is +9% with σ=22% (standard deviation about the mean bias). The separation of tracer and emission gas sources in the mobile transect analysis is the largest cause for uncertainty. The mean bias when sources are separated is +83% (σ=99%), as opposed to transect analyses of co-located sources which have a mean bias of +33% (σ=31%).

The PSG technique, which involves a 20 minute stationary analysis, contains more inconsistent results compared to the stationary approach performed by the TRM (mean bias of methane emission rate prediction +34%, σ=123%). Most interesting of note is that for nearly every sample the bias in the prediction of the emission rate of acetylene is more negative than the bias in methane emission rate predictions (mean bias of acetylene emission rate prediction -19%, σ=128%). This suggests possible biases in the acetylene release rate or concentration measurement; however, at this time the issue cannot be located. Regardless, a stationary TRM technique produces the best results, and its use is recommended when site access is available for tracer release.

TABLE OF CONTENTS

Chapter 1 Introduction

1.1 Motivation

The known rate of pollutant emissions is critical in determining air pollutant concentrations and human exposure to potentially toxic compounds. For many sources of pollutants, their emission rates can be quantified at their source through straightforward means [e.g. *Schauer et al.*, 1999; *Johnson et al*., 1994]. However, for many pollution sources, this factor cannot be easily obtained at their source. There are challenges in estimating source emissions: emissions may be from multiple points or areas with no easy way to directly determine an emission rate budget, such as landfills [*Galle et al*., 2001], or unintended emissions may occur throughout many stages of an industrial process, referred to as fugitive emissions [*Howarth et al*., 2011]. There may not be access to the area of a source. In these cases, it is far easier to determine the concentrations of pollutants downwind of their source and use this value, along with other information, to estimate the emission rate. This may also be a more cost-effective strategy than measuring emission rates directly [*Thoma et al*., 2012]. Energy production, more specifically extraction and production of fossil fuels, can have complex source geometries that may be difficult to access, as well as fugitive emissions [*Howarth et al*., 2011], thus making the goal of setting an accurate emission rate a difficult problem.

Oil and natural gas production has been dramatically increasing in recent years throughout the United States, due in large part to hydraulic fracturing processes that allow for extraction of these fuels from "unconventional wells" [*EIA*, 2014]. This has raised concerns about local air quality impacts. In Colorado especially, the oil and natural gas industry has seen substantial growth and makes up a sizeable fraction of the state's economy [*Lewandowski*, 2012]. The recent

growth in the number of producing wells in Colorado is shown in **Figure 1.1**. This large increase in well production, combined with the uniqueness of well completion processes specific to unconventional wells [*Stephenson et al.*, 2011], makes it important to characterize volatile organic compounds (VOCs) and quantify their emission rates at these well sites. *Gilman et al.* [2013] attribute many different VOCs that are specific to O&NG production in Northeastern Colorado that act as precursors to tropospheric ozone formation. Other VOCs that may originate from unconventional wells are classified as air toxics that could negatively impact human health [*Pacsi et al.*, 2013]. Additionally, methane, a potent greenhouse gas, can be emitted throughout many processes of well completion and has become an area of extensive study [*Brantley et. al.*, 2014; *Howarth et. al.*, 2011].

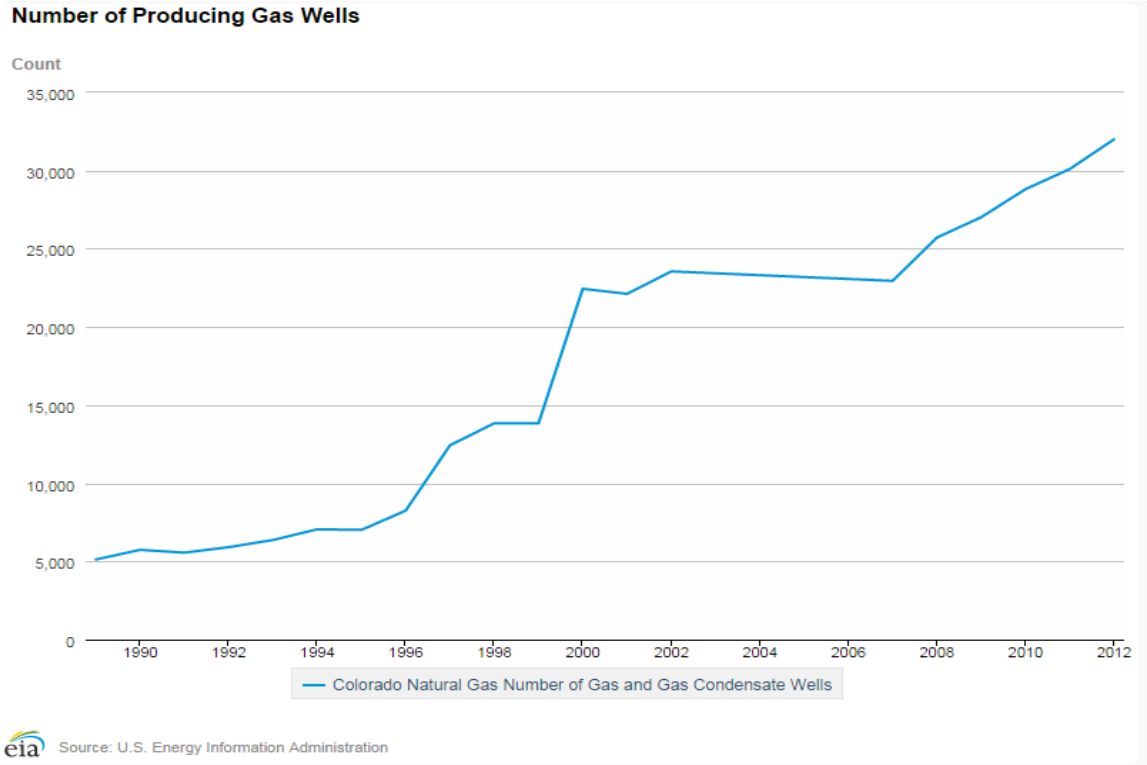

Figure 1.1 A graph of the number of producing natural gas wells within the state of Colorado from 1989 to 2012, courtesy of the U.S. Energy Information Administration (EIA) [http://www.eia.gov/dnav/ng/ng_prod_wells_s1_a.htm].

Where concentration measurements can only go so far as to give a snapshot in time of air quality downwind of an unconventional well, estimating emission rates gives us a tool to predict how an unconventional well may impact different regions during different completion processes and how these impacts could change given the number of new producing wells in a region. This next step in O&NG examination is mentioned in *Warneke et. al.* [2014].

A research team from Colorado State University's Atmospheric Science Department is conducting experiments to quantify VOC emission rates from a variety of oil and natural gas extraction processes throughout Colorado. Using gas chromatography (GC) and proton transfer reaction – mass spectrometry (PTR-MS), the concentrations of a range of VOCs, including toxic organic compounds, are determined from ambient air downwind of a natural gas well using stainless steel, evacuated and air tight canisters.

Given the intricacies of well production and the novelty of unconventional extraction techniques, combined with difficult access to emission sources, the task of estimating emission rates using concentration sampling techniques is difficult. Complicated terrain and rapidly changing weather patterns that are common to Colorado only add to this difficulty, rendering many emission rate estimation methods that rely on modeling gas plume dispersion difficult or impossible to use. It is then imperative to use a method that can be mobile, rely on as few variables as possible, and requires merely a good approximation of the location and geometry of emission sources.

Our team will attempt to estimate the emission rates of many different VOCs via a technique that can fulfill all the requirements mentioned above. This will be accomplished by releasing a chemically inert gas near the source of emissions at a known emission rate from a point that is co-located with the source VOC emissions. The concentration of this inert "tracer gas" will also

be determined at the same point downwind as the VOCs. Upwind "background" samples are also collected to establish a local background concentration of VOCs and tracer gas. The ratio of a background-subtracted VOC concentration to the background-subtracted tracer concentration multiplied by the emission rate of the tracer gas will provide an estimate for that VOC's emission rate from the source. This method for estimating emission rates is known as the tracer ratio method (TRM).

To best accomplish the goals of our field work and to develop a way to determine the magnitude of errors to expect in the TRM, there is a need to create a controlled experiment in which we can examine the method. These controlled experiments, performed at Christman airfield in Fort Collins, CO, were done by releasing a tracer gas as well as another "emission gas" that simulated a VOC being released at a well site. This emission gas had a known flow rate as well so an error in the method could be obtained.

These controlled experiments provided an opportunity to practice the approach so as to be as efficient and methodical as can be at a well site. It also allows us to evaluate a range of variables that could alter the ability of the TRM to accurately predict a gas emission rate. We also tested the TRM against another method used for predicting emission rates that require similar source types and downwind sampling distances. Error analysis of the TRM will better constrain our results. These findings will help to quantify our error in field samples, leaving us with a set of emission rate inventories that is as robust and accurate as possible.

1.2 Current State of Research

1.2.1 The Tracer Ratio Method

The TRM has been used as a technique for estimating the emission rates of gases from a variety of source types [*Lamb et al*., 1986; *Lassey et al*., 1997; *Rumburg et al*., 2008; *Scholtens*

et al., 2004] as well as a tool to predict emission rates of roadside coarse particulate matter [*Kantamaneni et al*., 1996]. The process involved in performing the TRM is straightforward, with the core instrumentation being a way to release a tracer gas near the source of emission gas(es) and the ability to measure these gas concentrations downwind. In this way the method can be expressed as an equation in a similar fashion to that found in *Lamb et al*. [1986]:

$$Q_i = Q_t \frac{\int [\chi_i] d\alpha}{\int [\chi_t] d\alpha} \quad \textbf{1.1}$$

where Q and χ represent emission rate and concentration, respectively, and the subscript i refers a specific species of VOC analyzed along with a tracer gas, subscripted t. These concentrations are integrated over some variable, α, which is usually either time or distance. In cases where the profile of the downwind concentrations of tracer and emission gases is along two dimensions, **Eq**. **1.1** can be a double integral, such as over the crosswind and vertical distance of the plume as performed in *Kaharabata et al*. [2000]. For many TRM measurements that involve stationary canister sampling, the total concentrations accumulated over the amount of sample collection time acts as the integrated concentration [*Rumburg et al*., 2008].

This method is enticing because in theory it does not rely on meteorological parameters in its calculation, allowing for less instrumentation in the field [*Ludwig et al*., 1983], and on-site or quick analysis if mobile real-time measurements are used [*Galle et al*., 2001]. For the TRM to be accurate, however, certain conditions must be met. The emission source geometry must be similar for both tracer and emission gas and the plumes of both gases must disperse downwind in a similar manner [*Scholtens et al*., 2004]. The tracer must be inert and subject to the same chemical and/or physical removal processes as the emission gas [*Scholtens et al*., 2004]. The concentration of both gases must also be sufficiently elevated above local ambient background levels so a distinct plume signal can be determined [*Lassey et al*., 1997; *Scholtens et al*., 2004].

Under these conditions, it can be assumed that both plumes are behaving in a similar fashion and are therefore analogous to one another. *Ludwig et al*. [1983] also recommends for the TRM to be used under stable atmospheric conditions. They observed source emissions estimates increasing for increasingly unstable atmospheres, therefore leading to larger uncertainties in predicted emission rates when unstable conditions are present. This parameter will also be evaluated in our study.

The sensitivity of the TRM to a wide range of meteorological conditions has been evaluated in several studies [*Lassey et al*., 1997; *Ludwig et al*., 1983; *Rumburg et al*., 2008]. As mentioned above, atmospheric stability has been shown to affect the accuracy of the method. As expected, wind direction and its change over the sampling time are very important factors in sensitivity as well [*Ludwig et al*., 1983]. The TRM obviously cannot be used if the wind direction is pointed away from the location(s) that sampling equipment can be placed, and the accuracy of the method can come into question if the standard deviation of the wind direction during the sampling period is too large. *Ludwig et al*. [1983] recommends the TRM be used at night, when the atmosphere is most stable and with less chance for rapid wind changes. Wind direction change is less of an issue if mobile and real-time downwind concentration measurements are used, as in *Scholtens et al*. [2004] where their mobile measurement system could relocate into the plume. It is thought that the TRM is less sensitive to wind speed, but a non-negligible wind speed is needed so advection is the dominant transport mechanism of gases as opposed to molecular diffusion [*Kaharabata et al*., 2000; *Rumburg et al*., 2008].

The mechanics of the TRM, such as how the release system is set up, may also influence the sensitivity of the method. The majority of TRM experiments attempt to release the tracer gas as close as possible to the sources of the emission gases [*Galle et al*., 2001; *Rumburg et al*., 2008;

Scholtens et al., 2004]. *Catalano* [1987] observed that the distance from a line source of tracer to the area source of emission gas had a relatively small impact on the sensitivity of the emission rate prediction, observing that "In general the farther the line source was from the area source in the direction of the samplers, the smaller the estimate of the source strength. The farther the line source was on the side away from the samplers, the larger the source strength." Most TRM experiments attempt to arrange their tracer release set up to mimic the geometry of the emission gas source(s) by releasing the tracer as a true line source or simulated line source using a mobile point source behind the area of emissions [*Kantamaneni et al*., 1996; *Ludwig et al*., 1983], as multiple point sources at or near emissions [*Galle et al*., 2001; *Lamb et al*., 1986; *Mønster et al.*, 2014], or allowing the tracer to mix with emission gases that originate within a building before it is released into the atmosphere [*Karahabata et al*., 2000; *Scholtens et al*., 2004].

It has been recommended that the tracer is released at the same height as the emission gases [*Ludwig et al*., 1983]. The distance downwind where samples are taken may affect the estimation of emission fluxes as well, with most studies making measurements at least 100 m downwind [*Catalano,* 1986; *Kaharabata et al*., 2000; *Lamb et al*., 1986]. In their validation study of the TRM, *Scholtens et al.* [2004] made downwind measurements between 30 and 70 m and found relatively large biases between predicted and actual emission rates of ammonia (NH_3), their emission gas of study. *Catalano* [1986] found that in distances further than 3 km there is little disparity in downwind tracer concentrations released by either point, line, or area release set ups.

The *Ludgwig et al*. [1983] paper did not test the TRM against a source of emission gas emitting at a known flow rate. Indeed, most papers examined the validity of the TRM not through a controlled emission rate release of an emission gas, but by comparing the TRM-estimated emission flux against the emission flux calculated from other flux calculation methods.

Lamb et al. [1986] found that estimated isoprene emissions through the TRM were in good agreement with an established vegetation enclosure technique; *Johnson et al*. [1994] validated the TRM for estimating CH_4 emissions from ruminating livestock against a respiration chamber technique for estimating emission rates and found that, through a total of 55 TRM measurements and 25 respiratory chamber measurements, there was very good agreement between the two methods (mean CH_4 emissions at 11.03 and 11.00 liters per hour for TRM and chamber methods, respectively). *Scholtens et al*. [2004] directly controlled NH_3 emissions for a slurry store and cattle house in which simulated surface sources of NH_3 were controlled via a thermal mass flow controller. This study involved the release of a commonly used tracer gas, sulfur hexafluoride (SF_6), at points within the slurry store and cattle house. Taking continuous measurements over a six-week period and after considerable data screening, well-correlated NH_3 and SF_6 downwind concentrations were observed. However, a -25% bias in the TRM was calculated for the slurry store and a +43% bias calculated for the cattle house. The study concluded that while the method shows promise for real farms there are real discrepancies between measured and estimate emission rates that need to be addressed.

More recently, *Mønster et al.* [2014] performed a sensitivity analysis with a controlled flow of both CH_4 and C_2H_2 to investigate the performance of the TRM when mobile, real-time measurements offered the ability to perform mobile plume transects. This controlled experiment utilized the same downwind concentration measurement instrumentation as our research group. For co-located CH_4 and C_2H_2 sources, the uncertainty in the TRM estimation was found to be on the order of less than ±10%. However, source separation lead to a much larger uncertainty: up to a 36% error.

There appears to be a lack of studies that estimate errors in the TRM via a controlled release of an emission gas. Furthermore, while parameters that may affect the overall performance of the TRM have been evaluated on a theoretical bases or through passive observations as mentioned in this section, the act of independently exploring the influence of many different variables has not been fully realized. We see that there is a need to explore the sensitivities of the TRM further under a controlled setting given this lack of validation.

1.2.2 The EPA Point Source Gaussian Method

The emission rate estimation technique to be compared to the TRM comes from the EPA's Geospatial Measurement of Air Pollution (GMAP) program that has developed a new technique for evaluating emission rates known as the Remote Emission Quantification (REQ) method. This technique uses a point source Gaussian plume (PSG) approach [*Thoma and Squier*, 2012]. This approach can be performed from a mobile vehicle that can identify the plume and perform analysis off site and downwind of the source, much like the TRM. The PSG technique utilizes the downwind distance as well as atmospheric stability to obtain standard deviations of the plume size in the crosswind and lateral directions (σ_y and σ_z), along with downwind concentrations. Stability parameters require the input of data from a 3-D sonic anemometer, an instrument that measures wind speed in all 3 directions. The GMAP-REQ package also uses a backwards Lagrangian stochastic (bLs) approach for estimating emission rates, with detail on this method given in *Thoma et al.*, [2012]. For this study, only the PSG approach was used.

The PSG GMAP-REQ method is recommended for flat terrain with few obstructions and steady winds, making it unsuitable for many well locations in Colorado that feature complex terrain and changing wind patterns, though the method has been evaluated at a gas well in Greeley, CO, as well as sites in Texas and Wyoming. *Thoma and Squier* [2012] have also

outlined a validation experiment, conducted in a similar fashion to what we will be performing for the TRM and PSG, in which CH_4 was emitted at a controlled rate (0.6 g/s) and evaluated both GMAP-REQ methods under a range of distances and meteorological conditions. The two methods appear to be in good agreement with each other, but ongoing experiments are being conducted to further constrain the model [*Thoma et al*., 2012].

The EPA has labeled the PSG technique the Other Test Method (OTA) 33A in the literature, but it will be referenced as the PSG technique within this thesis. This technique contains a novel way of determining wind variables from a stationary location within a plume, but the core equation utilized is a simple two-dimensional evaluation of a Gaussian plume in the cross-wind and vertical directions, as seen in *Turner* [1970]:

$$Q = 2\pi\chi\sigma_y\sigma_z \qquad \textbf{1.2}$$

Similar to **Eq. 1.1**, Q and χ represent emission rate and peak average concentration, respectively. u (mean wind speed) and σ_y and σ_z, mentioned above, are also factors in the prediction. This OTM 33A PSG technique has been utilized at O&NG sites, as described in *Brantley et. al.* [2014].

This Gaussian method has been analytically inspected over a range of conditions, with *Carrascal et al*. [1993] determining that a PSG approach is most sensitive to stability conditions, which factor into the calculation of σ_y and σ_z in **Eq. 1.2**. *Neumann and Halbritter* [1980] found wind speed and emission height to be the values that most affect a PSG model's sensitivity in the "near field", or a distance less than 1 km downwind of a source [*Rella et al*., 2010]. While *Thoma et al*. [2012] validates our specific PSG approach, *Miller and Hively* [1987] have laid out a review of 2-Dimensional Gaussian plume models across a range of experimental validation studies and found that this approach has accuracy generally within a factor of 2 to 4. It is seen

that, in general, the more technical the meteorological and terrain conditions, the more likely this simple plume model's assumptions may not be valid. Averaging time may also affect the overall performance of these simple Gaussian models. *Thoma et. al*., [2012], however, report that a 20 minute averaging time is adequate for obtaining accurate results. Given the flat terrain presented to us at Christman field, as well as the meteorological conditions we sample under (for further information on tests for ideal meteorological conditions, see **Appendix E**), this method should be a sound tool for estimating emission rates as a point or line source.

Our GMAP-REQ method does not require a tracer gas like the TRM does, although a tracer gas may be used to estimate errors in each method. Canister measurements cannot be used for the PSG like they can for the TRM, meaning that this method can be used at Christman airfield in comparison to the stationary TRM validation but cannot be utilized at a field site using GC methods for VOC quantification alone because high time resolution gas concentration measurements are required to perform an emission rate estimation.

1.3 Thesis Goal

What was borne out of a necessity for our field team to test our instruments and practice the operating procedures of the TRM in a controlled setting has led to a validation study of the method to explore unanswered questions about its accuracy and conditions for which it is most applicable. This thesis explores what errors to expect for the TRM given a variety of conditions, both controlled and uncontrolled. We have seen that the TRM is a widely used approach for estimating emission rates, and our team will be using this technique for a large number of experiments. Is this method best suited to accomplish our goals given our experimental needs and limitations?

Because of a lack of direct validation experiments on the TRM, we will need to explore variables such as release system set up, how far downwind we sample, and meteorological parameters in a controlled environment at Christman airfield in Fort Collins, CO. *Scholtens et al*. [2004] attempted to validate the TRM by remaining stationary in a plume, integrating downwind concentrations over the sampling time, while *Mønster et. al.* [2014] validated the TRM as well as Gaussian dispersion model using a mobile transect approach. While our canister samples will be stationary, time-integrated measurements, our experiments at Christman airfield can also focus on mobile transects of downwind plumes, with each plume transect analyzed through the TRM. We are doing so because where *Scholtens et al*. [2004] had essentially one TRM data point for both a slurry store and cattle house, mobile measurements will allow us to have many plume data points even after data screening. This will also allow us to compare our findings to those from *Mønster et. al.* [2014]. Evaluating every plume over as many variables as possible, we hope to develop a system to quantify the errors in the TRM under a range of conditions. This will ultimately constrain our results out in the field.

Stationary plume analysis will be another subset of our TRM analysis. ~20 minute plume samples will be evaluated using both the TRM and the GMAP-REQ model. These models will be compared against the true emission gas emission rate as well as each other. Results from our PSG analysis may be compared to those from a similar controlled experiment performed by the EPA. Both techniques are recommended for use in similar situations, and it would be useful for developing recommendations for what conditions are more suitable for one technique over the other.

In short, a formal list of objects to be covered in this thesis are as follows:

1. Develop a reliable, transportable gas release mechanism for controlled release of emission and tracer gases.
2. Measuring downwind concentrations, either through mobile plume transects or by remaining stationary within a plume, estimate the emission rate of an “emission gas” that is being released under controlled conditions and determine the differences between predicted and actual emission rates.
3. Alter the physical characteristics of gas release setup as well as downwind sampling distance in order perform a sensitivity analysis of variables that can be controlled by the experiment team.
4. Perform these controlled release studies on multiple days to examine the sensitivities to meteorological parameters that each emission rate estimation method may have.

Chapter 2 Methods

2.1 Experimental Design

Our TRM and PSG validation experiments occurred during 2013 and 2014 at Christman Field, a private-use airfield located on the northwestern edge of Fort Collins, CO owned by Colorado State University. Christman Field contains one north/south oriented runway, 1220 m in length, and is surrounded by grass and small shrubs that can be driven over. This allowed for better maneuvering of the mobile sampling system (referred to here as the "plume analyzer") outfitted inside a Chevrolet Tahoe hybrid. In this way we were able to transect or sit in plumes at a range of distances from the source, depending on wind direction. These are the corresponding distances the experiment team usually samples at when performing experiments at an oil and gas well.

Experiments were not performed at Christman Field during days that contained forecasted precipitation or unfavorable wind patterns. The experiments were performed near mid-day, as these times generally correspond to stronger and more consistent winds. An example of wind conditions from an experiment from the spring of 2014 is shown in **Figure 2.1**, taken from a weather station located at the airfield. Though experiments were performed on days forecasted to be most favorable, wind speed and direction nevertheless could vary widely throughout an experiment, as Christman Field's close proximity to the foothills of the Rocky Mountains means that wind patterns are subject to rapid changes due to small-scale eddy turbulence, diurnal mountain breezes, and synoptic-scale patterns.

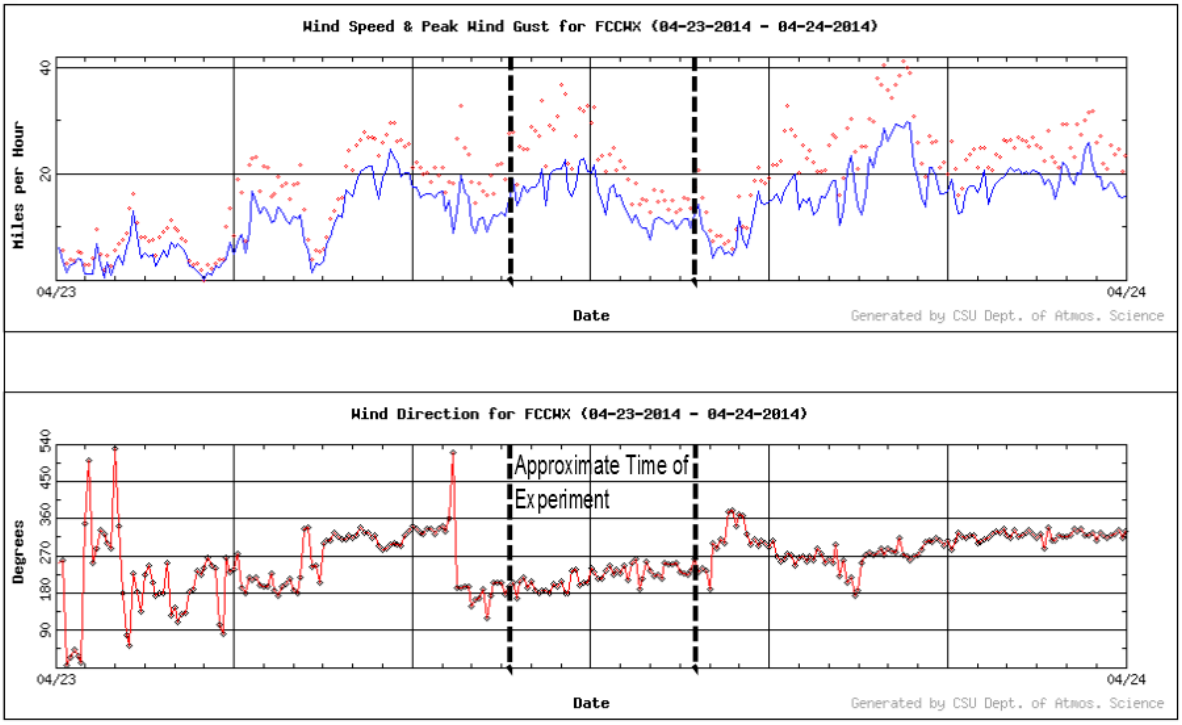

Figure 2.1 Wind speed and peak gust (above) and wind direction (below) averaged over five-minute intervals at a permanent weather station at Christman Field, Fort Collins, CO during a validation study. Dashed vertical lines indicate the beginning and end of the experiment.

Methane (CH_4) is the emission gas used in the Christman experiments. CH_4 is a VOC that is known to leak from natural gas wells and is the main component of natural gas. CH_4 also has a similar density to and is measured with the same speed and accuracy as our tracer gas, which makes it an ideal emission gas to use as a simulation of a VOC source in our Christman studies. These experiments comprise of one tracer gas, acetylene (C_2H_2). Also known as ethyne, C_2H_2 is a very stable alkyne and is considered one of the least reactive species in the atmosphere [*Whitby and Altwicker*, 1978]. It is also almost entirely generated by industrial sources and has a very low naturally-occurring concentration [*Rella et al.*, 2010]. These gases are considered non-reactive for the length and time scales over which they are released from our source and subsequently analyzed with our plume analyzer. Both gases are accessible through the Airgas branch in Fort Collins [Airgas.com]. The flow of these gases was controlled through a custom-built release

system, and their downwind concentrations readily quantifiable via instrumentation on the mobile plume analyzer. As we will see in the instrumentation section below, both C_2H_2 and CH_4 can be explosive within a certain range of ratios of their concentration to that of O_2, denoted as $[O_2]$, in the air. The ratios of both gases need to be monitored throughout certain experimental set ups.

A schematic of the experimental setup at Christman Field is shown in **Figure 2.2**. Both emission and tracer gases are released from a manifold designed as a point or line source at fixed emission rates. Quantification of the plume downwind was accomplished by drawing air in through a sampling inlet which directs air to the analyzer within the vehicle which instantaneously determines the concentrations of C_2H_2 and CH_4 via cavity ring-down spectroscopy. The time-integrated gas concentrations across a plume transect or stationary sample period were used to predict the known CH_4 emission rate. For times of uncertain wind patterns our team released a smoke signal at the point of emissions to help trace their trajectories, as seen in **Figure 2.3**.

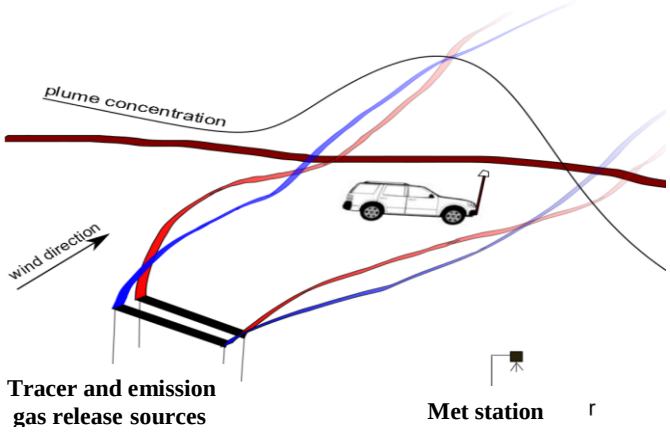

Figure 2.2 A simplified diagram of the Christman Field experiments set up. In this version, plumes flowing downwind from co-located line sources of our tracer and emission gases are traversed by an SUV with real-time analyzer equipment. The instantaneous concentrations of these plumes plotted along the SUV path may look like the "plume concentration" line shown. A met station is also located nearby to record 3-D wind measurements.

Figure 2.3 A line source release during a Christman field study in which a smoke canister is released at a co-located source. The plume's trajectory can be traced from the smoke path.

As mentioned in the introduction, the Christman experiments are meant to test as wide a range of variables that may affect the performance of the TRM and PSG as possible. Some of these variables are within our control, others are not. The following is a list of variables both controllable and uncontrollable that we will be examining:

Emission rate. We are able to control the emission rate of both tracer and emission gases. The flow rates we use for our emission rates range from 2.5 to 40 liters per minute (LPM). We can set the emission rates of each gas to the same flow or examine the outcome when the emission rate of each gas is different. The PSG should not be affected by a difference in emission rates between the gases, as this technique evaluates both gases independently of each other.

Source geometry. As shown in the introduction, the configuration of the sources of each gas can play a substantial role in how the TRM and PSG performs. The configurations for our gas release include tracer and emission gases both released as a point source, seen in **Figure 2.4** or both as a

short line source, as seen above in **Figure 2.3**. The sources can be co-located or they may be separated from each other by placing the tracer gas source downwind of the emission gas, or by separating the sources in the crosswind direction. They may also be separated in the vertical direction.

Figure 2.4 A point source release set up at Christman Field. Estimate and tracer gases flow up and out of their respective tube seen on the right. Our meteorological station is also seen on the left.

Distance. A range of downwind distances were tested, with analysis ranging from about 40 m to nearly 200 m away from the release point. The maximum distance downwind that can be sampled is heavily dependent on wind direction. Given the configuration of Christman Field, there can be a wider range of sampling distances when the wind is moving parallel to the N-S oriented runway than if the wind is moving east or west. The distance it takes for the plume analyzer to traverse a plume (i.e. the plume width) is another variable that will be recorded.

These distance measurements can be accomplished using the GPS onboard the plume analyzer through the haversine formula:

$$d = 2r \sin^{-1}\left(\sqrt{\sin^2\left(\frac{\varphi_f - \varphi_i}{2}\right) + \cos\varphi_i \cos\varphi_f \sin^2\left(\frac{\lambda_f - \lambda_i}{2}\right)}\right) \quad \textbf{2.1}$$

where distance *d* is determined using *r*, the radius of the Earth, and latitude and longitude, φ and λ, from an initial point to a final point (subscripts *i* and *f*, respectively). For determining plume width, the points in which the plume analyzer entered and exited the plume are used as initial and final GPS coordinates. For distance from the source, we mark the release point's GPS by driving the plume analyzer to the source release. The coordinates at the center of a plume are used as the final latitude and longitude.

Background Effects. We can set a value for defining how elevated above its background concentration a gas plume reaches. The simplest approach is to record the mean concentration in excess of background for both tracer and emission gases. As we will see for CH_4, our emission gas, its concentrations within background can vary significantly, so a more rigorous form of this equation examines in greater detail how changing background effects may influence the results:

$$\chi_{\text{above}} = \frac{\chi_{mean} - \chi_{\text{background}}}{\sigma_{background}} \quad \textbf{2.2}$$

χ_{above} is the mean plume concentration, χ_{mean}, above its background value, $\chi_{\text{background}}$, divided by $\sigma_{background}$, the standard deviation of all concentrations that are used in determining a background value. This is essentially a signal to noise ratio.

Meteorological parameters. As shown in the literature review, wind direction plays a very critical role for both the TRM and the PSG program. To examine the influence of this variable, we will look at the standard deviation of the wind direction throughout the width of a mobile transect or throughout a stationary sampling time. Wind speed will also be a variable considered. For days in which high-resolution 3-D wind speed data is available, micrometeorological parameters and stability may be evaluated as well. To determine the stability regime of the lower atmosphere at Christman Field during an analysis, we assign an integer value from 1 to 7, 1 being very unstable and 7 being neutral. The parameters used in determining the stability class are the standard deviation in the 2-D wind direction, σ_θ, and an average value of the turbulent intensity (TI), which is described as:

$$TI = \sigma_{u_z} \times [\bar{u}]^{-1} \qquad \textbf{2.3}$$

TI is the standard deviation of the vertical component of the wind speed, σ_{u_z}, divided by the mean wind speed $\bar{u}$, both of which are determined via 3-D wind measurements. *TI* and σ_θ are averaged together and this value classifies the stability class based off the following:

Stability Class 1, if $(\overline{\sigma_\theta, TI}) < 1.5$

Stability Class 2, if $1.5 \leq (\overline{\sigma_\theta, TI}) < 2.5$

Stability Class3, if $2.5 \leq (\overline{\sigma_\theta, TI}) < 3.5$

Stability Class 4, if $3.5 \leq (\overline{\sigma_\theta, TI}) < 4.5$

Stability Class 5, if $4.5 \leq (\overline{\sigma_\theta, TI}) < 5.5$

Stability Class 6, if $5.5 \leq (\overline{\sigma_\theta, TI}) < 6.5$

Stability Class 7, if $(\overline{\sigma_\theta, TI}) \geq 6.5$

This method for determining stability class is used in the PSG program as well for the calculation of predicted gas emission rates, and is in fact a more robust interpretation of stability based on the original Pasquill-Gifford stability class table [*Gifford*, 1961].

Lastly, we've shown that one of the largest assumptions in the TRM is that the plumes of both gases mix together downwind of their source points. It's also been shown that the PSG program assumes deviations in wind direction near the surface across a sample period in order to determine plume width. These assumptions are due to turbulent motions within the lowest levels of the atmosphere (the surface boundary layer), and so we will also examine the effect of turbulence on the performance of the methods. The variable u_*, or friction velocity, is a measure of shear in the surface boundary layer. Because turbulence itself is an instability that is generated by forces of shear, this variable will provide insight into the effects of turbulence near ground-level that is expressed in terms of a wind speed. We can determine u_* in this way:

$$u* = \sqrt{\frac{\tau}{\rho}} = \sqrt[4]{(\overline{u'w'})^2 + (\overline{v'w'})^2} \qquad \textbf{2.4}$$

Friction velocity is generally calculated analytically as the square root of the shear stress τ divided by the ambient atmospheric density ρ. However, we can come to a numeric solution as seen in *Weber* [1999] that uses the three components of wind speed, *u*, *v*, and *w*, in an un-rotated coordinate system. Here, the products of the instantaneous fluctuations of the wind speed components, averaged over 20 minutes, are taken into consideration. Stability class and friction velocity can be determined for mobile and stationary method evaluations from experiments with available high-resolution 3-D wind speed.

2.2 Instrumentation

2.2.1 Gas Release

The 2013 Christman Field experiments contained our most preliminary gas release setup. In these experiments, emission and tracer gases were released from their respective canisters through a regulator that controls the pressure as it exits into non-reactive plastic tubing (Bev-A-Line IV). This tubing transported it to a rotameter (Thorpe tube type, controlled by a dial and ball) which can fully restrict or fully open the flow of gas. From here, the gas was introduced into a stream of ambient air, which flows to either a point or line source. The plume release system comprised of a fan, accordion hose, and a stand to elevate the source. The gas flowed through the opening of the accordion hose where a 12V cooling fan drew in ambient air that mixed the two gases and drew them through to the elevated source. The point source is simply the opposite end of the hose, usually with a plastic tube joint connected at the end, seen in **Figure 2.4**. The line source consists of a solid 3 m tube manifold connected to the opposite end of the hose with two rows of holes, 3 cm in diameter, drilled 10 cm apart. The gas mixture is able to diffuse through these holes across the manifold (see: **Figure 2.5**).

A Mesa Labs Bios Defender 510 [Mesa Labs, Lakewood CO, USA] volumetric flow meter calibrated the rotameter on-site to give us an accurate measurement of the emission rates of gases for the 2013 Christman Field experiments. This flow meter was attached to the Bev-A-Line tubing carrying tracer or emission gas before it entered the accordion hose. The Defender was not connected to our release system through the duration of an experiment. Rather, it was connected to calibrate new emission rates when needed.

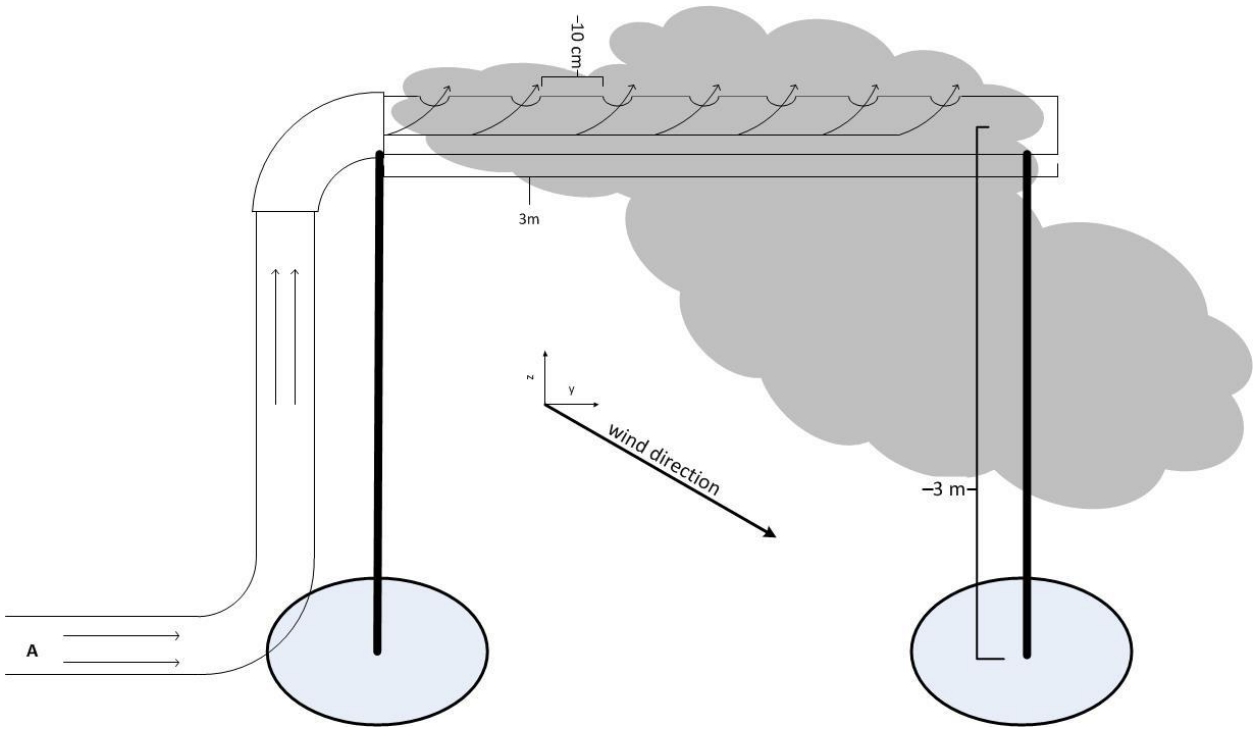

Figure 2.6 The mix of ambient air and release gas flows through the 4" rubber tube and into a line source. In this line source example, we see the manifold located 3m above the ground, though it can also be lowered to ground-level. Point source releases involve tracer and emission gases released into the atmosphere through separate tubes located near each other (see **Figure 2.4**).

A schematic of our 2014 gas-release system, in its most complete form, is given in **Figure 2.7**. A three-layer removable, stackable, rolling toolbox (henceforth called the "DeWalt Stack") is modified to contain a mass flow controller, data logger, and fan speed controller (upper chamber), a mixing chamber with inflow of a specific gas and ambient air (middle chamber), and a housing for the power source (lower chamber). The tracer or emission gas flowed out of its cylinder and pressure regulator, similar to our 2013 experiments, and into the top stack, where its flow was set to a constant rate. This information is fed to the data logger. The gas then continued to flow into the mixing chamber where it diluted in ambient air with the help of a vertical wall with three holes drilled in order to help generate turbulent eddies that aid in the mixing process. The gas's lower explosive limit (LEL) was monitored in this chamber as well, which was

installed to ensure that field study participants were operating in a safe environment in which both [CH_4] and [C_2H_2] within their chambers were diluted to levels that inhibit their flammability if introduced to an ignition source. The mix then flowed out of the chamber into the accordion hose to its release as a point or line source (**Figure 2.6**). A list of all equipment used in our gas release system is given in **Table 2.1**.

Our primary emission rate measurement for our 2014 experiments was obtained by an Alicat M-Series mass flow controller [Alicat Scientific, Inc., Tucson AZ, USA]. This device allows us to record our emission rates as either a mass or volumetric flow rate. The M-Series contains no moving parts, and can compensate for temperature and pressure changes allowing for readings in standard temperature and pressure (STP). With the M-Series, we can record flow rates (in terms of mass or volume), temperature, and pressure. This gives us a time series of emission rate data throughout an experiment, as opposed to a single measurement from the Defender 510 at the moments it was connected to the emission system. We recorded our emission rates as a volumetric flow with the M-Series. The Defender 510 was occasionally connected to our release system during the experiment as well to assure that the M-Series was recording correct volumetric flow rates. This was done by rerouting gas flow through the Defender 510 after it had exited the upper chamber and before it entered into the middle chamber to be diluted.

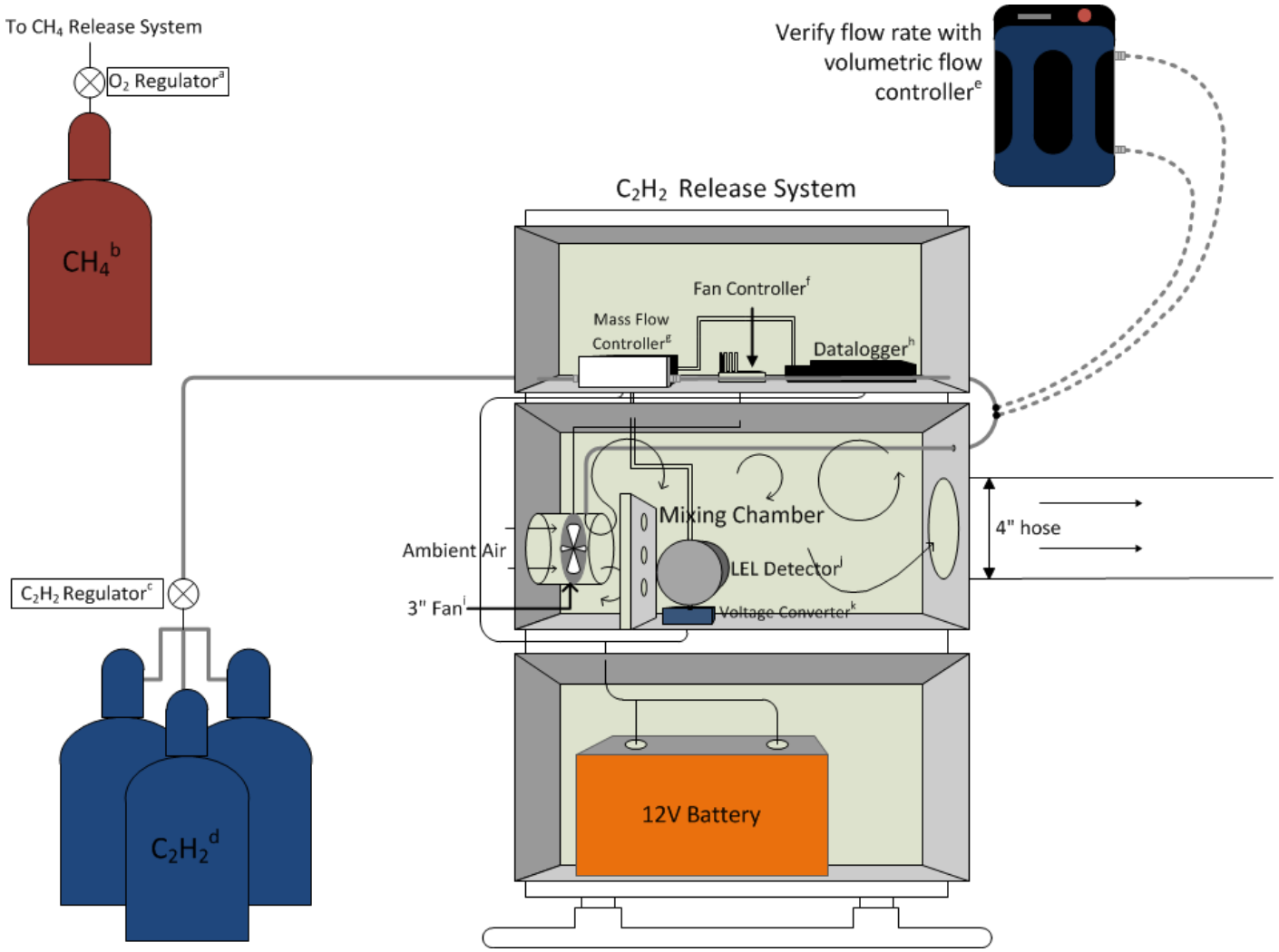

Figure 2.7 The final form of our Christman Field experiment gas release set up. Here, C_2H_2 flows out of its canisters, through the C_2H_2 regulator and into the top DeWalt stack. The flow rate is regulated by a mass flow controller which is controlled by a data logger. The C_2H_2 then flows out of the top stack and into the middle, where it is injected into a 3" tube containing a fan that draws in ambient air so the two may dilute within the middle DeWalt stack. The C_2H_2 LEL is recorded, and the mix of gases flows out of the chamber and through 4" plastic hose to a source setup.

Table 2.1: Gas Release Instrumentation			
Instrument	**Maker**	**Model**	**Remarks**
[a] O_2 Regulator	Radnor	CGA350	Used on CH_4 canisters
[b] CH_4 Canister	Airgas	-	
[c] C_2H_2 Regulator	Airgas	CGA 510	
[d] C_2H_2 Canister	Airgas	AC 4	Contains solid acetone inside canister
[e] Volumetric Flow Meter	Defender	510	
[f] DC Motor Speed Controller	CanaKit	UK1102	
[g] Mass Flow Meter	Alicat	M-Series	
[h] Data Logger	Campbell Scientific, Inc.	CR850	Micrologger that records data at one second and/or one minute summaries
[i] Fan	Rule	140	
[j] LEL Detector	Sensor Electronics	SEC Millenium	
[k] Voltage Converter	Dimensional Engineering	AnyVolt 3	

2.2.2 Downwind Concentration Measurements

The instrumentation used for analyzing downwind concentrations is the Picarro A0941 mobile measurement kit with G2203 analyzer for simultaneous [CH_4] and [C_2H_2] determination [Picarro Inc., Santa Clara CA, USA]. These analyzers utilize cavity ring-down spectroscopy (CRDS), in which a laser is focused into a cavity containing both gases and three reflective mirrors. The laser pulse emitted into this cavity reflects off of these mirrors, traveling around the chamber. A small amount of radiation is able to leak out of the cavity and onto a photodetector that measures its intensity for each pass of the laser pulse. The rate of change in intensity over time due to this energy decay is measured and can be expressed in the following equation:

$$I(t) = I_0 \exp\left[\frac{-t}{\tau} - \alpha c t\right] \quad \textbf{2.5}$$

The intensity at time t, $I(t)$, follows an exponential decay and is essentially controlled by the decay function τ, or the time it takes for the intensity to decrease to $1/e$ of its initial value I_0, as well as the molecular absorption coefficient of the gas being measured, α. This time-dependent decay rate is called the "ring-down time".

We see that this α value can increase the ring-down time compared to the ring-down time if the cavity contained no gases, which we will call τ_0. α is determined at various wavelengths that correspond to the absorption spectra of the gas being measured. Say τ equals the decay function at a certain wavelength λ in the presence of this gas, then:

$$\alpha(\lambda) = \frac{1}{c}\left(\frac{1}{\tau(\lambda)} - \frac{1}{\tau_0}\right) \quad \textbf{2.6}$$

This absorbance at different wavelengths is fitted to a line shape, and the area under its curve is proportional to the concentration of the gas being measured. This technique for concentration measurement is attractive, as it has a very fast response time (>1 Hz) and experiences no noise from laser interference because the laser is shut off during measurement on the photodetector. A schematic of the Picarro CRDS is given below in **Figure 2.8**.

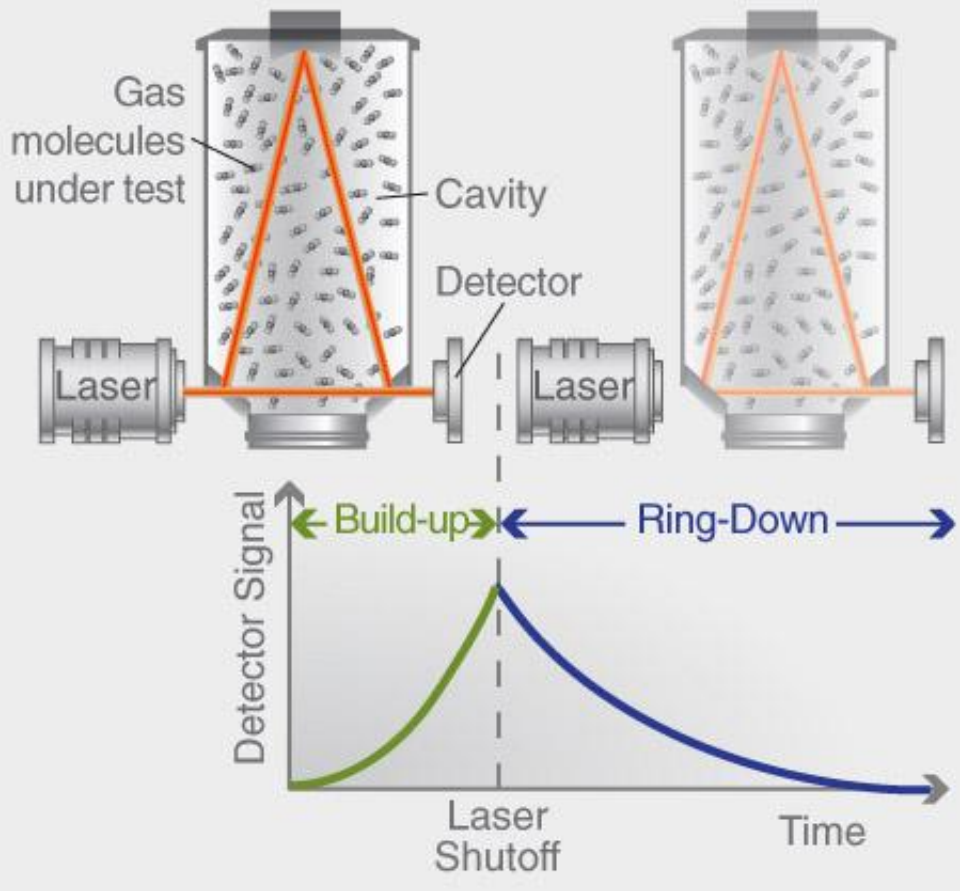

Figure 2.8 Schematic of a Picarro cavity ring-down spectroscopy analyzer, courtesy of Picarro, Inc. [http://www.picarro.com/technology/cavity_ring_down_spectroscopy]

Our CRDS analyzers are housed inside of the plume analyzer. The inlet to draw in ambient air is located on a mast mounted at the front of the SUV. The ambient air flows into the inlet port and through a Teflon tube at ~5 LPM into the CRDS, with the time it takes to travel the length of the tube and into the Picarro being 1.3 seconds. With the average speed of our SUV at around 2 m/s this gives about a 3 m delay in terms of the location gas concentrations are recorded. Given that the average plume transect during our experiments was over 50 m and all plumes are screened to assure that the plume analyzer traversed the entire plume before turning or stopping (see data processing section below), this delay has little effect on the outcome of our mobile measurements. However, when we would like to perform an emission rate estimate via the PSG program, which requires fast-response and time-sensitive sonic anemometer data, we

need to correct for this slight delay to ensure gas concentrations align with sonic data at each time stamp. The Picarro system was calibrated during the 2014 experiments on 2 May 2014 using concentration standards of both CH_4 and C_2H_2 as well as Zero Air canisters. This calibration is noted in **Appendix D**.

2.2.3 Meteorological Measurements

Meteorological measurements are used primarily for our PSG approach and for the calculation of wind parameters and turbulent boundary layer statistics (the TRM itself does not employ any meteorological parameters). **Table 2.2** contains a list of all meteorological equipment used as well as the variables measured from each.

Table 2.2: Meteorological Instrumentation

Instrument	Model	Maker	Variables Measured
Sonic Anemometer	WindMaster	Gill[a]	u, v, w wind components, sonic temp.
All-In-One Weather Station	All-In-One	Climatronics[b]	Wind speed and direction, temperature, pressure, relative humidity.
Temp and RH Probe	HMP45C	Campbell Scientific[c]	Temperature and relative humidity.
Data logger	CR1000	Campbell Scientific[c]	Met data acquisition and memory.

[a] Gill Instruments Limited, New Milton, UK

[b] Climatronic Corportation, Bohemia NY, USA

[c] Campbell Scientific, North Logan UT, USA

Our met station contains a WindMaster, All-in-One, HMP45C, and a data logger. An all-in-one is located on our plume analyzer used for determining wind speed and direction at our downwind sampling points. The met station samples 1 m above the ground for the 2013 experiments. Some of the 2014 experiments utilize two heights with duplicate instrumentation;

one at 2 m and the other at 10 m at the same location via a crank-up tower attached to a trailer also containing a large storage compartment for data loggers for both sampling levels. This gives us a better understanding of the state of the atmosphere throughout our experiments.

Sonic anemometer data from the WindMaster collected 3D wind and temperature variables at a rate of 20 Hz. This high-resolution data is input in the PSG program. Some of this information is decomposed into its mean component (i.e. wind speed in **Eqn. 2.3**) or fluctuation component (3D wind speeds in **Eqn. 2.4)** to calculate flux values. This technique, used in eddy covariance methods, is a statistical tool that carries with it certain assumptions and limitations. Data in this study is screened using tests outlined by *Foken and Wichura* [1996] to ensure that all major assumptions in eddy covariance are met. More detail on these tests are given in **Appendix E**.

2.3 Data Processing

2.3.1 The Tracer Ratio Method

To perform the TRM on mobile transects, gas concentrations downwind are plotted in Matlab [MathWorks, Natick MA, USA] which allows the user to identify the beginning and end of each individual plume. The plumes of CH_4 and C_2H_2 are evaluated separately, meaning that the initial and final times corresponding to the elevated concentration of each gas plume may be different. To constitute a plume during a mobile transect, both tracer and emission gas must have a distinct increase in concentrations during the same transect by the mobile plume analyzer, before it turns another direction or stops.

Background concentrations are determined for each plume, as in *Hecobian et al*. [2011], where the background concentration is determined by averaging the gas concentrations before and after a plume. The length of this averaging varies depending on the length of time from one

plume to another. The standard deviation of the values used as background is also calculated in order to evaluate **Eqn. 2.2**. With background values established for each gas, we can then perform the TRM by integrating the concentrations of both tracer and emission gas over the sampling time. To ensure that concentrations within each plume are sufficiently elevated above their background values, only those concentrations that are larger than 3 standard deviations (3σ) of that plume's background value are used in the integration. An example of mobile transects with clearly defined plumes is given in **Figure 2.9**.

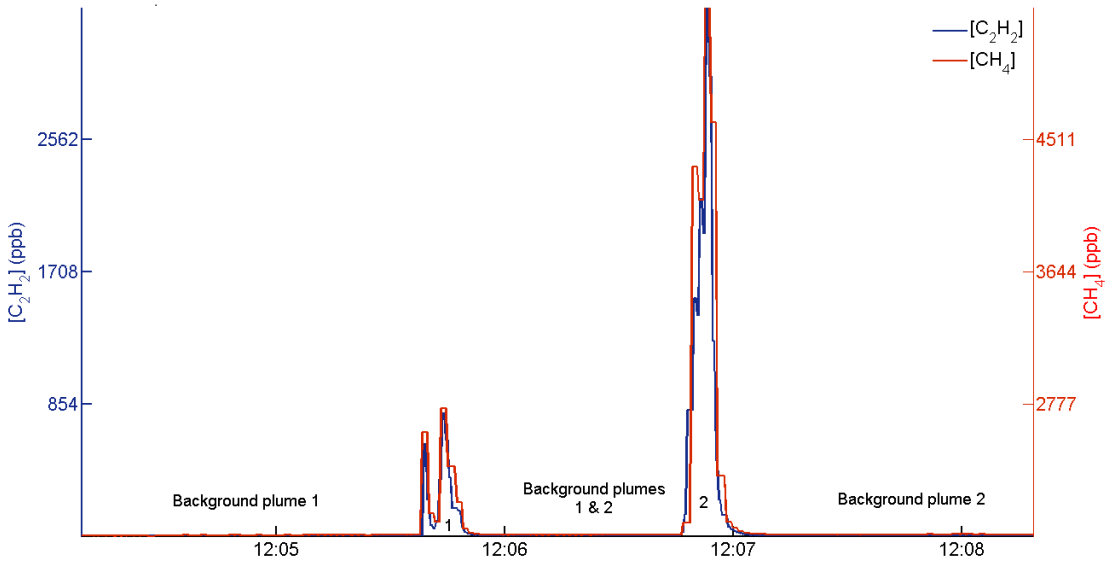

Figure 2.9 Two transected plumes (1 and 2) are plotted. The areas used for determining background values are also labeled, noting that the length of time between plumes 1 and 2 is used in both plume's set background value. Total length of time used for background determination varies between plumes.

The TRM is also used when performing a stationary analysis. In **Figure 2.10** an entire stationary experiment is plotted from 19 September, 2014. A total of nine sample periods were recorded and marked by dividing vertical lines. Two background determination techniques are used in the stationary analysis. The fist and simplest technique involves taking the average of the lowest 5% of concentration values for each gas and subtracting this number from each elevated gas concentration throughout the sample time. This technique is shown in **Figure** 2.11**.** The stationary analysis is then performed like the mobile analysis, in which these background-subtracted concentration measurements for each gas are integrated over the sample period.

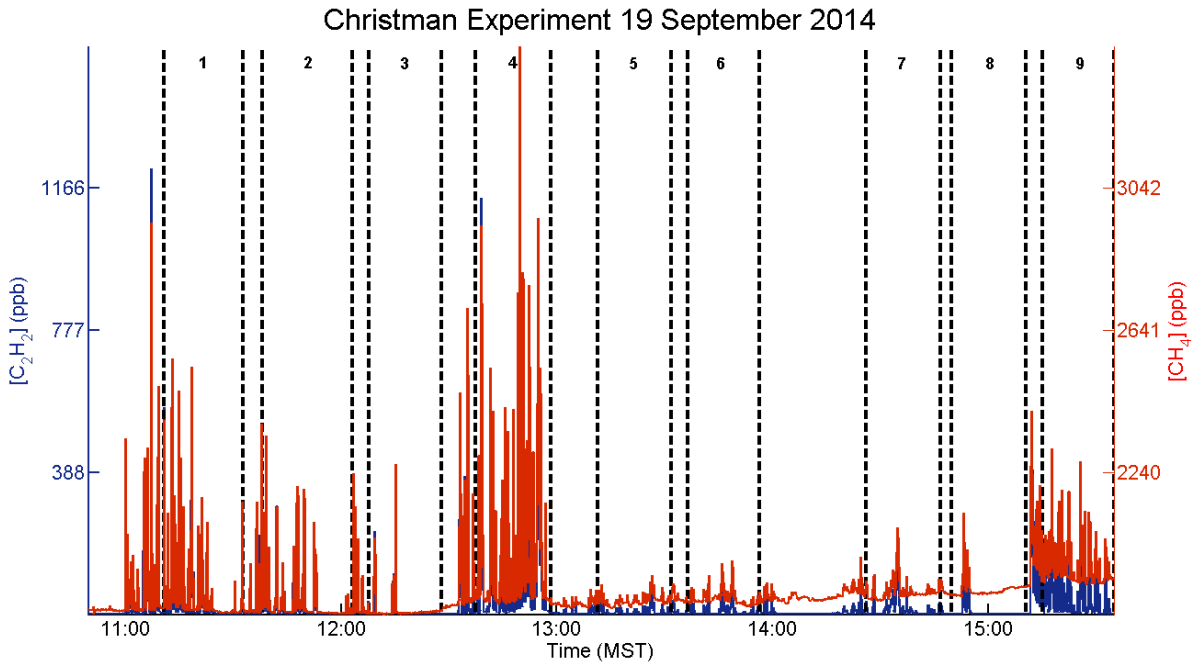

Figure 2.10 The entire Christman field experiment on 19 September, 2014. The vertical lines separate the beginning and end times for each of the stationary samples, with sample numbers labeled at the top of the figure. During this experiment day it is clear that the background of CH_4 varied significantly from beginning to end of the experiment.

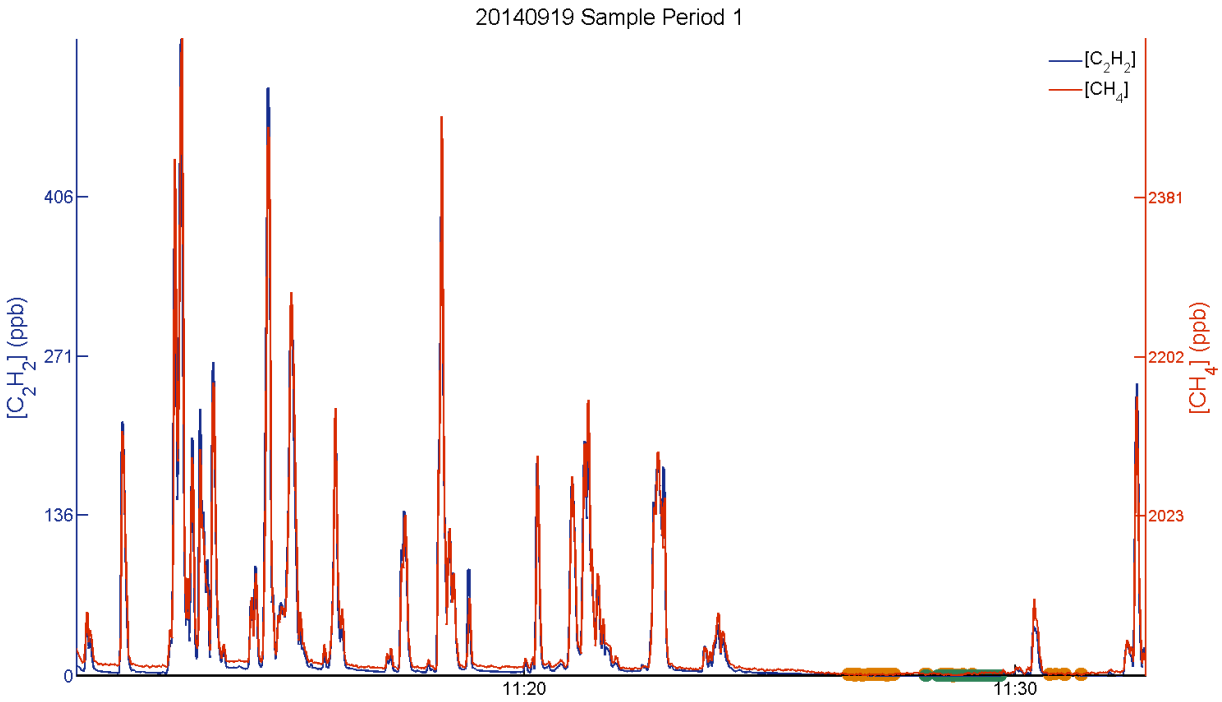

Figure 2.11 Plot of the first sample period during the experiment of 19 September, 2014. Here, an example of the standard background subtraction is shown, with the bottom 5% of CH_4 concentration values highlighted in orange, and the bottom 5% of C_2H_2 concentration values highlighted in green. These values are averaged for each gas, and this value is subtracted off the concentration values within the plume.

The most sophisticated approach involves linearly interpolating a gas concentration time series during periods of elevated concentrations. In **Figure 2.12**, $[CH_4]$ is seen to be highly variable, and so the values of $[C_2H_2]$ are used to indicate whether the gas plume is flowing across the plume analyzer location (assuming that both gases are mixing downwind in a similar manner). The CH_4 background values during elevated concentration measurements are interpolated between the points immediately before and after $[C_2H_2]$ elevates to 3σ above its background value (which is still the lowest 5% of concentrations averaged together). Thus, unlike the previous method for stationary TRM analysis, each $[CH_4]$ value during elevated concentrations has its own unique background concentration that is subtracted off. As we can see in **Figure 2.12** the elevated portions at the beginning and end of a sample time may or may not be used in our analysis, depending on whether or not a background point before and after this

time period can be accurately obtained (in this case, a value before the elevated portion at the beginning of the sample cannot be determined, as the SUV was moving into the plume before the stationary sampling began). Due to the nature of determining an interpolated background correction, the concentration values of both gases outside of these interpolated areas are discarded from the analysis. This leaves us with a smaller series of points for each sample than for the standard background correction technique.

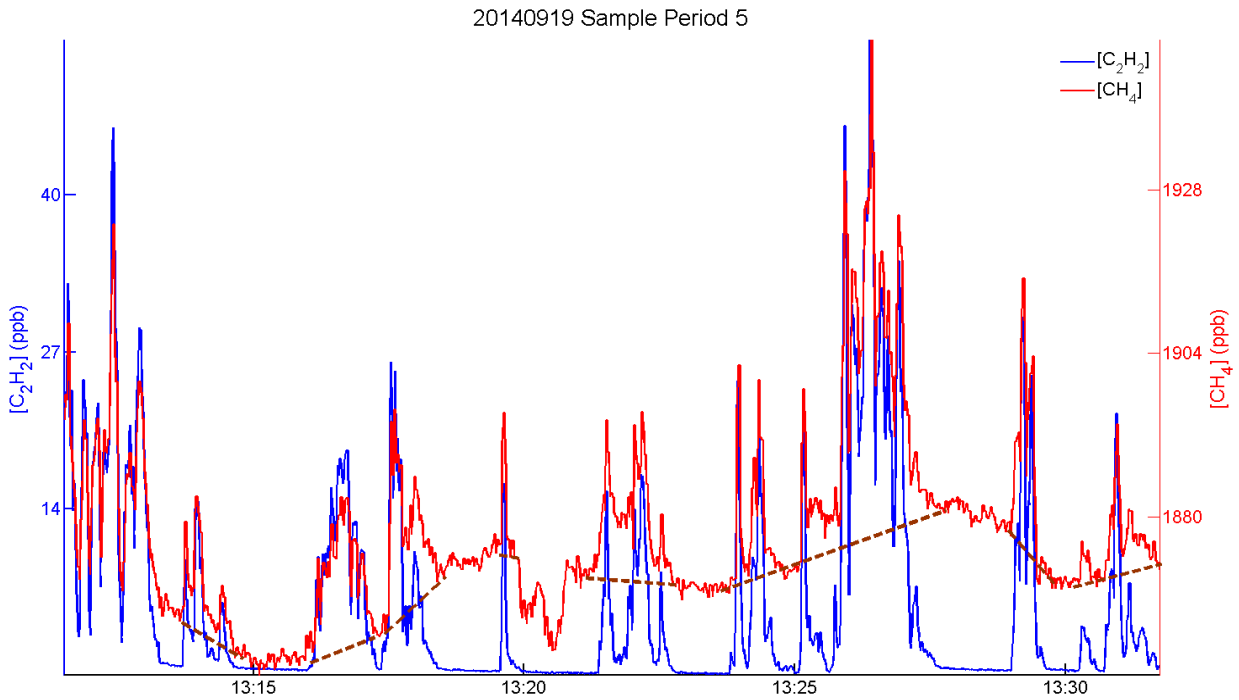

Figure 2.12 Example of a plume evaluated using linearly interpolated CH_4 background values. The dotted lines represent these interpolated concentrations. The beginning and end of an interpolation is determined when $[C_2H_2]$ rises above and falls below 3σ above its background value (average of the lowest 5% of concentration values).

2.3.2 Tracer Slope Methods

An alternate tracer method for estimating emission rates is considered for our validation experiments as well. The ratio of total integrated concentrations of emission and tracer gases that is used in the computation of **Eq. 1.1** is our primary objective because gas canisters at a natural gas well can only serve to give us a total concentration over a set amount of time. However, for

our Christman validation experiments we may also perform the TRM using the correlation between tracer and emission gas at every time step throughout an analysis (mobile or stationary). This technique, which we will call the slope method, uses linear regression with least squares between the instantaneous concentrations of emission gas and tracer gas to determine the slope of the line between the two gases. This slope is then multiplied by the tracer gas emission rate to derive an estimate for the emission gas emission rate.

Another technique, the modified slope method, estimates the delay between the signals of the tracer and emission gas plumes and subtracts this delay to align the plumes. This is accomplished using the built-in align signals program in Matlab. A new linear regression is then calculated and this modified slope is then be used to predict the emission rate of the emission gas. An example of these two techniques performed on a mobile plume is given in **Figure 2.13**. On the top, the instantaneous concentrations of both CH_4 and C_2H_2 from a mobile plume transect are plotted as a time series on the left, and as a scatter plot between the two on the right. The bottom shows the two plumes aligned in the time series as well as the new scatter plot and slope value. If there is no estimated delay between the signals of both gas plumes, the modified slope method is not performed on that transect. This modified slope method was performed on mobile transect analysis only, because over the course of a 20 minute stationary analysis multiple delays may be determined through the program.

For stationary error analysis, the linear regression calculated for the slope method will be the product of every instantaneous concentration of CH_4 and C_2H_2 within a sample period (to compare to the standard background correction for the TRM) or the product of all elevated instantaneous concentrations that will be used in an interpolated background scheme, with a

unique background subtracted off of CH_4 in the exact same manner as the TRM background correction. Thus, there will be two background correction schemes for the slope method as well.

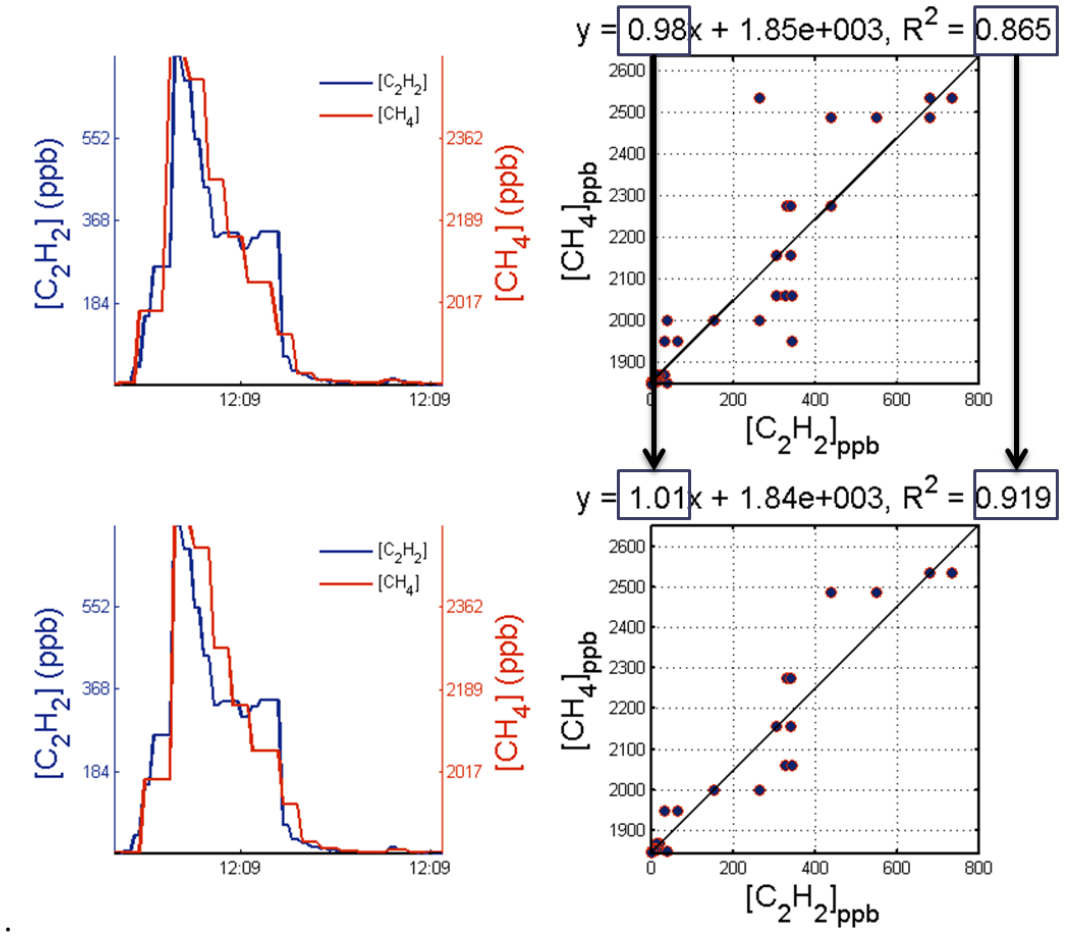

Figure 2.13 In the top panels, the time series (left) and scatter plot (right) of $[CH_4]$ and $[C_2H_2]$ within a mobile transect are plotted. A linear regression is calculated between the two concentrations and the slope of the line (boxed off in the equation above the scatter plot) is used to predict the CH_4 emission rate. In the bottom panels, the same transect is plotted, but after the signals of both $[CH_4]$ and $[C_2H_2]$ are aligned. The modified slope value in the new regression line (also boxed off above the scatter plot) is then used to predict the CH_4 emission rate. Note that the correlation between the two plumes changes when aligning the signals, which is boxed off above the scatter plots as well.

Plots of $[CH_4]$ and $[C_2H_2]$ time series and scatter plot data for mobile transects with co-located sources are given in **Appendix A**, along with the % biases in the TRM, slope

method, and modified slope method (labeled as MSM). The same information is plotted in **Appendix B** for mobile transects with separated gas sources.

2.3.3 The Point Source Gaussian Method

The point source Gaussian program operates under the assumption that, over the course of a 20-minute sample run, the plume analyzer will be stationed directly downwind of the prevailing wind direction. It follows then that the majority of the time the Picarro will sample the largest volumetric concentrations along the centerline of the plume. There are times, however, that disturbances in the localized mean wind flow will drive the plume out of the path of the plume analyzer, allowing lower concentrations that are more representative of background values to be sampled. Gas concentrations are recorded along 10^o wind direction bins over the course of the sampling time. Background-subtracted mean concentrations are recorded in each wind direction bin. These values are then used as reference points to fit a Gaussian curve to the data using the Ezfit Matlab function.

The peak average gas concentration, χ, along this fitted Gaussian curve (in g/m3) is input into **Eq. 1.2** to determine a predicted emission rate in g/s. The mean wind speed $\bar{u}$ contained in the equation is determined by averaging the recorded sonic anemometer 3D wind speed across the entire sampling time. σ_y and σ_z (both in terms of length m) are a function both of downwind distance and atmospheric stability parameters.

An example of the output of a PSG stationary analysis is given in **Figure 2.14**, where concentrations recorded across the 10^o wind direction bins as well as the fitted Gaussian plume. The PSG program rotates the sonic coordinate system to a streamlined coordinate system set at 180^o from the downwind measurement location.

The two methods for determining background values for the PSG program are the same as the within-sampling time methods mentioned above for the stationary TRM analysis. The lowest 5% method is built into the PSG program and requires no modifications to the program. The linearly interpolated program again corrects for a unique background value for each CH_4 concentration measurement.

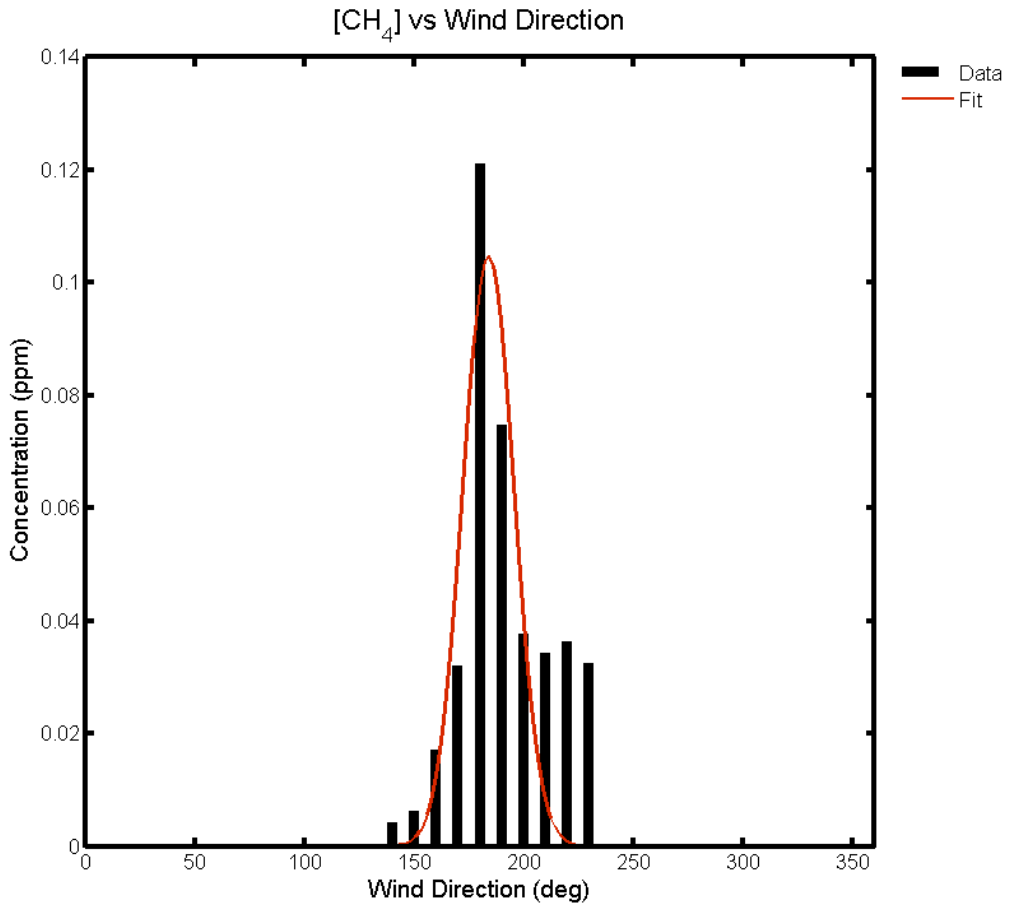

.

Figure 2.14 Example of the PSG output during a stationary sample run during a 2014 Christman field experiment. Black bars are the average concentration in each wind direction bin, and the red curve is the fitted Gaussian distribution determined by the Matlab Ezfit function.

Stationary plume analysis for each sample period is given in **Appendix C**, with plots of time series data in the same manner as **Appendix A** and **Appendix B**, as well as PSG plot

outputs for both CH_4 and C_2H_2 plume fits. The % biases in the TRM, slope method, and PSG programs for both the standard and interpolated background corrections are also shown.

2.3.4 The Point Source Gaussian Tracer Ratio Method

We've noted that χ is determined so it can be used in the calculation of the predicted emission rate via the PSG program. This can be multiplied by the y and z stability parameters along with 2π to obtain an integrated concentration value in g/m (this is essentially **Eq. 1.2** without the multiplication of $\bar{u}$). If we were to perform the PSG analysis on both tracer and emission gases we could obtain an integrated concentration for each. We can input these values into the TRM in place of the standard integrated values to obtain a PSG TRM predicted emission rate. This method will also be evaluated using the two background correction methods as well.

2.4 Analysis

Mobile plume transects are filtered based on a few criteria, one being the correlation between tracer and emission gas concentrations across the width of the plume. If the R^2 value for tracer to emission concentrations is below 0.7, these plumes are considered to behave too differently to evaluate using tracer techniques and are discarded. The timestamps used in this correlation analysis are ones in which both tracer and estimate gases are above their 3σ background threshold. We also filter out plumes in which the plume analyzer made rapid changes in its motion, stopped, or turned at any point during a plume transect. The aim is to evaluate a completely mobile transect across an entire plume under a steady speed and any of the analyzer motions mentioned above may significantly affect the outcome of the analysis.

Stationary analysis contained filtering similar to that of the mobile analysis, although now instead of filtering out plumes with slow or no vehicle motion, the stationary analysis requires

the plume analyzer to be stationary for an entire experiment. For the PSG program, we will filter results based on the criteria used in the original EPA validation experiments, outlined in *Thoma et al.* [2012], which includes an average wind speed of less than 1 m/s during a sampling time, peak [CH_4] concentrations less than 50ppb above their background values, and an R^2 value of the Gaussian fit to the concentration bins less than 0.7. To fairly evaluate both the stationary TRM and PSG methods against each other, stationary TRM measurements corresponding to any sampling time that cannot be processed using the PSG program are discarded as well. Sonic Anemometer data used for the stationary analysis is also evaluated using the tests mentioned in **Appendix E**. This high-frequency micrometeorological data must meet the criteria outlined in this section.

The recorded emission rates in the field are in LPM, i.e. a rate in the form of a volume of gaseous emissions per time. A more conventional way of expressing the flow of gases out of a source is through its total mass released into the atmosphere per time. This representation of emission rate in terms of a mass is more consistent with the literature (e.g. *Rumburg et al*. [2008] and *Zavala-Araiza et al*. [2014] report emissions as a mass per time, while *Stephenson et al*. [2011] report emissions in a similar fashion as a unit of mass per amount of energy generated during a span of time: grams per kilowatt-hour). While a conversion from LPM to g/s will not affect the outcome of our error analysis, we will report our values in this way.

The conversion from liters to grams can be accomplished by multiplying the volumetric unit by the standard density of each gas (recorded at 1013.25 hectopascals (hPa) and 25° C) for measurements in standard liters per minute (SLPM) for the mass flow meter. However, because Christman airfield is located nearly 1 mile above sea level, using this conversion of recorded emission rates in LPM is inaccurate as the average atmospheric pressure at this height is

generally ~25% less than that at sea level. To account for this, we use the ideal gas law, expressed as follows:

$$pV = \left(\frac{m}{M}\right)\bar{R}T \qquad \textbf{2.7}$$

We can solve this equation for density, or mass *m* over volume *V*, using atmospheric pressure *p*, molar mass *M*, temperature *T*, and the universal gas constant $\bar{R}$ (8.314 J K^{-1} mol^{-1}). In this way we see that the calculated mass accounts for actual pressure and temperature. $M_{acetylene}$ = 26.0373 g/mol and $M_{methane}$ = 16.0425 g/mol, [National Institute of Standards and Technology Chemistry WebBook].

The predicted emission gas emission rates, $Q_{predicted}$, for each plume can be compared to their true emission rates, Q_{true}, in this manner:

$$\%Bias = 100 \times \frac{Q_{predicted} - Q_{measured}}{Q_{measured}} \qquad \textbf{2.8}$$

The percent bias in a method will allow us to determine the error in the technique as well as whether it leads to an over-prediction or under-prediction of the emission gas emission rate. This percentage bias can be helpful as it is intuitive to think in this manner, but we will also evaluate our findings as a ratio value between predicted over the measured emission rates. A logarithmic plot of this ratio gives an equal spacing for both a positive and a negative bias in the methods, which is helpful in a graphical evaluation of the results. With the bias in our methods calculated, we can then evaluate the effectiveness of the tracer techniques and PSG against the variables mentioned above.

Chapter 3 Results

3.1 2013 Christman Field Experiments

Six Christman field experiments were performed during the spring and summer of 2013. These experiments only contain mobile transect analysis. Based on the criteria for defining a good plume transect in **Section 2.4**, there are 101 total plumes that meet all these requirements. All plumes are evaluated on an individual basis so each plume transect may have a predicted CH_4 emission rate via the TRM and the slope method. The modified slope method is also performed on plumes that can be realigned to offer a maximum correlation between C_2H_2 and CH_4.

In **Table 3.1** we see parameters that are evaluated for each experiment day. These are divided into categories based off controlled and uncontrolled variables that can be examined. Some controlled variables are only marked as evaluated if multiple configurations of that parameter are assessed throughout a given experiment. For example, every downwind measurement must be some distance away from the source, but the parameter *distance* is checked only if multiple downwind distances are evaluated during that experiment day. Uncontrolled meteorological variables are checked as yes if the proper instruments were onsite and functioning during that experiment day. We also see that meteorological data has been divided into two sections, basic met and micro met, with basic met comprising met data that is obtained from the all-in-one sensor onboard the plume analyzer, while micro met involves more detailed analysis from our on-field met station. The micro met data include information from the 3-D sonic anemometer and thus give us information about frictional velocity. **Table 3.1** also includes the number of plumes (N) evaluated for both the TRM and slope method and for the modified slope method

(recall that a plume that is maximally aligned as-is is not evaluated using the modified slope method), as well as the mean biases for each of the three methods.

Table 3.2. Record of all controlled and uncontrolled variables for each 2013 Christman Field experimental day. A green Y indicates that that parameter was evaluated on that given day, while a red N indicates it was not. The number of plumes (N) evaluated during each experimental day is also recorded as well as the mean biases in each method. A range in values in the parameter evaluated is given, where applicable.

Table 3.1: Parameters Evaluated during 2013 Christman Experiment Days

Date	26-Jun	11-Jul	20-Aug	23-Aug	30-Aug	05-Sept
N	20	9	10	25	22	15
CH_4 emission rate	Y	N	N	N	Y	N
C_2H_2 emission rate	N	N	N	N	Y	N
Source height (m)	N	N	N	N	Y (2)	N
Separation	N	Y (2)	N	N	N	Y (2)
Downwind distance (m)	Y (58-194)	N	Y (48-116)	Y (40-190)	Y (42-184)	Y (110-255)
Meas. Above background	Y	Y	Y	Y	Y	Y
Basic met	Y	Y	Y	Y	Y	Y
Micro met	Y	Y	N	Y	Y	N
Mean TRM bias (%)	48.4	45.7	45.7	44.1	60.1	54.2
Mean slope method bias (%)	41.9	37.3	33.5	33.7	75.4	55.6
Mean modified slope method bias (%)	46.6	44.9	37.5	36.5	78.6	66.1
Modified N	15	5	7	19	11	14

There is another 2013 experiment, performed on 30 May of 2013, which is not included in this analysis, because key information such as GPS coordinates and vehicle speed is not available. This missing information prevents us from determining parameters such as downwind distance and more importantly plume filtering criteria related to vehicle speed. This day then cannot be evaluated like our other experiments as it's impossible to use the same filtering criteria for these plume transects as we do for our other experiment days.

In **Table 3.1** we see that for the overall mean biases for each different method there is a persistent positive bias over all experiment days generally on the order of 30 to 50% error. The 20 and 23 August experiments contain the lowest biases for each method, while the 30 August

and 05 September experiments contain the highest biases, and so it appears that there is some consistency between all three methods. It is unclear based off **Table 3.1** what parameters may be affecting these biases, and we will individually explore these parameters further. Curiously, the modified slope method performs worse than the standard slope method in all cases. Out of all methods evaluated, the standard slope method contains the lowest mean biases for most experiments, although those values are not far better than the other two methods.

We will examine the spread in predicted CH_4 emission rates via the TRM and slope methods for each experiment day in **Figure 3.1**. Here we evaluate our methods using the ratio of the predicted to the measured CH_4 emission rate. **Figure 3.1** only includes those plumes that are not maximally correlated initially, i.e. the plume transects that are able to be evaluated through both slope methods. Here, a value of one indicates that the method perfectly predicted the CH_4 emission rate, and we again notice the persistent positive bias among all methods and across each experimental day. Across each experiment day and each method, the median predicted values are fairly consistent, with the major difference being the spread of predicted values. There is a much larger spread in predictions on 30 August and 05 September, and to a lesser extent 26 June, than for the other experiment days. These three days are the only experiments to sample with a source separation of some kind (either in the cross/downwind direction or through source heights), which could be influencing the larger spreads in ratios.

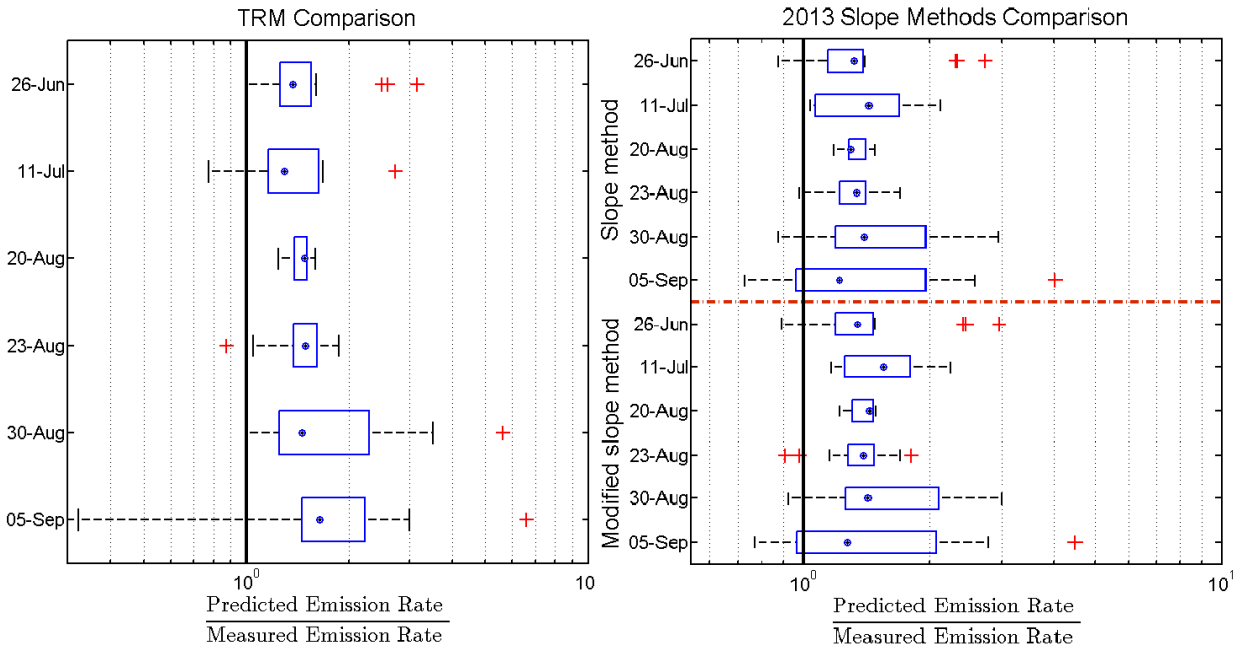

Figure 3.1 Box and whisker plots of the ratio of predicted to measured CH_4 emission rates for each 2013 Christman Field experiment day. The point within the box represents the median error ratio while the edges of the box represent the 25th and 75th percentiles of the error ratios. The whiskers extending to the edge of the ratios show the 95th percentiles of the error ratios. Large outlying ratios are plotted individually and marked by the red plus signs. Results for the TRM are plotted in the left panel, while results from both the slope method and modified slope method are plotted in the right panel.

It's been noted that the modified slope method appears to perform worse than the slope method in **Table 3.1**, however the spread in predicted values in **Figure 3.1** is very similar between the two methods. This is explained in **Figure 3.2**, in which the slope method results of plume transects of CH_4 and C_2H_2 that are already aligned, without the need to modify their time series, are plotted. It is shown that plumes that are already aligned also tend to have a bias that is relatively close to the median value of errors for each given day. This indicates that the modified slope method is generally performed on plumes that have larger outlying biases to begin with, and that aligning tracer and emission gas plumes on these lesser-aligned transects does not necessarily lead to a significantly better emission rate estimate. Our 30 August experiment seems to be an exception, with large % biases plumes that are not included in the modified slope method predictions.

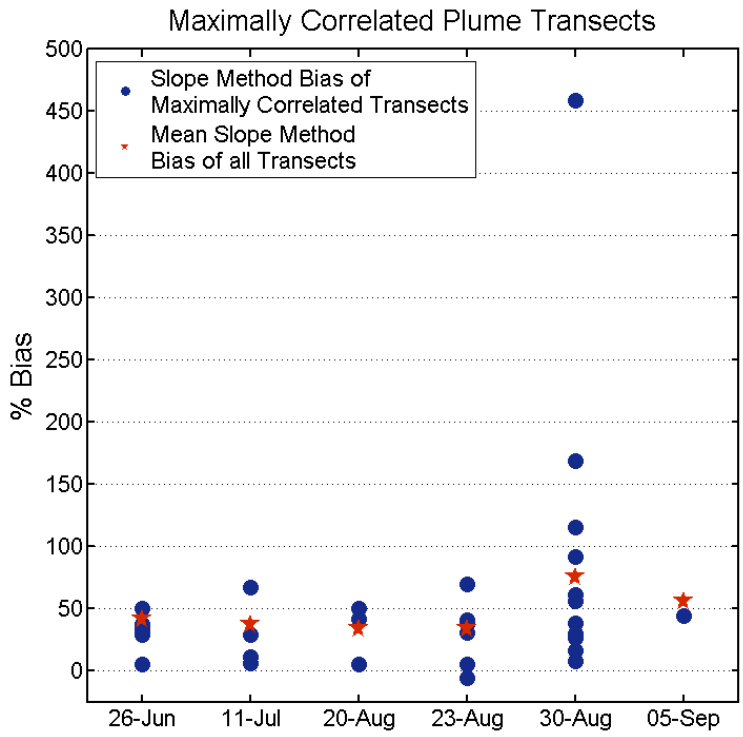

Figure 3.2 Scatter plot of the % bias of plumes that are not included in the modified slope method predictions because their CH_4 and C_2H_2 are maximally aligned to begin with. Red stars for each experimental day denote the mean % bias in the slope method for all transects evaluated.

The correlation between the results of the slope method and the modified slope method is 0.98 with a *p*-value (here, the probability that the two variables are uncorrelated) on the order of 10^{-66}, or ≈ 0 (in the results section, any *p*-value less than 10^{-3} will be written as ≈ 0). The R^2 value between the slope method and the TRM is 0.75 ($p \approx 0$). In general, the three methods perform similarly across all situations encountered during these six experiment days. However, we will now evaluate plume transects originating from sources that were co-located separately from sources that were separated (either vertically or horizontally), as we would expect this to introduce biases in the data. The co-located and separated cases will be evaluated side-by-side to allow for a clearer comparison.

In **Figure 3.3** each method is tested to see how probable its distribution of errors fits a lognormal distribution. There is a great deal of consistency between these methods for co-located sources, with all containing a similar distribution. For the bulk of error values, there appears to be log normality; however, the largest 20% (and to a lesser extent, the bottom 20%) is not lognormally distributed, and this large tail of high ratios exists for each method. The methods are also similar in their distributions, although they are shifted slightly in the cumulative distributions of their error ratios. The TRM distribution is shifted most in the positive bias direction, while the slope method's distribution is centered closest to a perfect prediction (although again, still relatively far from a perfect ratio of one). Transects with separated sources are less consistent in terms of following a lognormal distribution, although there are no large outlying error ratios like those seen in the co-located transects.

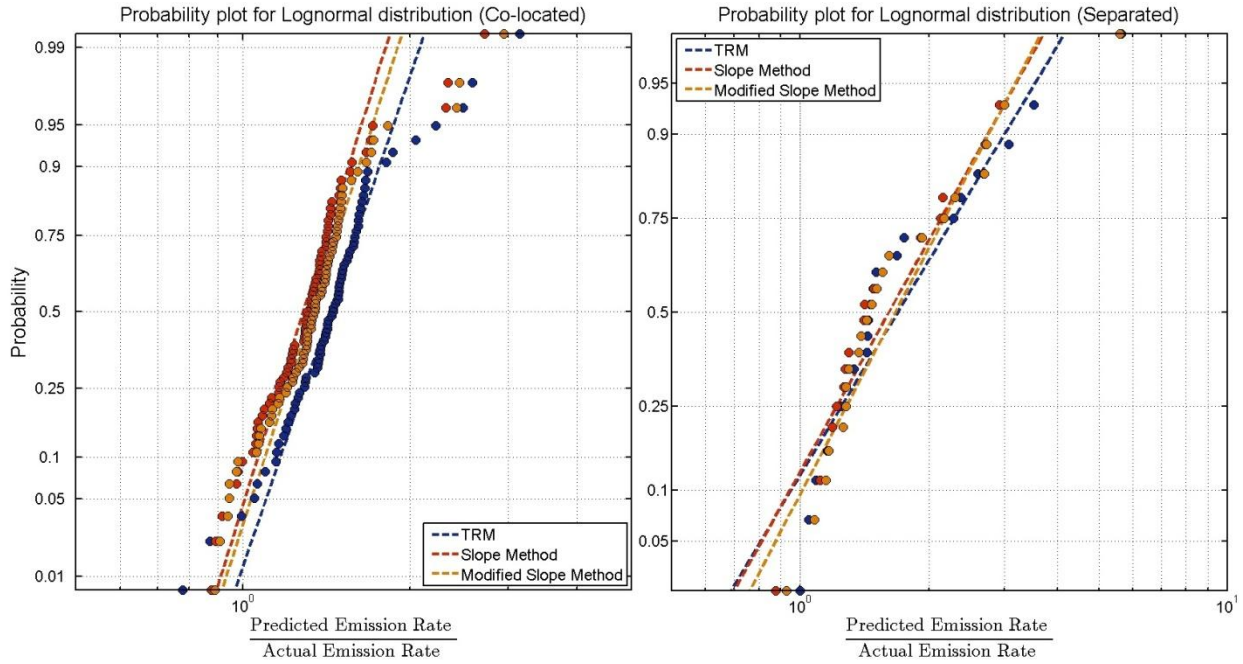

Figure 3.3 Probability plot that tests for lognormal distributions for each of the three methods evaluated in this section. The scatter of points for each method represent the predicted to the actual, measured CH_4 emission rate for a plume transect. If a method's ratios followed a perfect lognormal distribution, all points would fall on that method's respective reference line. Errors from plume transects with co-located sources are evaluated on the right, while those from separated sources are on the left.

All three methods perform very similarly, while the slope methods overall hold a mean error that is closer to the actual emission rate. Because of this, we will evaluate these three methods against the parameters outlined in **Section 2.3.3**. These methods will also be evaluated against each other when examining these parameters.

The correlation between the time series of CH_4 and C_2H_2 instantaneous concentrations measured onboard the plume analyzer across an entire plume is shown in **Figure 3.4**, compared to the absolute value of the percent bias for each method. In this figure, and for the rest of the figures for the 2013 evaluation, circular points denote sources separated vertically, square points denote sources separated in the upwind direction, and triangular points for crosswind separations for the analysis of separated sources. It is clear from these two plots that the co-located plume transects contain a smaller spread in errors compared to those from separated sources. The errors are much more constrained at the very highest correlations between the two gas concentrations for both co-located and separated sources, with the worst-predicted plume transects between R^2 values of 0.7 and 0.8. This is true more so for separated sources. All three methods perform similarly across the range as well, indicating that there is no distinguishable pattern between R^2 and a difference in individual method performance.

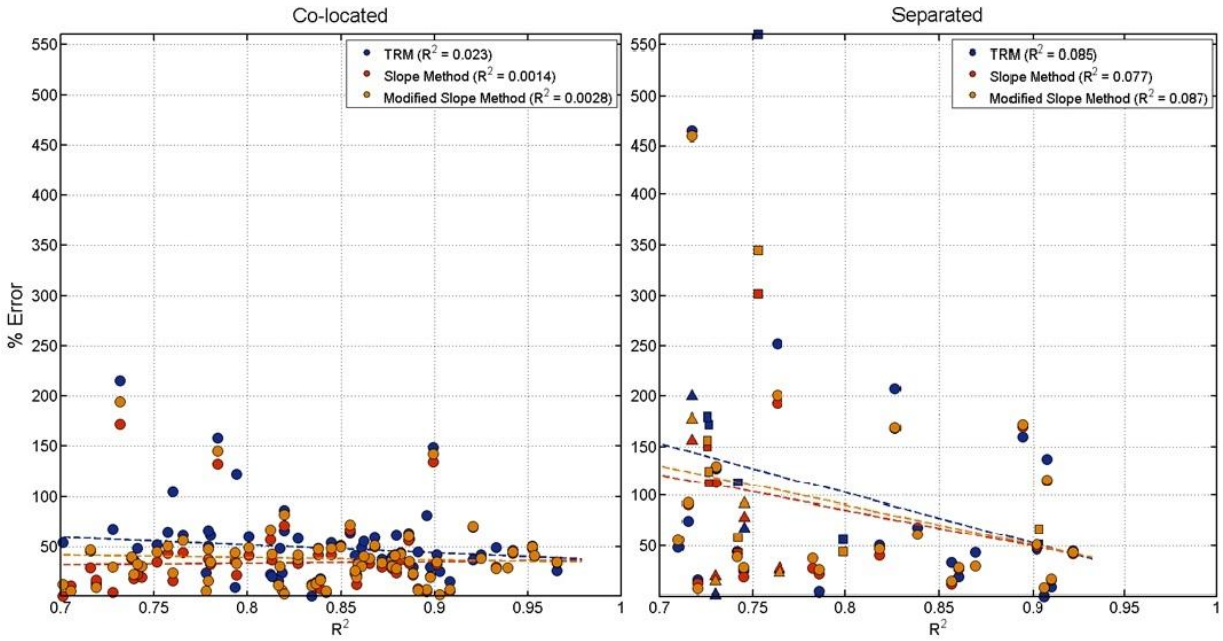

Figure 3.4 The absolute error in CH_4 emission rate predictions for each method, as a function of the R^2 value between instantaneous CH_4 and C_2H_2 concentrations measured on the plume analyzer, for co-located sources (left) and separated sources (right).

Parameters that can be controlled by the experiment team are shown in **Figure 3.5** for co-located plume transects and for separated source plume transects in **Figure 3.6**. Here, the ratio of predicted to measured CH_4 emission rates are plotted with respect to the correlation between $[CH_4]$ and $[C_2H_2]$ and color-coded by the ratio of the emission rate of C_2H_2 to that of the CH_4 emission rate in the top plot and the distance from the sources the plume analyzer transected the plumes in the bottom plot. Changing the ratio of the emission rate of C_2H_2 to that of the CH_4 emission rate, which ranges from around 0.5 to 2, doesn't have a major effect on the performance of the methods evaluated. We would not expect and wouldn't want this factor to significantly alter the performance of our methods, keeping in mind that this exact ratio cannot be known at an oil and natural gas well site. The distance from the sources the plume analyzer transected a plume shows no distinct pattern either, and this also agrees with the theory behind the tracer ratio methods. From this analysis it is hard to find a parameter that has a noticeable effect on the outcome of the methods.

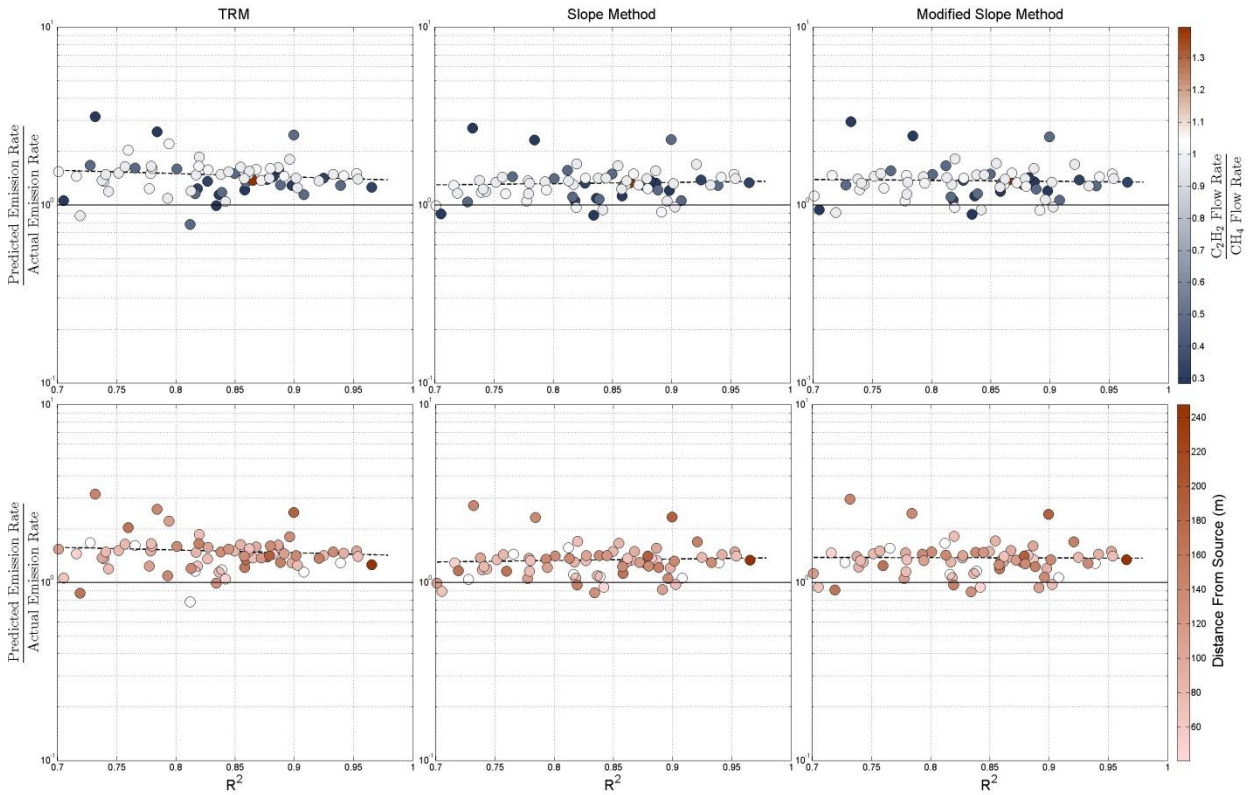

Figure 3.5 Variables that may affect the different tracer ratio methods that are controlled by the experiment team for co-located plume transects. Bias ratio and R^2 values for the TRM (left column), slope method (middle column), and modified slope method (right column) are plotted with respect to the ratio of tracer to emission gas emission rates (top row), source set-up configuration (middle row), and distance from the sources the plume analyzer transected the plume.

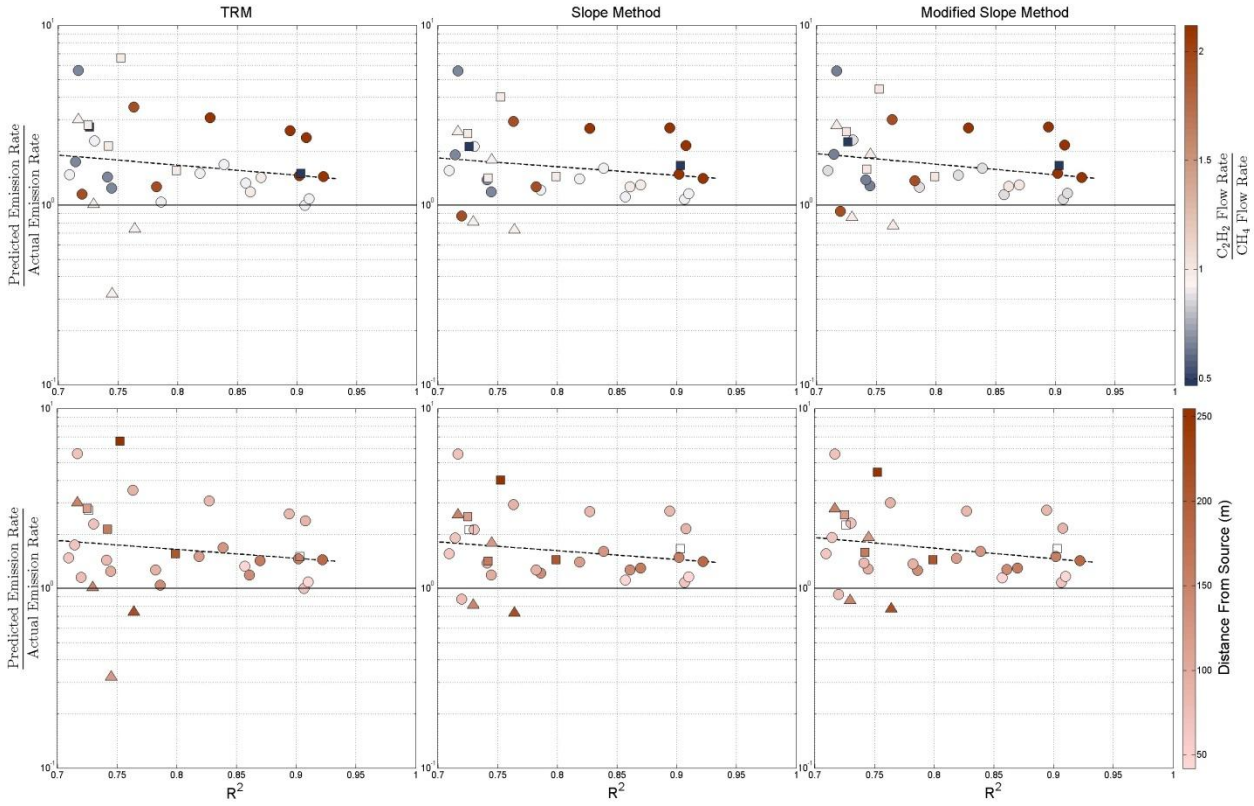

Figure 3.6 Separated plume transects, plotted in the same manner as **Figure 3.5**.

The effect of plume width is plotted in **Figure 3.7**. The majority of the widths for both co-located and separated sources are between 25 and 100 m. Some plumes were very narrow and were still able to meet all criteria for a good plume. It is hard to deduce if a larger plume width decreases the spread in error ratios or if it leads to more accurate predictions for either co-located or separated plumes.

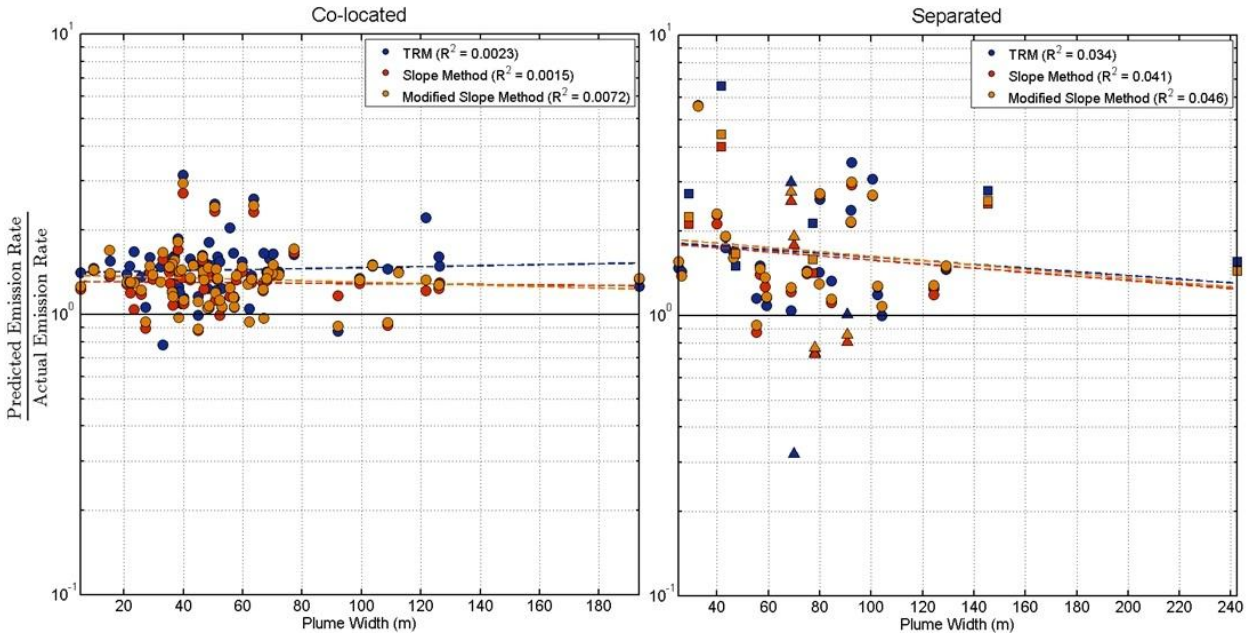

Figure 3.7 The ratio of the predicted to actual CH4 emission rate for each plume transect as a function of plume width for plume transects with co-located sources (left) and separated sources (right).

Meteorological variables are plotted in **Figure 3.8** with standard deviation in wind direction shown in the top row, mean wind speed in the middle row, and friction velocity in the bottom row. There is little dependence associated with standard deviation in wind direction, with the spread in errors remaining almost constant across what is a very wide range in wind deviations. The spread in errors when plotted against wind speed, however, decreases with decreasing wind speed notably for the separated cases. The spread in error ratios remains more or less the same throughout the range of wind speed values. Friction velocity shows little effect across its range of values as well.

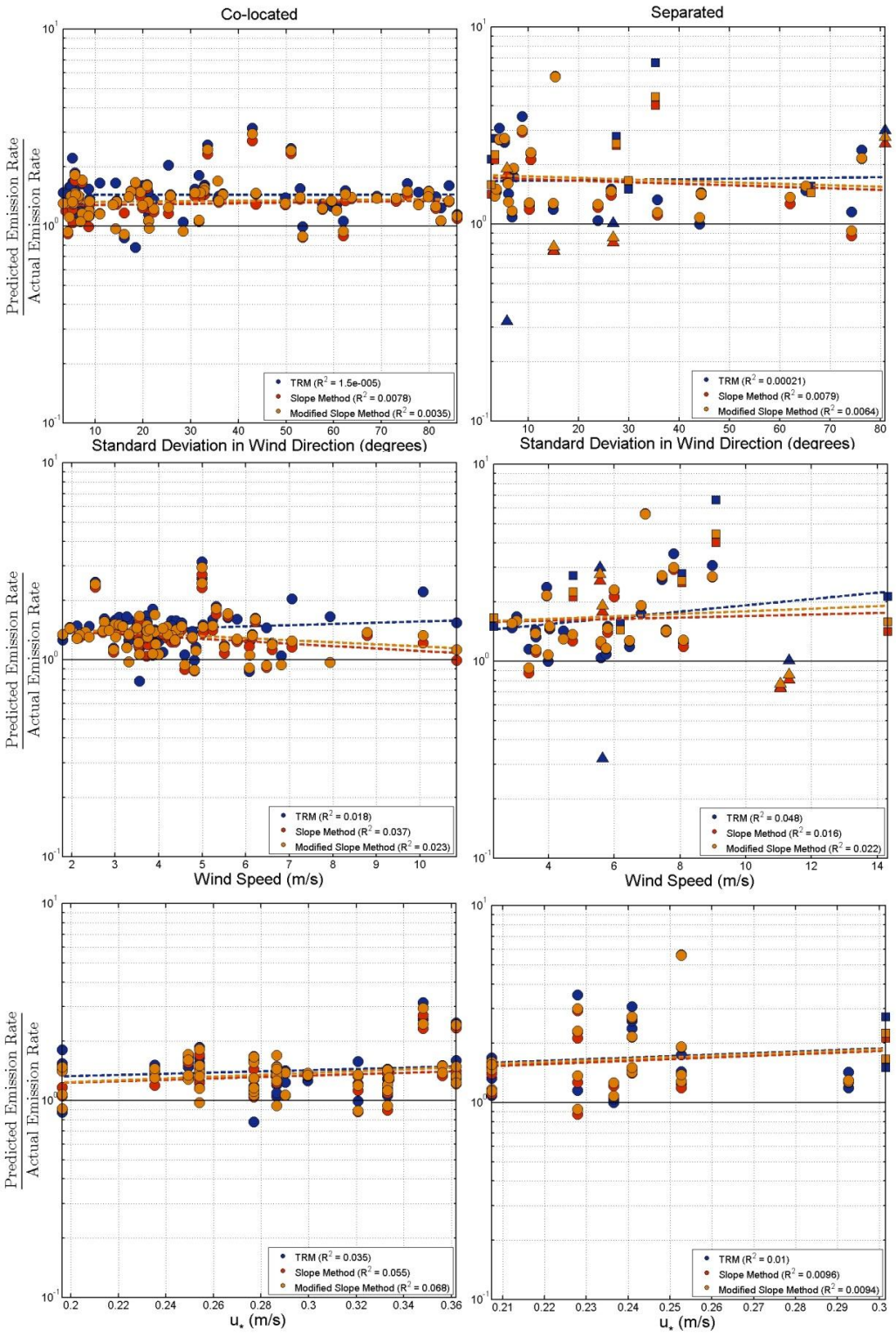

Figure 3.8 The ratio of the predicted to actual CH4 emission rate as a function of mean wind speed (top row), the standard deviation in wind direction (middle row), and friction velocity (bottom row). Plume transects with co-located sources are evaluated on the left while separated sources are evaluated on the right.

In the last figure we will evaluate the errors in predicting CH_4 emission rates against measures of the plume transect above background. In the top row of **Figure 3.9,** the mean $[C_2H_2]$ above background in a plume transect is plotted. There is a much larger spread in error ratios the closer C_2H_2 concentrations are to background. There are, however, far less points significantly above background to evaluate. This is true for the co-located and separated cases. In the separated cases, only transects where the sources were separated vertically (the circular points) show a large elevation above background. The middle plot is the same as the top, only for CH_4, and there appears to be less of a pattern compared to the C_2H_2 plot. The plume transects with separated sources contain large error ratios even at higher elevation above background, although we again see only vertically separated sources containing transects with CH_4 concentrations far above background. Lastly, the concentrations of CH_4 are evaluated with **Equation 2.2** in the bottom row. These two plots look very similar to their counterparts in the middle row. This indicates that in terms of a signal-to-noise ratio, the noise in our background measurements scales similarly to the plume signal of CH_4 for most transects.

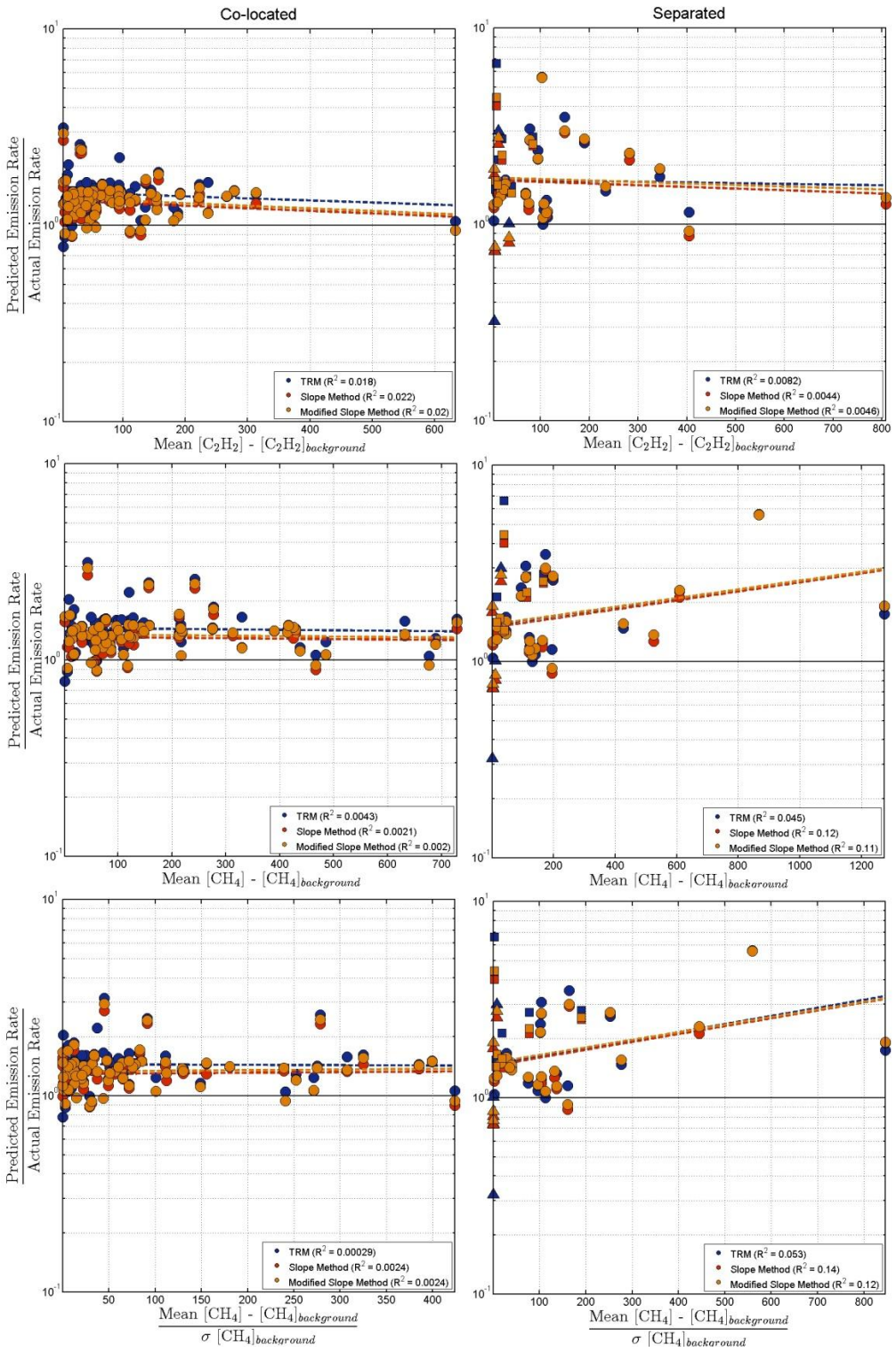

Figure 3.9 The ratio of the predicted to actual CH_4 emission rate as a function of the mean C_2H_2 concentration above background (top row), the mean CH_4 concentration above background (middle row), and the mean CH_4 concentration above background normalized by the standard deviation in CH_4 background concentrations (bottom row). Plume transects with co-located sources are evaluated on the left while separated sources are evaluated on the right.

As stated in the methods section, the rotameter used to maintain a set flow rate during the 2013 experiments was always calibrated (via volumetric flow meter) at least once for each gas during an experiment, and often multiple times if the emission rate of either gas was to be changed. Rotameters, however, are very sensitive to deviations in the ambient pressure and temperature from the pressure and temperature at which it was calibrated, as well as the density of the gas flowing through the rotameter, and thus the emission rate we presume to be releasing at may not be accurate.

Any changes in density of the gas that is flowing through the rotameter is not recorded and so we cannot comment on this potential cause for error. However, ambient air temperature and pressure is recorded at Christman Field, and here we will perform a simple sensitivity test for each 2013 experiment day using the following formula:

$$Q_{actual} = Q_{calibrated} \times \sqrt{\frac{p_{actual} T_{calibrated}}{p_{calibrated} T_{actual}}} \qquad \textbf{3.1}$$

The actual emission rate at a point during an experiment is calculated using the emission rate, temperature and pressure at calibration as well as temperature and pressure at that point in time. In this analysis, we will only concern ourselves with the extreme temperatures and pressures in each experiment to see if large deviations in emission rates could be major contributor to the large errors seen in the 2013 experiments. This will be done by taking the smallest and largest recorded temperature and pressure measurements during each experiment time and inputting them into **Equation 3.1** to determine the maximum possible difference between the actual to calibrated emission rate value that could occur during an experiment.

Table 3.2: Sensitivity of Rotameter on Temperature/Pressure Changes	
Date	Maximum % Deviation From Calibrated Emission Rate
26-Jun	1.41
11-Jul	0.85
20-Aug	2.03
23-Aug	2.06
30-Aug	4.73
05-Sep	1.6

The largest percent difference in this analysis occurs on 30 August and would account for a nearly 5% error. This factor doesn't seem to explain the sometimes 100% or greater bias in the predicted CH_4 emission rates in the 2013 cases.

3.2 2014 Christman Field Experiments

3.2.1 Mobile Analysis Results

Mobile transect analysis included three experiment days on the 8th, 23rd, and 25th of April. The marked difference between these experiments and the 2013 experiments is the difference in emission rate control, in which the research team's DeWalt stack set up for both tracer and emission gas was in use in 2014, which allowed for much more control over the release process. Due to less experiment days and many transects having R^2 values below 0.7, there are fewer points to analyze this year compared to the 2013 experiments. In **Table 3.4** the record of all parameters evaluated for the 2014 experiments is recorded in the same fashion as we did in **Table 3.1** for the 2013 experiments.

Table 3.3. Record of all controlled and uncontrolled variables for each 2014 Christman Field experimental day that included mobile transects. A green Y indicates that that parameter was evaluated on that given day, while a red N indicates it was not. The number of plumes (N) evaluated during each experimental day is also recorded as well as the mean biases in each method. A range in values in the parameter evaluated is given, where applicable.

Table 3.4: Parameters Evaluated in the 2014 Mobile Analysis Experiments

Date	08-Apr	23-Apr	25-Apr
N	8	4	15
CH_4 emission rate	N	N	Y
C_2H_2 emission rate	N	N	Y
Source height (m)	N	N	N
Separation	N	N	N
Point Source	Y	N	Y
Line Source	Y	Y	N
Downwind distance (m)	Y (69-118)	N	Y (37-103)
Meas. Above background	Y	Y	Y
Basic met	Y	Y	Y
Micro met	N	N	N
Mean TRM bias (%)	5.3	48.6	33.9
Mean slope method bias (%)	11.0	32.1	18.2
Mean modified slope method bias (%)	8.4	29.3	24.1
Modified N	5	3	14

For the 2014 mobile transects there are fewer parameters that were evaluated compared to the 2013 experiments. This was due partially to the knowledge that the 2013 analysis contained large errors and a consistent positive bias, and so for 2014 the experiment team decided to use a more elementary approach that consisted of no separation or height differences between the sources and equal emission rates between each gas. In essence, these experiments were largely meant to see if the recorded emission rate errors were more constrained under the new release system than for our 2013 measurements. Although there are fewer samples to analyze, what is seen are mean biases that are in general smaller than for the 2013 experiments. The exception is 23 April, which has mean biases closer to those seen in 2013, however only 4 good samples are taken from this experiment day.

In **Figure 3.10** the range in errors of the ratio of predicted to actual CH_4 emission rates for each method are plotted. There is again an almost universal positive bias; however, in general these error ratios are closer to one and there are many fewer large outlying errors than in the 2013 experiments. Of the three methods, the standard TRM appears to have the largest range in predictions, while the slope method and modified slope method perform very similarly (R^2 = 0.98, $p \approx 0$). The correlation between the TRM and the slope method leads to an R^2 value of 0.49 ($p \approx 0$).

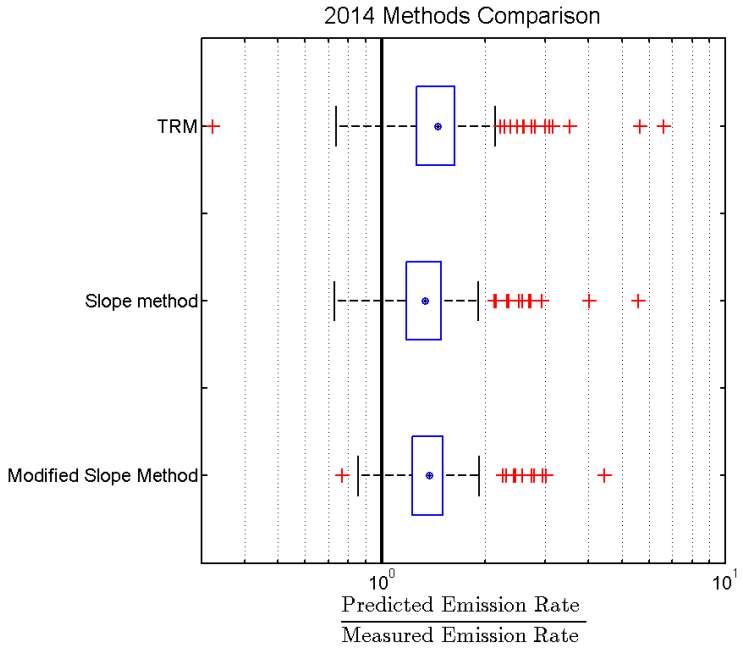

Figure 3.10 Box and whisker plots of the range in predicted to measured CH_4 emission rates for all three methods during the 2014 mobile experiments. The point within the box represents the median error ratio while the edges of the box represent the 25th and 75th percentiles of the error ratios. The whiskers extending to the edge of the ratios show how large/small the majority of the error ratios expand. Large outlying ratios are plotted indivually and marked by the red plus signs.

The difference in performance in the TRM compared to the slope methods is further shown in probability plots of lognormal distribution in **Figure 3.11**. The TRM error ratio is distributed quite differently than the error ratios for the slope methods, whose distributions are very similar. For the 2014 experiments, there are fewer large outlying predictions like in the 2013 cases,

which shows that in general the method results are more constrained than in 2013, which may be due to the more controlled gas release setup in 2014 vs. 2013 as well as only co-located source configurations. It looks like there may be a long tail on the under-predicted side although there are really only two large under-predictions to support this, and regardless for the majority of the distribution in error ratios both the slope method and the modified slope method behave almost exactly like a lognormal distribution. The distribution in TRM error ratios does not seem to follow a lognormal distribution as much as the slope methods.

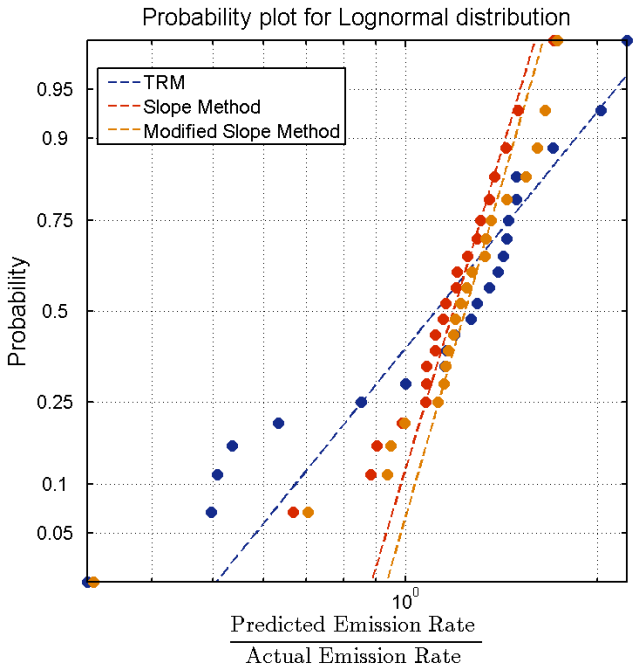

Figure 3.11 Probability plot that tests for lognormal distributions for each of the three methods evaluated in this section. The scatter of points for each method represent the predicted to the actual, measured CH_4 emission rate for a plume transect. If a method's ratios followed a perfect lognormal distribution, all points would fall on that method's respective reference line.

The absolute value in the % bias for each method is plotted as a function of the correlation between the instantaneous concentrations of CH_4 and C_2H_2 in **Figure 3.12**. The spread in errors does not decrease with increasing R^2 values, and no transect contained an R^2 value greater than 0.9, meaning many there were many transects with a greater correlation in 2013 compared to

2014. The correlation between the two gas concentrations for this analysis is not then a good indicator of method performance.

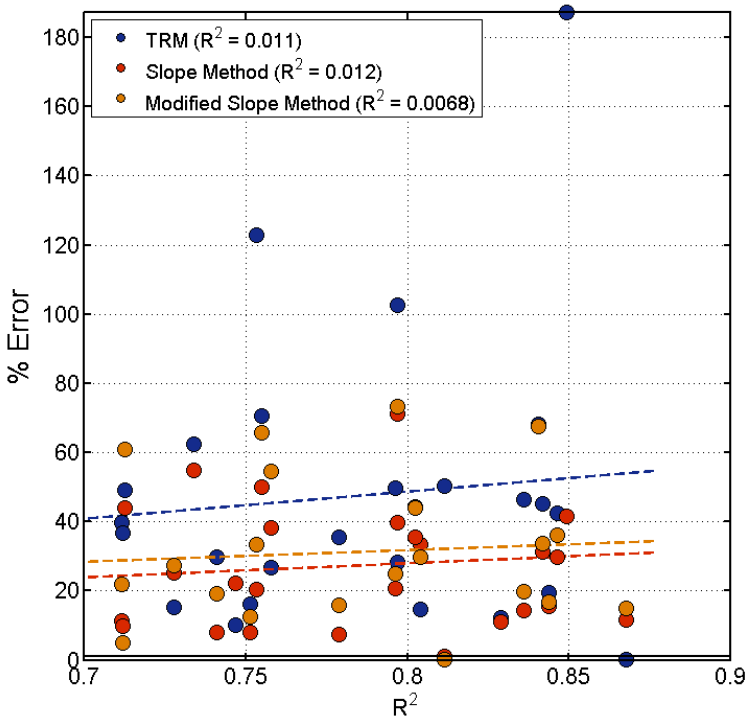

Figure 3.12 The percent error (i.e. the absolute value of the percent bias) as a function of the R^2 value between CH_4 and C_2H_2 instantaneous concentrations in a plume transect.

Below in **Figure 3.13** the effect controlled variables on the bias ratios are examined as a function of the correlation between the instantaneous gas concentrations. In the top row, the distance downwind the plume analyzer traversed the plume is plotted for all methods. This does not appear to have an effect on the performance of any method. The same can be said of the source geometry, shown in the bottom row. Both point and line sources seem to affect the outcome of each method similarly. The two large under-predicted traverses for the two slope methods were from point sources, and in the TRM the outlying values came from point and line sources equally.

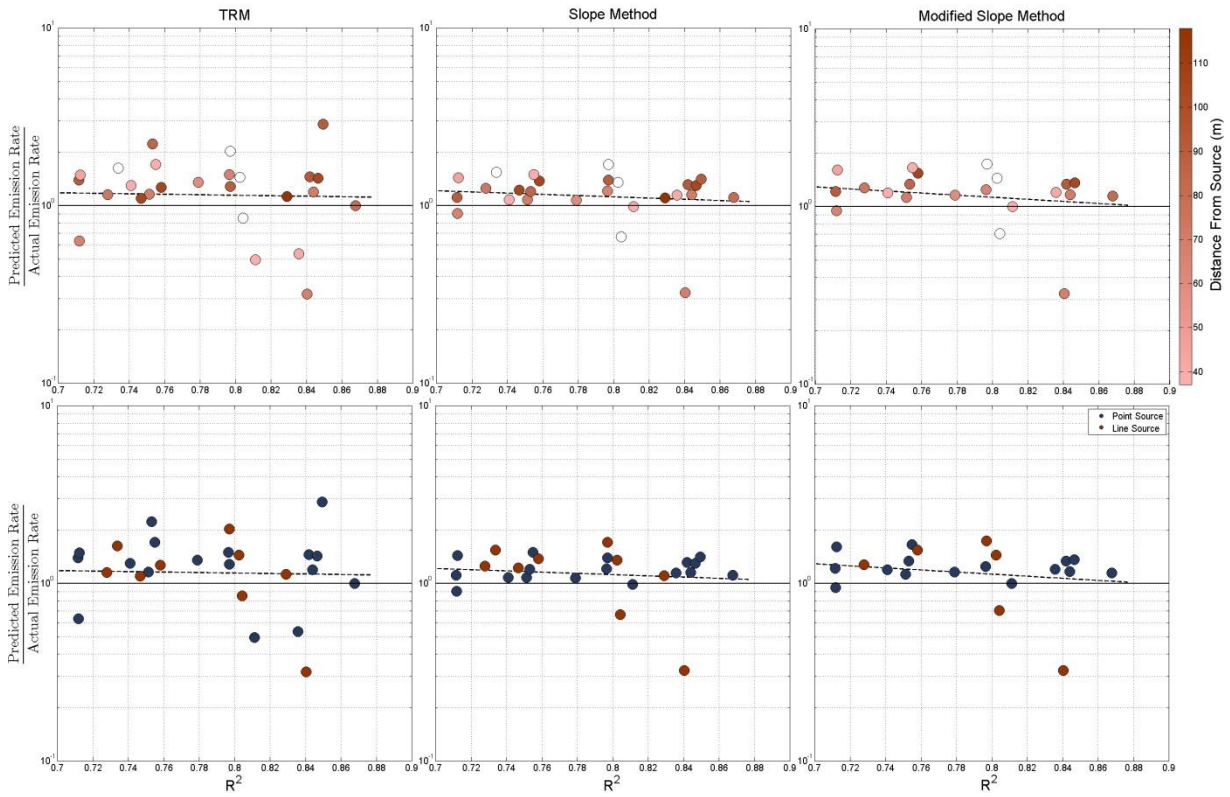

Figure 3.13 The effect of parameters that can be controlled by the experiment team are examined for the TRM (left column), slope method (middle column), and the modified slope method (right column) as a function of R^2 between CH_4 and C_2H_2 instantaneous concentrations. The distance from the source the plume analyzer traversed the plume is shown in the top row, and the source geometry (point or line source) is shown in the bottom row.

The width of the plume traversed and its effect on the outcome of the methods is shown below in **Figure 3.14**, and it appears that there exists a larger range in error ratios in smaller plumes than in large ones. This finding is consistent with the 2013 results, shown in **Figure 3.7**; however, the same caution must be exercised because there are fewer points with large plume widths than for smaller ones. The two largest recorded plume widths have very similar error ratios between all three methods and between each other. This ratio is about 1.7, or a 70% over-prediction in all methods. This is much larger than the average biases shown in **Table 3.4**.

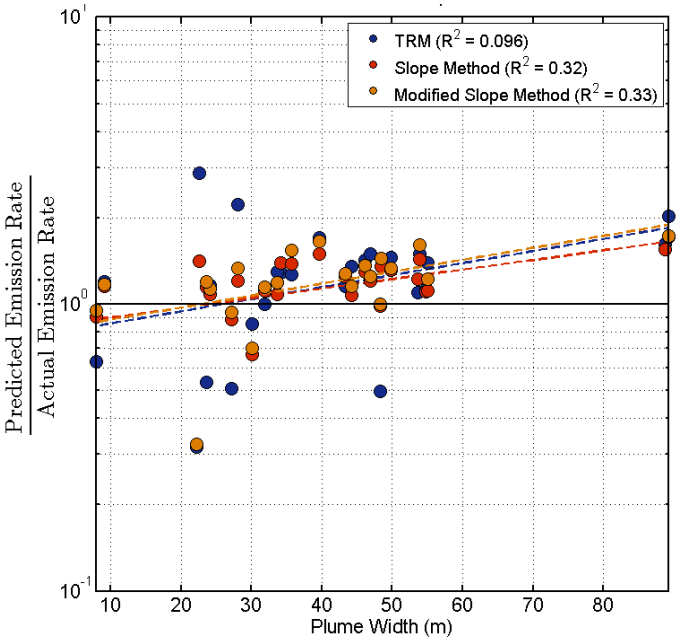

Figure 3.14 The ratio in predicted to actual emission rates of CH_4 as a function of plume width for all methods evaluated.

Meteorological variables are now analyzed in **Figure 3.15**. Again, as in the 2013 analysis, the standard deviation in wind direction across a plume traverse does not have a very noticeable effect on the performance of any of the methods analyzed, although the largest spread in errors for the TRM does appear to exist for the smallest standard deviations. Mean wind speed does not show a very discernible pattern, especially for the TRM. For the slope methods it could be argued that with increasing wind speed there is an upward trend in the bias in the predictions in CH_4 emission rates, leading to larger over-predictions with faster wind speeds, reflected in the slightly positive R^2 values given in the legend.

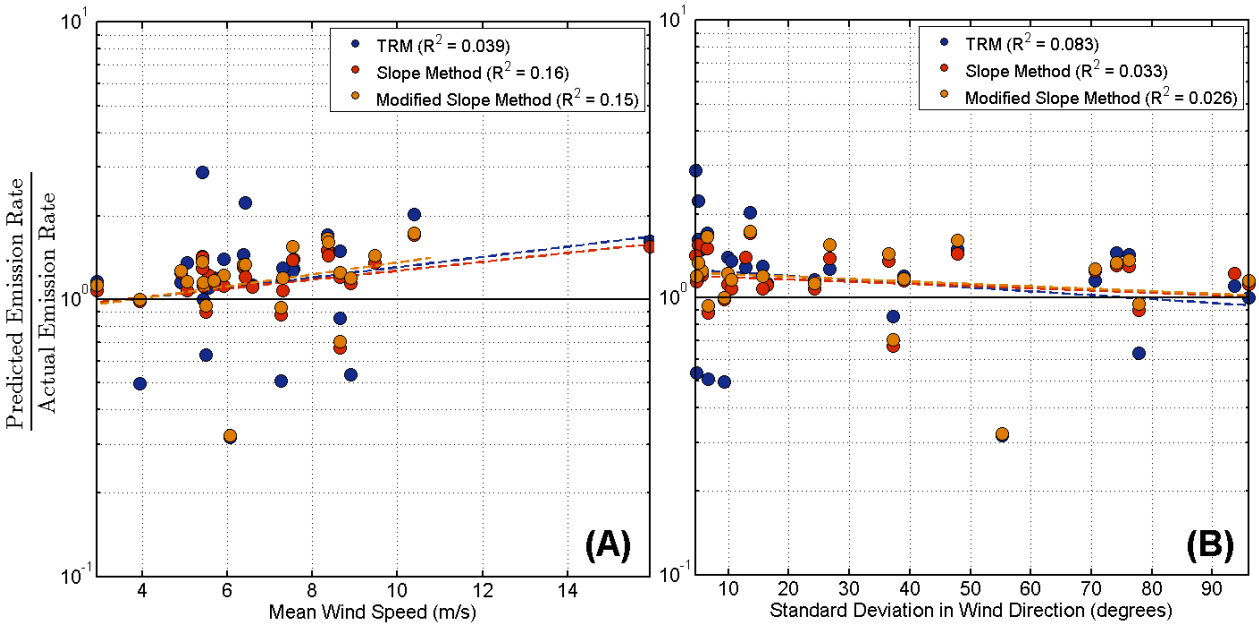

Figure 3.15 The relationship between mean wind speed **(A)** and standard deviation in the wind direction **(B)** across a plume traverse and the ratio of the predicted to actual CH_4 emission rate.

Measures of the gas plumes above background are given in **Figure 3.16**. As in **Figure 3.9** for the 2013 experiments, **(A)** and **(B)** show mean $[CH_4]$ and $[C_2H_2]$ above background, while in **(C)** the concentrations of CH_4 are evaluated with **Equation 2.2**. As in the 2013 experiments for C_2H_2, the largest spread in error ratios lies where the plume is not significantly elevated above background. All three plots show a very similar trend, with slope method and modified slope method error ratios approaching 1 with increasing signal. The standard TRM seems to approach error ratio values near 0.5, curiously. However, as we have seen before, there are fewer points at these higher measurements above background than near background, so it is difficult to confirm a clear pattern in this data.

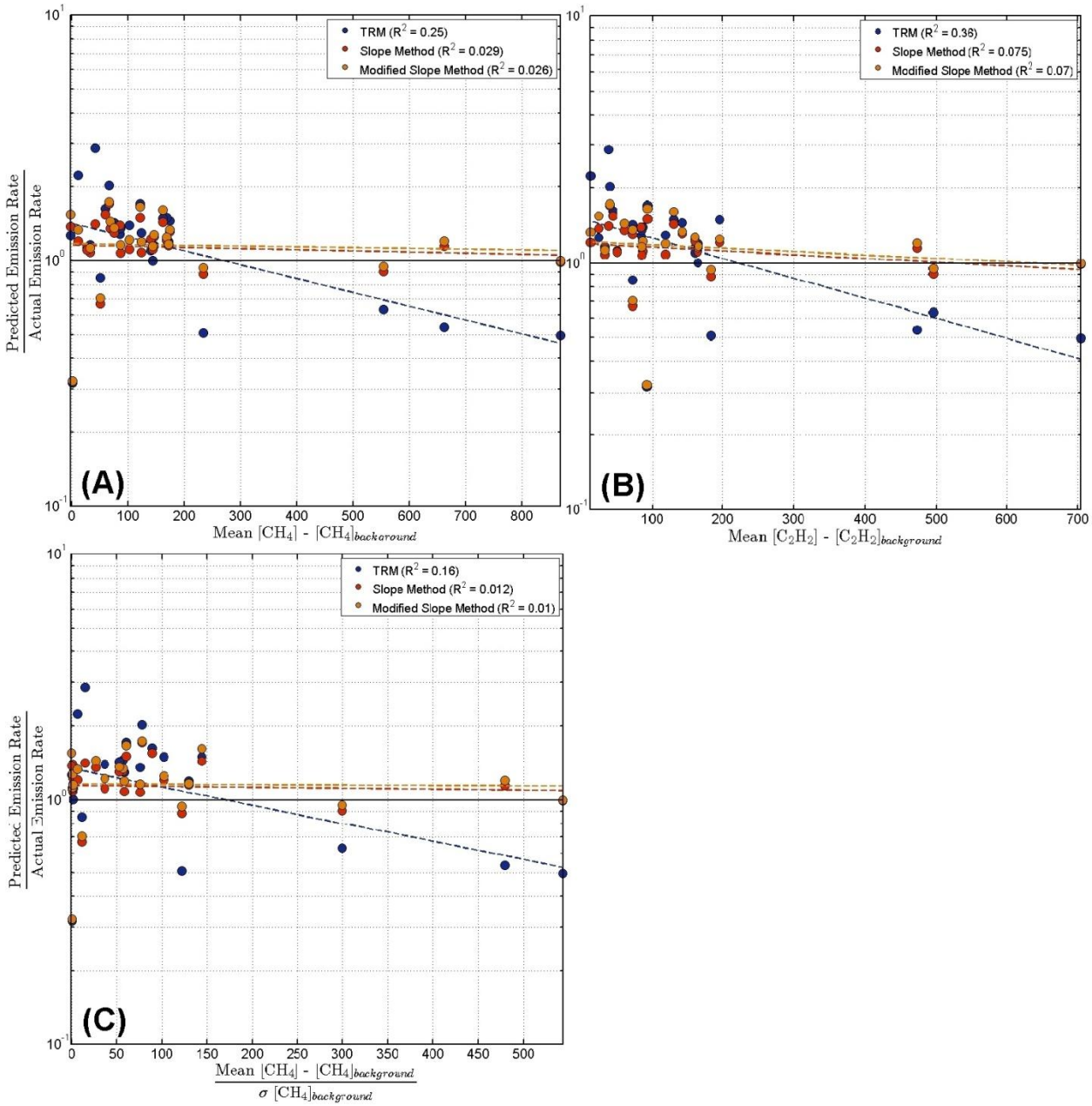

Figure 3.16 Bias in all methods as a function of the mean $[CH_4]$ above background within a sample period **(A)**, the same formula for C_2H_2 **(B)**, or the standard deviation of measurements used to establish the background value of CH_4 .

3.2.2 Stationary Analysis Results

Three experiment days in 2014 contain stationary measurements: 14 March, 23 April, and 19 September. As can be seen in **Table 3.6**, many parameters are evaluated during all three

experiments, despite there being relatively few samples to analyze compared to the mobile transect analysis. As in the 2014 mobile transects analysis, the full gas release system set up has evolved over the course of our stationary experiments. Our 14 March experiment saw CH_4 released from the newly-built DeWalt stack, explained in the methods section. For the 23 April and 19 September experiments, a C_2H_2 DeWalt stack was also used. For all three experiments, CH_4 was released from a single canister. This is also the case for C_2H_2 for our first two experiments, while the 19 September field experiment has C_2H_2-released through three canisters connected to a single regulator, as shown in **Figure 2.7**. Micrometeorological data was obtained from the release team's own met station on 14 March and 19 September, while on the 23 April experiment this data were given to us by a team from the University of Wyoming that was on-site at Christman Field as well. All meteorological data used in these evaluations was recorded from 2 m above the surface to allow for a true side-by-side comparison of variables pertaining to meteorology.

Table 3.5. Record of all controlled and uncontrolled variables for each 2014 Christman Field stationary experimental day. A green Y indicates that that parameter was evaluated on that given day, and a range of values, where applicable, is given. The number of plumes (N) evaluated during each experimental day is also recorded as well as the mean biases in each method.

Table 3.6: Parameters Evaluated During 2014 Stationary Experiments

Date	14-Mar	23-Apr	19-Sep
N	6	6	9
CH_4 emission rate (g/s)	Y (0.1-0.5)	Y (0.05-0.1)	Y (0.03-0.1)
C_2H_2 emission rate (g/s)	Y(~0.2)	Y(0.09-0.2)	Y(0.04-0.2)
Source height	Y	N	N
Separation	Y	Y	N
Point Source Release	N	Y	N
Line Source Release	Y	Y	Y
Downwind distance	Y(40-74)	Y(33-109)	Y(63-180)
Meas. Above background	Y	Y	Y
Basic met	Y	Y	Y
Micro met	Y	Y	Y

Results obtained from the tracer methods and PSG methods will be evaluated together here, as we will see that these two techniques share many similarities as well as differences. In **Figure 3.17** there is a comparison of all techniques that are used to predict emission rates from a stationary sample period, with the error analysis being the ratio of the predicted CH_4 or C_2H_2 emission rate to its actual, measured emission rate. These values are plotted on a logarithmic scale, with a perfect prediction being shown by the horizontal line at 1.

The top plot of the figure contains the results from the PSG program, which can individually predict CH_4 and C_2H_2 emission rates without the input of the other gas. The mean bias ratios of each of the three methods are 1.34 (CH_4 prediction with standard background correction), 1.76 (CH_4 prediction with interpolated background correction), and 0.81 (C_2H_2 prediction). The positive bias in CH_4 predictions is driven by a few very large over-predictions primarily on 23

April. There is a very large spread in results for the PSG method for both gas estimates, but unlike the results obtained for our mobile TRM measurements (and for stationary TRM analysis as well, as can also be seen in **Figure 3.17**) there is no persistent positive or negative bias among emission rate predictions. However, the prediction of C_2H_2 emission rates is smaller than the predicted emission rate of CH_4 in all cases except two (the first two sample times for 23 April). The interpolated technique had larger predicted CH_4 emission rates compared to the standard technique in all cases except two as well (note: not the same two cases as in the comparison of CH_2 and CH_4 predictions). These relationships are intriguing to the analysis of the tracer techniques in the mobile analysis section, as this pattern between CH_4 and C_2H_2 emission rate estimations indicates that the persistent positive bias in these methods may be due to an incorrect measured emission rate or downwind concentration value of one of the gases. There might be a small positive correlation between the two methods, as the R^2 value between both estimate techniques is 0.14 (p = 0.098). The correlation between CH_4 emission rates predicted with the program's built-in background calculation and through a linearly interpolated technique does show to be positively correlated (R^2 = 0.74, $p \approx 0$). There is no indication that the more sophisticated background interpolation method leads to better predictions, only that it leads to a consistently higher emission rate prediction.

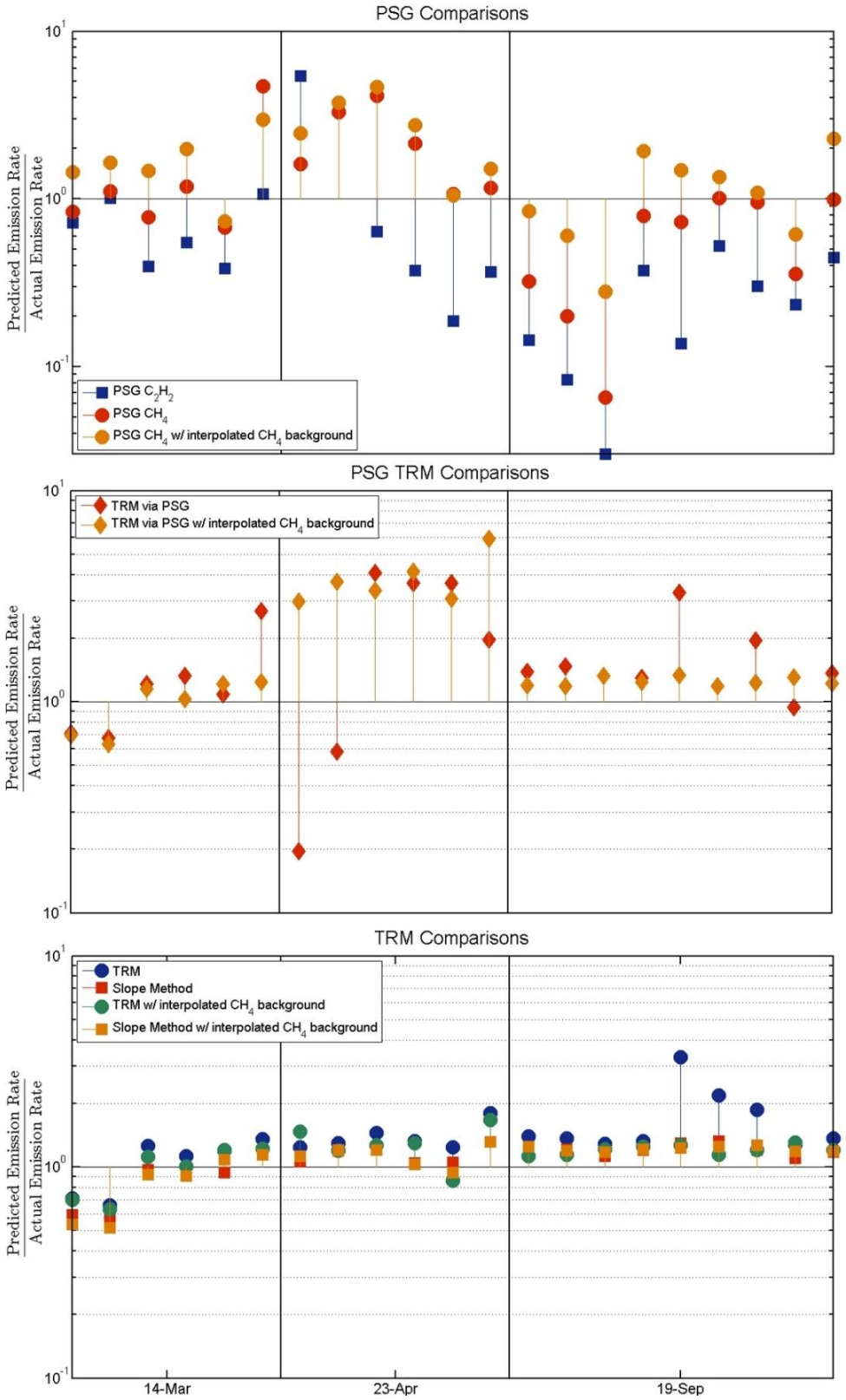

Figure 3.17 A comparison of all techniques used for predicted gaseous emission rates from a stationary analysis. PSG methods (above), the TRM via the PSG (middle), and the standard TRM and slope method (below) are shown.

The middle plot in **Figure 3.17** shows the results of techniques used to predict the emission rate of CH_4 through the ratio of integrated plume concentrations of CH_4 to C_2H_2 determined through the PSG program. These are the PSG TRM methods. There's nearly a consistent positive bias for both methods shown here (mean bias ratios of 1.72 and 1.92 for the PSG TRM with standard and interpolated CH_4 background corrections, respectively), and they are slightly positively correlated with each other (R^2 = 0.38, p = 0.0028). The standard PSG program accounts for mean wind speed as well, so there is not a perfect correlation between the standard PSG vs. PSG TRM, with an R^2 value of 0.31 between these two methods using the standard background-correcting technique (p = 0.0090) and 0.32 when using an interpolated background correction (p = 0.0074). This overall positive bias is strikingly similar to that of the overall positive biases seen in the standard TRM methods on the bottom plot, however. The built-in background correction technique yields an R^2 value of 0.86 (p = 0.006) and 0.66 (p = 0.008) between the PSG-TRM and TRM for 14 March and 19 September, respectively. These correlations rise even further for the interpolated background technique, with R^2 = 0.99 and $p \approx 0$ for both days. 23 April does not see this high a correlation between the two tracer techniques, with R^2 = 0.024 (p = 0.77) and 0.48 (p = 0.13) for the standard background correction and the interpolated approach, respectively. For this day there appears to be something unique to the PSG program sensitivity that is driving these larger biases, which is perhaps caused by a bias introduced by the use of data from a different met station, but it is unclear why this would lead to different results for these methods only.

The bottom plot shows the results from the standard tracer techniques for both types of background correction. What we see are values that are very similar for the TRM and slope method as well as both background calculation techniques. All mean bias ratios are between ~1.1

and 1. The correlation between the TRM and slope method is 0.96 ($p \approx 0$) for the standard background calculation and 0.99 ($p \approx 0$) for the interpolated CH_4 background calculation. For the cases during 19 September where the standard TRM performs poorly the interpolated background technique corrects the large bias. We also note that there is an overall positive bias in the tracer techniques that is similar to the mobile transects experiments.

Table 3.7 contains the accuracy (the mean and median biases) and the precision (the interquartile range and standard deviation of the predicted to measured emission rates) for each method evaluated. This again shows how consistent the (non PSG) tracer techniques are compared to the PSG techniques, and that the PSG C_2H_2 program is the only program this is negatively biased.

Table 3.7. Accuracy and Precision of Emission Rate Estimation Methods

	Median Bias (%)	Mean Bias (%)	25th Percentile (%)	75th Percentile (%)	Standard Deviation in Bias(%)
TRM	**32.96**	**43.13**	**24.1**	**40.2**	**54.4**
TRM w/ Interpolated Background	**20.66**	**16.74**	**12.8**	**26.9**	**22.9**
Slope Method	**17.64**	**9.27**	**4.5**	**20.7**	**20.5**
Slope Method w/ Interpolated Background	**18.35**	**9.05**	**2.69**	**21.4**	**21.9**
TRM via PSG	**32.92**	**71.62**	**8.5**	**97.3**	**111**
TRM vias PSG w/ Interpolated Background	**24.07**	**92.14**	**18.5**	**198**	**138**
PSG CH_4	**-0.92**	**33.77**	**-21.9**	**18.6**	**123**
PSG CH_4 w/ Interpolated Background	**47.80**	**76.42**	**4.51**	**128**	**108**
PSG C_2H_2	**-60.48**	**-19.34**	**-76.5**	**-36.3**	**128**

We will now more robustly determine if these methods for emission predictions are similar in their results. The most common way of determining this is to compare the means of two methods through a T-test. However, for the stationary analysis caution must be exercised, because the assumption of a normal distribution of values may not be accurate. For this reason, we will use the non-parametric two-way K-S test, which compares the means and distributions of two methods without any assumptions about their distribution shapes. Continuous distribution functions for our tracer and PSG techniques are plotted in **Figure 3.18**.

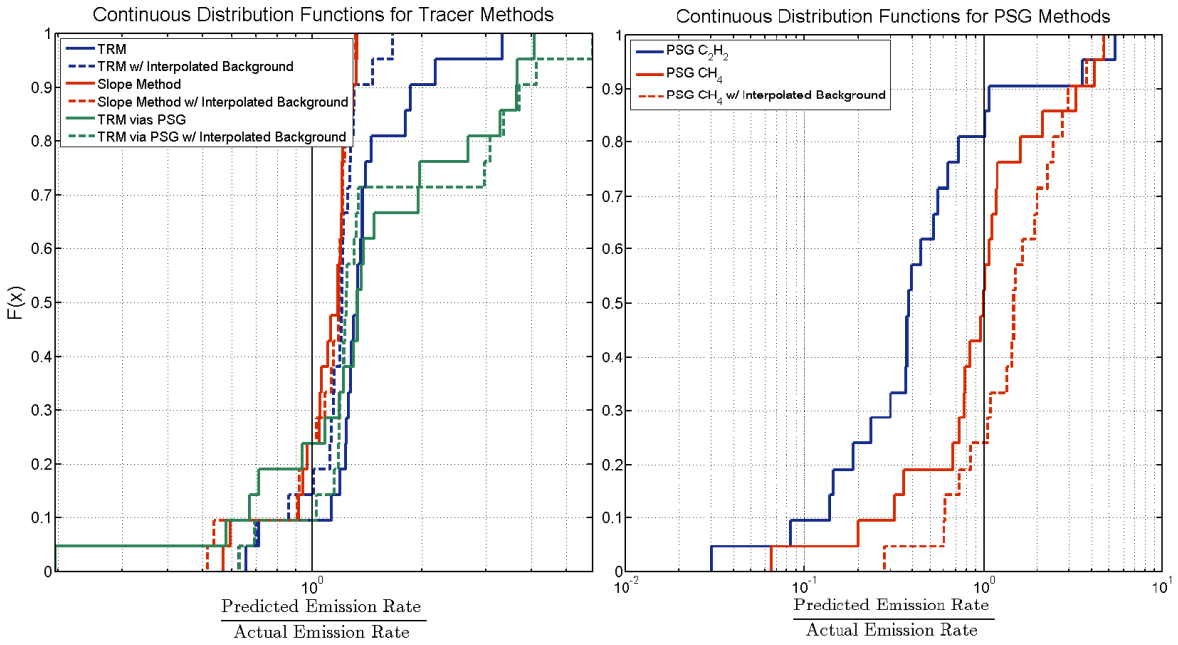

Figure 3.18 Continuous distribution functions for the ratio of the predicted to the actual CH_4 emission rate for the tracer methods (left) and PSG methods (right).

The TRM and slope methods appear to have similar distributions, more so to each other than to the TRM via the PSG method. All techniques that utilize a standard background correction as well as an interpolated correction appear to show similarity as well. **Table 3.8** indicates that many of our methods have the same distribution of predicted CH_4 emission rates. What we do find with certainty (p = 0.01) is that the TRM and slope method predictions that are obtained through the standard background correction do not have a similar distribution, which seems to be

counter-intuitive based off of **Figure 3.18**, but large biases in the TRM during the 19 September cases do not allow for the null hypothesis that the two distributions are the same to be valid. Most of the other method comparisons do not reject this null hypothesis; however, large *p* values for many of the cases indicate that this cannot be asserted with certainty. Another observation is that the predicted emission rates of CH_4 from the TRM and the PSG method have a different distribution for both background correction techniques, each with very low *p* values. In all, it is difficult to say with certainty whether many of these methods actually are statistically different in their performance, so we will continue to evaluate both the tracer and PSG methods side-by-side together below.

Table 3.8 R^2 and Kolmogorov-Smirnov Test of distribution similarity of the results between two separate methods emission rate predictions using the standard background correction and between two separate methods using the interpolated background correction. A K-S value of 0 indicates that the null hypothesis that the two methods have the same distribution cannot be rejected. *p* values for each test are also given.

Standard Background Comparison					**Interpolated Background Comparison**				
	R^2	***p***	**K-S**	***p***		**R^2**	***p***	**K-S**	***p***
TRM | Slope Method	0.96	≈ 0	1	≈ 0	**TRM | Slope Method**	0.99	≈ 0	0	0.53
TRM | TRM via PSG	0.62	≈ 0	0	0.531	**TRM | TRM via PSG**	0.59	≈ 0	0	0.304
TRM | PSG CH4	0.25	0.02	1	≈ 0	**TRM | PSG CH4**	0.38	0.003	1	0.001
PSG CH_4 | PSG C_2H_2	0.14	0.098	0	0.155					

In **Figure 3.19** the errors in the different prediction methods are compared to the R^2 value for a correlation between $[CH_4]$ and $[C_2H_2]$ during the entirety of a stationary analysis. There is little variation across R^2 values, although it appears that there is a decrease in the spread in errors for the standard TRM as R^2 values increase, which is corrected using an interpolated background scheme. Slope method values cluster more around a roughly +20% bias for both background

corrections. There does not seem to be a pattern between R^2 and percent error for the TRM via PSG method.

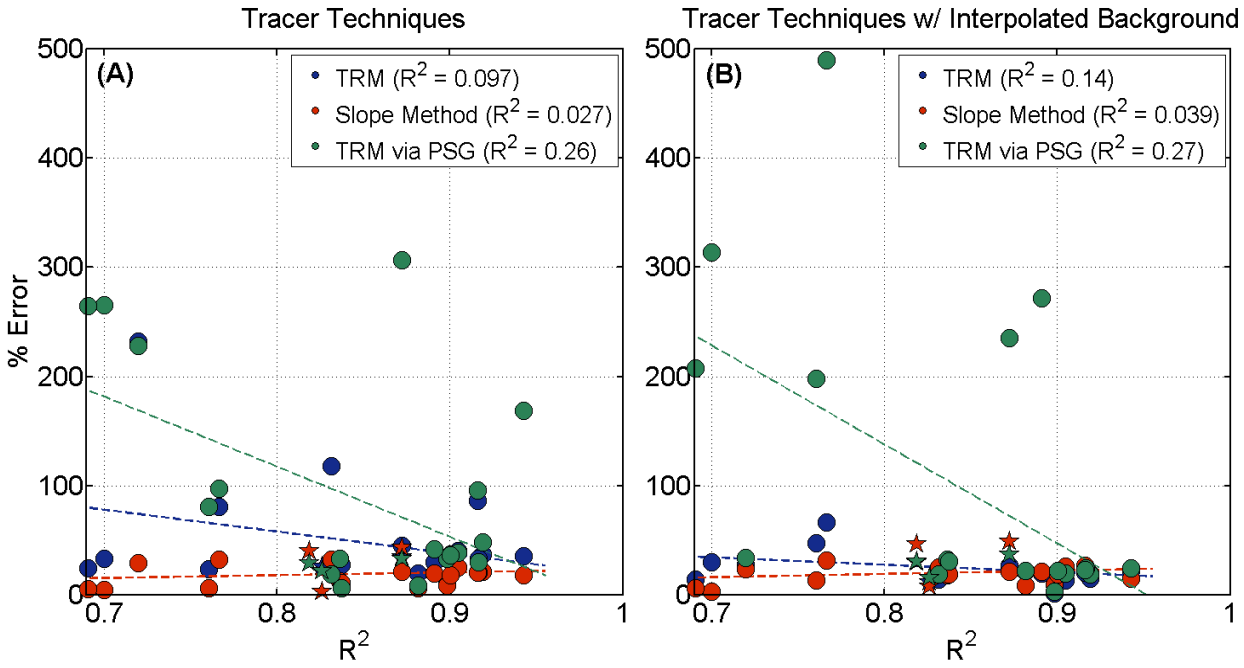

Figure 3.19 A comparison of the absolute value of the percent bias (the percent error) for tracer techniques and the R^2 value between [CH_4] and [C_2H_2] for each stationary sample measurement using the standard background correction technique **(A)** and from using an interpolated CH_4 background **(B)**.

We will now compare the error in CH_4 emission rate predictions to controlled variables. The majority of measurements were done with co-located line source releases located 3 m above the ground. The first three measurements during the 14 March experiment saw C_2H_2 released 1 m upwind of CH_4. Two of these three measurements correspond to the only sample times throughout the 2014 stationary analysis experiments to have an emission rate estimate via the standard TRM that is lower than the measured emission rate. It also appears that these three measurements hold some of the most constrained results for the PSG techniques, however with only three data points we cannot make any conclusive comments. In the following plots, these first three sample periods from 14 March will be indicated with as star for all tracer techniques to distinguish them from the rest of the sample periods that contained co-located sources.

The first four measurements from 23 April are the only measurements to use a point source of gas release instead of a line source release across 3 m manifolds. Standard (non-PSG) tracer method emission rates are similar to the other sampling times. It should be noted here again that the PSG program assumes a point source, and so these measurements are the only sampling experiment times where this assumption is valid. However, the spread in biases in the PSG program techniques is not noticeably different during these experiments than for the others. An observation of note is that the sample periods in which the C_2H_2 emission rate were over-predicted with respect to the CH_4 emission rate using the standard PSG program occur during this time. This gives us large negative biases in the TRM via PSG program during these sampling times.

The effect of the distance downwind that gas concentrations are collected is evaluated. Our stationary experiments contained downwind concentration measurements at distances between roughly 40 and 200 m away from the sources of gas emissions. In **Figure 3.20 (A)** and **(B)** the effect that downwind sampling distance has on the tracer techniques is evaluated for both background correction techniques. There is no real pattern discern from these plots, although there could be less of a spread in error ratios in the tracer methods (the TRM via PSG most notably) at further downwind sampling distances when an interpolated background correction scheme is used instead of the standard background correction. There are only a couple of points at these distances to demonstrate this, so we cannot say for certain this is an actual pattern. This range in distances may be too narrow to illustrate what its true effect may be on the tracer methods (as also stated in the mobile transect analysis sections). The same may also be true for the PSG results, given in **(C)**, in which the methods do not seem to have a dependence on sampling distance.

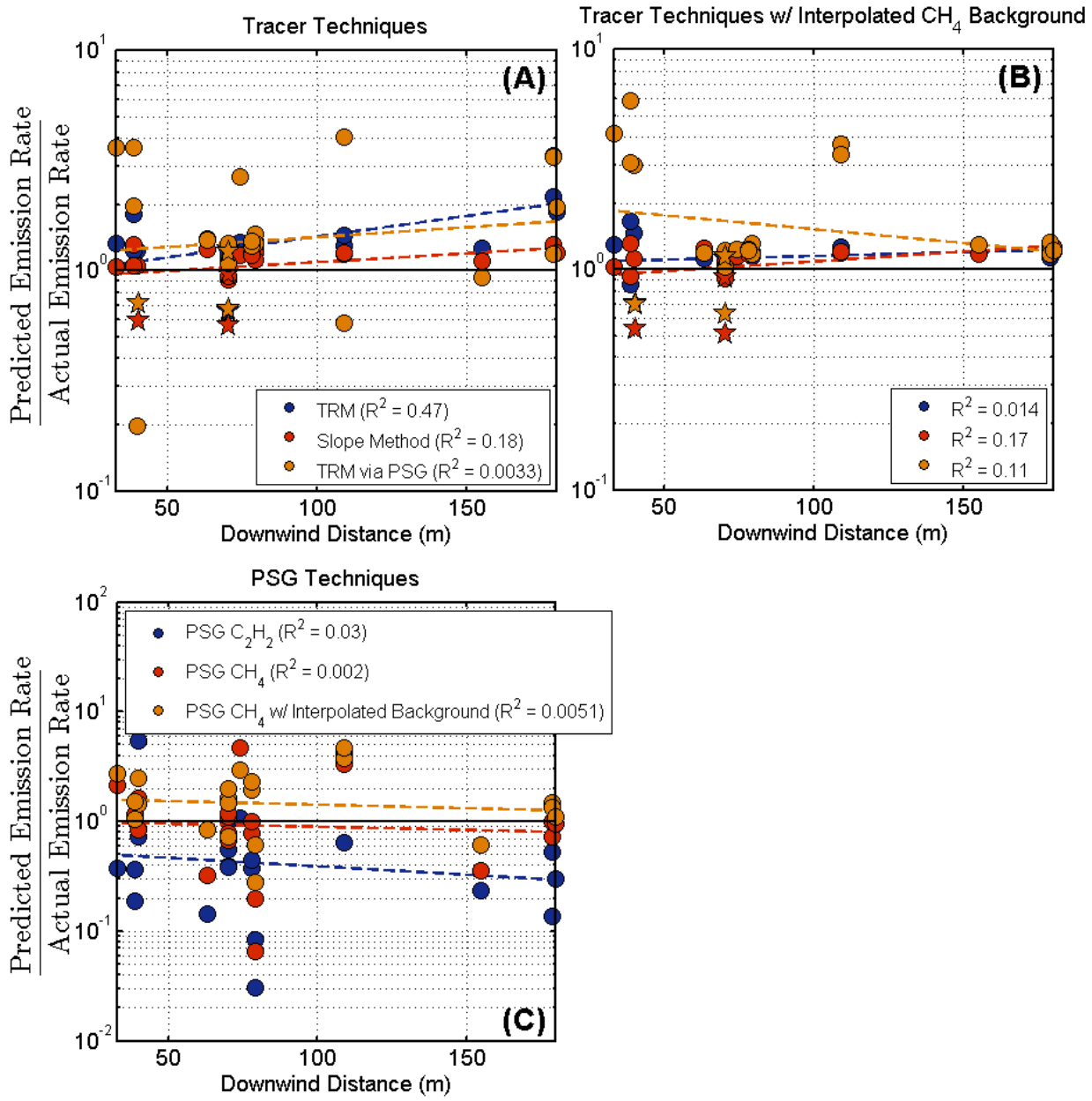

Figure 3.20 A comparison of the bias in tracer methods with the standard background correction **(A)**, an interpolated CH_4 background correction **(B)**, and PSG methods **(C)** to downwind sampling distance for each stationary sample period

Unlike the tracer methods, the PSG methods are dependent on the knowledge of a precise record of distance from the emission source and stability of the boundary layer, as the calculation of both the σ_y and σ_z values are dependent on these two variables. To evaluate the implications of using an incorrect distance or stability class value, a sensitivity analysis is given in **Figure 3.21**.

Here, the percent change in the CH_4 emission rate predicted via the PSG program with standard background correction is plotted against deviations both downwind sampling distance and stability class from a sample period with a recorded distance of 33 m and stability class of 3. The PSG program is sensitive to both these variables, with the largest changes in predicted emission rates occurring when both variables deviate from their true values. Larger predictions of CH_4 occur when either a further downwind distance is recorded or the atmosphere is predicted to be more unstable, while smaller predictions occur for the opposite cases. For unstable cases (low stability class values), there seems to be the greatest change in predicted emission rates. This sensitivity appears to be very important for PSG calculations, as even small deviations in the recorded values (e.g. a roughly 5 m change in distance recording) can lead to around a ±25% prediction of emission rates.

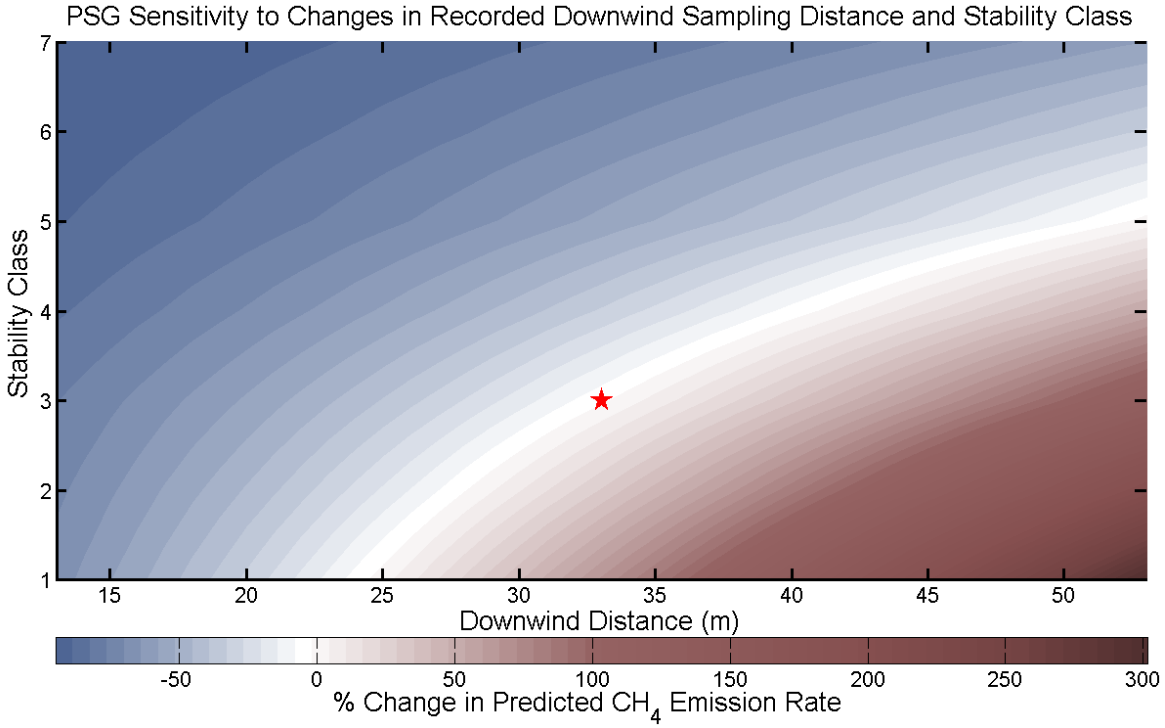

Figure 3.21 Sensitivity of the PSG program to changes in the recorded downwind distance from the source and stability class. The star in the plot represents the recorded downwind sampling distance and stability class (33 m and a stability class of 3) for the sample analyzed, and the plot is color-mapped by the % change in the predicted CH_4 emission rate via the standard PSG approach when these two values are altered within the program.

In **Figure 3.22** we evaluate the bias in the predictions through the tracer and PSG methods as a function of both the CH_4 and C_2H_2 measured emission rates. For all sample times that contain an emission rate value for CH_4 and C_2H_2 below of 0.15 g/s the emission rates of both gases are equal. Emission rates larger than this value correspond to experiments in which the CH_4 emission rate was higher than the emission rate for C_2H_2. Plots **(A)** and **(B)** compare TRM estimates. The emission rate of CH_4 shows a large spread in biases for low recorded emission rate values. However, the two sets of measurements in which the CH_4 emission rate was above 0.3 g/s contain very well-predicted emission rate values. This pattern is even more noticeable for the PSG methods, which are plotted in **Figure 3.22 (C)** and **(D)**. Keeping in mind that there are fewer points at large emission rate values, there is a much larger spread in biases towards the lower end of CH_4 emission rates than for higher rates, where all the methods performed very well. There is no distinctive pattern for C_2H_2 emission rates for either the PSG or tracer methods.

The highest range of CH_4 emission rates that correspond to the least amount of spread in biases come from sample periods in which the CH_4 emission rate is greater than that for C_2H_2, so it is difficult to say whether the increase in either gas's measured emission rate can lead to a more accurate prediction. What we will also note is that for both figures there are more sample periods with smaller measured emission rates vs. periods with higher rates, which also decreases the strength in these plots in determining a pattern. That being said, both the TRM and PSG methods do require the emitted gas to be sufficiently elevated about its background concentration, and it could be possible the lowest emission rates in these experiments were affected by background noise, more so from that of the CH_4 background as opposed to the C_2H_2 background, as it is essentially non-existent compared to the CH_4 background. A noisy and highly variable background should be accounted for in the methods that use an interpolated

background, and for both the tracer and PSG comparisons the techniques with an interpolated background correction in general do yield better results.

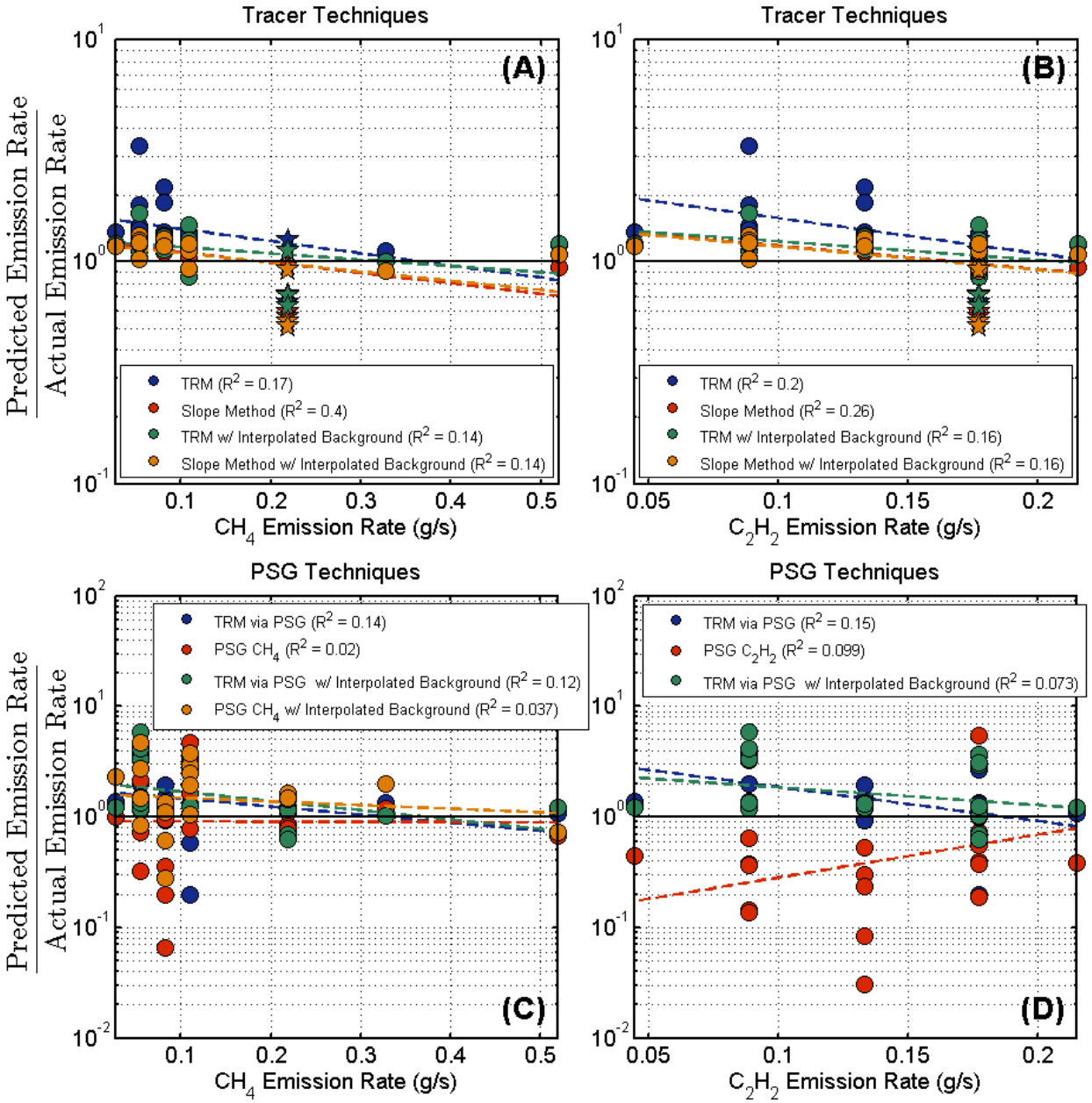

Figure 3.22 Comparisons of the bias in predictions as a function of emission rates. Plots **(A)** and **(B)** compare CH_4 and C_2H_2 emission rates to biases in tracer methods while **(C)** and **(D)** compare these emission rates to PSG method biases.

The effect of changing background will now be evaluated in closer detail. In **Figure 3.23** the influence of varying CH_4 background concentrations across an entire stationary sampling time is compared to its bias in emission rate predictions. This is accomplished using **Equation 2.2** by taking the mean CH_4 concentration (in ppb) in excess of background during an analysis and normalizing it by the standard deviation in the lowest 5% of concentration values (i.e. the values used for the standard background determination). The methods examined here are from analyses using the standard background correction only, because in the interpolated technique each measured concentration within a plume has its own unique background value. The standard deviation in C_2H_2 concentrations is in general two orders of magnitude smaller than that for CH_4, and so it does not have a large effect on the outcomes of the methods evaluated. The spread in biases is largest at the lower values of this plot for both the standard PSG method and for the TRM via the PSG. This is less-so for the TRM and the slope method, which stay somewhat consistent.

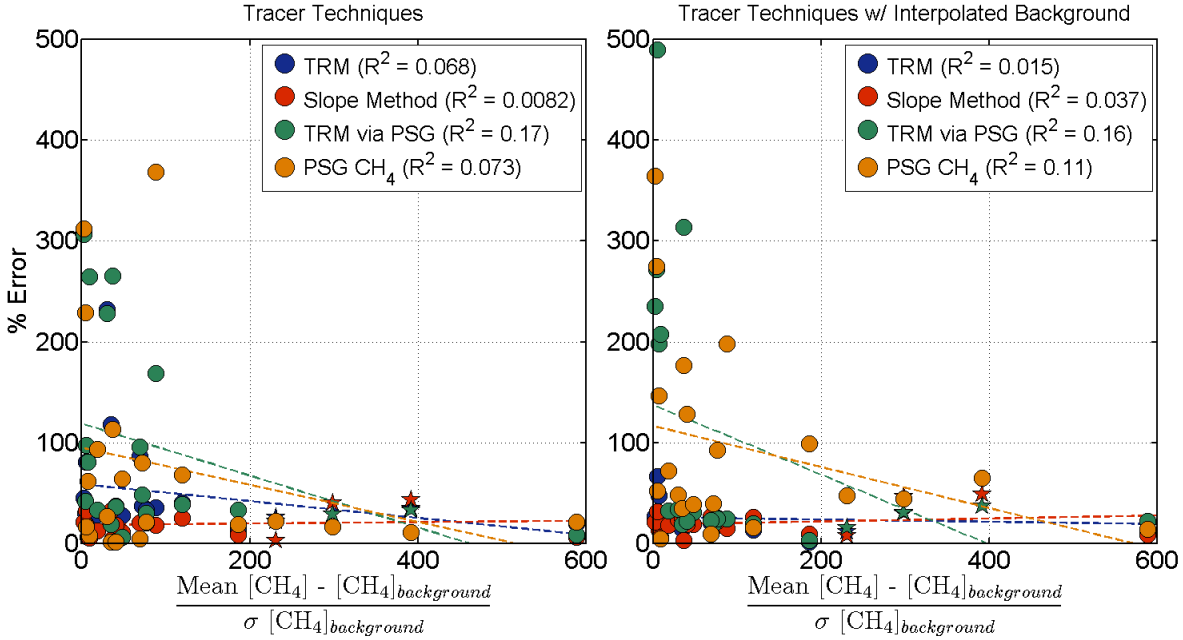

Figure 3.23 Bias in all methods that use the standard background correction as a function of the mean $[CH_4]$ above background within a sample period, normalized by the standard deviation in the concentrations used to obtain the background CH_4 value.

This plot looks similar to **Figure 3.22 (A)** and **(C)**, and the same sample periods clustered towards the lowest end of **Figure 3.23** are indeed the samples with the lowest CH_4 and C_2H_2 emission rates. This is an indication that the large spread in biases for low emission rates could be due to a small signal strength in the sources downwind.

An illustration of this background/emission rate comparison is shown in **Figure 3.24**, where sampling periods are color-coded by sampling day and evaluated based on their measured CH_4 emission rate and standard deviation in background CH_4 values used in the ordinary background correction technique. There is a stark contrast between all three experimental days. 14 March contained the highest emission rate values with very low σ CH_4 background with 23 April representing the opposite. 19 September had low measured emission rates and mostly steady background values, despite the overall background increasing considerably during the entire sample run (see: **Figure 2.11**). The major difference between the 23 April experiment compared to the other two experiment days is that the TRM via the PSG program performed objectively worse during this day compared to the others.

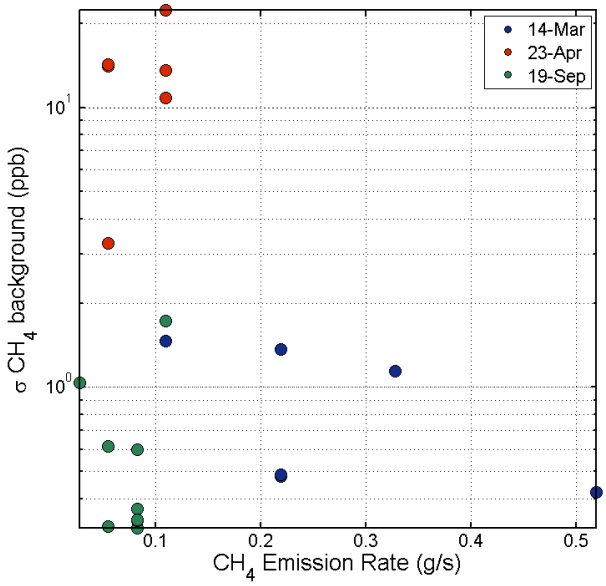

Figure 3.24 A comparison of the measured CH_4 emission rate and the standard deviation of the concentrations used in calculating the ordinary CH_4 background value for each sample period. Points are color-coded by the experiment day it was taken from.

In measuring what effect meteorological conditions may have on the performance of the methods we will first evaluate the sensitivity of the methods to the standard deviation in wind direction throughout a sample time, shown in **Figure 3.25**.

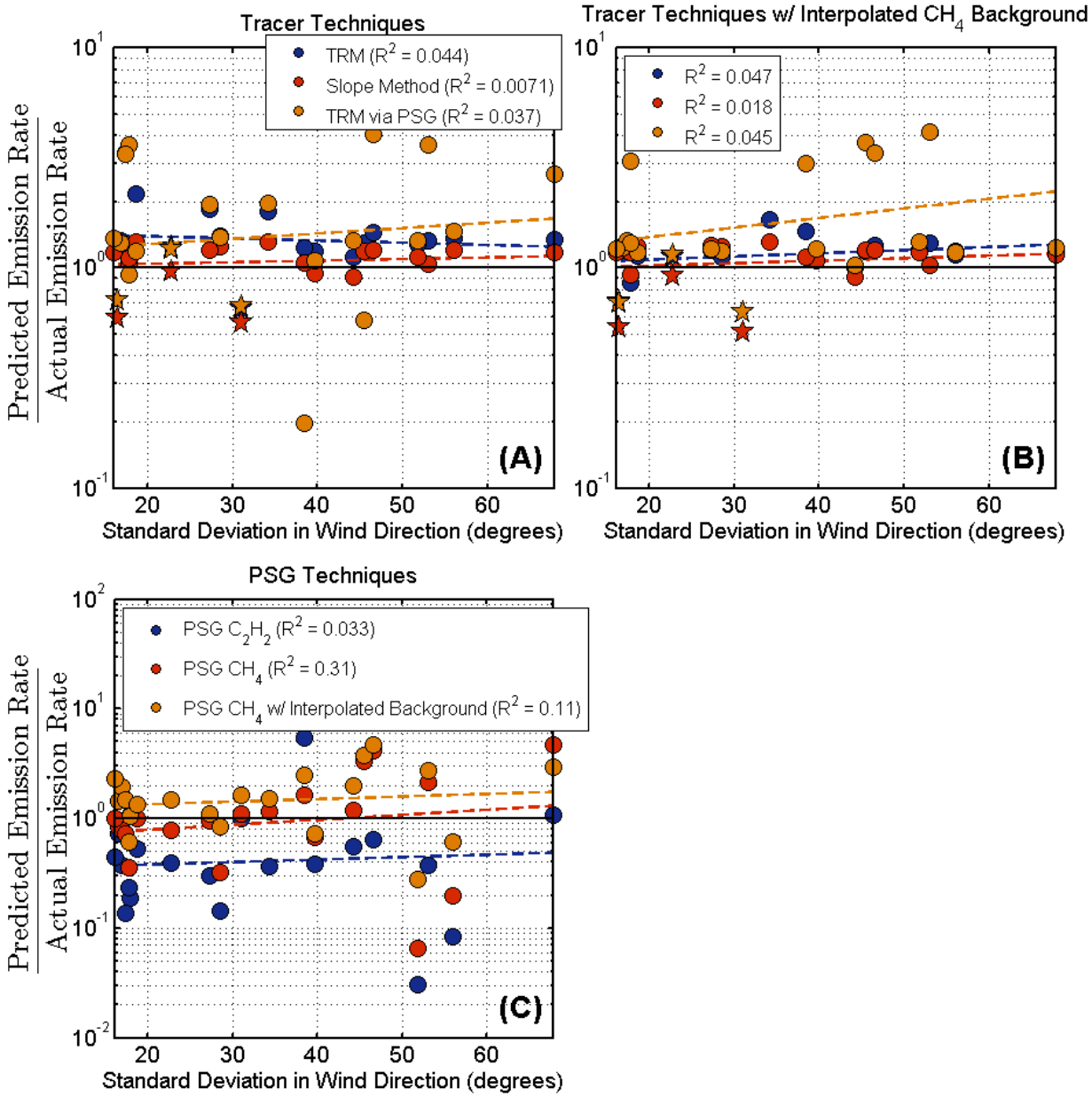

Figure 3.25 Influence of the standard deviation in wind direction across a sample period on the bias in the predicted CH_4 emission rate from standard tracer techniques **(A)**, tracer techniques with an interpolated CH_4 background correction scheme **(B)**, and for PSG techniques **(C)**.

We would not expect the deviation in wind direction over the course of a sample period to affect our tracer method estimates if the assumption that both tracer and emission gases are behaving in

a similar fashion is valid, and indeed we see no effect over the range in wind direction deviations for any tracer method. The effect the standard deviation may have on the PSG estimates is more complicated, as the variable σ_y estimated within the program relies heavily on this value: too small a deviation in wind direction over the course of a sample time may have a detrimental effect on the accuracy of the method, because it requires a sizeable shift in wind direction to allow for the plume analyzer to sample measurements at the centerline of the plume all the way to the outer edges to obtain background concentrations. Conversely, very large deviations in wind direction over the sample period may mean the fitting of a Gaussian curve to the data is not an accurate assumption.

There is no pattern to distinguish for the PSG techniques in **Figure 3.25**, but this variable alone plotted against the bias ratio may not be reveal a pattern. This is because bias ratios may be a function of both the size of the standard deviation in wind direction as well as downwind sampling distance for our PSG methods. For example, to measure the complete width of a plume would require a larger deviation in wind direction over the course of a sample period the further downwind measurements take place, and vice versa. **Figure 3.26** evaluates the bias in the PSG methods as a function of both standard deviation in wind direction and downwind sampling distance, marked by experiment day. Keeping in mind the small number of samples to evaluate, there may be two modes on these plots: increasing wind direction change at a shorter downwind distance, and large downwind distance and small wind direction change. The latter is from the 19 September case only, and this experiment day contains samples across both modes. The other days are contained within the former mode.

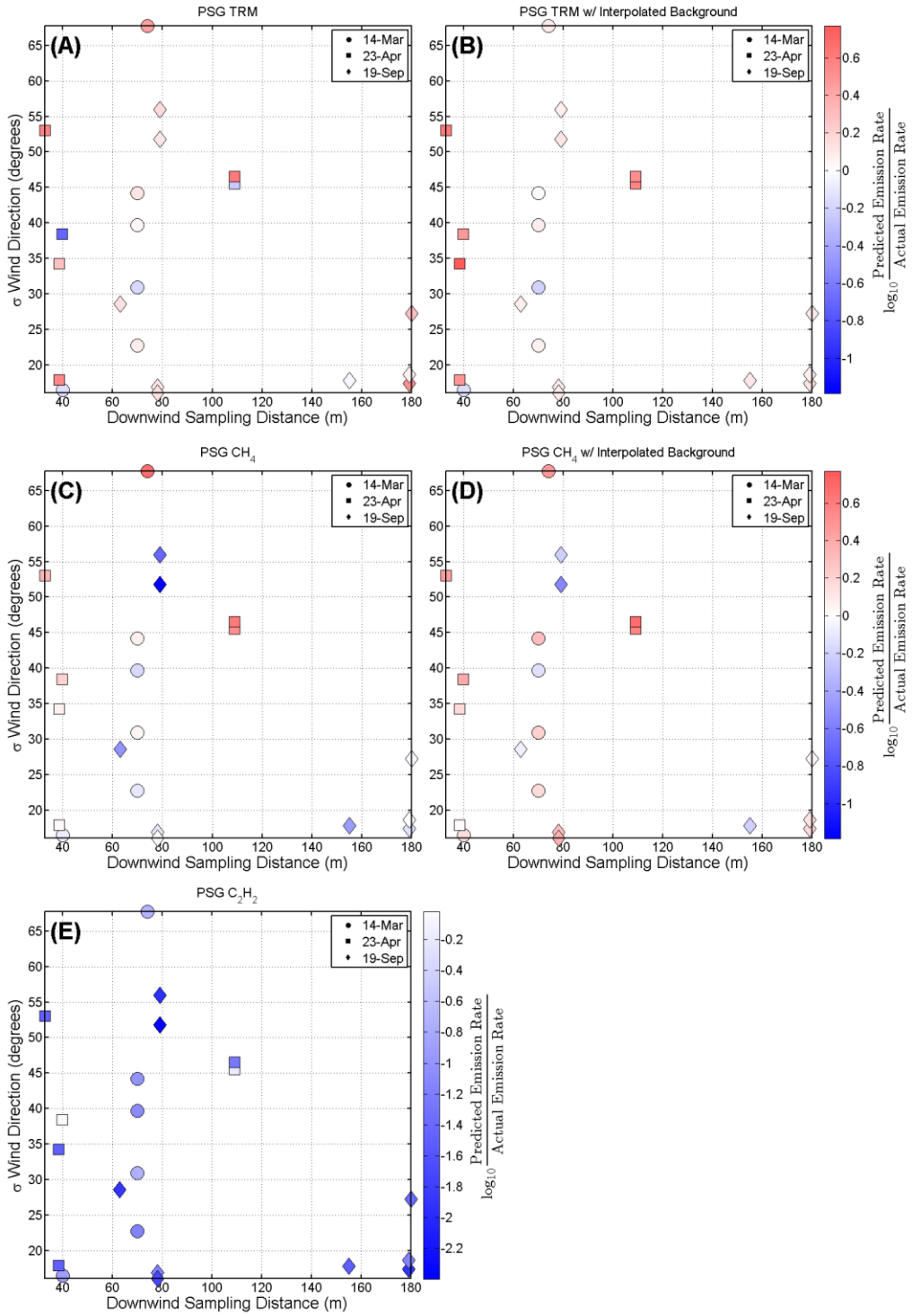

Figure 3.26 Comparison of downwind sampling distance, standard deviation of wind direction, and the $\log_{10}$ of the ratio of predicted to measured CH_4 emission rates through PSG methods, labeled by the experiment day. The standard method for estimating CH_4 emission rates is given in **(A)** and **(B)**, while CH_4 emission rates estimated through a tracer ratio technique via the PSG program is given in **(C)** and **(D)**. Plot **(E)** shows the results for the standard PSG program in estimating C_2H_2 emission rates. Here, **(A)**, **(C)**, and **(E)** use the standard background correction while the **(B)** and **(D)** utilize an interpolated CH_4 background correction.

For the standard PSG method for predicting CH_4 emission rates (plots **(A)** and **(B)**), at short downwind distances the bias in the method generally increases with increasing standard deviation in wind direction, with small biases at large downwind distances. This is not true for the prediction of C_2H_2 emission rates, given in plot **(E)**, in which there exist large biases in all sections of the plot. The largest biases in the TRM via PSG methods, plot **(C)** and **(D)**, are present in the middle and upper portions of the plot, corresponding to a standard deviation in wind direction between 40 and 70 degrees, and downwind sampling between 60 and 120 meters.

Mean wind speed across a stationary sample period is shown in **Figure 3.27**. This variable does not seem to affect the performance of the tracer techniques with the standard background correction scheme, shown in plot **(A)**. When an interpolated CH_4 background correction is utilized, shown in plot **(B)**, it appears that for lower wind speeds this technique lowers the spread in ratio of predicted to measured emission rate values compared the standard background correction scheme. This is not true for larger wind speeds, where we see the spread in biases about as large as they are in plot **(A)**. Note that for all techniques that utilize the PSG program, the predicted gaseous emission rate increases with increasing wind speed. While the average wind speed is used in the direct calculation of the predicted emission rate for the standard PSG methods, seen in **Eqn. 1.2**, it should scale with stability parameters. Also noting that wind speed is not directly used in the predictions using the TRM via PSG, this suggests there may be issue with the method itself in calculating plume width. This pattern does not necessarily say anything about the accuracy of the PSG programs as a function of mean wind speed, only that they continually estimate a larger emission rate value as wind speed increases, regardless of whether or not this increase brings the estimate closer or farther from the measured emission rate, as illustrated in the TRM via PSG programs in **(A)** and **(B)**.

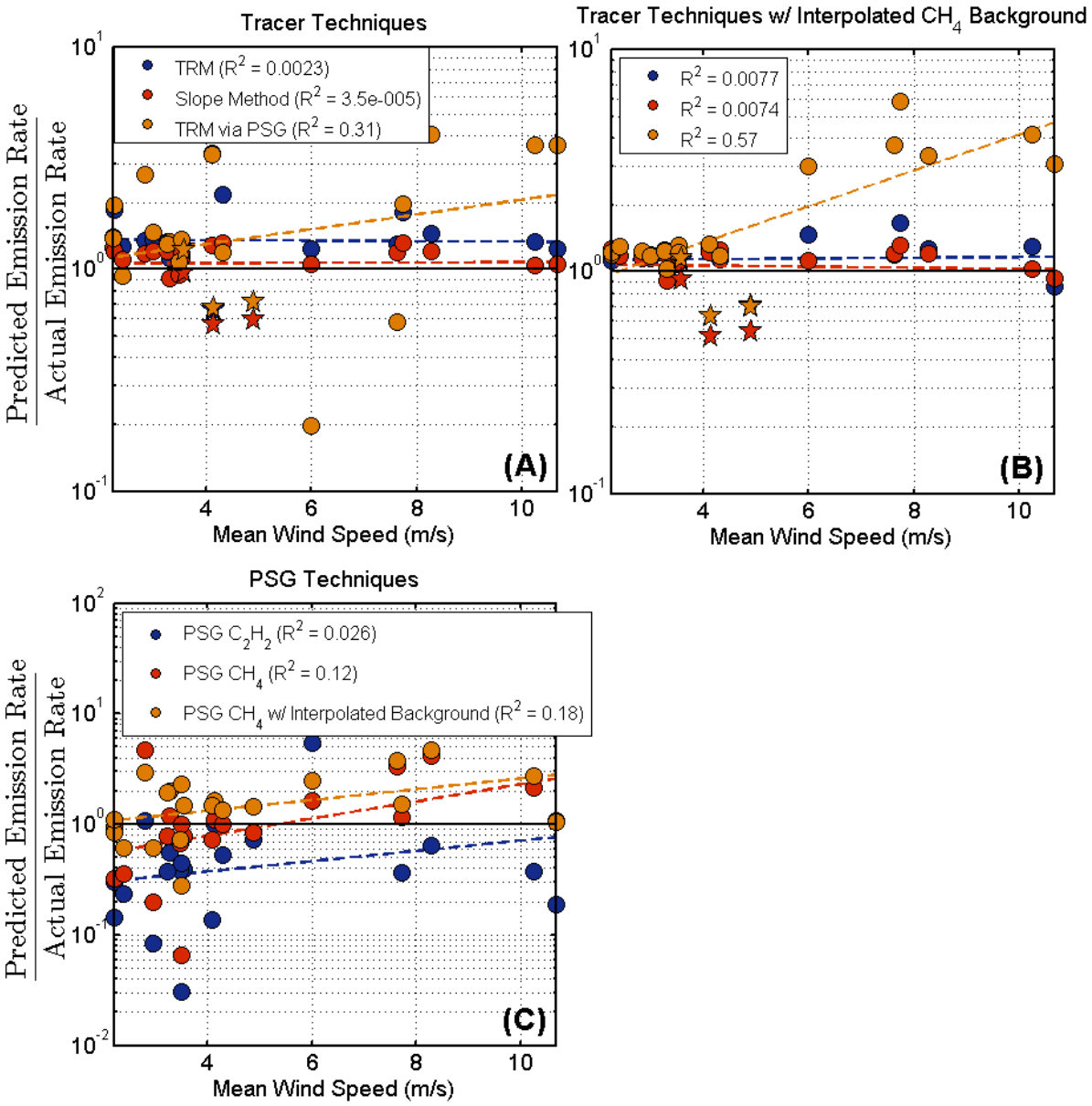

Figure 3.27 A comparison of the bias in tracer methods with the standard background correction **(A)**, an interpolated CH_4 background correction **(B)**, and PSG methods **(C)** to mean wind speed during each stationary sample period.

Friction velocity, u_* is given in **Figure 3.28**. Much like mean wind speed, for the tracer methods with the standard background correction there is not a very distinguishable pattern, but when an interpolated technique is used, the samples with the lowest recorded u_* values have a more constrained prediction in emission rate, with a tighter spread around the mean bias for the

tracer techniques. Another similarity between u_* and the mean wind speed is that for the PSG methods there is a general increase in predicted emission rate values as the value of u_* increases.

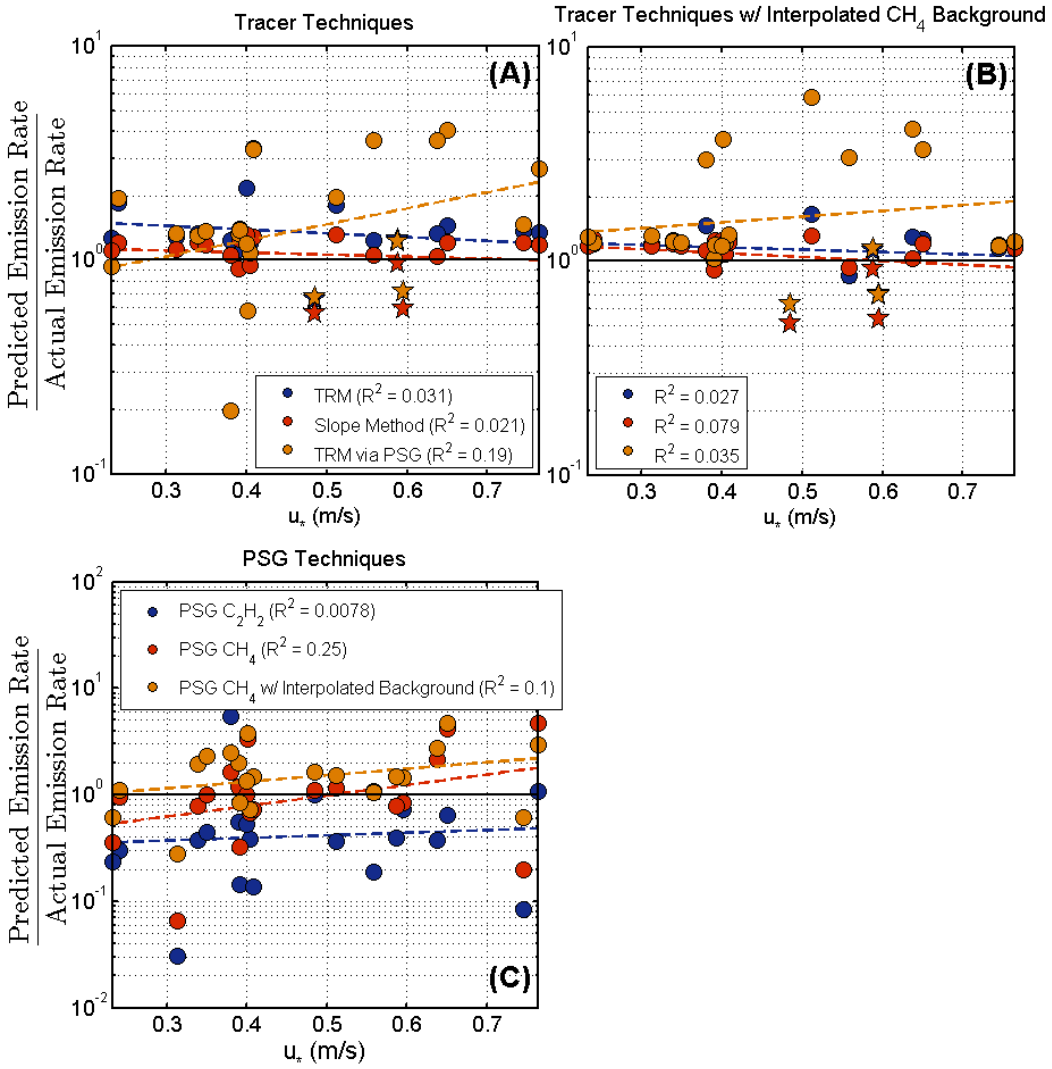

Figure 3.28 A comparison of the bias in tracer methods with the standard background correction **(A)**, an interpolated CH_4 background correction **(B)**, and PSG methods **(C)** to u_* during each stationary sample period.

The last meteorological parameter to evaluate is the stability class of the atmosphere during each sample period, shown in **Figure 3.29**. Through all three sample experiments, we were able to evaluate stability across a wide range of conditions, from a stability class of 2 (unstable) up to 7 (neutral). An increase in stability seems to decrease the predicted to actual emission rate for the

PSG methods, which again may be tied to its sensitivity to the other meteorological measurements discussed above.

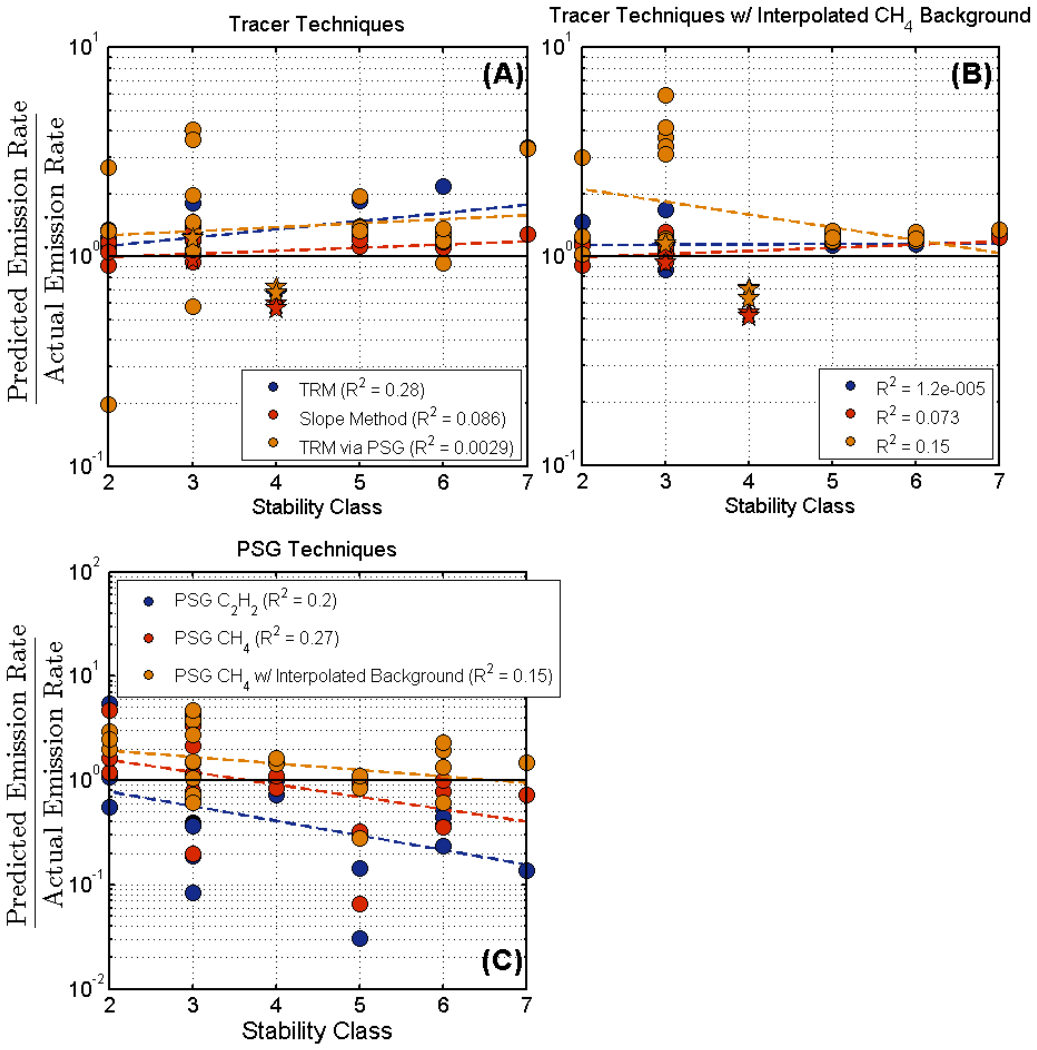

Figure 3.29 A comparison of the bias in tracer methods with the standard background correction **(A)**, an interpolated CH_4 background correction **(B)**, and PSG methods **(C)** to stability class during each stationary sample period. A low number represents unstable conditions, while higher numbers represent a stable atmosphere.

One final analysis on the tracer and PSG techniques for stationary analysis concerns how long one must remain stationary downwind of the gas sources before one can confidently say that the estimated emission rate value obtained through a tracer technique will unlikely contain a relatively large error. We have seen in our mobile analysis that there are numerous and large

outlying bias ratio values in the tracer techniques compared to these same techniques used in the stationary analysis; however, the median error values are more or less similar for mobile and stationary analysis. It appears that a long sampling time decreases this chance for large error (although we should make the distinction here that we are referring to random errors and not the systematic positive bias seen throughout this analysis).

To get a representative illustration of the effect of smaller sample periods in the stationary analysis, one, two, three, five, and ten minute sample times were chosen at random start times from within each original 20 minute sample period. The locations of these intervals within the time series are chosen randomly, but on the condition that the entire interval exist within the original sample period and the correlation between [CH_4] and [C_2H_2] throughout the interval is greater than 0.7. 20 of these random intervals were generated for the one through five minute intervals and 10 were used for the 10 minute intervals. Therefore, a total of 420 bias ratios are considered for sample periods of one to five minutes while 210 bias ratios are considered for the ten minute interval.

In **Figure 3.30** this time sensitivity is evaluated on the TRM and slope method with interpolated background corrections in **(A)** and **(B)**, respectively, and on the PSG CH_4 emission rate prediction with standard background correction **(C)**. Box plots showing the median, 25^{th} and 75^{th} percentiles, 95^{th} percentiles, as well as outlying bias ratios are shown for all shorter time intervals along with the box plot for the original 20 minute sample bias ratios. The horizontal dotted line represents the median bias ratio value for the 20 minute samples.

Results for both the TRM and slope method show both the length of the spread of values within the 95^{th} percentile and the largest outlying bias ratios decreasing in magnitude as one

increases the sampling time. The interquaritle range and median value of bias ratios, however, do not vary significantly across the different sample period lengths. The 25th percentile of bias ratios calculated using the TRM across one minute intervals is roughly 10% lower than 25th percentile for the 20 minute analysis. The 75th percentile and median values remain nearly identical throughout the analysis. Interquartile range values decrease slightly for the slope method analysis.

The PSG analysis in **(C)** contains results that show very large outlying bias ratios for all sample times. The interquartile range decreases significantly between five and ten minute sample periods from about 1.4 to 0.7. The median value of bias ratios for all shorter sampling periods are below one, which is also roughly the median bias ratio value for the original 20 minute samples. For sample periods of one to ten minutes, half of all percent biases are below about -30%. One explanation for this feature is that, at shorter sampling periods, a smaller total amount of wind fluctuations may lead to a smaller estimate of the full plume width, which in turn leads to a lower estimate of gas emission rates. This would help to explain the mostly negative percent biases seen for shorter sampling periods.

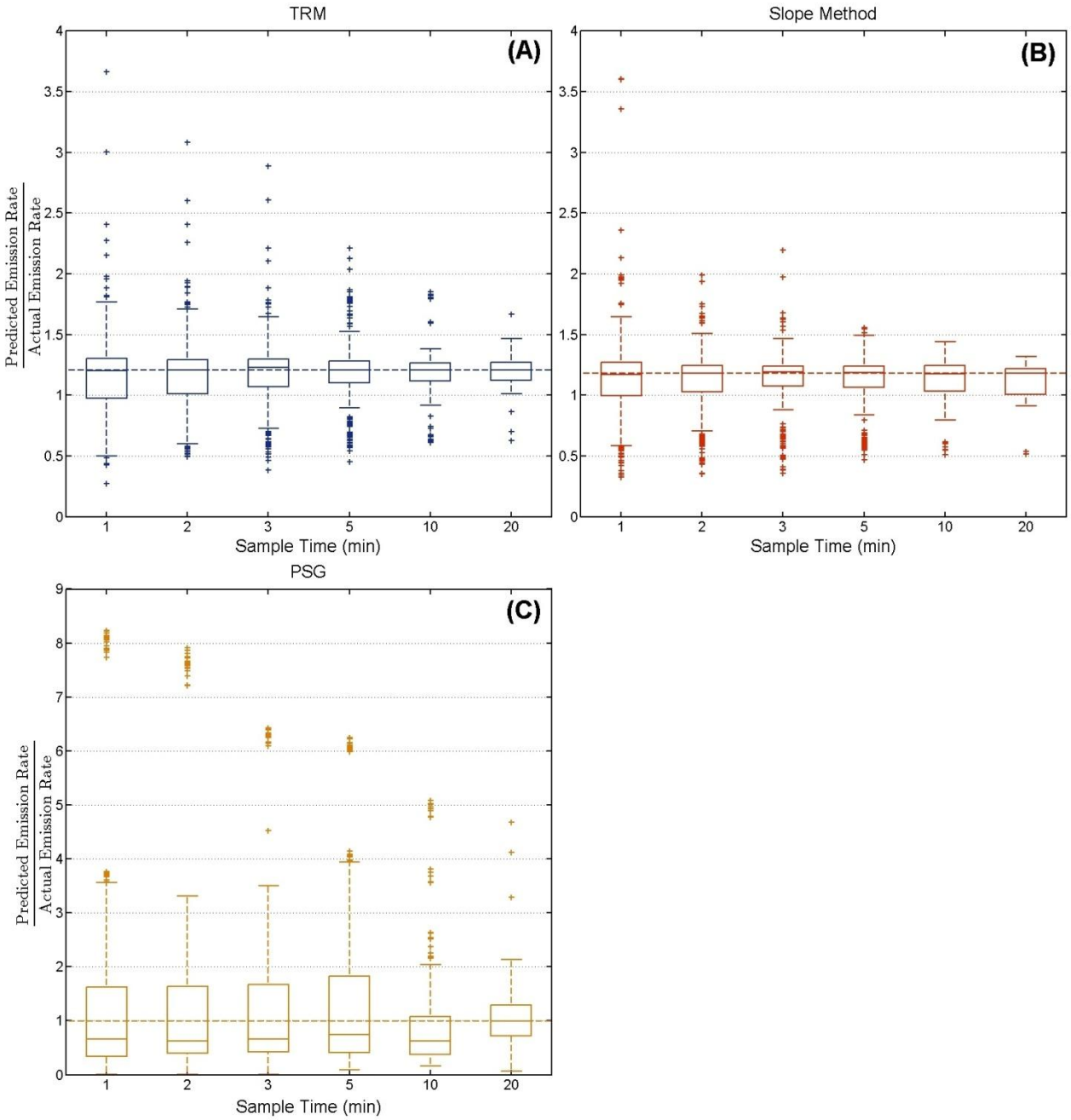

Figure 3.30 Sensitivity of sampling time on the TRM **(A)** and slope method **(B)** analysis with interpolated background correction, and on the PSG analysis with standard background correction **(C)**. In these figures a box plot of bias ratio values calculated in each different time step (contained within the original 20 minute sample period) are shown. The line within the box represents the median bias ratio while the edges of the box represent the 25^{th} and 75^{th} percentiles of the error ratios. The whiskers exending to the edge of the ratios show the 95^{th} percentiles of the error ratios. Large outlying ratios are plotted individually and marked by the red plus signs. The horizontal dashed line reiterates the median bias ratio value for the full 20 minute samples.

Chapter 4 Discussion

4.1 Conclusions

The mobile transect analyses during the 2013 and 2014 experiments share many similarities and differences. A consistent positive bias is present for each method and over all experiment days, and its cause is not yet known. 2013 analyses contained both co-located and separated sources of CH_4 and C_2H_2 while the 2014 experiments only contain co-located sources. The average % biases for co-located sources range from +35-50% in 2013 for all methods, and in 2014 +25-30% for slope methods and nearly 50% for the TRM. Separated sources contain average % biases around +100%. This is arguably the single largest cause for error, at least over the span of downwind distances recorded in our experiments, and so it is pertinent to release the tracer gas as close to the source of emission gases (in terms of both horizontal and vertical positioning) as possible. This is consistent with the findings of *Mønster et al*. [2014].

Other factors evaluated had influences, however minor, on the mobile tracer techniques as well. The R^2 value between the CH_4 and C_2H_2 instantaneous concentrations during a mobile transect seems to play a large part in the spread in errors in the tracer methods in the 2013 experiments, notably for experiments with separated sources. R^2 values from 0.7 to 0.8 are associated with errors from 0 to nearly 400%, while values over 0.9 are constrained to less than 100%. This pattern is not seen in the 2014 cases, although there are fewer data points to analyze and all values are from co-located sources. Here, all transects except for three contained errors less than 100%. For the 2013 experiments, plume transects in which the sources of tracer and emission gases where separated in either the crosswind or downwind directions contain a smaller R^2 value between the two gas concentrations as well as a large spread in error values.

In both years, the spread in error decreases and the models become more accurate, at least in terms of the positive bias, as the signal of the mean C_2H_2 concentration value in excess of background increases. The same can be said about CH_4 concentrations above background for co-located cases. The separated source cases in 2013 still contain a fairly large spread in error ratios even at high elevations above CH_4 background. Meteorological variables overall do not seem to play a large role in the sensitivity of the tracer methods, which is consistent with the theory behind the tracer ratio method. In all, the slope method and modified slope method perform very similarly, and in 2013 the TRM produces predictions that are nearly identical to the two slope methods. For the 2014 analysis, it appears that the slope methods contain errors that are much more constrained compared with the standard TRM method. If real-time analysis is in use, a slope method approach may be more reliable than the standard tracer ratio method for mobile analyses.

The stationary analysis in 2014 shows that tracer techniques in predicting CH_4 emission rates are very consistent with one another, with biases clustered around +10%, which is very similar to the mobile analysis with co-located sources, if not marginally better. This consistent positive bias again shows itself in these longer-integrated, stationary analyses. The main difference between this analysis and the mobile transect analyses is that the precision for stationary analysis is much better, with a standard deviation in the bias ratios being around 0.5 or less. We demonstrated that one needs to remain stationary for roughly five minutes or more to obtain this confidence in precision.

The PSG program contains very erratic results compared to our tracer methods, with standard deviations in the bias ratios for these methods all over 1. Most interesting of note is the bias ratio for CH_4 emission rates is nearly always larger than the bias ratio for C_2H_2 emission rates, with

C_2H_2 emission rates very consistently biased low. This is a very critical finding as this may indicate that there is a difference between the release rate observed and the actual release rate of C_2H_2, or within the downwind concentration recording of the gas. Downwind concentration recordings have been calibrated (see: **Appendix D**), as have the total flow rates out of our gas cylinders; however, one hypothesis is that solid acetone that exists in the C_2H_2 cylinder may be evaporating out as well during our experiments, causing a higher recording of C_2H_2 emission rates than is actually occurring. This would explain the low bias in C_2H_2 emission rate predictions in the PSG program and the high bias in the tracer techniques.

Despite the discrepancies between the two models, it does seem that larger emission rates and a higher signal against the change in background leads to more constrained results. The PSG program is also very sensitive to the input downwind distance value and stability class. These approaches show a systematic sensitivity to meteorological parameters, with a increasing trend in the predicted to actual emission rate ratios with increasing wind speed and u_*, and a decreasing trend with increasing stability class. In all, the tracer methods perform better under the given conditions at Christman Field as opposed the PSG methods, and their use is recommended in the field over PSG approaches.

4.2 Future Work

The most pressing matter to resolve in future studies is to determine where the persistent positive bias in the tracer methods is originating from. This systematic bias may be due to an issue in either the release system or in downwind concentration measurements. In future studies, Nitrous Oxide (N_2O) will be released as a tracer gas as well as C_2H_2. If the prediction in CH_4 still follows this positive bias when this new tracer is used, that would be indicative of a fault in the

release or downwind measurement of CH_4. The release rate or downwind measurement of C_2H_2 will be called into question if this bias is not present in the new experiments.

Furthermore, in a recent paper by *Roscioli, et al.* [2014], both C_2H_2 and N_2O were released as a dual tracer at oil and natural gas sites. A more specific validation of this dual-tracer method will be helpful in determining what conditions this approach may be most useful, and if the use of two tracers at a site can lead to an on-site calibration of our tracer techniques, such as that outlined in the paper.

As indicated in the literature review, many experiments involving tracer methods to estimate emission rates involve acquiring gas concentration measurements at least 1 km downwind of their sources. It may be useful to perform an analysis like the one we have done at Christman Field at a site that allows us to sample an entire plume at these distances. At these distances, we can more confidently say that the plumes of both tracer and emission gases have completely mixed together and this may lead to more constrained results with fewer large outlying error values.

We have seen that a stationary sample technique combined with an interpolated background correction leads to a precise prediction of CH_4 emission rates. Unfortunately, this technique cannot be directly used for many VOCs that may be measured at an oil and gas field site. This is because instantaneous concentration measurements cannot be determined for these VOCs onboard the plume analyzer; only their total concentrations over a sample period taken from canister samples (outlined in **Section 1.1**) will be retrieved. If CH_4 background concentrations vary significantly during analysis at an oil and gas site, warranting an interpolated background correction, the emission rate of CH_4 predicted using this technique and the emission rate of CH_4

predicted via the standard TRM with total integrated [CH_4] from a canister sample during the same period may be compared. The value of the ratio of these two predictions can be multiplied by the predicted emission rate of another VOC to attempt to obtain a more accurate and precise estimation of that VOC's emission rate. This correction is contingent on the change in background values of CH_4 and the other VOCs analyzed over the course of a sample to all be well correlated. A future project could focus on whether or not this is a valid assumption.

The PSG program contains more parameters within its calculation that may affect the outcome of the prediction. One area to explore is to determine the apparent systematic error associated with meteorological parameters and attempt to fix this. One of the potential shortcomings within the program is that σ_y and σ_z are assumed to be the entire crosswind and vertical widths of the plume, which is estimated from a stationary analyzer. The calculations of these two variables rely on meteorological parameters, so a first step would be to determine how different σ_y and σ_z are to the actual plume width over the course of a 20-minute sampling period.

References

2014 National Emission Inventory Information. (2014, December 9). Retrieved December 18, 2014, from http://www.epa.gov/ttn/chief/net/2014inventory.html

Baptista, F.J., Bailey, B.J., Randall, J.M., and J.F. Meneses (1999). Greenhouse Ventilation Rate: Theory and Measurement with Tracer Gas Techniques. *Journal of Agricultural Engineering Research* **72** (4), 363-374.

Brantley, H.L., Thoma, E.D., Squier, W.C., Guven, B.B., and D. Lyon (2014). Assessment of Methane Emissions from Oil and Gas Production Pads using Mobile Measurements. *Environ. Sci. Technol.* **48** (24), 14508-14515. DOI: 10.1021/es503070q

Carrascal, M.D., Puigcerver, M., and P. Puig (1993). Sensitivity of Gaussian Plume Model to Dispersion Specifications. *Theor. Appl. Climatol.* **48**, 147-157.

Catalano, J.A. (1987). Estimating Inaccessible Source Strengths Using Tracer Techniques: A Sensitivity Analysis. *EPA Project Summary*. Accessed online 20 Oct. 2014. http://nepis.epa.gov/Exe/ZyPURL.cgi?Dockey=2000TSVO.txt

"Continuous Emission Monitoring - Information, Guidance, Etc." *EPA*. Environmental Protection Agency, n.d. Web. 26 Aug. 2014.

EIA (2014). AOE2014 Early Release Overview. DOE/EIA-0383ER (2014), Energy Information Agency, U.S. Department of Energy. http://www.eia.gov/forecasts/aeo/er/pdf/0383er(2014).pdf.

Foken, T., and B. Wichura (1996). Tools for quality assessment of surface-based flux measurements. *Agricultural and Forest Meteorology* **78**, 83-105.

Galle, B., Samuelsson, J., Svensson, B.H., and G. Borjesson (2001). Measurements of Methane Emissions from Landfills Using a Time Correlation Tracer Method Based on FTIR Absorption Spectroscopy. *Environ. Sci. Technol.* **35** (1), 21-25.

Gifford, F.A., (1961). Use of Routine Meteorological Observations for Estimating Atmospheric Dispersion, *Nuclear Safety* **2**, 47-57.

Gilman, J. B., B. M. Lerner, W. C. Kuster, and J. A. de Gouw, (2013). Source Signature of Volatile Organic Compounds from Oil and Natural Gas Operations in Northeastern Colorado, *Env. Sci. and Tech* **47** (3), 1297-1305. DOI: 10.1021/es304119a

Hecobian, A., Liu, Z., Hennigan, C.J., Huey, L.G., Jimenez, J.L., Cubison, M.J., Vay, S., Diskin, G.S., Sachse, G.W., Wisthaler, A., Mikoviny, T., Weinheimer, A.J., Liao, J., Knapp, D.J., Wennberg, P.O., Kürten, A., Crounse, J.D., St. Clair, J., Wang, Y., and R.J. Weber (2011). Comparison of chemical characteristics of 495 biomass burning plumes intercepted by the NASA DC-8 aircraft during the ARCTAS/CARB-2008 field campaign. *Atmos. Chem. and Phys.* **11**, 13325-13337. DOI: 10.5194/acp-11-13325-2011

Heumann, G. and G. Halbritter, (1980). Sensitivity Analysis of the Gaussian Plume Model. *Studies in Environmental Science* **8**, 57-62.

Howarth, R.W., Santoro, R., and A. Ingraffea, (2011). Methane and the greenhouse-gas footprint of natural gas from shale formations. *Climate Change* **106** (4), 679-690 DOI: 10.1007/s10584-011-0061-5.

Johnson, K., Huyler, M., Westberg, H., Lamb, B., and P. Zimmerman, (1994). Measurement of Methane Emissions from Ruminant Livestock Using a SF6 Tracer Technique. *Eviron. Sci. Technol.* **28,** 359-362.

Kaharabata, S.K., Schuepp, P.H., and R.L. Desjardins (2000). Estimating Methane Emissions from Dairy Cattle Housed in a Barn and Feedlot Using an Atmospheric Tracer. *Environ. Sci. Technol.* **34** (15), 3296-3302. DOI: 10.1021/es990578c

Kantamaneni, R., Adams, G., Bamesberger, L., Allwine, E., Westberg, H., Lamb, B., and C. Claiborn (1996). The measurement of roadway PM_{10} emission rates using atmospheric tracer ratio techniques. *Atmos. Environ.* **30** (24), 4209-4223.

Lamb, B., Westberg, H., and G. Allwine (1986). Isoprene emission fluxes determined by an atmospheric tracer technique. *Atmos. Environ.* **20** (1), 1-8.

Lassey, K.R., Ulyatt, M.J., Martin, R.J., Walker, C.F., and I.D. Shelton (1997). Methane emissions measured directly from grazing livestock in New Zealand. *Atmos. Environ.* **31** (18), 2905-2914.

Lewandowski, B., (2012). Fueling Economic Growth: The Impact of Colorado's Oil and Gas Industry. http://www.coga.org/COGAContent/EconomicGrowth.pdf.

Ludwig, F.L., Liston, E.M., and L.J. Salas (1983). Tracer techniques for estimating emissions from inaccessible ground level sources. *Atmos. Environ.* **17** (11), 2167-2172.

Miller, C.W., and L.M. Hively (1987). A review of validation studies for the Gaussian plume atmospheric dispersion model. *Nuclear Safety*. **28** (4), 522-531.

Monin, A.S., and A.M. Obukhov (1954). Osnovnye zakonomernosti turbulentnogo peremesivanija v prizemnom sloe atmosfery. *Trudy geofiz. inst. AN SSSR*, **24** (151), 163-187.

Mønster, J.G., Samuelsson, J., Kjeldsen, P., Rella, C.W., and C. Scheutz (2014). Quantifying methane emission from fugitive sources by combining tracer release and downwind measurements – A sensitivity analysis based on multiple field surveys. *Waste Management*, **34** (8) 1416-1428.

Neumann, G., and G. Halbritter (1980). Sensitivity analysis of the Gaussian plume model. *Atmospheric Pollution 1980: Proceedings of the 14th International Colloquium.* May 5-8, 1980,

Paris, France. M.M. Banarie (Ed.), *Studies in Environmental Science*, **8**, 57-62. Elsevier Scientific Publishing Company, Amsterdam, Netherlands.

Pacsi, A.P., Alhajeri, N.S., Zavala-Araiza, D., Webster, M.D., and D.T. Allen (2013). Regional air quality impacts of increased natural gas production and use in Texas. *Environ. Sci. Technol.* **47** (7), 3521-3527. DOI: 10.1021/es3044714

Rella, C.W., Crosson, E.R., Dayton, D., Green, R., Hater, G., Merrill, R., Tan, S.M., and E. Thoma (2010). Quantifying Methane Fluxes Simply and Accurately: The Tracer Dilution Method. Poster Presented at the European Geosciences Union General Assembly. Presentation retrieved from http://www.picarro.com/assets/docs/Rella_EGU_2010_Poster_Picarro.pdf.

Roscioli, J.R., Yacovitch, T.I., Flourchinger, C., Mitchell, A.L., Tkacik, D.S., Subramanian, R., Martinez, D.M., Vaughn, T.L., Williams, L., Zimmerle, D., Robinson, A.L., Herndon, S.C., and A.J. Marchese (2014). Measurements of methane emissions from natural gas gather facilities and processing plants: measurement methods. *Atms. Measurement Techniques.* **7**, 12357-12406.

Rumburg, B., Mount, G.H., Filipy, J., Lamb, B., Westberg, H., Yonge, D., Kincaid, R., and K. Johnson (2008). Measurement and modeling of atmospheric flux of ammonia from dairy milking cow housing. *Atmos. Environ.* **42** (14), 3364–3379.

Schauer, J.J., Kleeman, M.J., Cass, G.R., and B.R.T. Simoneit (1999). Measurement of Emissions from Air Pollution Sources. 2. C_1 through C_{30} Organic Compounds from Medium Duty Diesel Trucks. *Environ. Sci. Technol.* **33**, 1578-1587.

Scholtens, R., Dore, C.J., Jones, B.M.R., Lee, D.S., and V.R. Phillips (2004). Measuring ammonia emission rates from livestock buildings and manure stores—part 1: development and validation of external tracer ratio, internal tracer ratio and passive flux sampling methods. *Atmos. Environ.* **38** (19), 3003–3015. DOI: 10.1016/j.atmosenv.2004.02.030

Stephenson, T., J.E. Valle, and X. Riera-Palou (2011), Modeling the relative GHG emissions from conventional and shale gas production. *Env. Sci. and Tech.* **45** (24), 10757-10764. DOI: 10.1021/es2024115

Thomas, C., and T. Foken (2002), Re-evaluation of integral turbulence characteristics and their parameterizations. *15th Conference on Turbulence and Boundary Layers*. Am. Meteorol. Soc., 129-132.

Thoma, E.D., and B. Squier (2012). Near-field production pad assessment with GMAP-REQ. *EDF Synthesis Workshop on Methane Leakage*. October 17-18, 2012, Boulder, Colorado.

Thoma, E.D., Squier, B.C., Olson, D., Eisele, A.P., DeWees, J.M., Segall, R.R., Amin, M.S., and M.T. Modrak (2012). Assessment of Methane and VOC Emissions from Select Upstream Oil and Gas Production Operations Using Remote Measurements, Interim Report on Recent Survey Studies. *Proceedings of 105th Annual Conference of the Air & Waste Management Association.* June 19-22, 2012, San Antonio, Texas. Control # 2012-A-21-AWMA.

Turner, D.B. (1970). Workbook on atmospheric dispersion estimates. Publication AP-26, U.S. Environmental Protection Agency, Research Triangle Park, N.C.

Warneke, C., Geiger, F., Edwards, P.M., Dube, W., Pétron, G., Kofler, J., Zahn, A., Brown, S.S., Graus, M., Gilman, J.B., Lerner, B.M., Peischl, J., Ryerson, T.B., de Gouw, J.A., and J.M. Roberts (2014). Volatile organic compound emissions from the oil and natural gas industry in the Uintah Basin, Utah: oil and gas well pad emissions compared to ambient air composition. *Atmos. Chem. Phys.* **14**, 10977-10988. DOI: 10.5194/acp-14-10977-2014

Weber, R.O. (1999), Remarks on the Definition and Estimation of Friction Velocity. *Boundary-Layer Meteorology* **93** (2), 197-209.

Whitby, R.A., and E.R. Altwicker (1978), Acetylene in the atmosphere: Sources, representative ambient concentrations and ratios to other hydrocarbons. *Atmos. Environ.* **12**, 1289-1296.

Zavala-Araiza, D., Sullivan, D.W., and D.T. Allen (2014). Atmospheric Hydrocarbon Emissions and Concentrations in the Barnett Shale Gas Production Region. *Environ. Sci. Technol.* **48** (9), 5314-5321. DOI: 10.1021/es405770h

Appendix A

MOBILE ANALYSIS CONCENTRATION PLOTS WITH CO-LOCATED SOURCES

26 June 2013

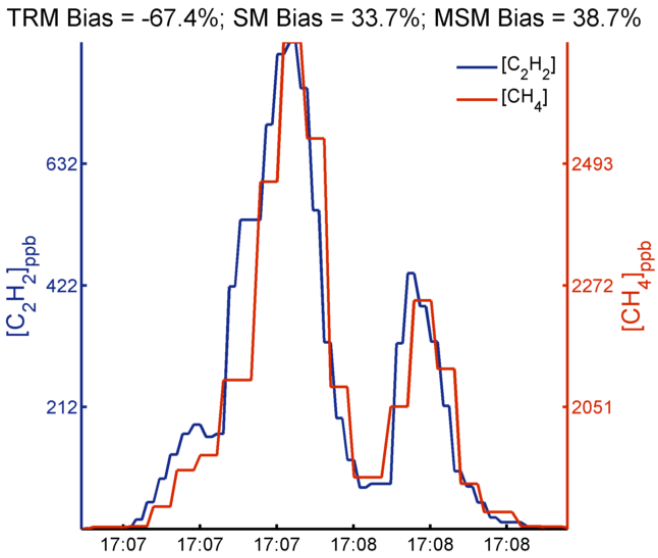
TRM Bias = -67.4%; SM Bias = 33.7%; MSM Bias = 38.7%
[C2H2]
[CH4]
632
422
212
2493
2272
2051
[C2H2]ppb
[CH4]ppb
17:07
17:07
17:07
17:08
17:08
17:08

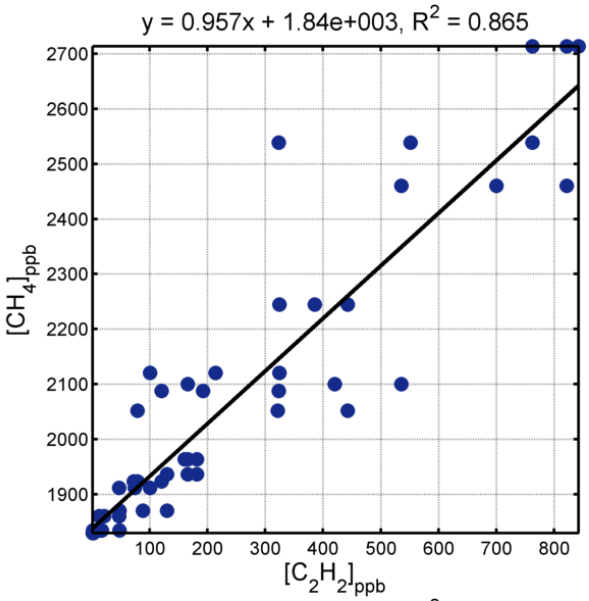
y = 0.957x + 1.84e+003, R2 = 0.865
2700
2600
2500
2400
2300
2200
2100
2000
1900
100
200
300
400
500
600
700
800
[CH4]ppb
[C2H2]ppb

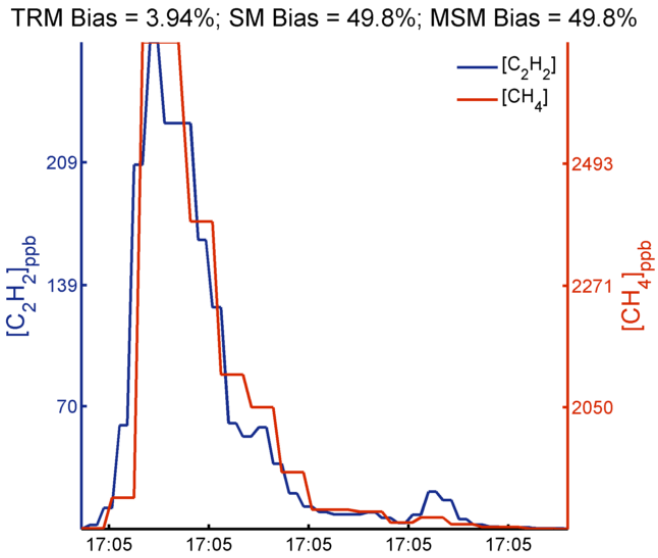
TRM Bias = 3.94%; SM Bias = 49.8%; MSM Bias = 49.8%
[C2H2]
[CH4]
209
139
70
2493
2271
2050
[C2H2]ppb
[CH4]ppb
17:05
17:05
17:05
17:05
17:05

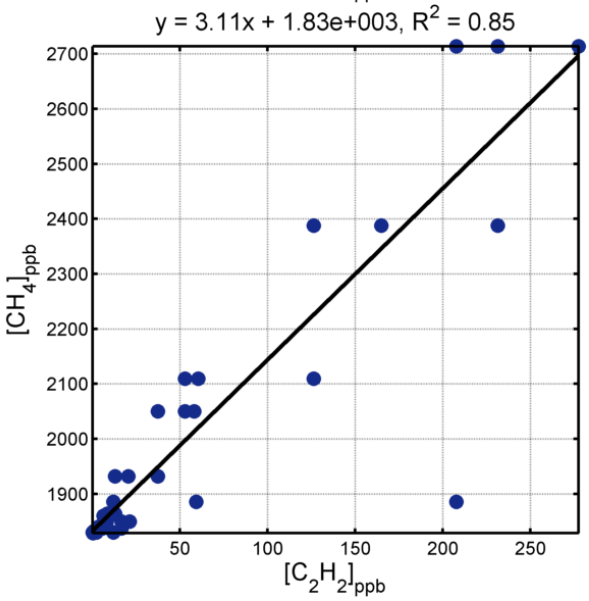
y = 3.11x + 1.83e+003, R2 = 0.85
2700
2600
2500
2400
2300
2200
2100
2000
1900
50
100
150
200
250
[CH4]ppb
[C2H2]ppb

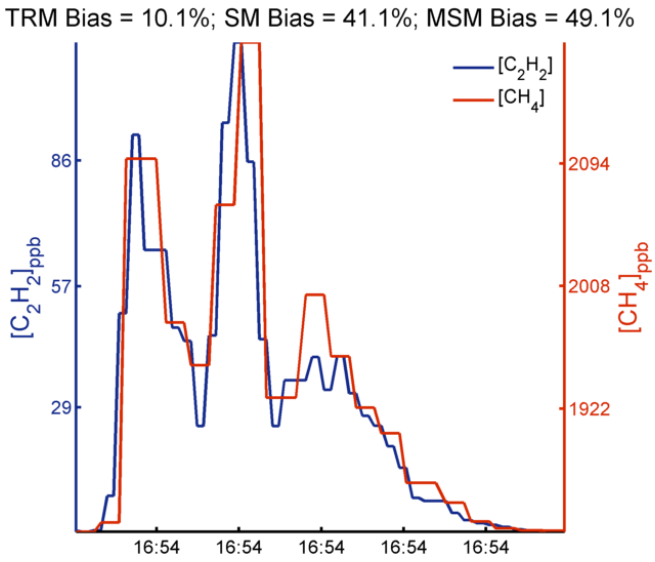
TRM Bias = 10.1%; SM Bias = 41.1%; MSM Bias = 49.1%
[C2H2]
[CH4]
86
57
29
2094
2008
1922
[C2H2]ppb
[CH4]ppb
16:54
16:54
16:54
16:54
16:54

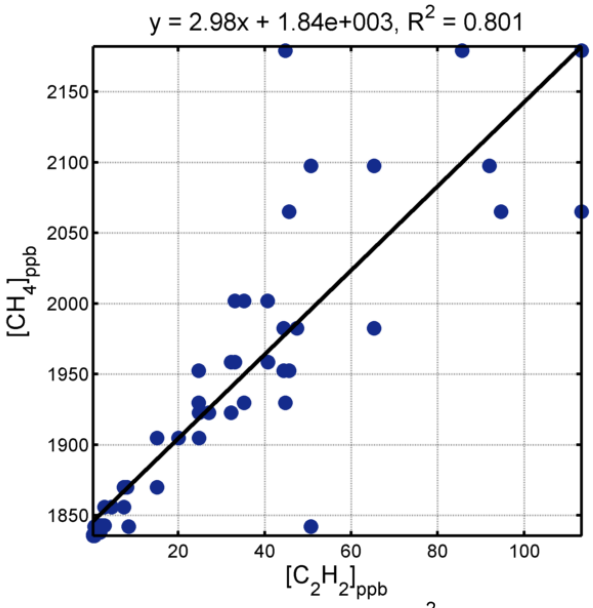
y = 2.98x + 1.84e+003, R2 = 0.801
2150
2100
2050
2000
1950
1900
1850
20
40
60
80
100
[CH4]ppb
[C2H2]ppb

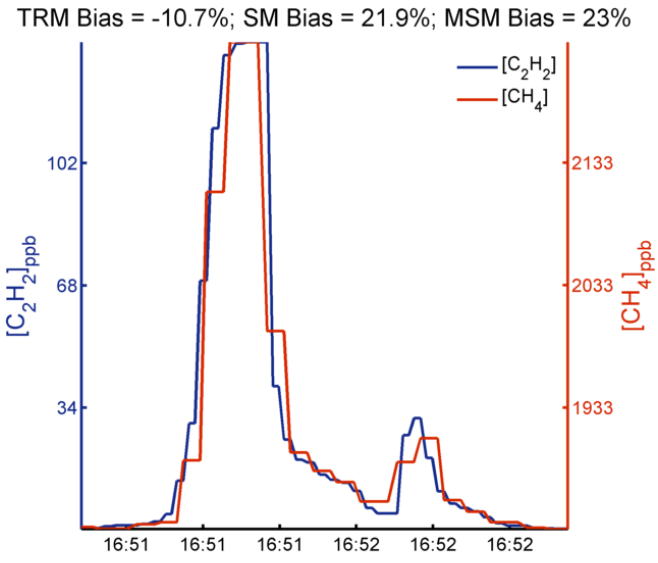
TRM Bias = -10.7%; SM Bias = 21.9%; MSM Bias = 23%
[C2H2]
[CH4]
102
68
34
2133
2033
1933
[C2H2]ppb
[CH4]ppb
16:51
16:51
16:51
16:52
16:52
16:52

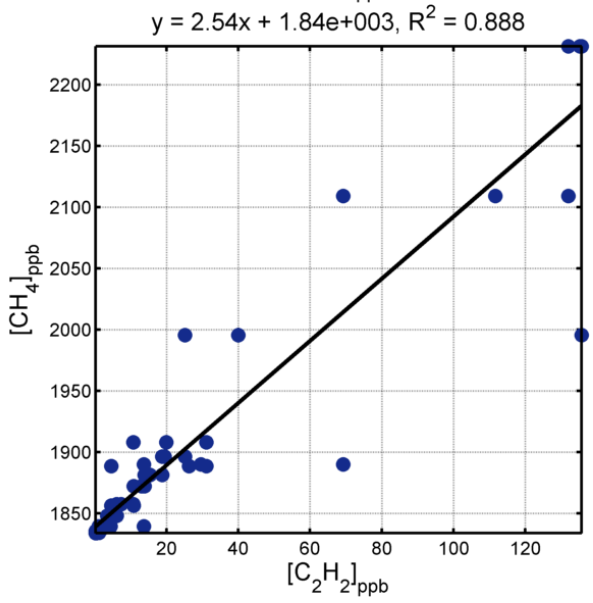
y = 2.54x + 1.84e+003, R2 = 0.888
2200
2150
2100
2050
2000
1950
1900
1850
20
40
60
80
100
120
[CH4]ppb
[C2H2]ppb

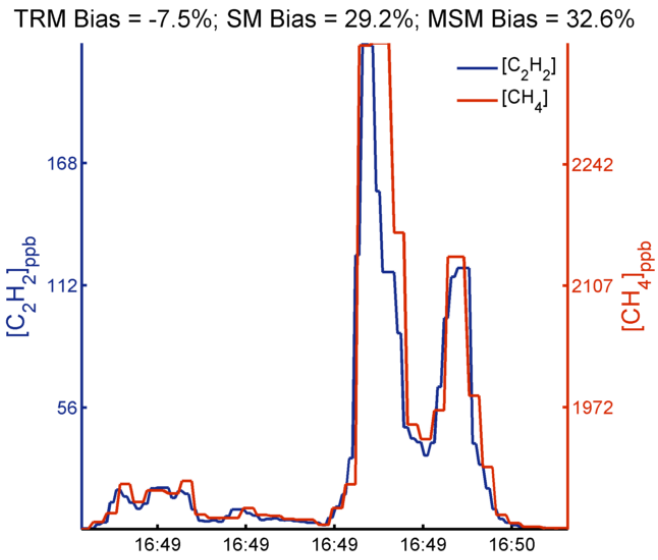
TRM Bias = -7.5%; SM Bias = 29.2%; MSM Bias = 32.6%
[C2H2]
[CH4]
168
112
56
2242
2107
1972
[C2H2]ppb
[CH4]ppb
16:49
16:49
16:49
16:49
16:50

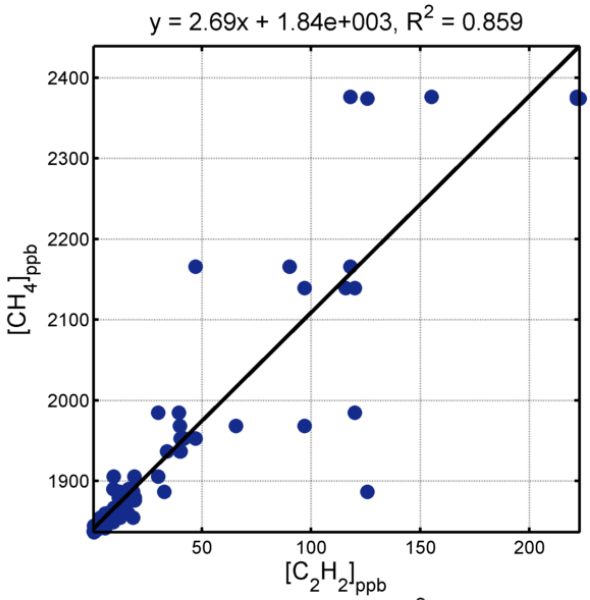
y = 2.69x + 1.84e+003, R2 = 0.859
2400
2300
2200
2100
2000
1900
50
100
150
200
[CH4]ppb
[C2H2]ppb

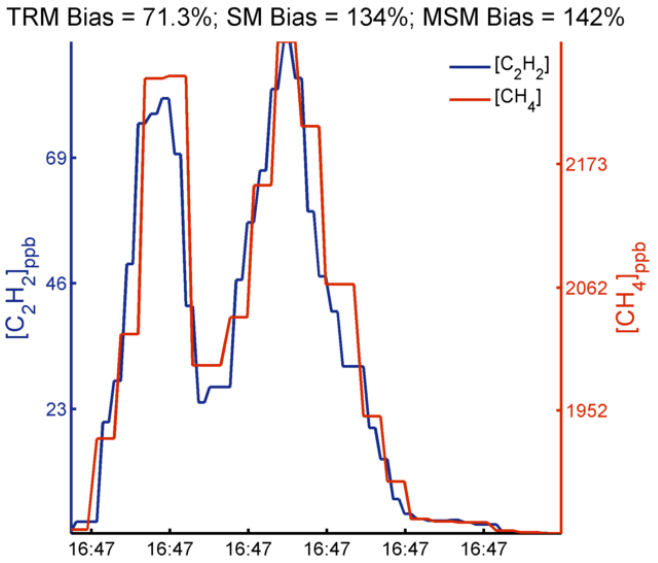
TRM Bias = 71.3%; SM Bias = 134%; MSM Bias = 142%
[C2H2]
[CH4]
69
46
23
2173
2062
1952
[C2H2]ppb
[CH4]ppb
16:47
16:47
16:47
16:47
16:47
16:47

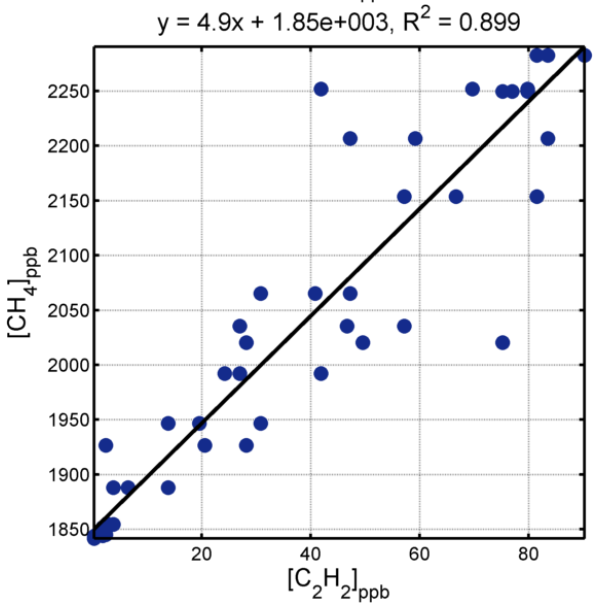
y = 4.9x + 1.85e+003, R2 = 0.899
2250
2200
2150
2100
2050
2000
1950
1900
1850
20
40
60
80
[CH4]ppb
[C2H2]ppb

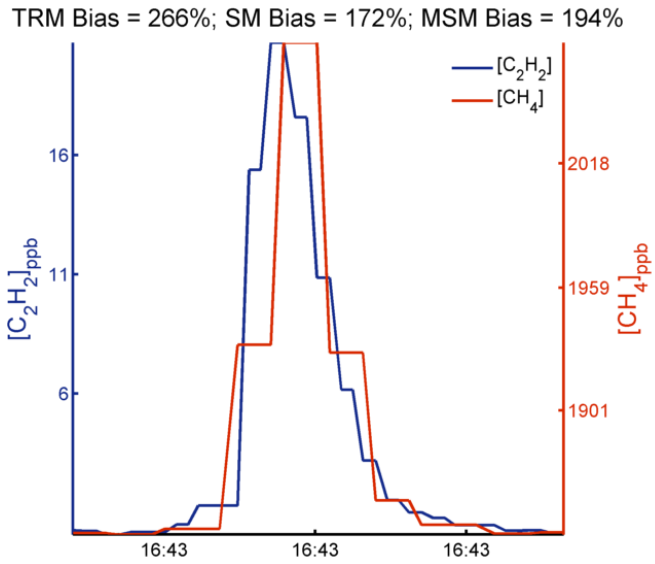
TRM Bias = 266%; SM Bias = 172%; MSM Bias = 194%
[C2H2]
[CH4]
16
11
6
2018
1959
1901
[C2H2]ppb
[CH4]ppb
16:43
16:43
16:43

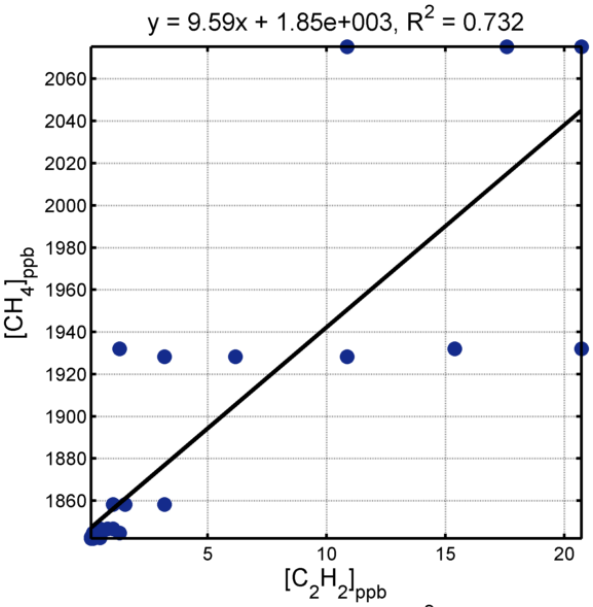
y = 9.59x + 1.85e+003, R2 = 0.732
2060
2040
2020
2000
1980
1960
1940
1920
1900
1880
1860
5
10
15
20
[CH4]ppb
[C2H2]ppb

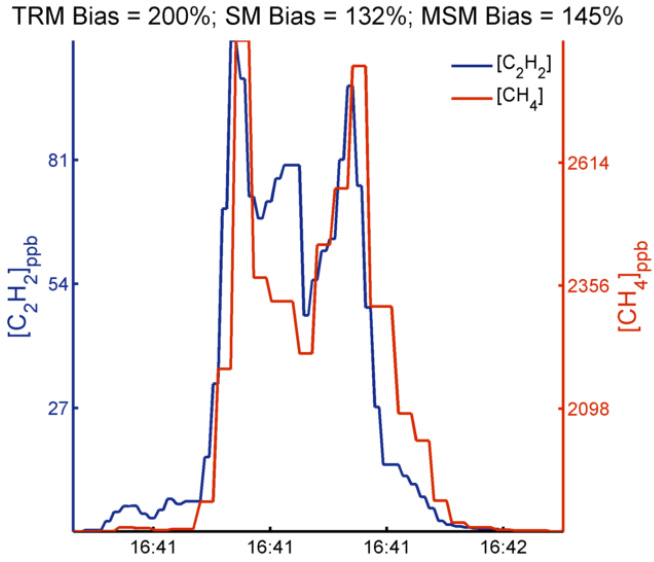
TRM Bias = 200%; SM Bias = 132%; MSM Bias = 145%
[C2H2]
[CH4]
81
54
27
2614
2356
2098
[C2H2]ppb
[CH4]ppb
16:41
16:41
16:41
16:42

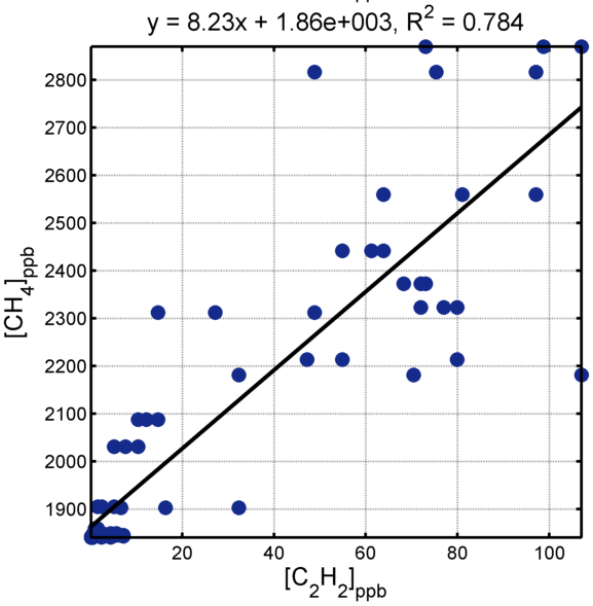
y = 8.23x + 1.86e+003, R2 = 0.784
2800
2700
2600
2500
2400
2300
2200
2100
2000
1900
20
40
60
80
100
[CH4]ppb
[C2H2]ppb

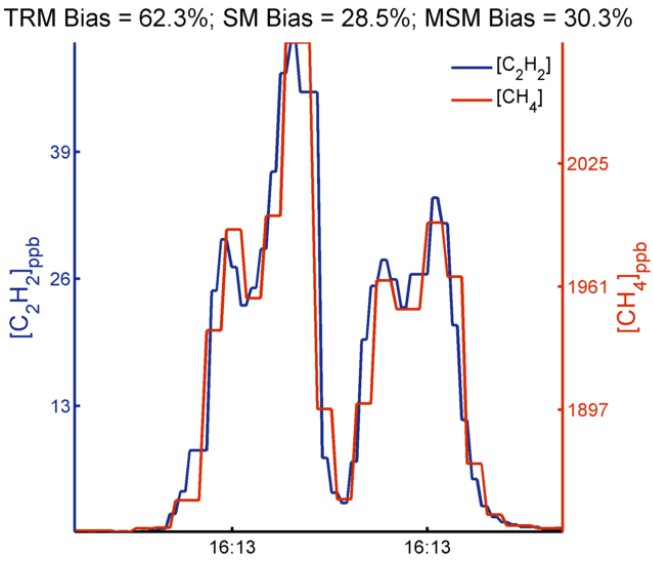
TRM Bias = 62.3%; SM Bias = 28.5%; MSM Bias = 30.3%
[C2H2]
[CH4]
39
26
13
2025
1961
1897
[C2H2]ppb
[CH4]ppb
16:13
16:13

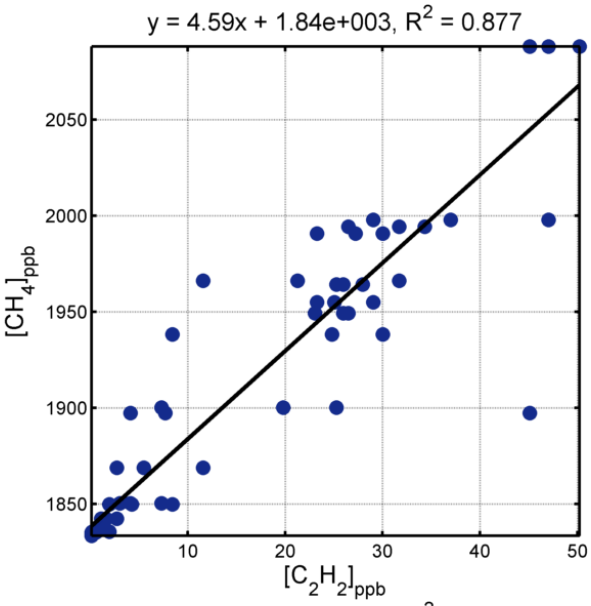
y = 4.59x + 1.84e+003, R2 = 0.877
2050
2000
1950
1900
1850
10
20
30
40
50
[CH4]ppb
[C2H2]ppb

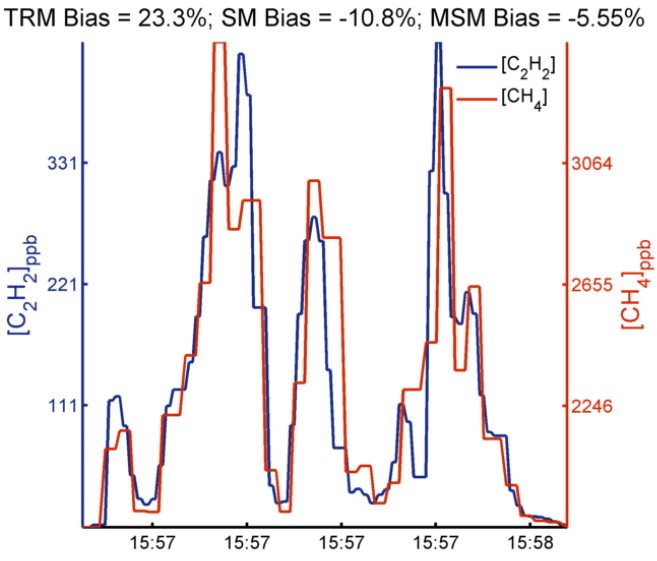
TRM Bias = 23.3%; SM Bias = -10.8%; MSM Bias = -5.55%
[C2H2]
[CH4]
331
221
111
3064
2655
2246
[C2H2]ppb
[CH4]ppb
15:57
15:57
15:57
15:57
15:58

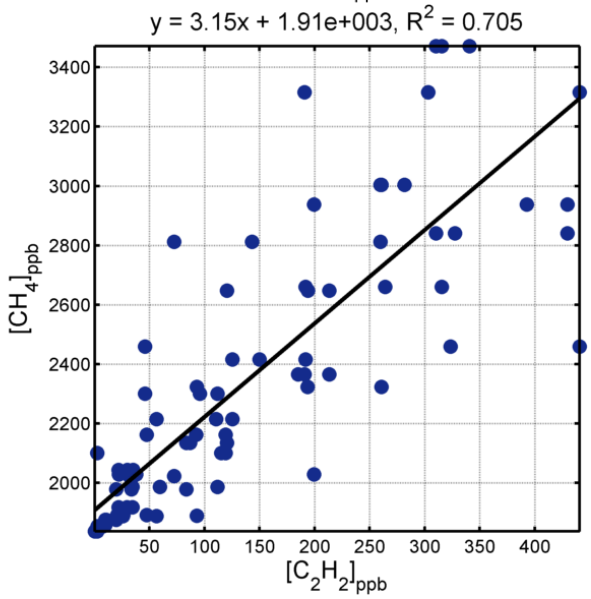
y = 3.15x + 1.91e+003, R2 = 0.705
3400
3200
3000
2800
2600
2400
2200
2000
50
100
150
200
250
300
350
400
[CH4]ppb
[C2H2]ppb

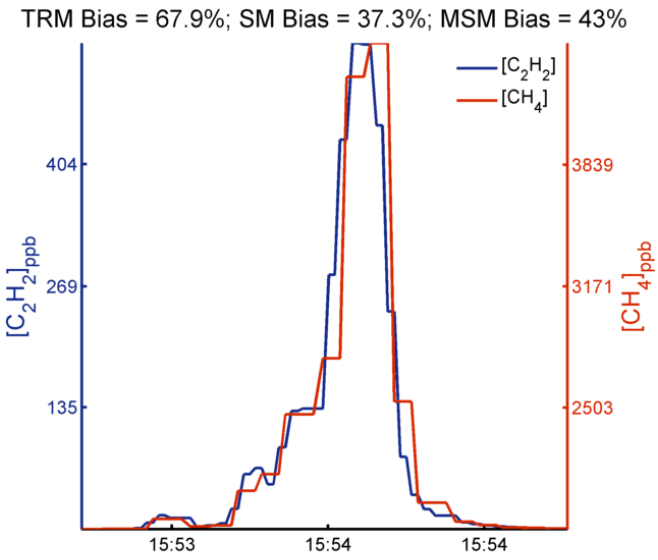
TRM Bias = 67.9%; SM Bias = 37.3%; MSM Bias = 43%
[C2H2]
[CH4]
404
269
135
3839
3171
2503
[C2H2]ppb
[CH4]ppb
15:53
15:54
15:54

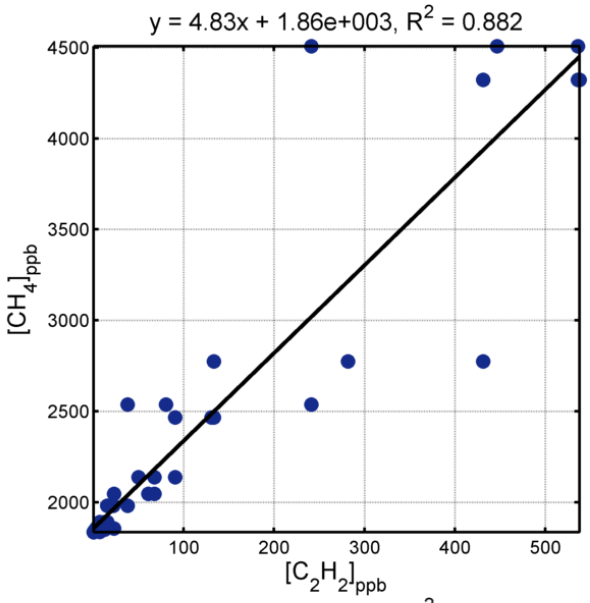
y = 4.83x + 1.86e+003, R2 = 0.882
4500
4000
3500
3000
2500
2000
100
200
300
400
500
[CH4]ppb
[C2H2]ppb

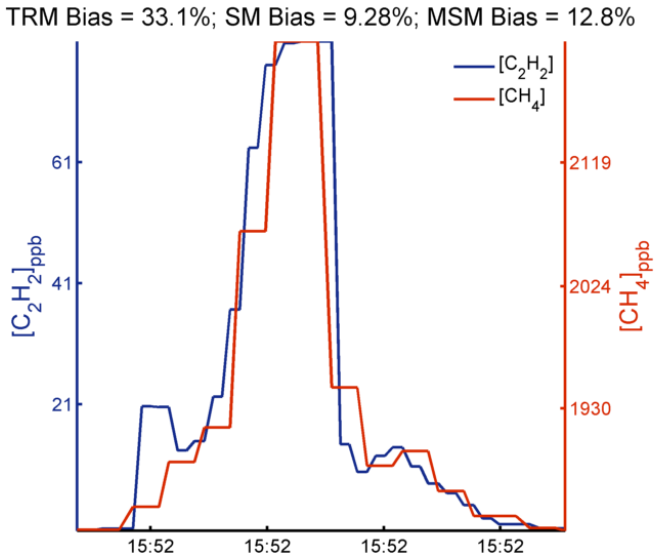
TRM Bias = 33.1%; SM Bias = 9.28%; MSM Bias = 12.8%
[C2H2]
[CH4]
61
41
21
2119
2024
1930
[C2H2]ppb
[CH4]ppb
15:52
15:52
15:52
15:52

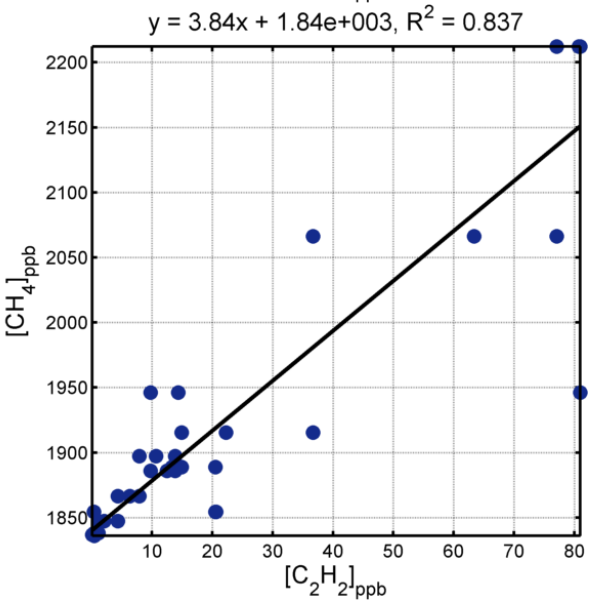
y = 3.84x + 1.84e+003, R2 = 0.837
2200
2150
2100
2050
2000
1950
1900
1850
10
20
30
40
50
60
70
80
[CH4]ppb
[C2H2]ppb

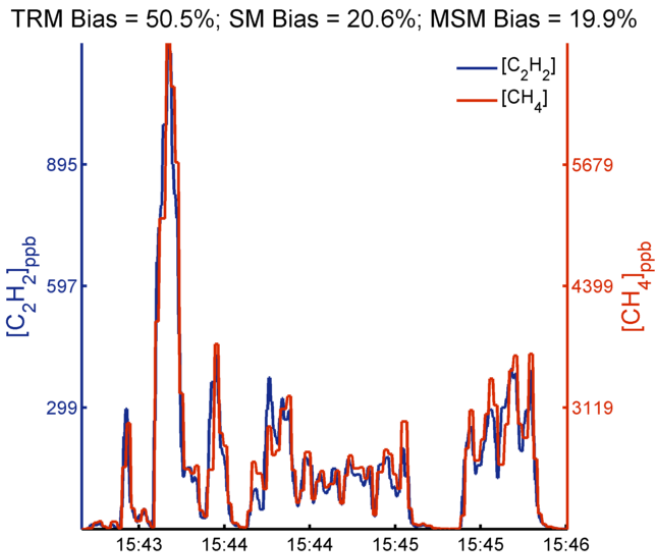
TRM Bias = 50.5%; SM Bias = 20.6%; MSM Bias = 19.9%
[C2H2]
[CH4]
895
597
299
5679
4399
3119
[C2H2]ppb
[CH4]ppb
15:43
15:44
15:44
15:45
15:45
15:46

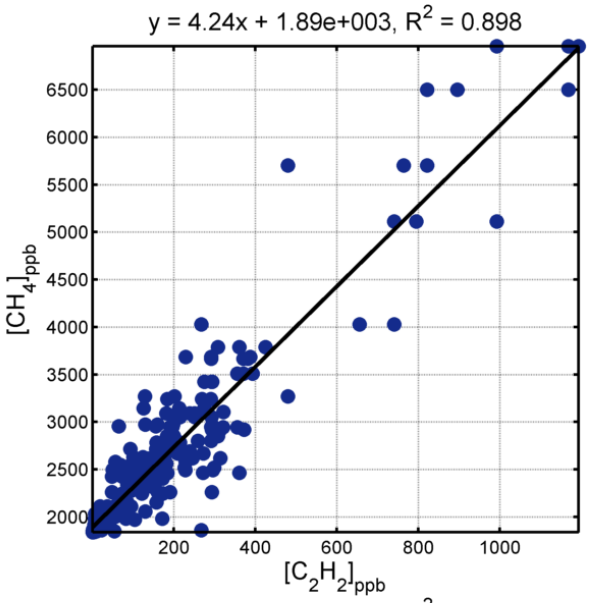
y = 4.24x + 1.89e+003, R2 = 0.898
6500
6000
5500
5000
4500
4000
3500
3000
2500
2000
200
400
600
800
1000
[CH4]ppb
[C2H2]ppb

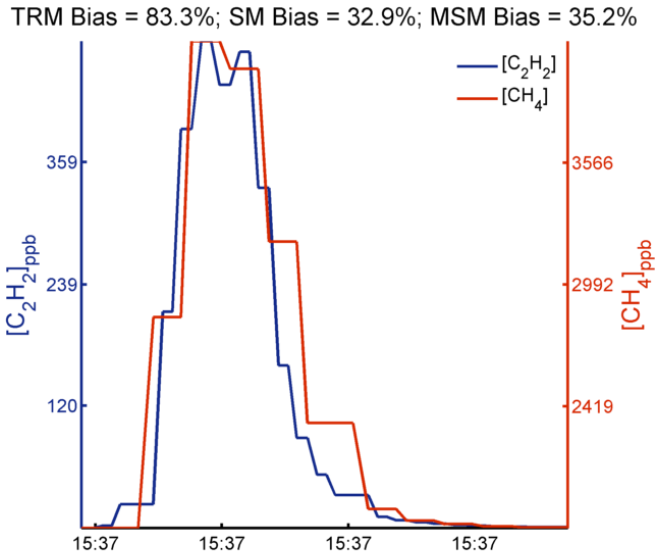
TRM Bias = 83.3%; SM Bias = 32.9%; MSM Bias = 35.2%
[C2H2]
[CH4]
359
239
120
3566
2992
2419
[C2H2]ppb
[CH4]ppb
15:37
15:37
15:37
15:37

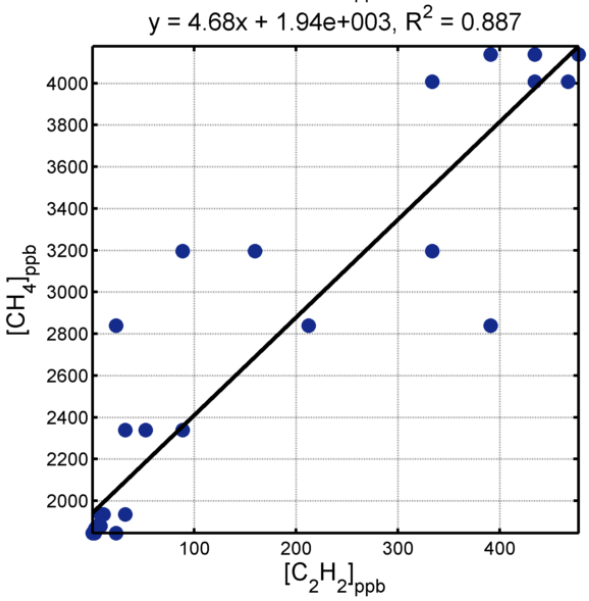
y = 4.68x + 1.94e+003, R2 = 0.887
4000
3800
3600
3400
3200
3000
2800
2600
2400
2200
2000
100
200
300
400
[CH4]ppb
[C2H2]ppb

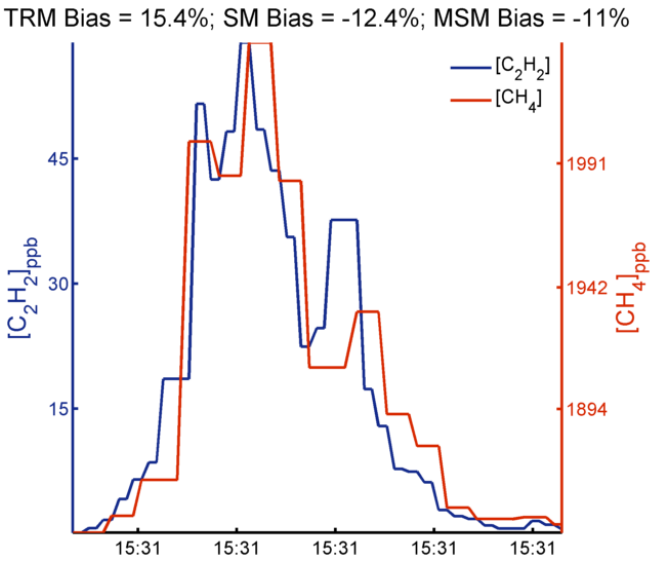
TRM Bias = 15.4%; SM Bias = -12.4%; MSM Bias = -11%
[C2H2]
[CH4]
45
30
15
1991
1942
1894
[C2H2]ppb
[CH4]ppb
15:31
15:31
15:31
15:31
15:31

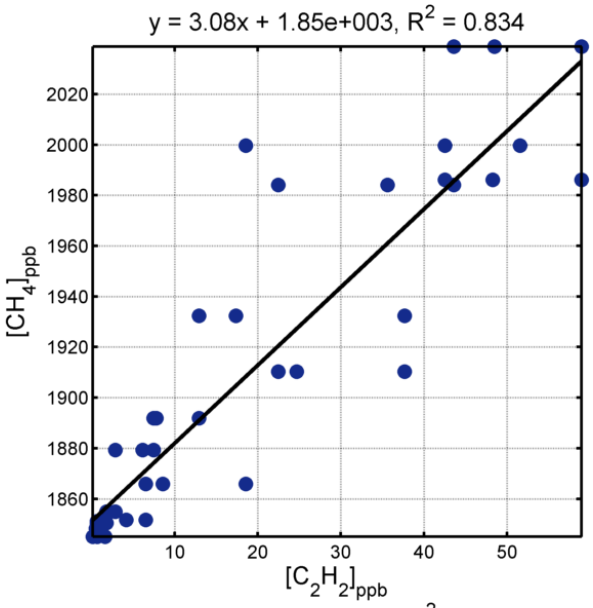
y = 3.08x + 1.85e+003, R2 = 0.834
2020
2000
1980
1960
1940
1920
1900
1880
1860
10
20
30
40
50
[CH4]ppb
[C2H2]ppb

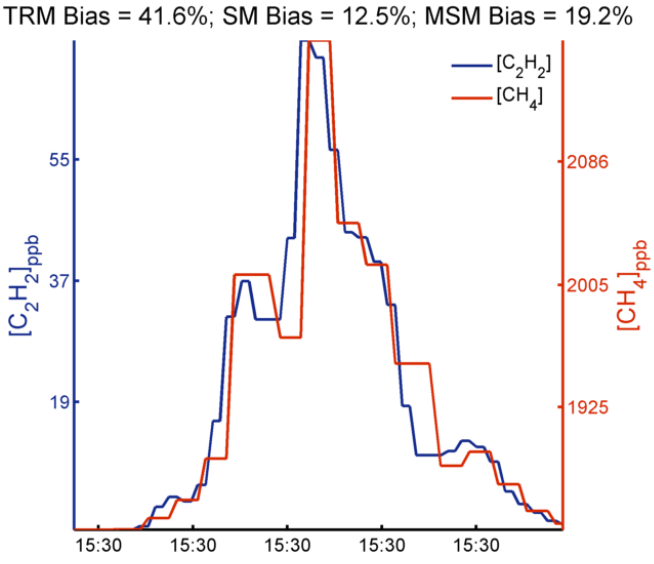
TRM Bias = 41.6%; SM Bias = 12.5%; MSM Bias = 19.2%
[C2H2]
[CH4]
55
37
19
2086
2005
1925
[C2H2]ppb
[CH4]ppb
15:30
15:30
15:30
15:30
15:30

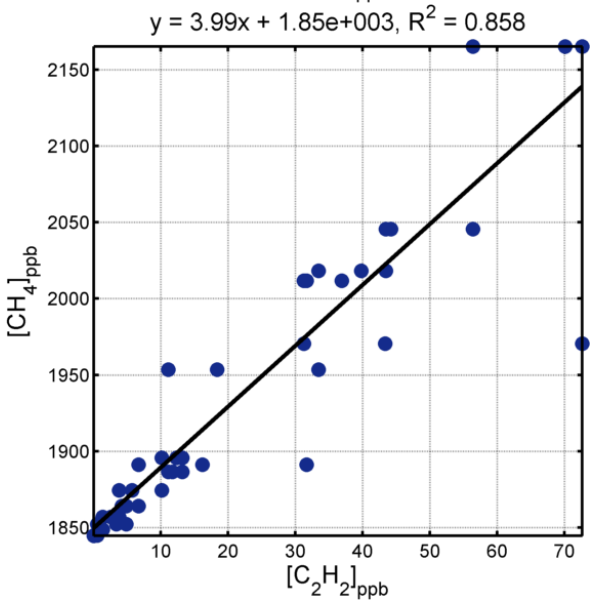
y = 3.99x + 1.85e+003, R2 = 0.858
2150
2100
2050
2000
1950
1900
1850
10
20
30
40
50
60
70
[CH4]ppb
[C2H2]ppb

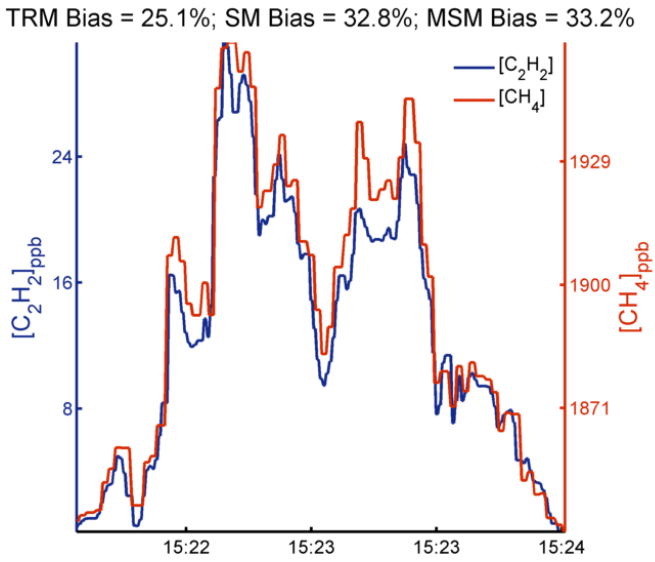
TRM Bias = 25.1%; SM Bias = 32.8%; MSM Bias = 33.2%
[C2H2]
[CH4]
[C2H2]ppb
[CH4]ppb
24
16
8
1929
1900
1871
15:22
15:23
15:23
15:24

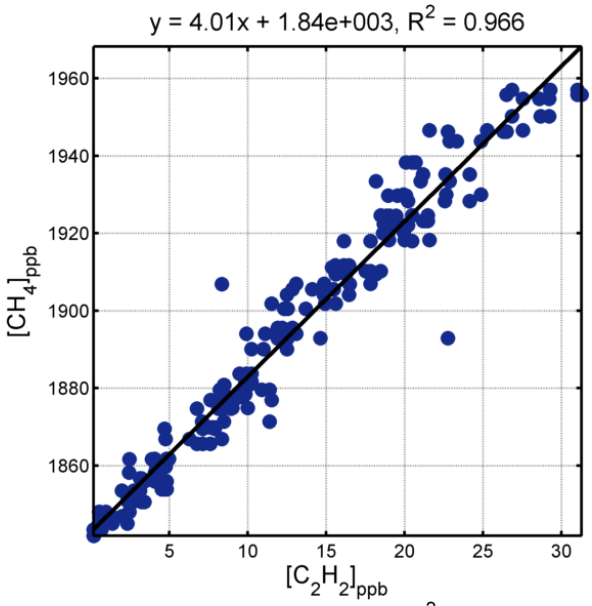
y = 4.01x + 1.84e+003, R2 = 0.966
[CH4]ppb
[C2H2]ppb
1960
1940
1920
1900
1880
1860
5
10
15
20
25
30

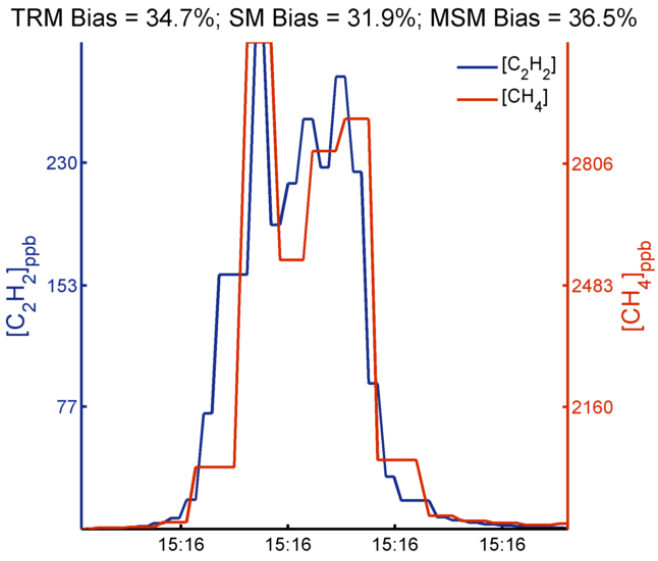
TRM Bias = 34.7%; SM Bias = 31.9%; MSM Bias = 36.5%
[C2H2]
[CH4]
[C2H2]ppb
[CH4]ppb
230
153
77
2806
2483
2160
15:16
15:16
15:16
15:16

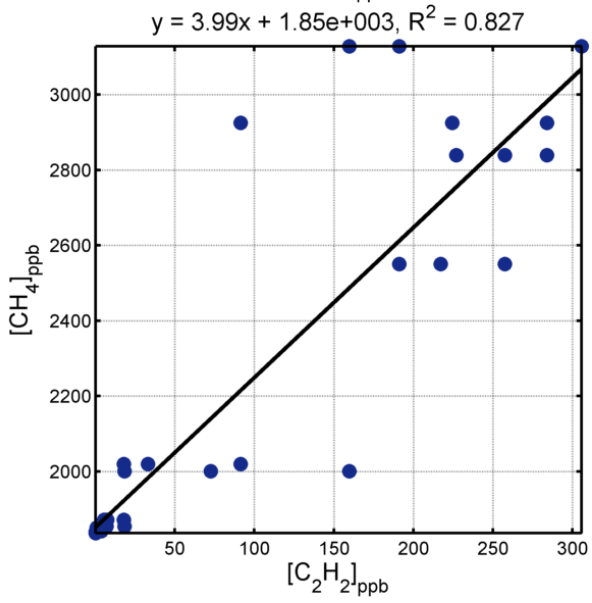
y = 3.99x + 1.85e+003, R2 = 0.827
[CH4]ppb
[C2H2]ppb
3000
2800
2600
2400
2200
2000
50
100
150
200
250
300

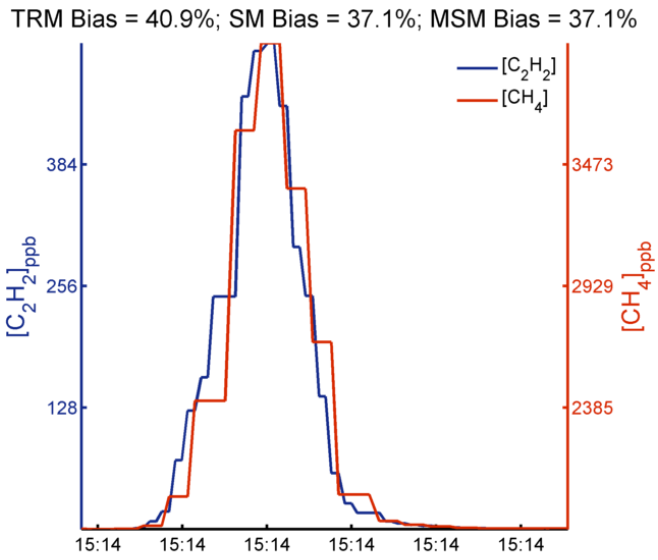
TRM Bias = 40.9%; SM Bias = 37.1%; MSM Bias = 37.1%
[C2H2]
[CH4]
384
256
128
3473
2929
2385
[C2H2]ppb
[CH4]ppb
15:14
15:14
15:14
15:14
15:14
15:14

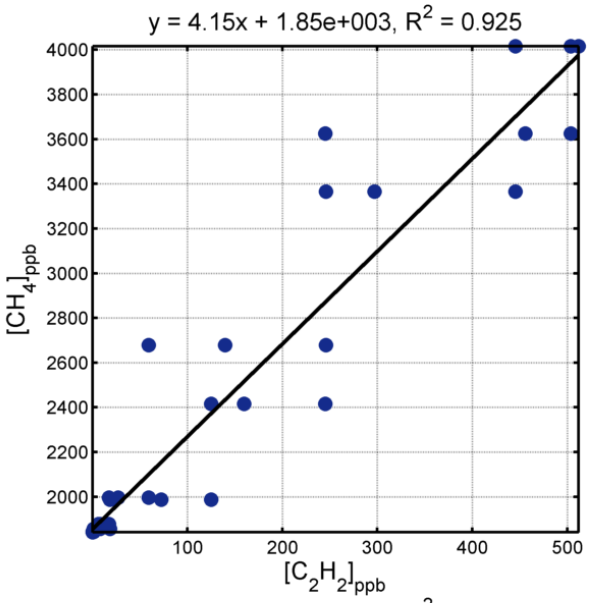
y = 4.15x + 1.85e+003, R2 = 0.925
4000
3800
3600
3400
3200
3000
2800
2600
2400
2200
2000
100
200
300
400
500
[CH4]ppb
[C2H2]ppb

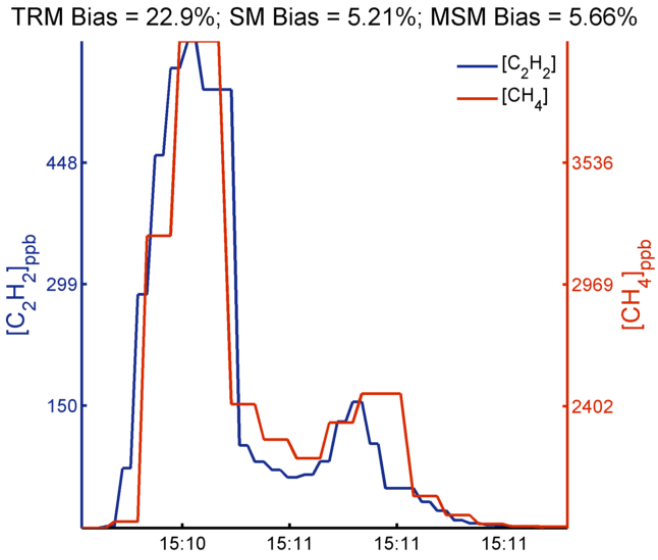
TRM Bias = 22.9%; SM Bias = 5.21%; MSM Bias = 5.66%
[C2H2]
[CH4]
448
299
150
3536
2969
2402
[C2H2]ppb
[CH4]ppb
15:10
15:11
15:11
15:11

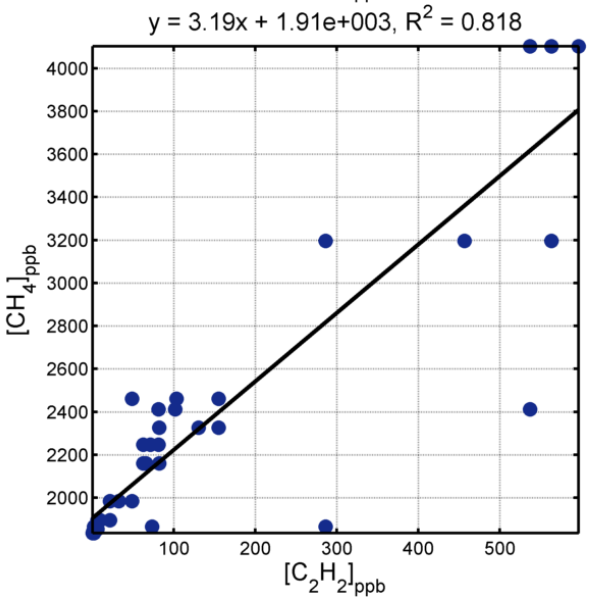
y = 3.19x + 1.91e+003, R2 = 0.818
4000
3800
3600
3400
3200
3000
2800
2600
2400
2200
2000
100
200
300
400
500
[CH4]ppb
[C2H2]ppb

11 July 2013

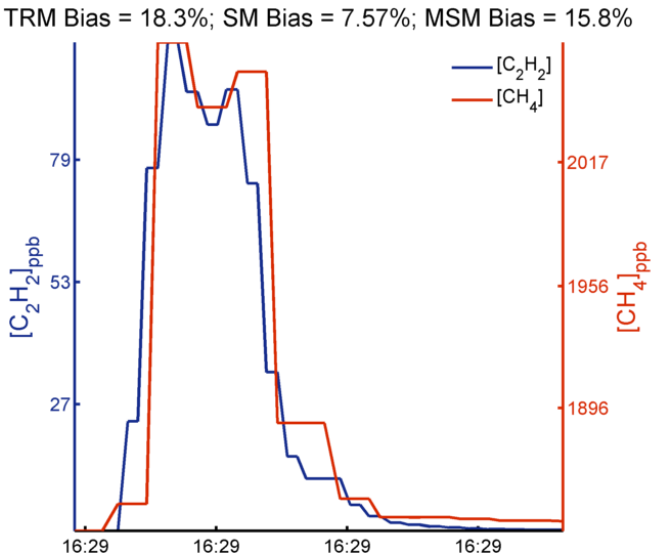
TRM Bias = 18.3%; SM Bias = 7.57%; MSM Bias = 15.8%
[C2H2]
[CH4]
79
53
27
2017
1956
1896
[C2H2]ppb
[CH4]ppb
16:29
16:29
16:29
16:29

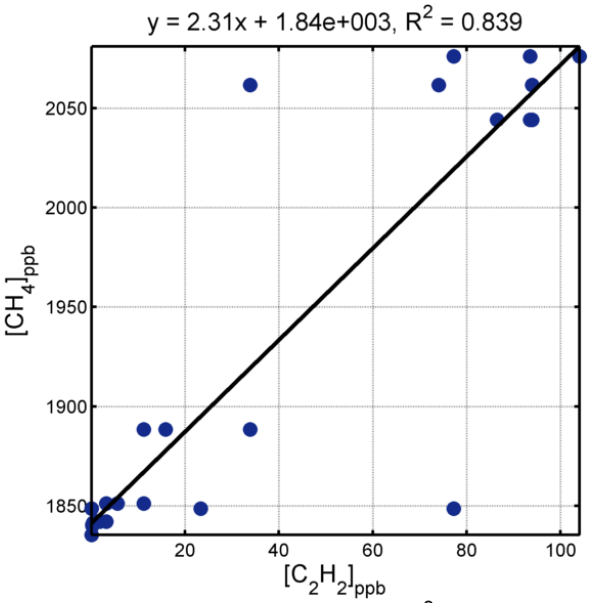
y = 2.31x + 1.84e+003, R2 = 0.839
2050
2000
1950
1900
1850
20
40
60
80
100
[CH4]ppb
[C2H2]ppb

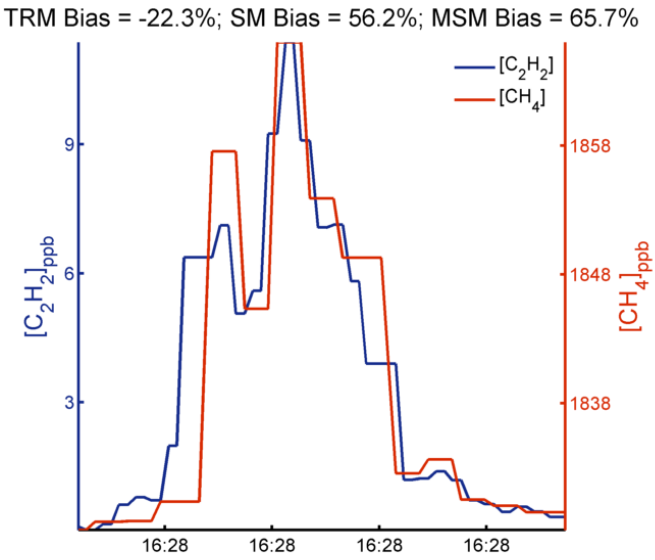
TRM Bias = -22.3%; SM Bias = 56.2%; MSM Bias = 65.7%
[C2H2]
[CH4]
9
6
3
1858
1848
1838
[C2H2]ppb
[CH4]ppb
16:28
16:28
16:28
16:28

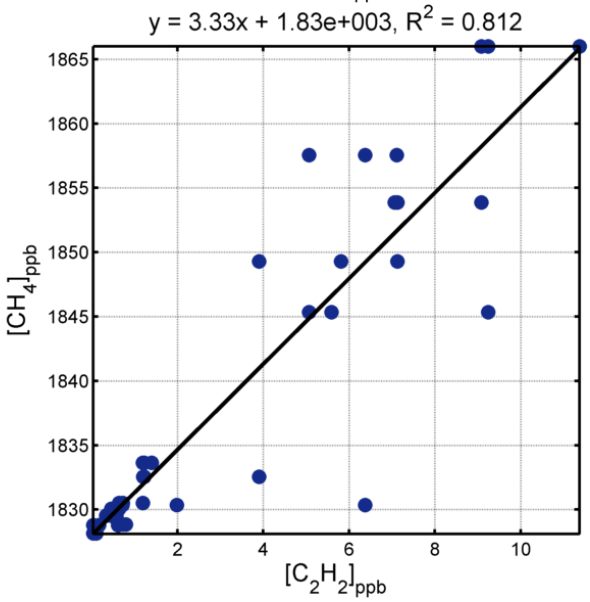
y = 3.33x + 1.83e+003, R2 = 0.812
1865
1860
1855
1850
1845
1840
1835
1830
2
4
6
8
10
[CH4]ppb
[C2H2]ppb

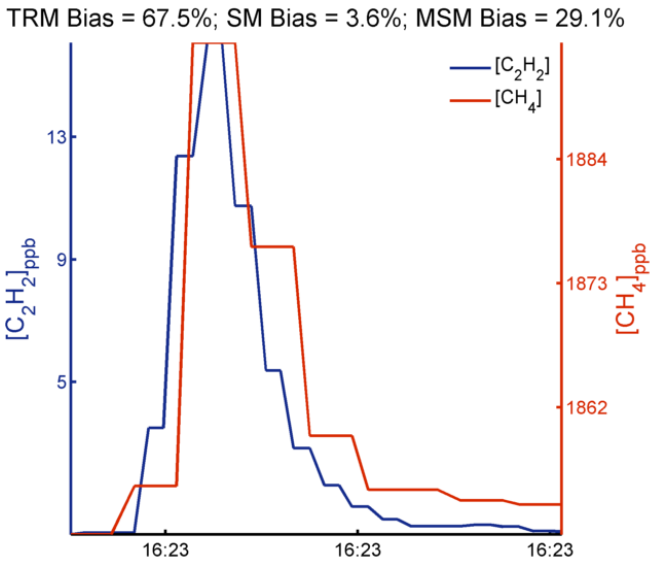
TRM Bias = 67.5%; SM Bias = 3.6%; MSM Bias = 29.1%
[C2H2]
[CH4]
[C2H2]ppb
[CH4]ppb
13
9
5
1884
1873
1862
16:23
16:23
16:23

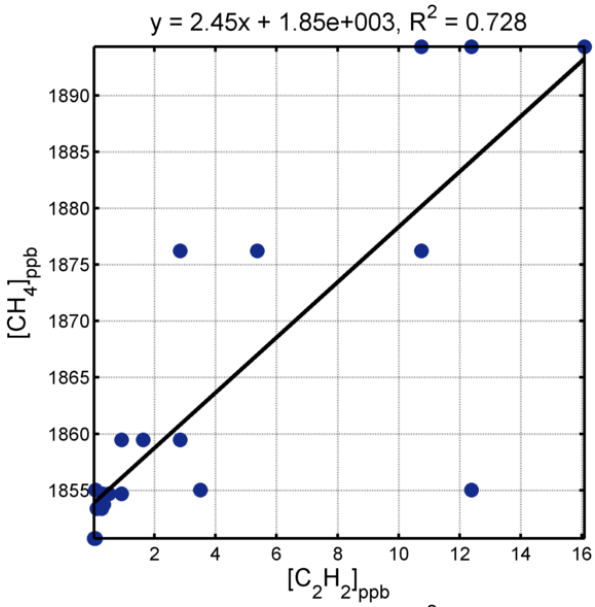
y = 2.45x + 1.85e+003, R2 = 0.728
[CH4]ppb
[C2H2]ppb
1890
1885
1880
1875
1870
1865
1860
1855
2
4
6
8
10
12
14
16

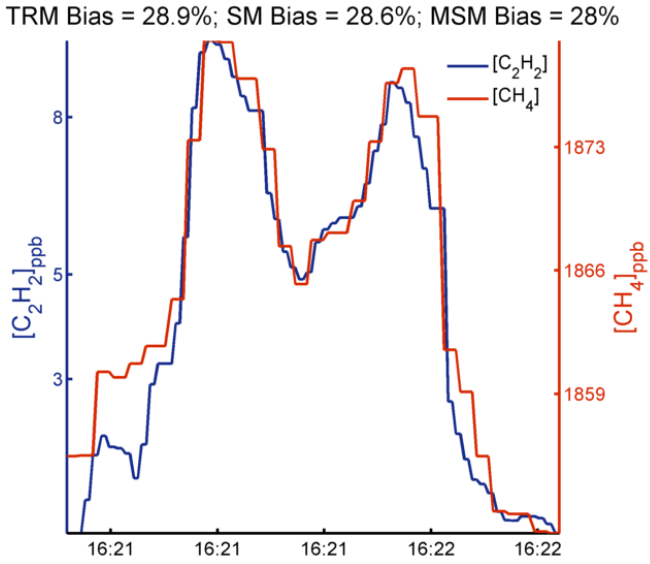
TRM Bias = 28.9%; SM Bias = 28.6%; MSM Bias = 28%
[C2H2]
[CH4]
[C2H2]ppb
[CH4]ppb
8
5
3
1873
1866
1859
16:21
16:21
16:21
16:22
16:22

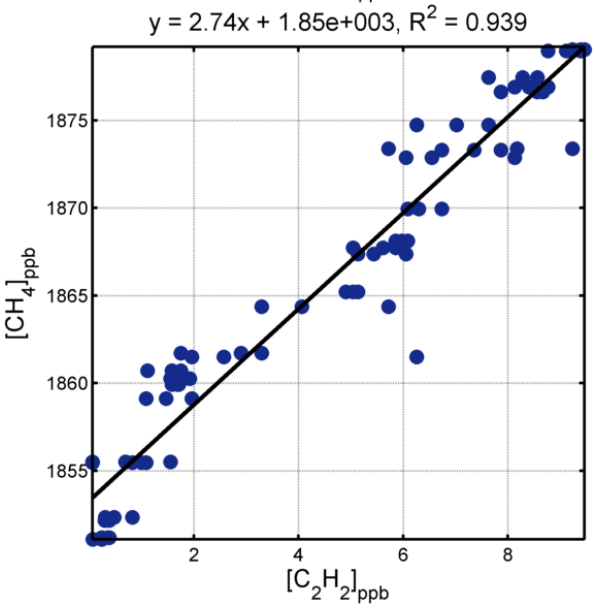
y = 2.74x + 1.85e+003, R2 = 0.939
[CH4]ppb
[C2H2]ppb
1875
1870
1865
1860
1855
2
4
6
8

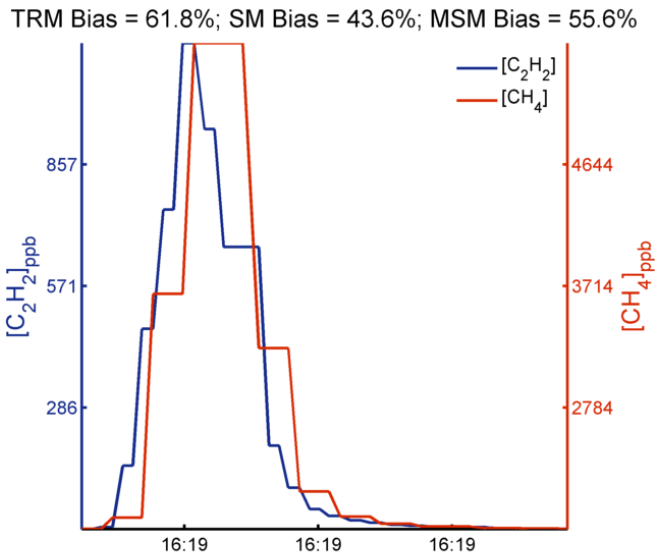
TRM Bias = 61.8%; SM Bias = 43.6%; MSM Bias = 55.6%
[C2H2]
[CH4]
857
571
286
4644
3714
2784
[C2H2]ppb
[CH4]ppb
16:19
16:19
16:19

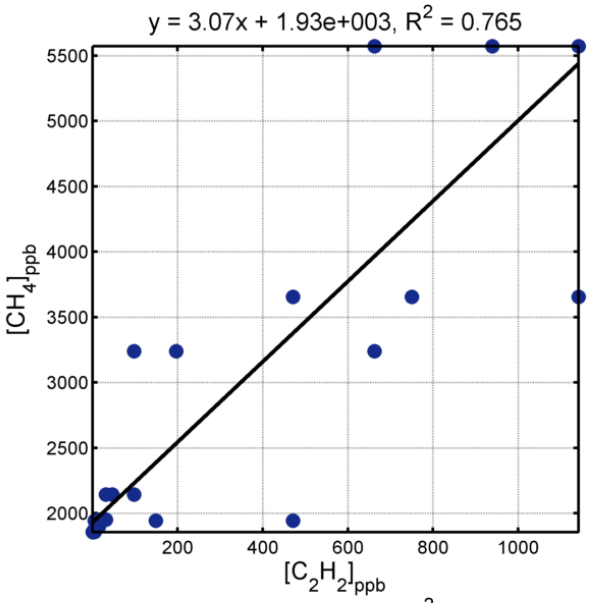
y = 3.07x + 1.93e+003, R2 = 0.765
5500
5000
4500
4000
3500
3000
2500
2000
200
400
600
800
1000
[CH4]ppb
[C2H2]ppb

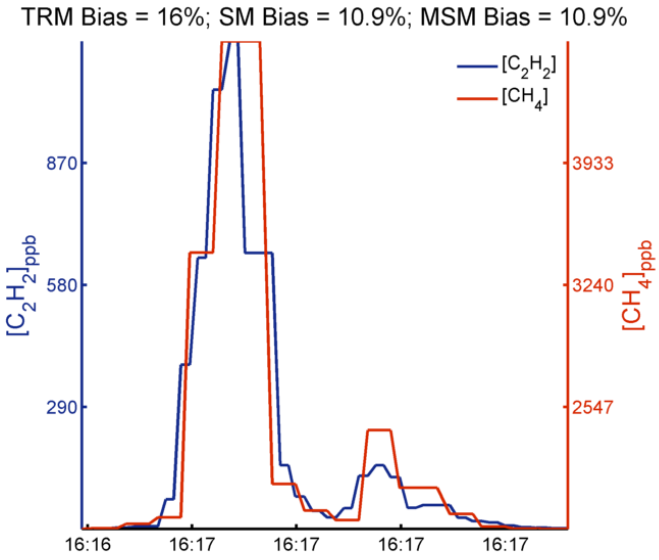
TRM Bias = 16%; SM Bias = 10.9%; MSM Bias = 10.9%
[C2H2]
[CH4]
870
580
290
3933
3240
2547
[C2H2]ppb
[CH4]ppb
16:16
16:17
16:17
16:17
16:17

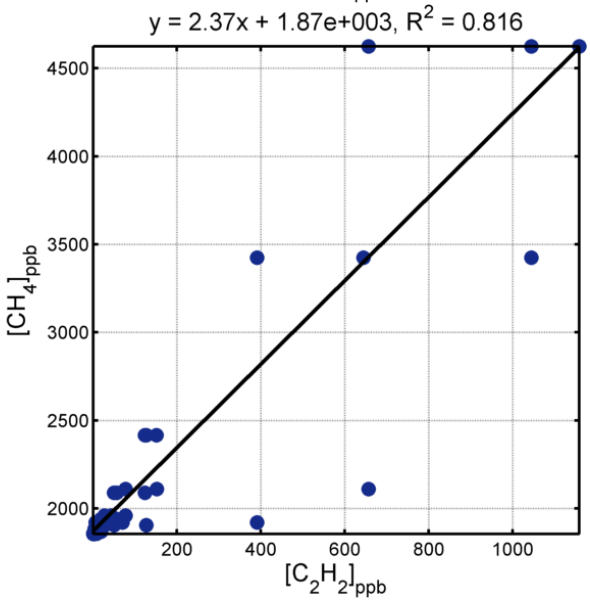
y = 2.37x + 1.87e+003, R2 = 0.816
4500
4000
3500
3000
2500
2000
200
400
600
800
1000
[CH4]ppb
[C2H2]ppb

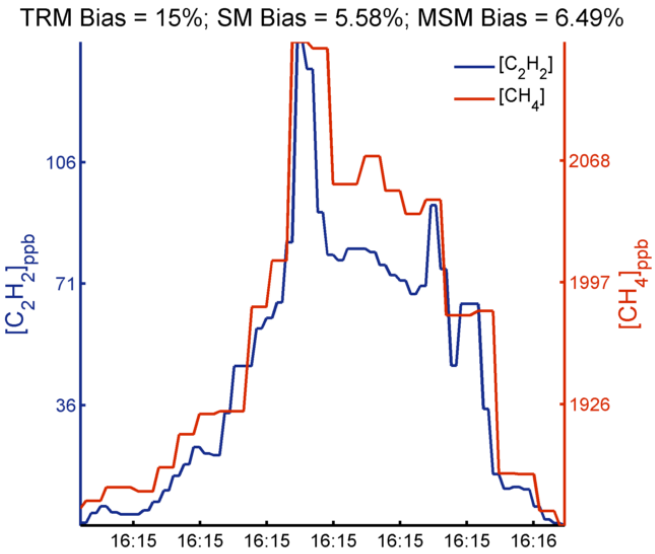
TRM Bias = 15%; SM Bias = 5.58%; MSM Bias = 6.49%
[C2H2]
[CH4]
106
71
36
2068
1997
1926
[C2H2]ppb
[CH4]ppb
16:15
16:15
16:15
16:15
16:15
16:15
16:16

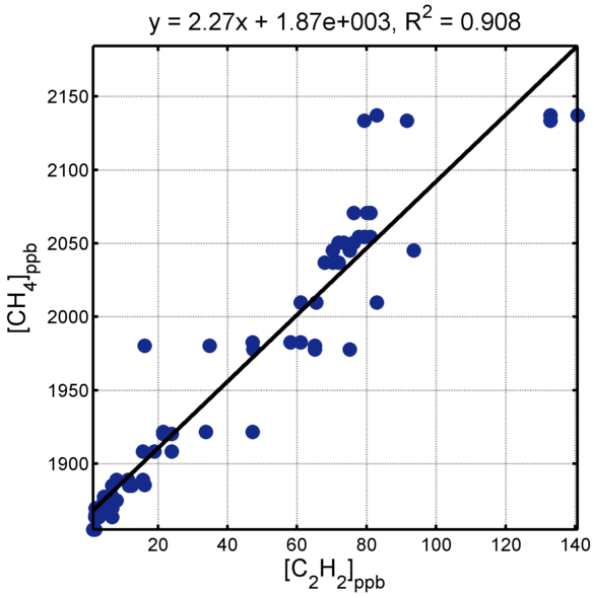
y = 2.27x + 1.87e+003, R2 = 0.908
2150
2100
2050
2000
1950
1900
20
40
60
80
100
120
140
[CH4]ppb
[C2H2]ppb

20 August 2013

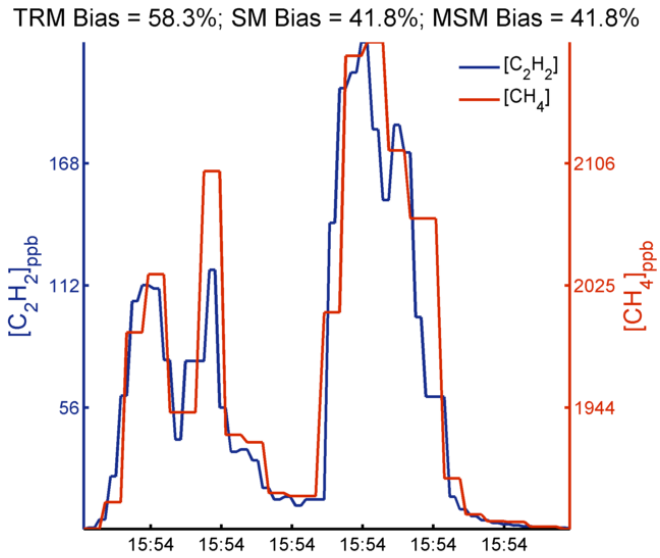

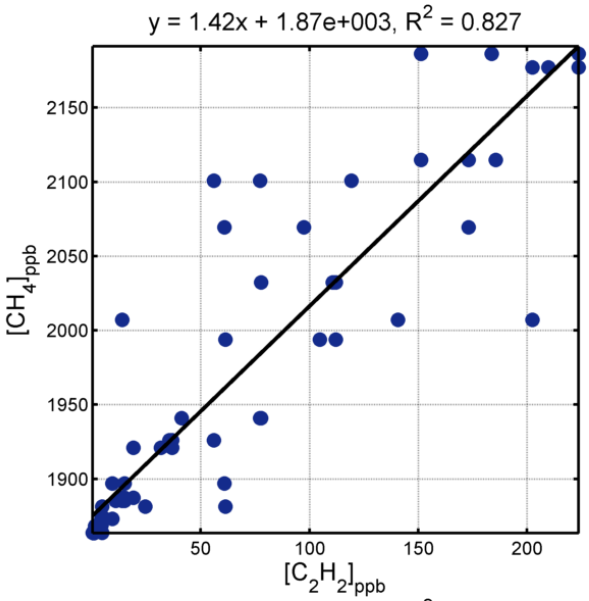

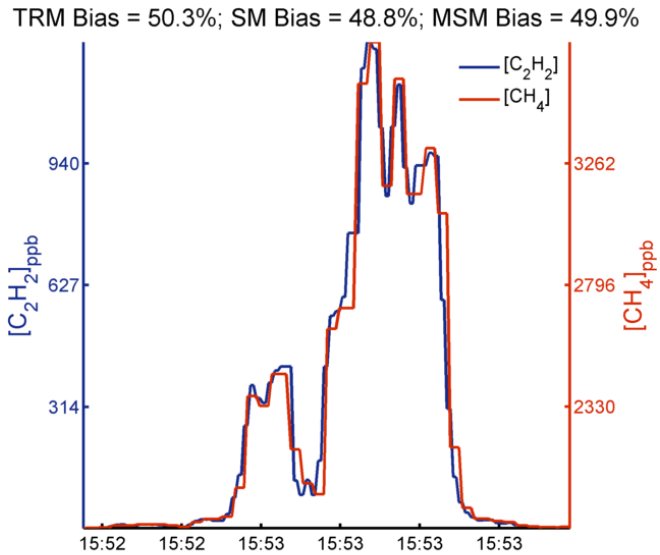

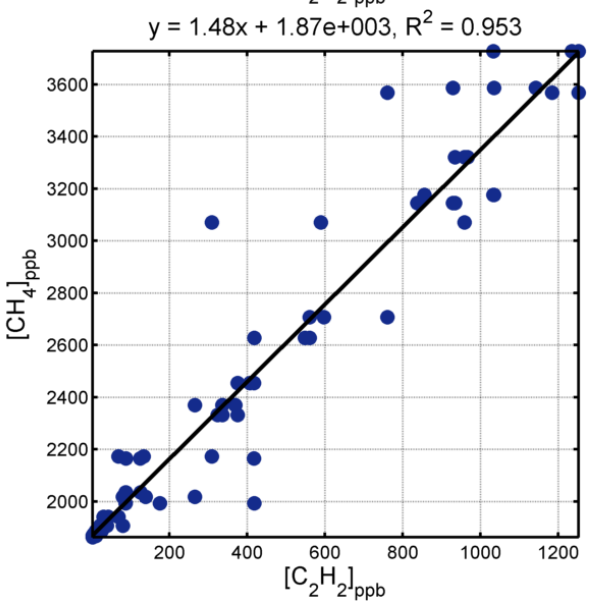

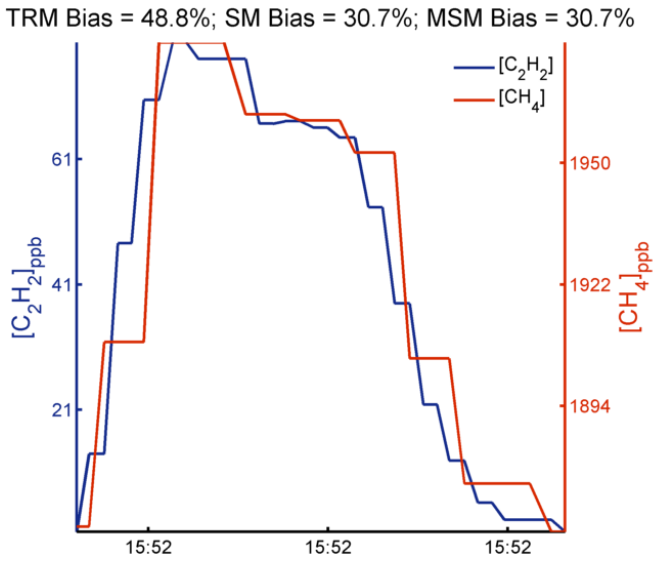
TRM Bias = 48.8%; SM Bias = 30.7%; MSM Bias = 30.7%
[C2H2]
[CH4]
61
41
21
1950
1922
1894
[C2H2]ppb
[CH4]ppb
15:52
15:52
15:52

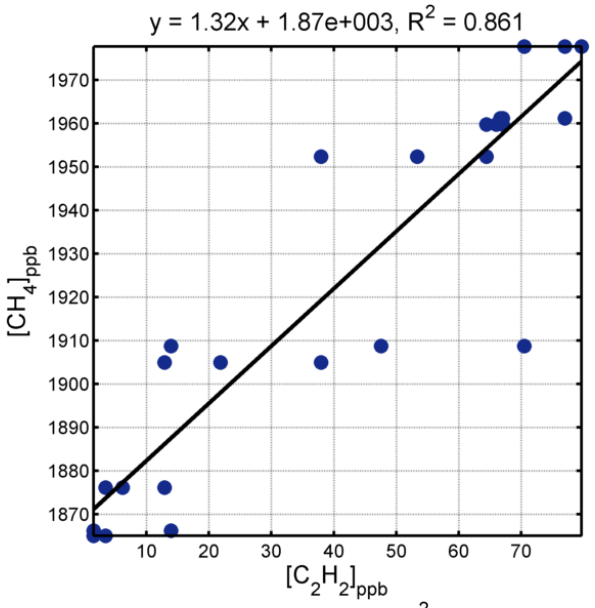
y = 1.32x + 1.87e+003, R2 = 0.861
1970
1960
1950
1940
1930
1920
1910
1900
1890
1880
1870
10
20
30
40
50
60
70
[CH4]ppb
[C2H2]ppb

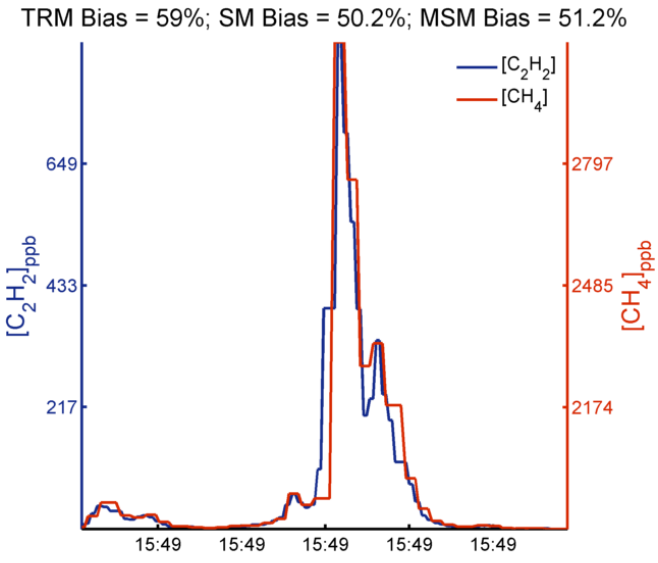
TRM Bias = 59%; SM Bias = 50.2%; MSM Bias = 51.2%
[C2H2]
[CH4]
649
433
217
2797
2485
2174
[C2H2]ppb
[CH4]ppb
15:49
15:49
15:49
15:49
15:49

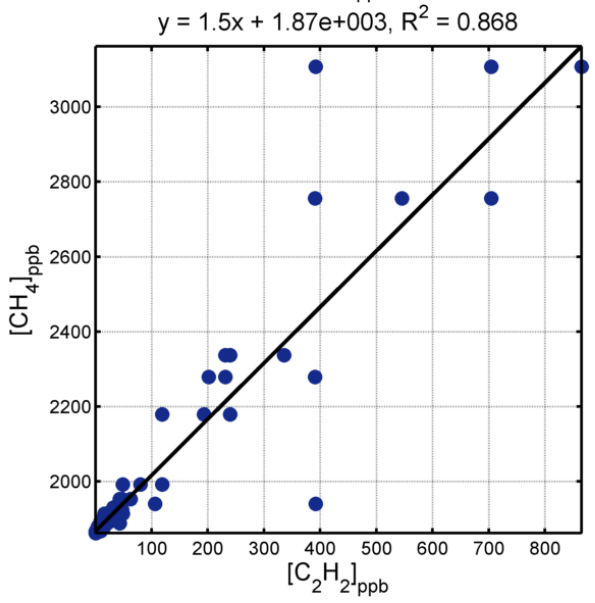
y = 1.5x + 1.87e+003, R2 = 0.868
3000
2800
2600
2400
2200
2000
100
200
300
400
500
600
700
800
[CH4]ppb
[C2H2]ppb

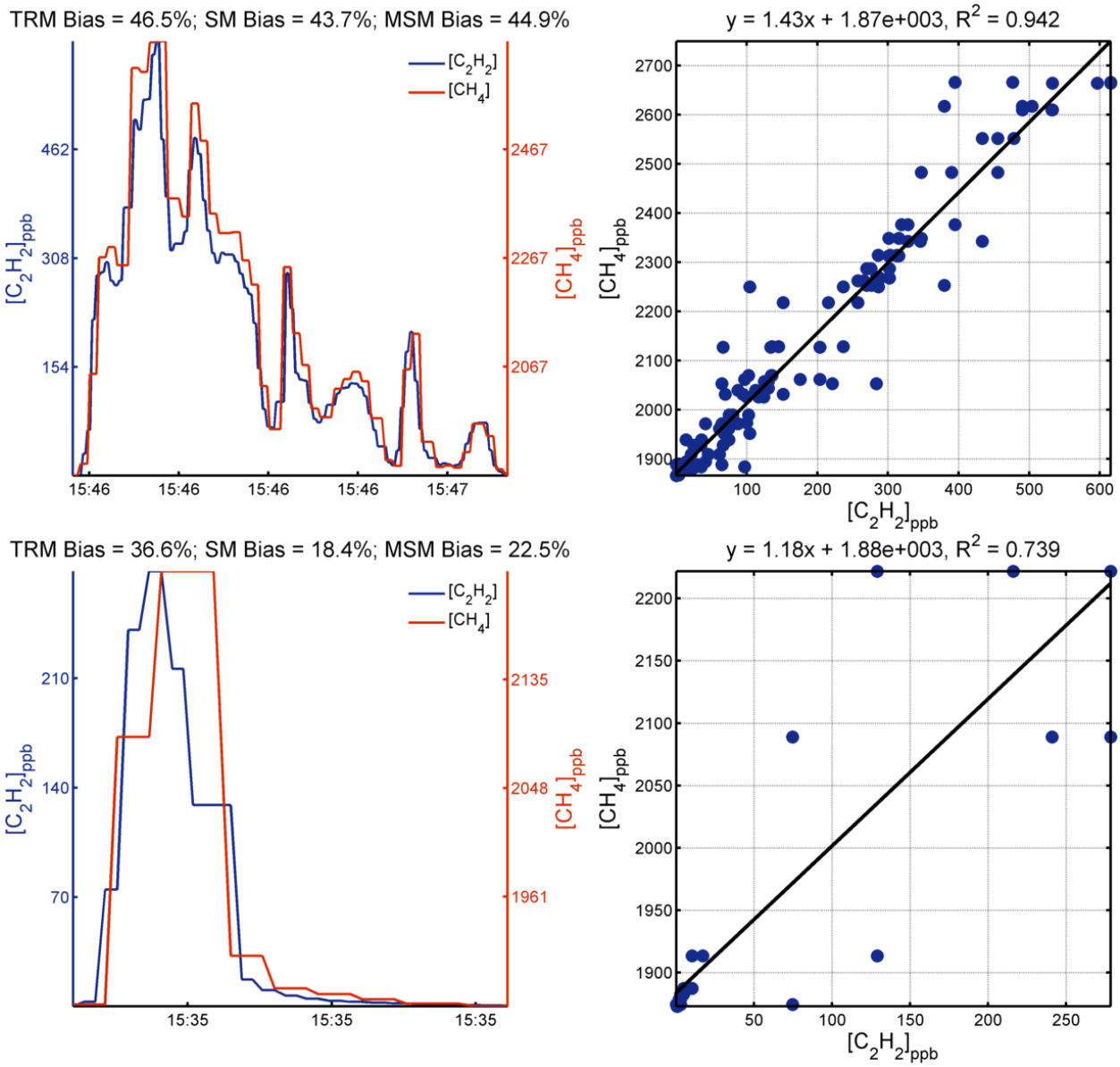
TRM Bias = 46.5%; SM Bias = 43.7%; MSM Bias = 44.9%
[C2H2]
[CH4]
462
308
154
2467
2267
2067
[C2H2]ppb
[CH4]ppb
15:46
15:46
15:46
15:46
15:47
y = 1.43x + 1.87e+003, R2 = 0.942
2700
2600
2500
2400
2300
2200
2100
2000
1900
100
200
300
400
500
600
[CH4]ppb
[C2H2]ppb
TRM Bias = 36.6%; SM Bias = 18.4%; MSM Bias = 22.5%
[C2H2]
[CH4]
210
140
70
2135
2048
1961
[C2H2]ppb
[CH4]ppb
15:35
15:35
15:35
y = 1.18x + 1.88e+003, R2 = 0.739
2200
2150
2100
2050
2000
1950
1900
50
100
150
200
250
[CH4]ppb
[C2H2]ppb

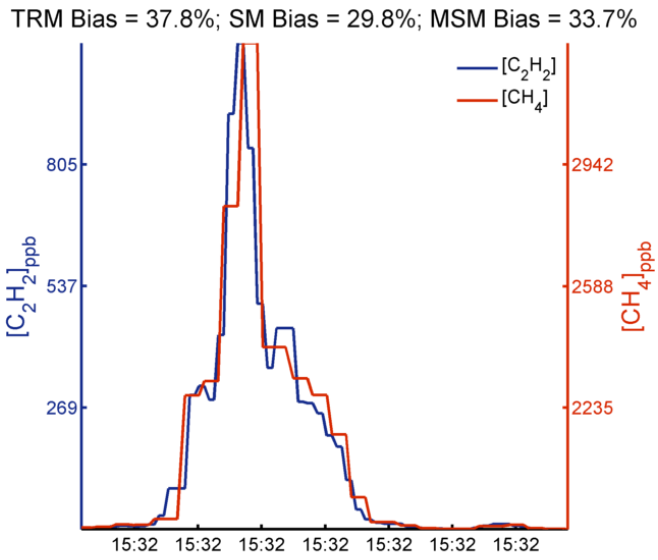
TRM Bias = 37.8%; SM Bias = 29.8%; MSM Bias = 33.7%
[C2H2]
[CH4]
805
537
269
2942
2588
2235
[C2H2]ppb
[CH4]ppb
15:32
15:32
15:32
15:32
15:32
15:32
15:32

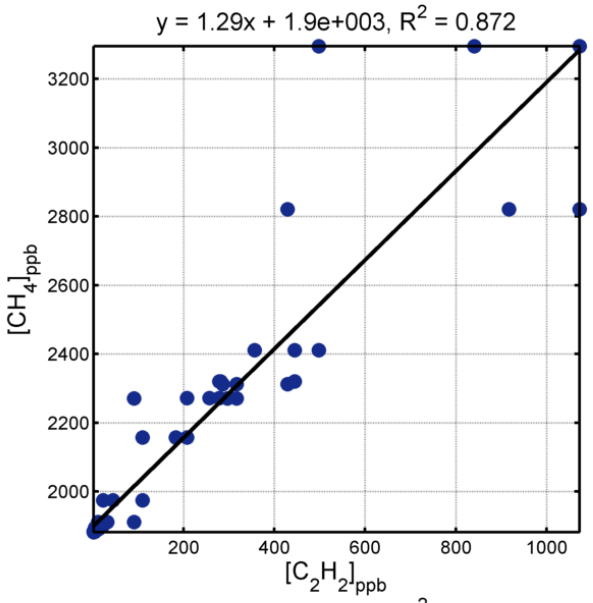
y = 1.29x + 1.9e+003, R2 = 0.872
3200
3000
2800
2600
2400
2200
2000
200
400
600
800
1000
[CH4]ppb
[C2H2]ppb

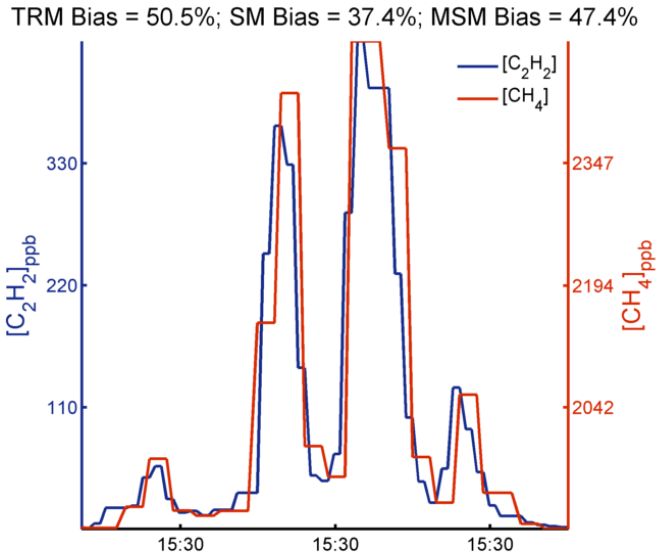
TRM Bias = 50.5%; SM Bias = 37.4%; MSM Bias = 47.4%
[C2H2]
[CH4]
330
220
110
2347
2194
2042
[C2H2]ppb
[CH4]ppb
15:30
15:30
15:30

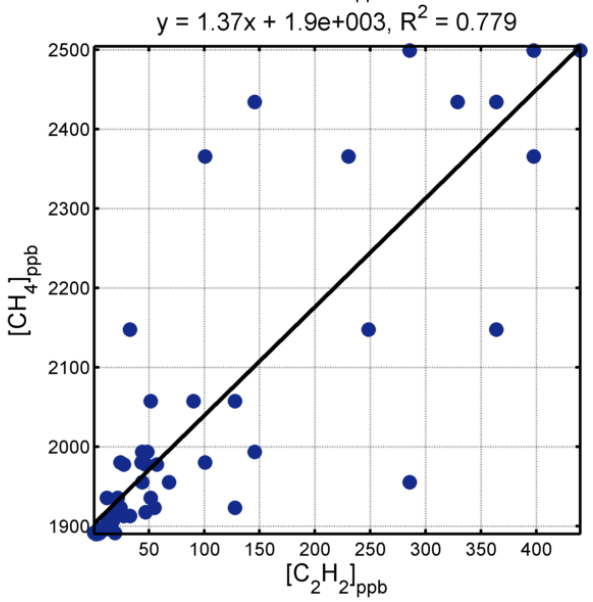
y = 1.37x + 1.9e+003, R2 = 0.779
2500
2400
2300
2200
2100
2000
1900
50
100
150
200
250
300
350
400
[CH4]ppb
[C2H2]ppb

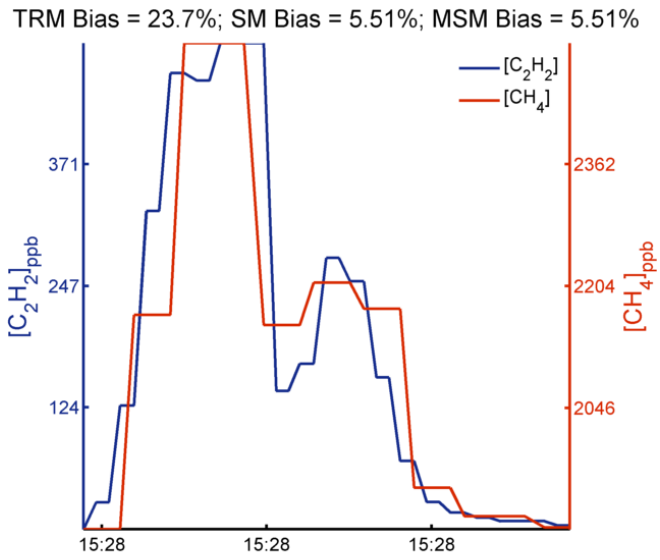
TRM Bias = 23.7%; SM Bias = 5.51%; MSM Bias = 5.51%
[C2H2]
[CH4]
371
247
124
2362
2204
2046
[C2H2]ppb
[CH4]ppb
15:28
15:28
15:28

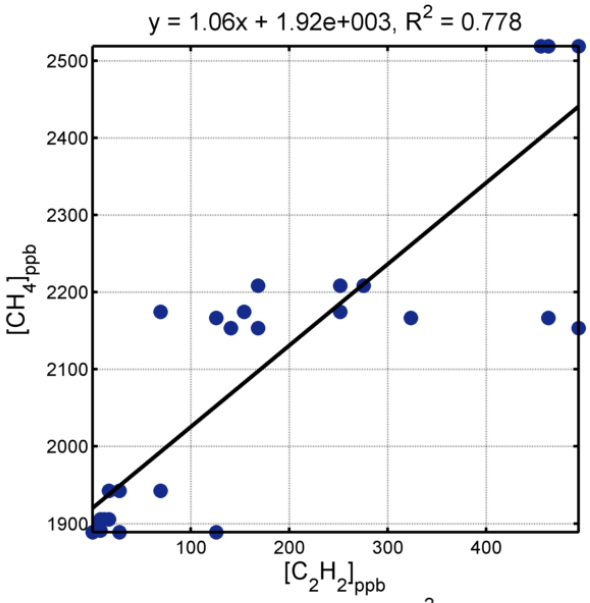
y = 1.06x + 1.92e+003, R2 = 0.778
2500
2400
2300
2200
2100
2000
1900
100
200
300
400
[CH4]ppb
[C2H2]ppb

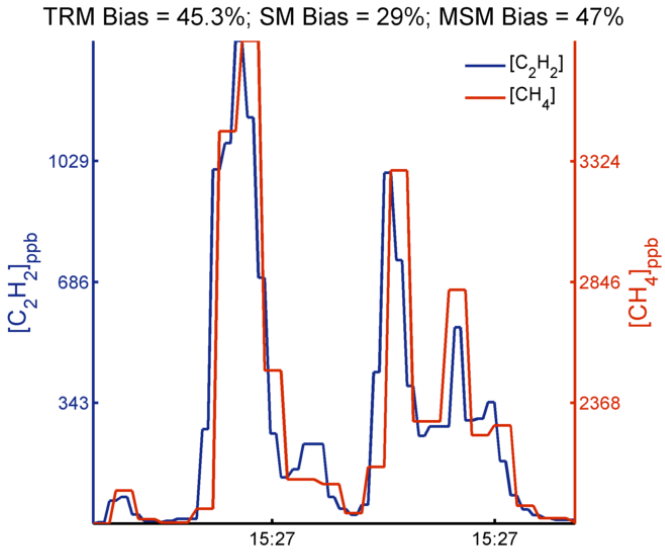
TRM Bias = 45.3%; SM Bias = 29%; MSM Bias = 47%
[C2H2]
[CH4]
1029
686
343
3324
2846
2368
[C2H2]ppb
[CH4]ppb
15:27
15:27

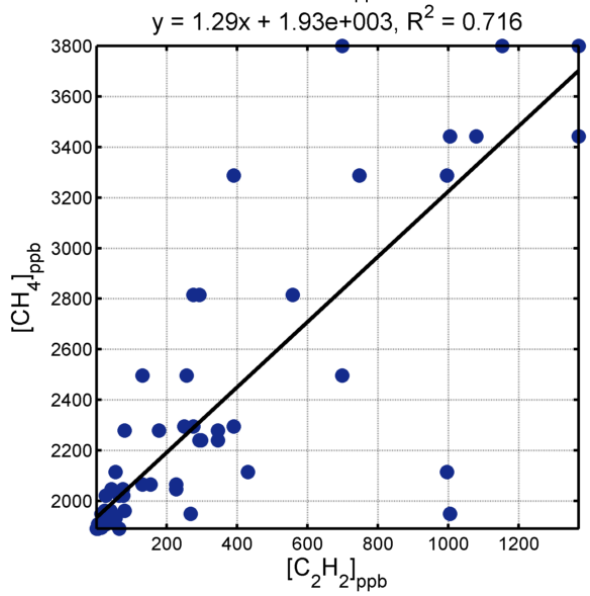
y = 1.29x + 1.93e+003, R2 = 0.716
3800
3600
3400
3200
3000
2800
2600
2400
2200
2000
200
400
600
800
1000
1200
[CH4]ppb
[C2H2]ppb

23 August 2013

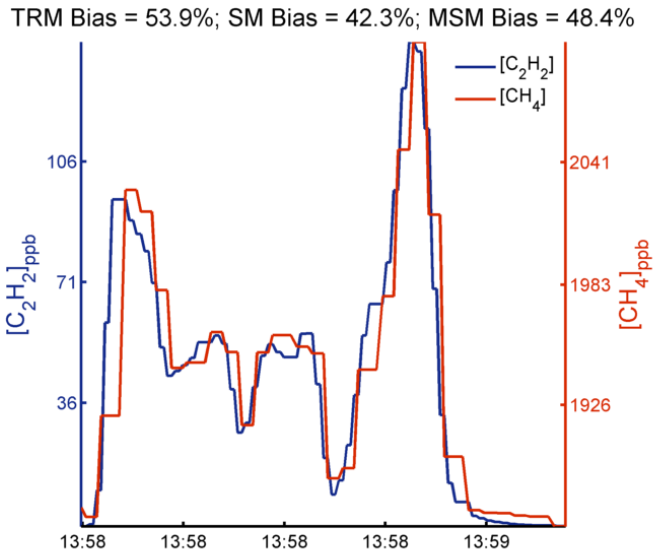

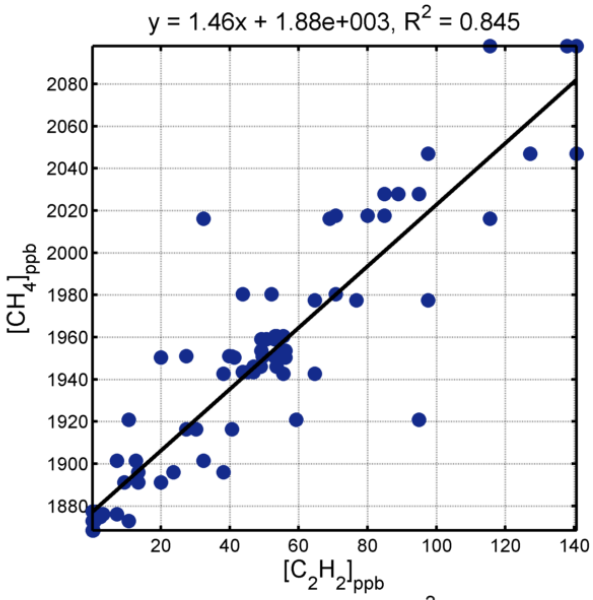

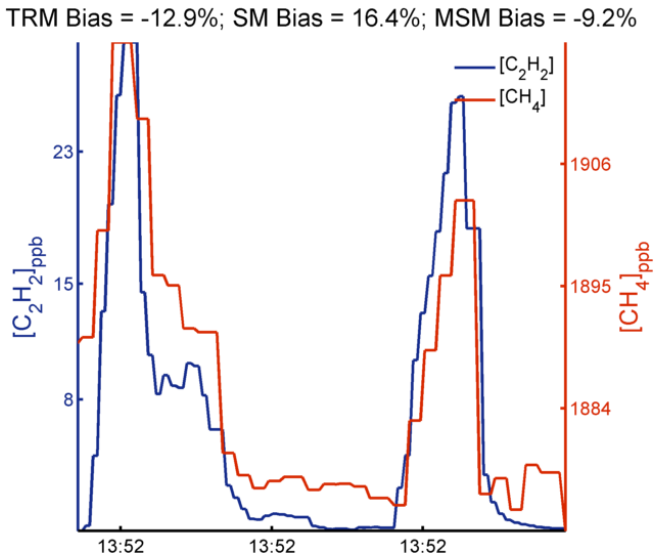

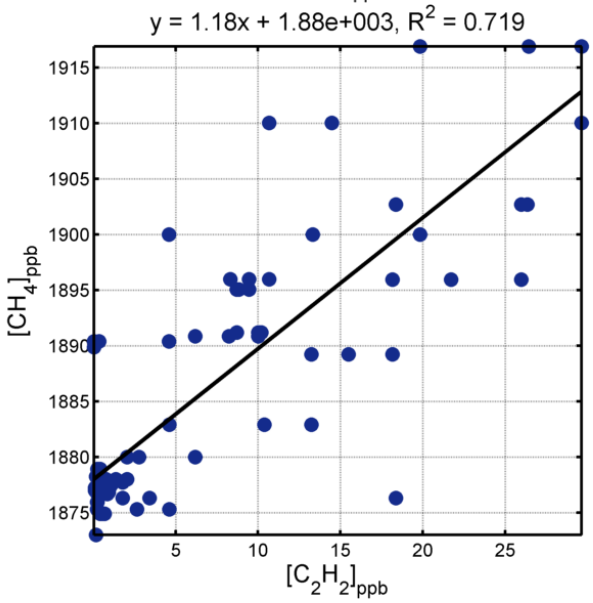

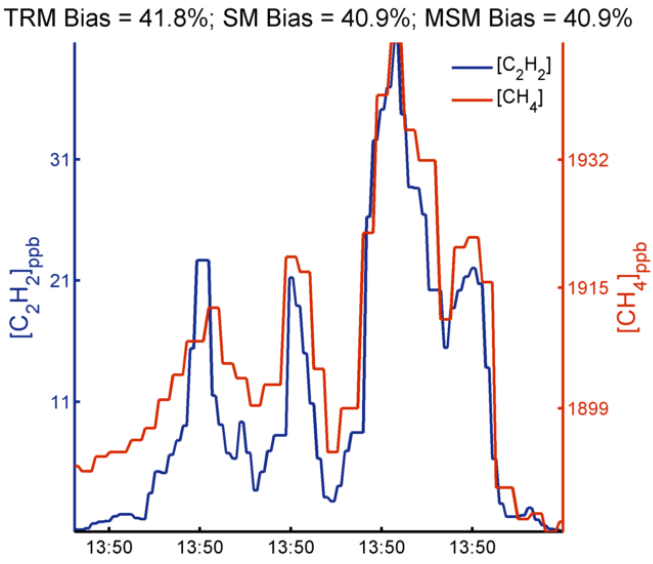
TRM Bias = 41.8%; SM Bias = 40.9%; MSM Bias = 40.9%
[C2H2]
[CH4]
[C2H2]ppb
[CH4]ppb
31
21
11
1932
1915
1899
13:50
13:50
13:50
13:50
13:50

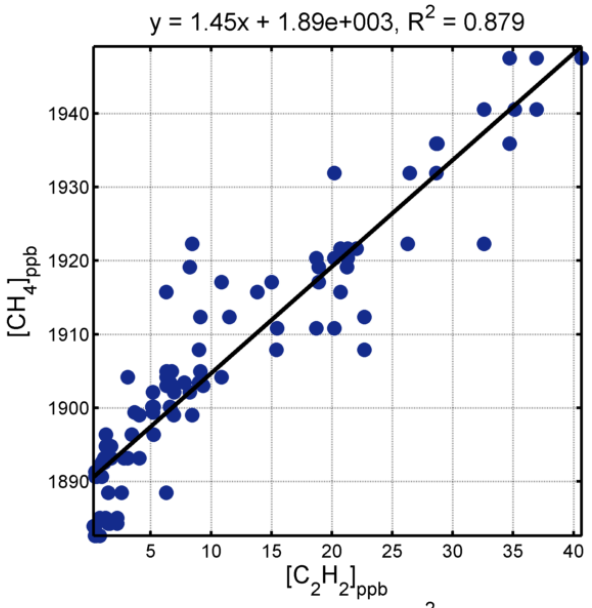
y = 1.45x + 1.89e+003, R2 = 0.879
[CH4]ppb
[C2H2]ppb
1940
1930
1920
1910
1900
1890
5
10
15
20
25
30
35
40

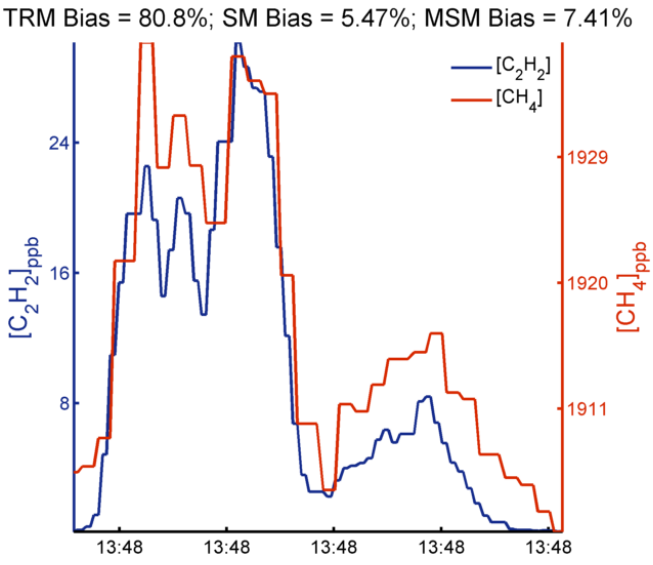
TRM Bias = 80.8%; SM Bias = 5.47%; MSM Bias = 7.41%
[C2H2]
[CH4]
[C2H2]ppb
[CH4]ppb
24
16
8
1929
1920
1911
13:48
13:48
13:48
13:48
13:48

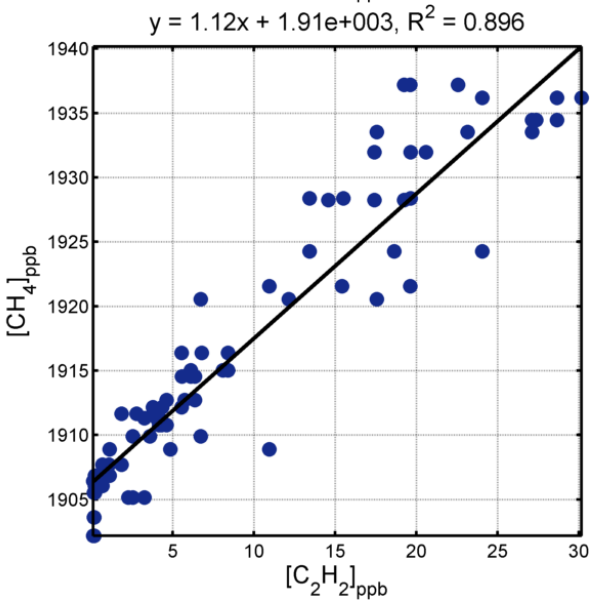
y = 1.12x + 1.91e+003, R2 = 0.896
[CH4]ppb
[C2H2]ppb
1940
1935
1930
1925
1920
1915
1910
1905
5
10
15
20
25
30

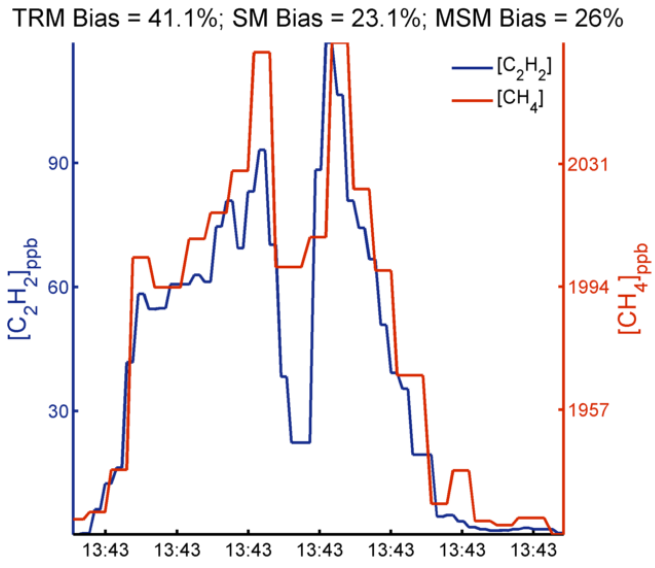
TRM Bias = 41.1%; SM Bias = 23.1%; MSM Bias = 26%
[C2H2]
[CH4]
90
60
30
2031
1994
1957
[C2H2]ppb
[CH4]ppb
13:43
13:43
13:43
13:43
13:43
13:43
13:43

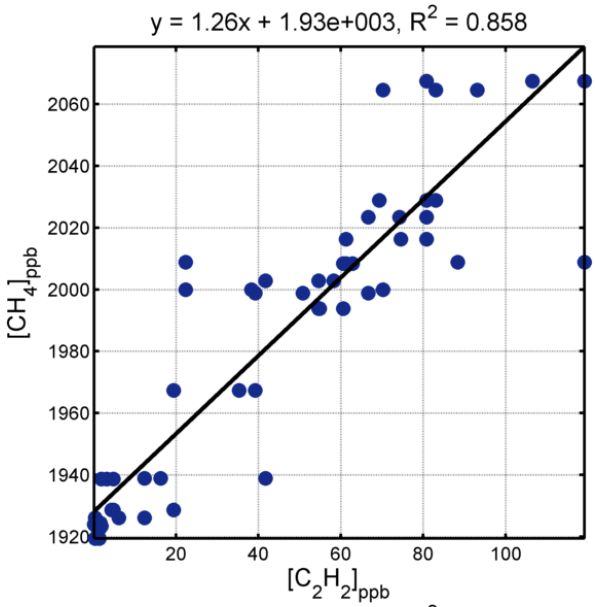
y = 1.26x + 1.93e+003, R2 = 0.858
2060
2040
2020
2000
1980
1960
1940
1920
20
40
60
80
100
[CH4]ppb
[C2H2]ppb

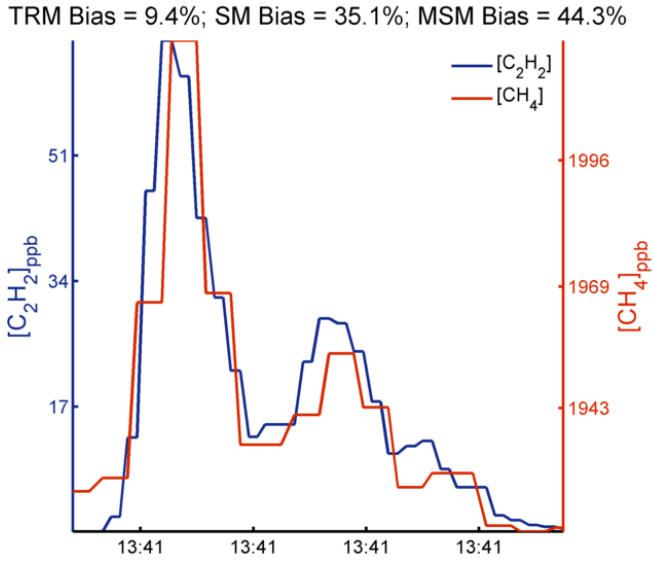
TRM Bias = 9.4%; SM Bias = 35.1%; MSM Bias = 44.3%
[C2H2]
[CH4]
51
34
17
1996
1969
1943
[C2H2]ppb
[CH4]ppb
13:41
13:41
13:41
13:41

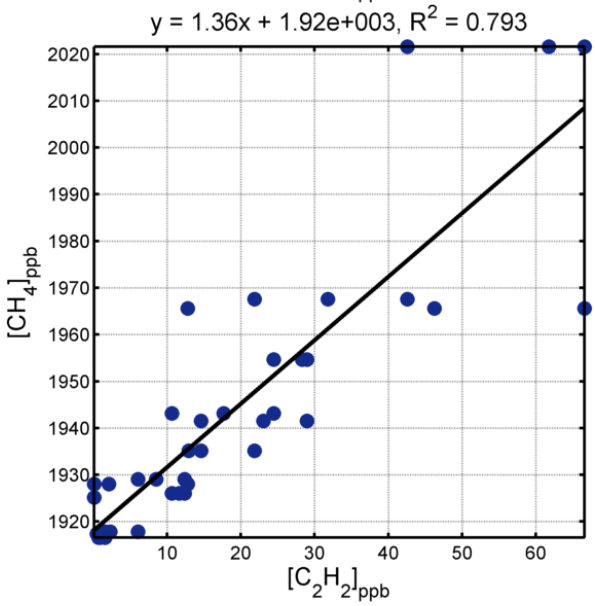
y = 1.36x + 1.92e+003, R2 = 0.793
2020
2010
2000
1990
1980
1970
1960
1950
1940
1930
1920
10
20
30
40
50
60
[CH4]ppb
[C2H2]ppb

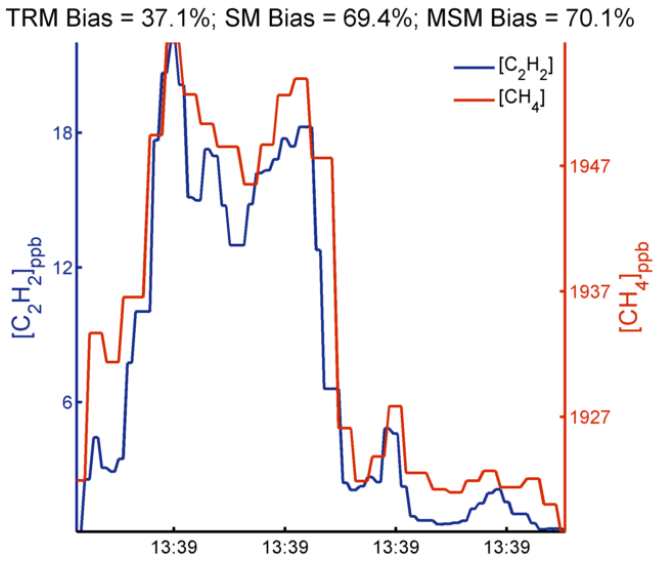
TRM Bias = 37.1%; SM Bias = 69.4%; MSM Bias = 70.1%
[C2H2]
[CH4]
[C2H2]ppb
[CH4]ppb
18
12
6
1947
1937
1927
13:39
13:39
13:39
13:39

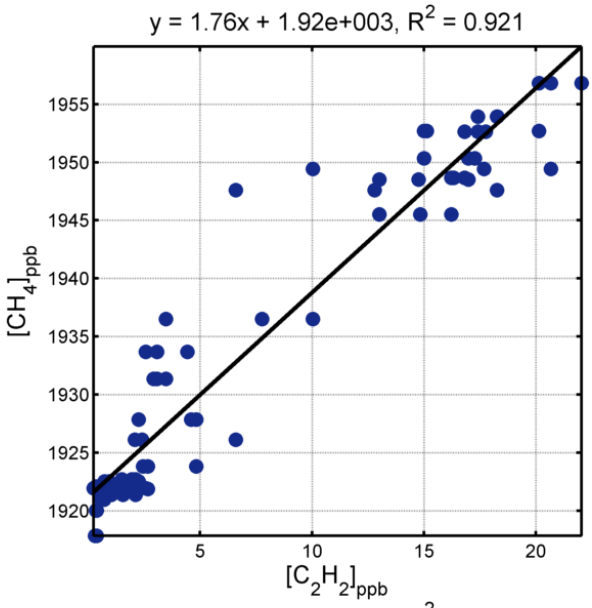
y = 1.76x + 1.92e+003, R2 = 0.921
[CH4]ppb
[C2H2]ppb
1955
1950
1945
1940
1935
1930
1925
1920
5
10
15
20

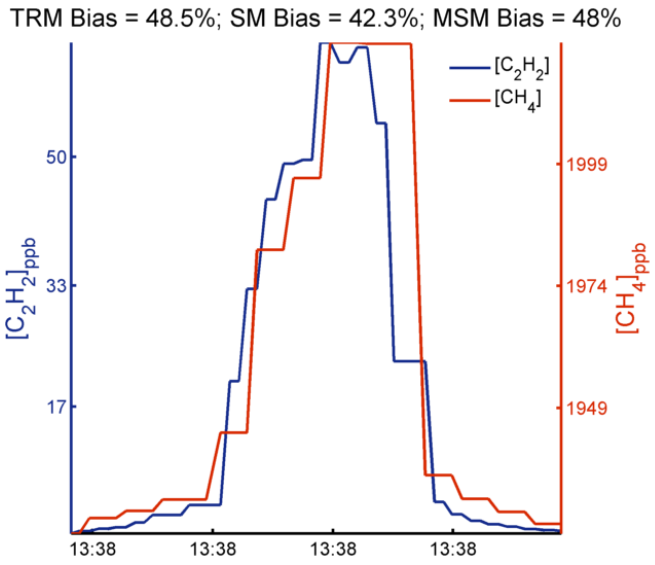
TRM Bias = 48.5%; SM Bias = 42.3%; MSM Bias = 48%
[C2H2]
[CH4]
[C2H2]ppb
[CH4]ppb
50
33
17
1999
1974
1949
13:38
13:38
13:38
13:38

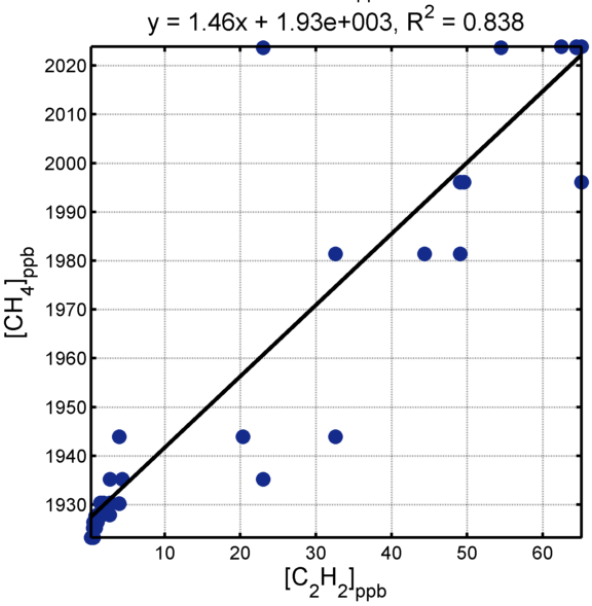
y = 1.46x + 1.93e+003, R2 = 0.838
[CH4]ppb
[C2H2]ppb
2020
2010
2000
1990
1980
1970
1960
1950
1940
1930
10
20
30
40
50
60

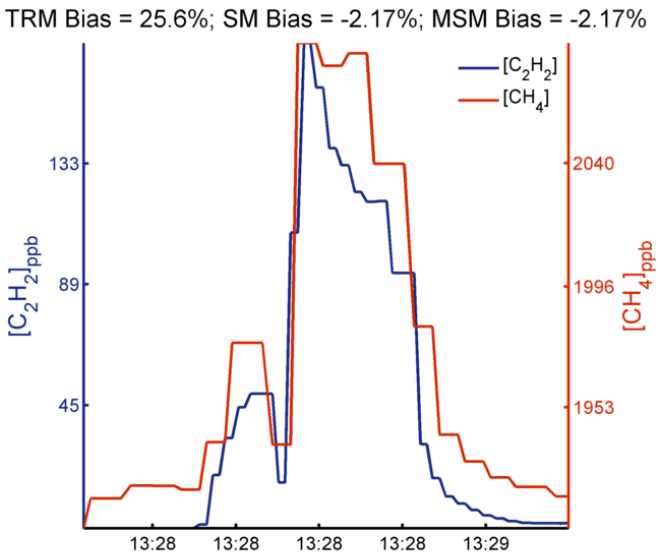
TRM Bias = 25.6%; SM Bias = -2.17%; MSM Bias = -2.17%
[C2H2]
[CH4]
133
89
45
2040
1996
1953
[C2H2]ppb
[CH4]ppb
13:28
13:28
13:28
13:28
13:29

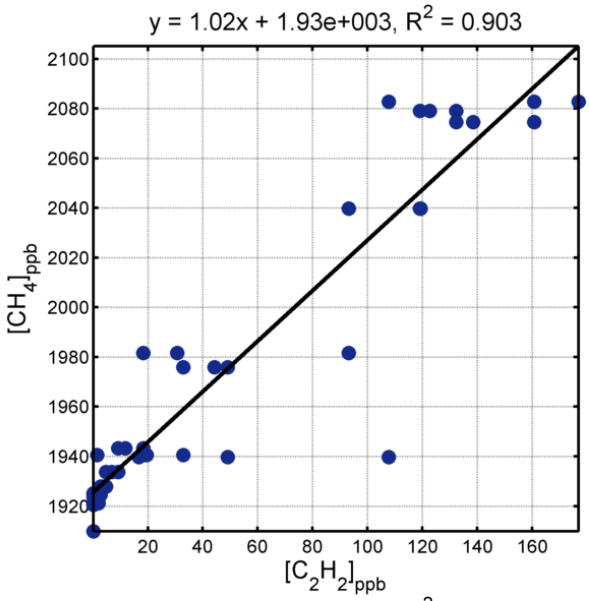
y = 1.02x + 1.93e+003, R2 = 0.903
2100
2080
2060
2040
2020
2000
1980
1960
1940
1920
20
40
60
80
100
120
140
160
[CH4]ppb
[C2H2]ppb

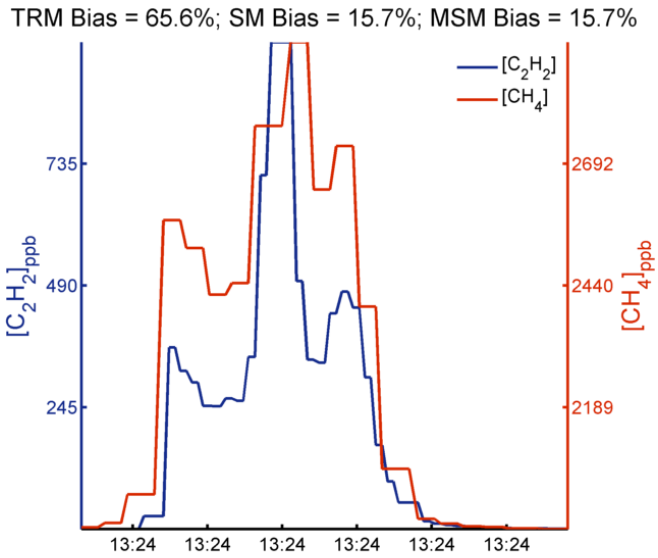
TRM Bias = 65.6%; SM Bias = 15.7%; MSM Bias = 15.7%
[C2H2]
[CH4]
735
490
245
2692
2440
2189
[C2H2]ppb
[CH4]ppb
13:24
13:24
13:24
13:24
13:24
13:24

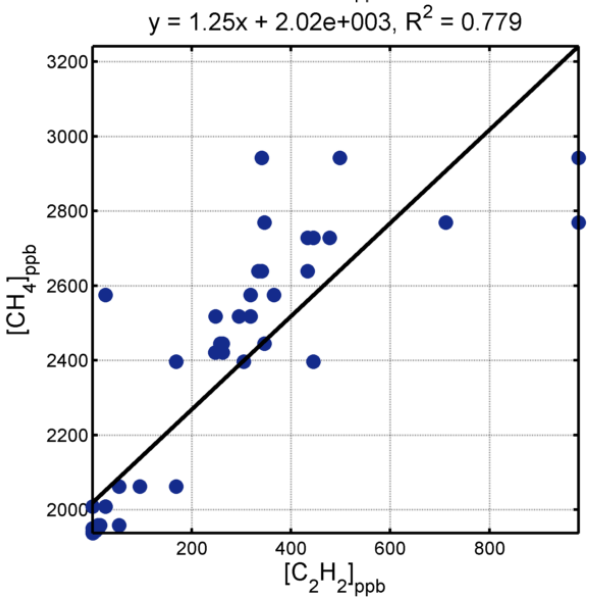
y = 1.25x + 2.02e+003, R2 = 0.779
3200
3000
2800
2600
2400
2200
2000
200
400
600
800
[CH4]ppb
[C2H2]ppb

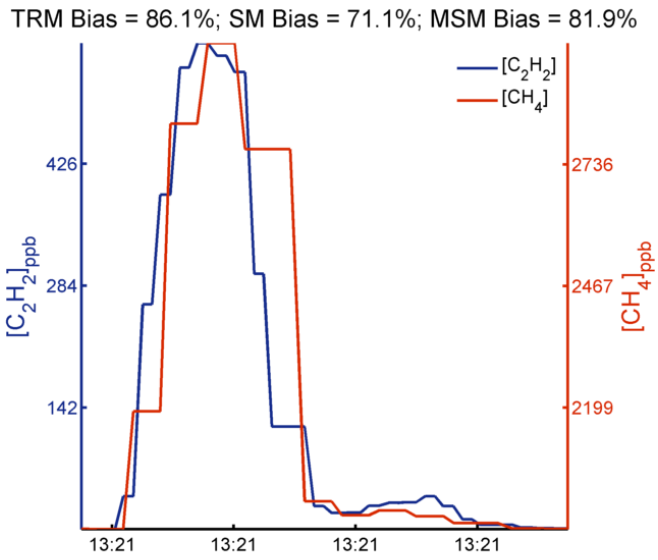
TRM Bias = 86.1%; SM Bias = 71.1%; MSM Bias = 81.9%
[C2H2]
[CH4]
426
284
142
2736
2467
2199
[C2H2]ppb
[CH4]ppb
13:21
13:21
13:21
13:21

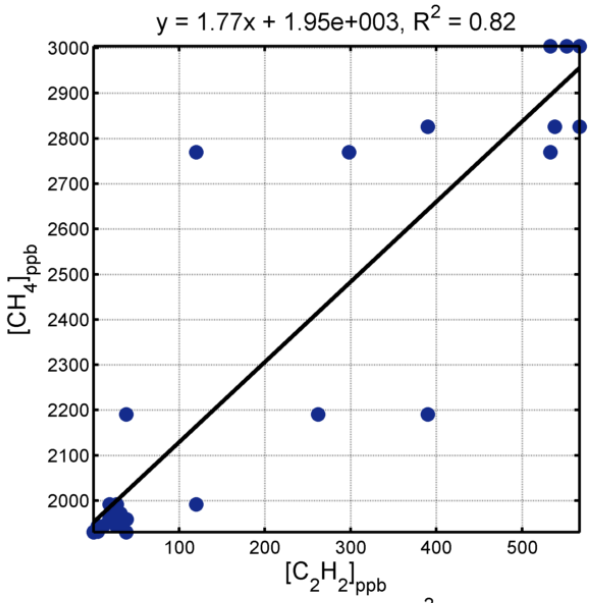
y = 1.77x + 1.95e+003, R2 = 0.82
3000
2900
2800
2700
2600
2500
2400
2300
2200
2100
2000
100
200
300
400
500
[CH4]ppb
[C2H2]ppb

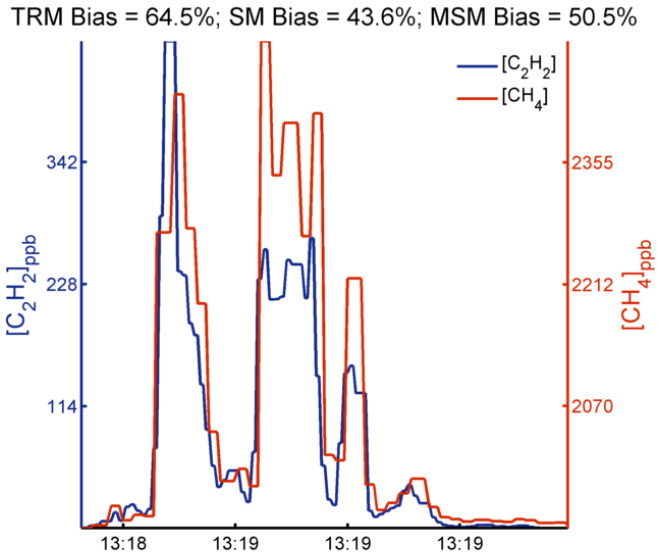
TRM Bias = 64.5%; SM Bias = 43.6%; MSM Bias = 50.5%
[C2H2]
[CH4]
342
228
114
2355
2212
2070
[C2H2]ppb
[CH4]ppb
13:18
13:19
13:19
13:19

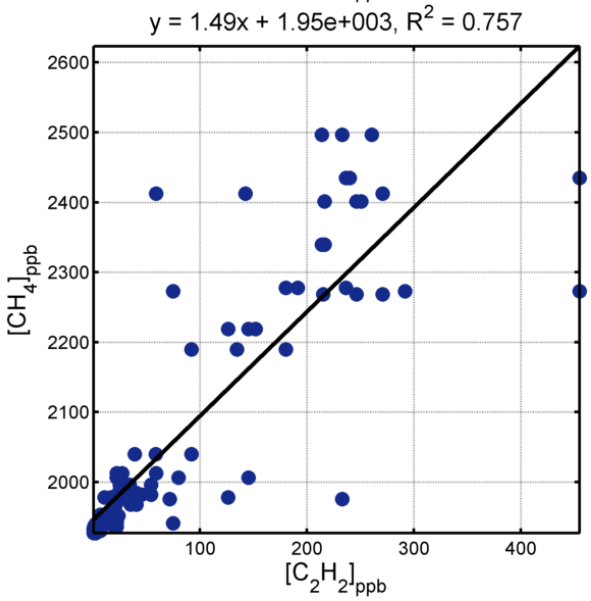
y = 1.49x + 1.95e+003, R2 = 0.757
2600
2500
2400
2300
2200
2100
2000
100
200
300
400
[CH4]ppb
[C2H2]ppb

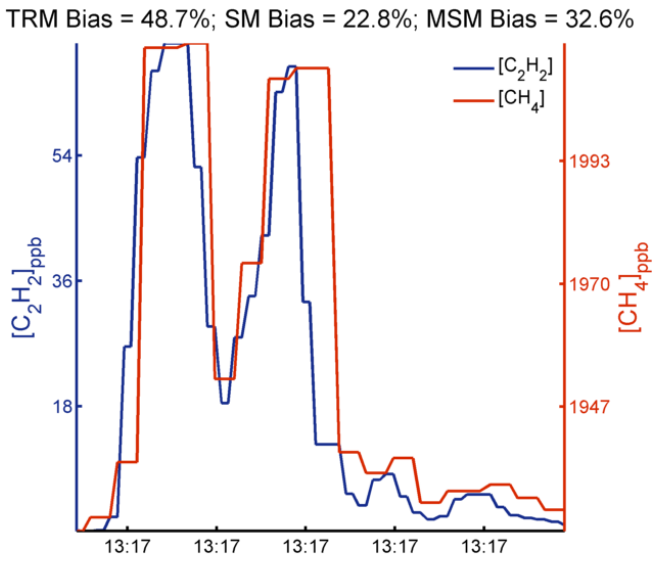
TRM Bias = 48.7%; SM Bias = 22.8%; MSM Bias = 32.6%
[C2H2]
[CH4]
54
36
18
1993
1970
1947
[C2H2]ppb
[CH4]ppb
13:17
13:17
13:17
13:17
13:17

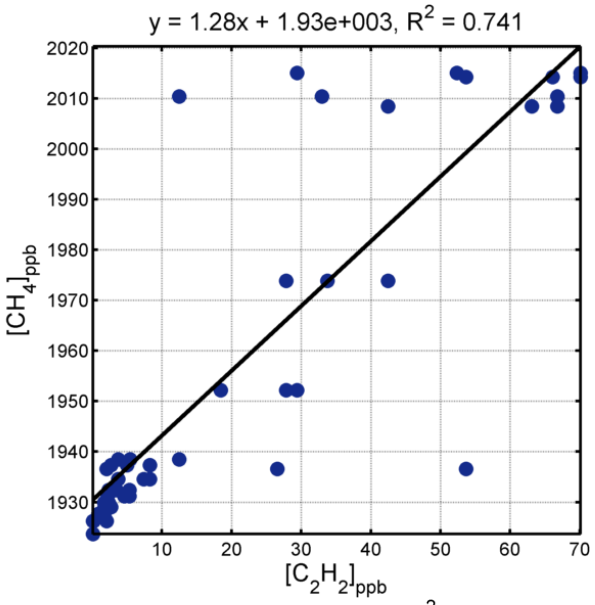
y = 1.28x + 1.93e+003, R2 = 0.741
2020
2010
2000
1990
1980
1970
1960
1950
1940
1930
10
20
30
40
50
60
70
[CH4]ppb
[C2H2]ppb

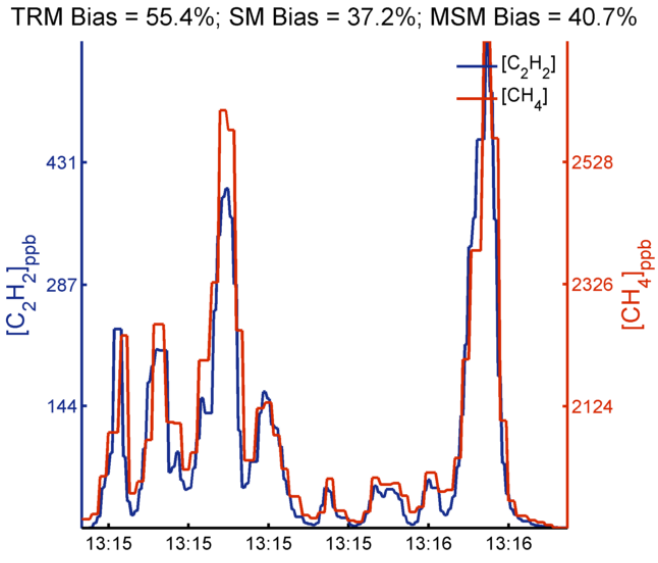
TRM Bias = 55.4%; SM Bias = 37.2%; MSM Bias = 40.7%
[C2H2]
[CH4]
431
287
144
2528
2326
2124
[C2H2]ppb
[CH4]ppb
13:15
13:15
13:15
13:15
13:16
13:16

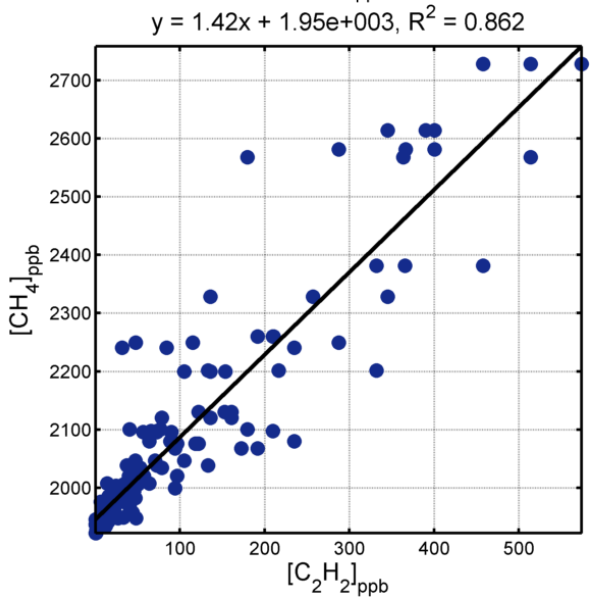
y = 1.42x + 1.95e+003, R2 = 0.862
2700
2600
2500
2400
2300
2200
2100
2000
100
200
300
400
500
[CH4]ppb
[C2H2]ppb

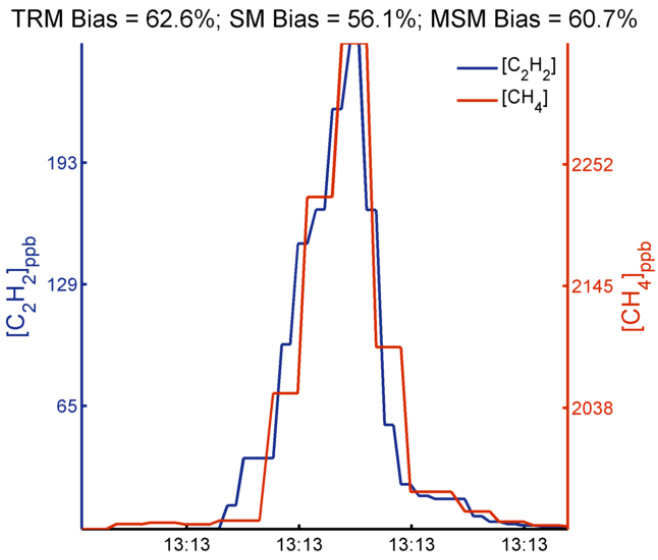
TRM Bias = 62.6%; SM Bias = 56.1%; MSM Bias = 60.7%
[C2H2]
[CH4]
193
129
65
2252
2145
2038
[C2H2]ppb
[CH4]ppb
13:13
13:13
13:13
13:13

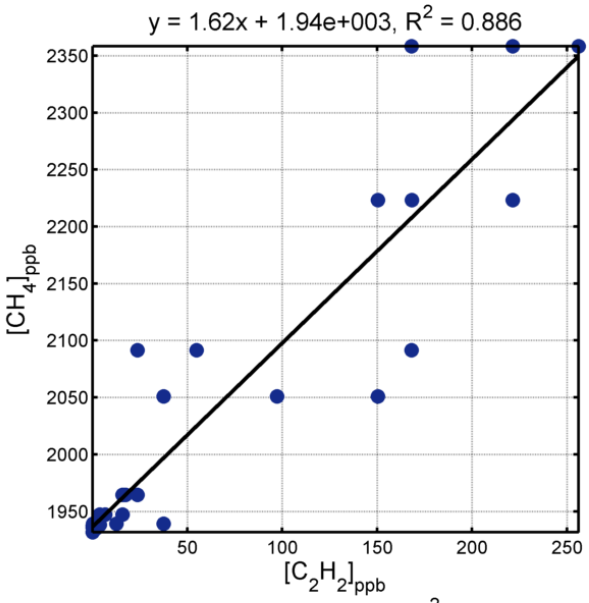
y = 1.62x + 1.94e+003, R2 = 0.886
2350
2300
2250
2200
2150
2100
2050
2000
1950
50
100
150
200
250
[CH4]ppb
[C2H2]ppb

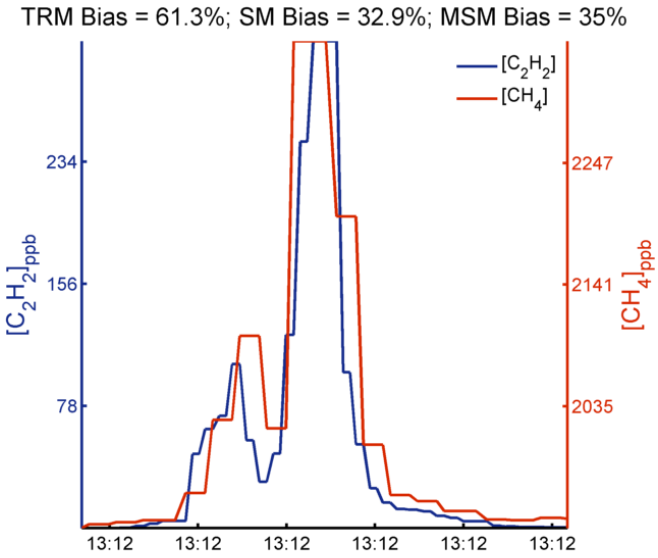
TRM Bias = 61.3%; SM Bias = 32.9%; MSM Bias = 35%
[C2H2]
[CH4]
234
156
78
2247
2141
2035
[C2H2]ppb
[CH4]ppb
13:12
13:12
13:12
13:12
13:12
13:12

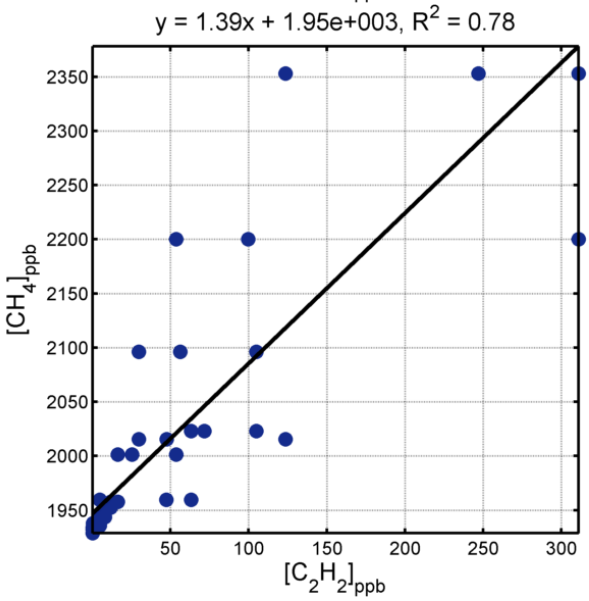
y = 1.39x + 1.95e+003, R2 = 0.78
2350
2300
2250
2200
2150
2100
2050
2000
1950
50
100
150
200
250
300
[CH4]ppb
[C2H2]ppb

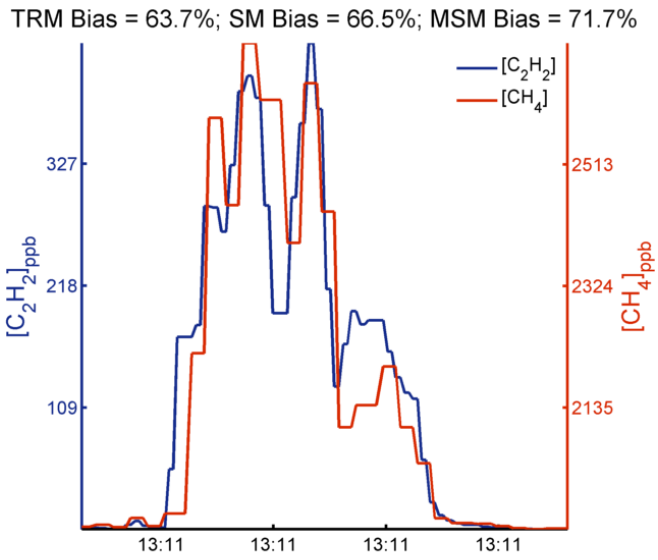
TRM Bias = 63.7%; SM Bias = 66.5%; MSM Bias = 71.7%
[C2H2]
[CH4]
327
218
109
2513
2324
2135
[C2H2]ppb
[CH4]ppb
13:11
13:11
13:11
13:11

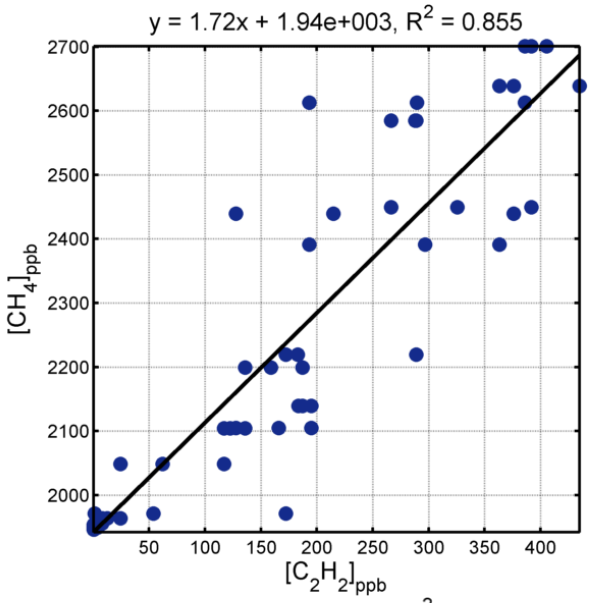
y = 1.72x + 1.94e+003, R2 = 0.855
2700
2600
2500
2400
2300
2200
2100
2000
50
100
150
200
250
300
350
400
[CH4]ppb
[C2H2]ppb

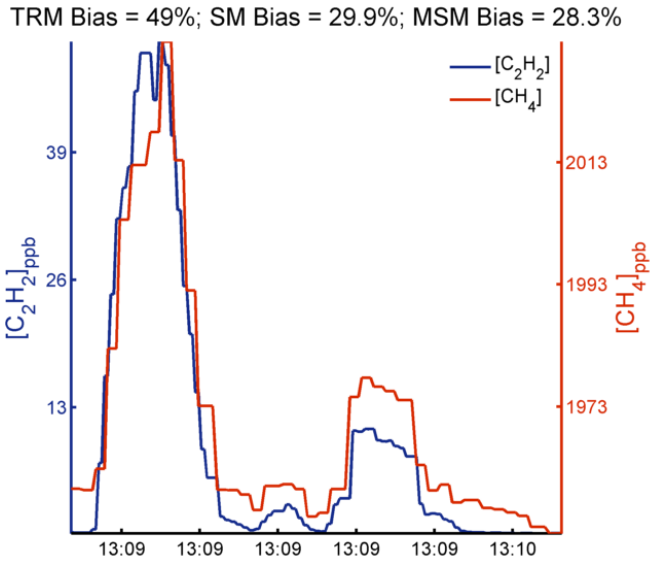
TRM Bias = 49%; SM Bias = 29.9%; MSM Bias = 28.3%
[C2H2]
[CH4]
39
26
13
2013
1993
1973
[C2H2]ppb
[CH4]ppb
13:09
13:09
13:09
13:09
13:09
13:10

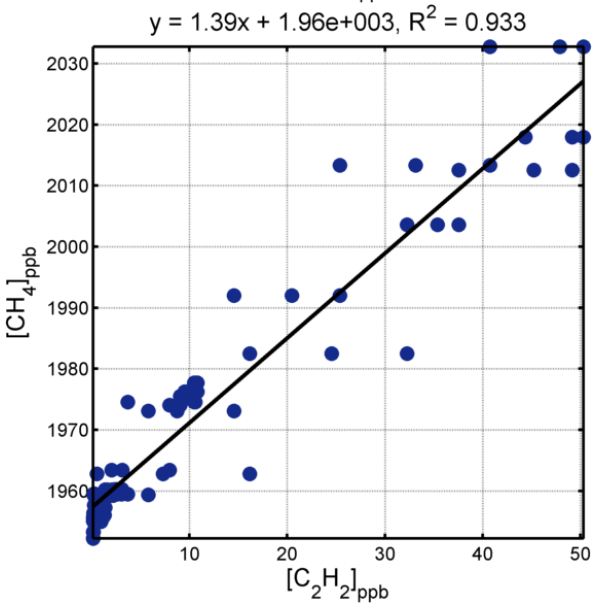
y = 1.39x + 1.96e+003, R2 = 0.933
2030
2020
2010
2000
1990
1980
1970
1960
10
20
30
40
50
[CH4]ppb
[C2H2]ppb

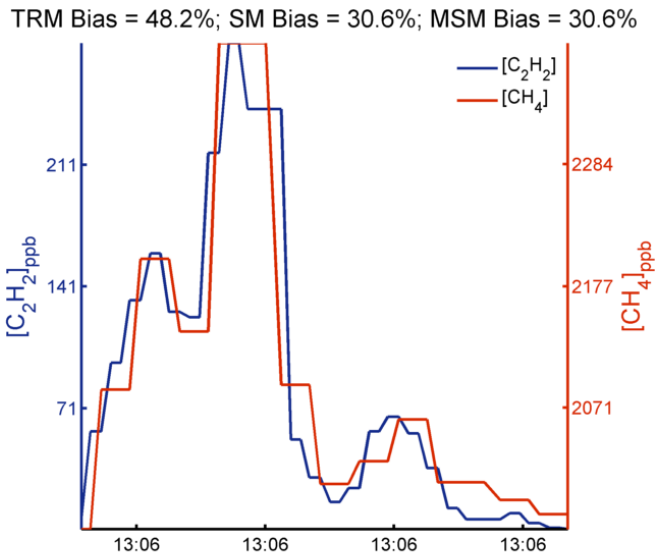
TRM Bias = 48.2%; SM Bias = 30.6%; MSM Bias = 30.6%
[C2H2]
[CH4]
211
141
71
2284
2177
2071
[C2H2]ppb
[CH4]ppb
13:06
13:06
13:06
13:06

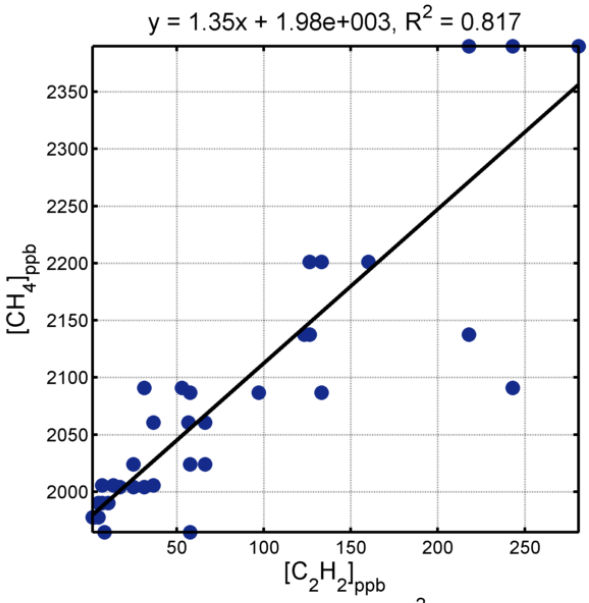
y = 1.35x + 1.98e+003, R2 = 0.817
2350
2300
2250
2200
2150
2100
2050
2000
50
100
150
200
250
[CH4]ppb
[C2H2]ppb

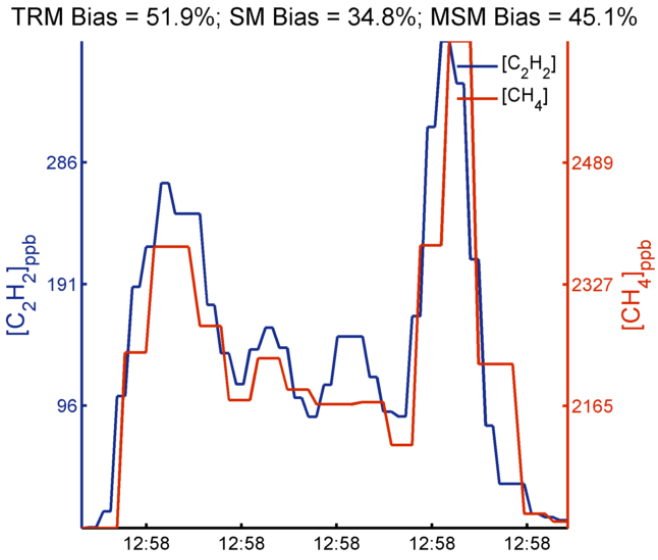
TRM Bias = 51.9%; SM Bias = 34.8%; MSM Bias = 45.1%
[C2H2]
[CH4]
286
191
96
2489
2327
2165
[C2H2]ppb
[CH4]ppb
12:58
12:58
12:58
12:58
12:58

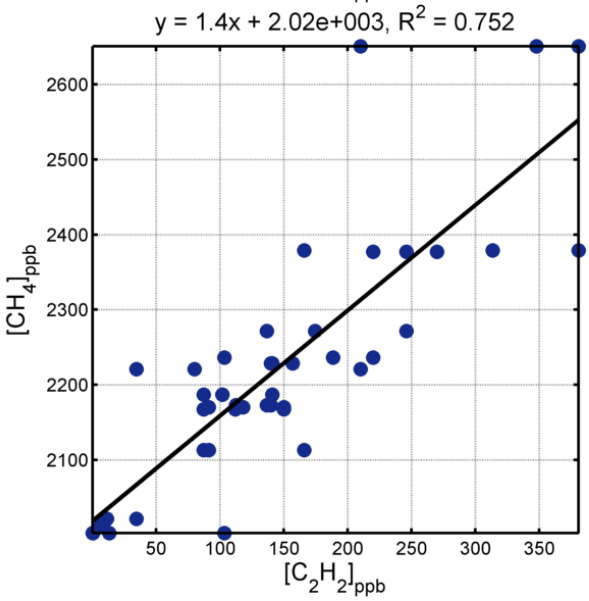
y = 1.4x + 2.02e+003, R2 = 0.752
2600
2500
2400
2300
2200
2100
50
100
150
200
250
300
350
[CH4]ppb
[C2H2]ppb

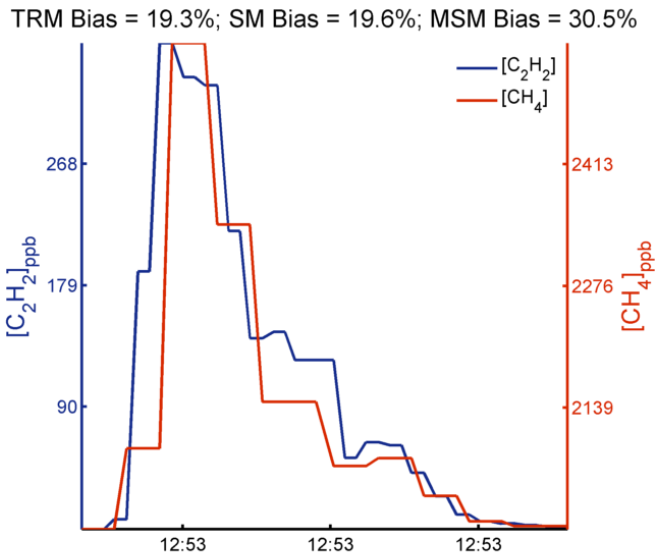
TRM Bias = 19.3%; SM Bias = 19.6%; MSM Bias = 30.5%
[C2H2]
[CH4]
268
179
90
2413
2276
2139
[C2H2]ppb
[CH4]ppb
12:53
12:53
12:53

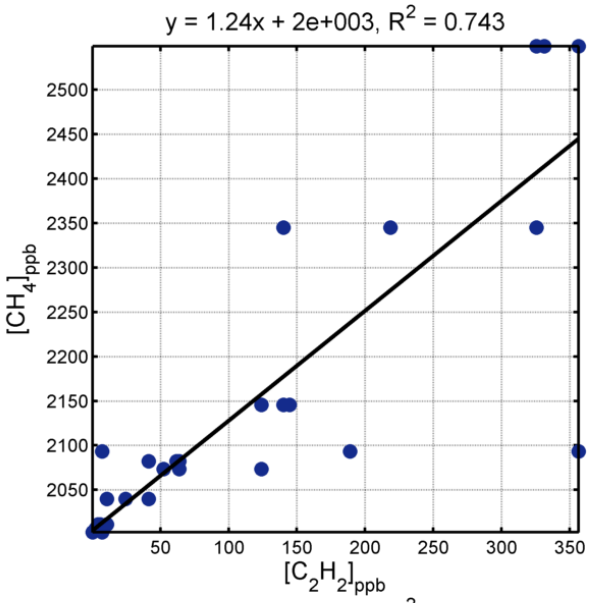
y = 1.24x + 2e+003, R2 = 0.743
2500
2450
2400
2350
2300
2250
2200
2150
2100
2050
50
100
150
200
250
300
350
[CH4]ppb
[C2H2]ppb

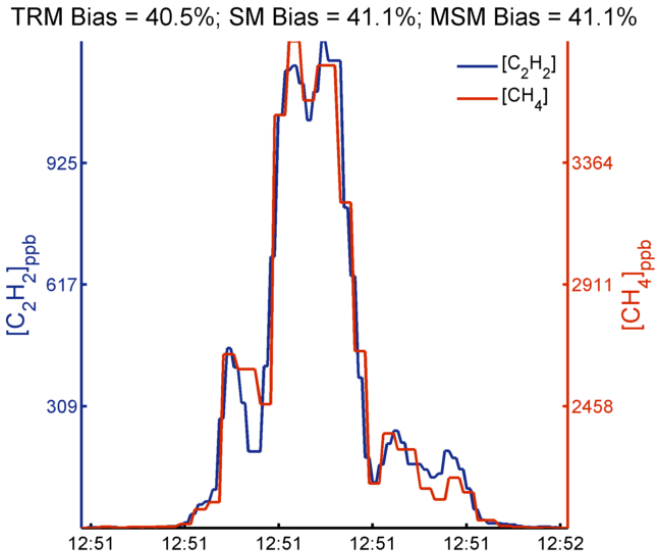
TRM Bias = 40.5%; SM Bias = 41.1%; MSM Bias = 41.1%
[C2H2]
[CH4]
925
617
309
3364
2911
2458
[C2H2]ppb
[CH4]ppb
12:51
12:51
12:51
12:51
12:51
12:52

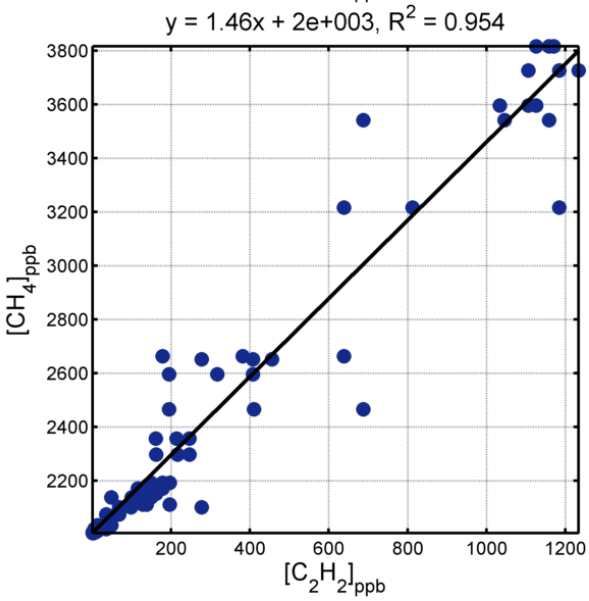
y = 1.46x + 2e+003, R2 = 0.954
3800
3600
3400
3200
3000
2800
2600
2400
2200
200
400
600
800
1000
1200
[CH4]ppb
[C2H2]ppb

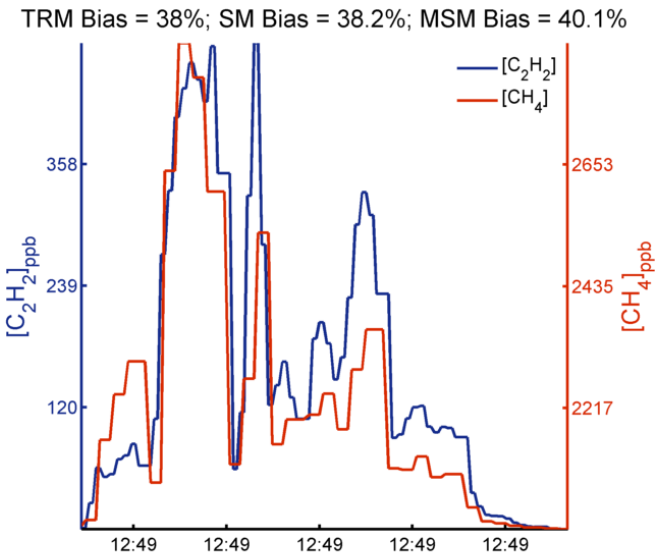
TRM Bias = 38%; SM Bias = 38.2%; MSM Bias = 40.1%
[C2H2]
[CH4]
358
239
120
2653
2435
2217
[C2H2]ppb
[CH4]ppb
12:49
12:49
12:49
12:49
12:49

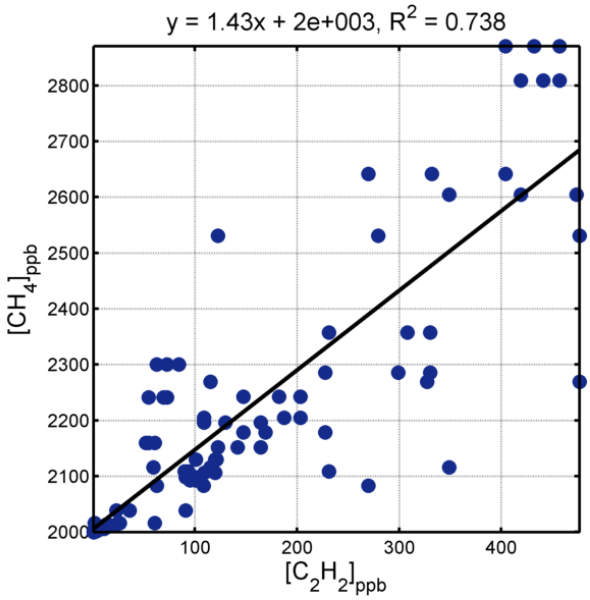
y = 1.43x + 2e+003, R2 = 0.738
2800
2700
2600
2500
2400
2300
2200
2100
2000
100
200
300
400
[CH4]ppb
[C2H2]ppb

05 September 2013

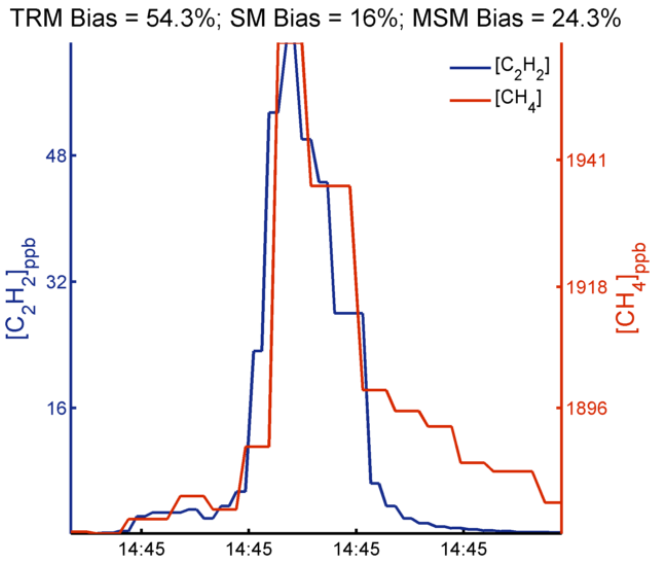

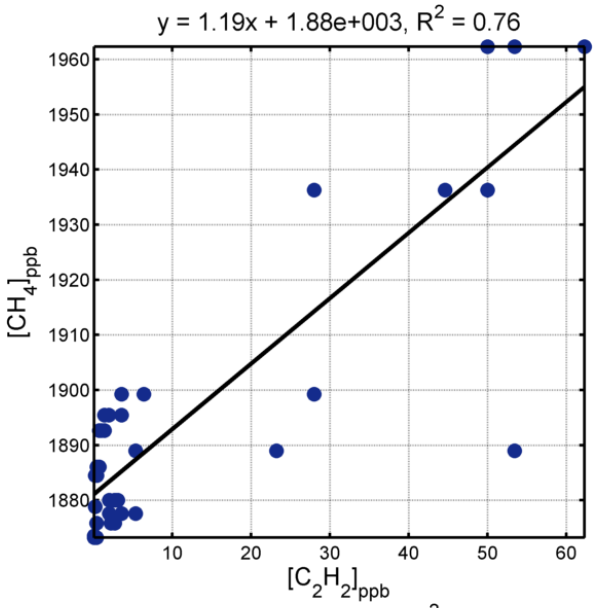

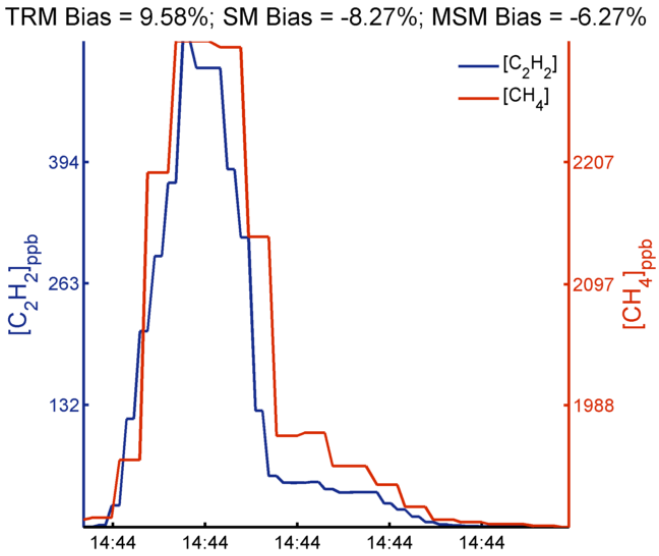

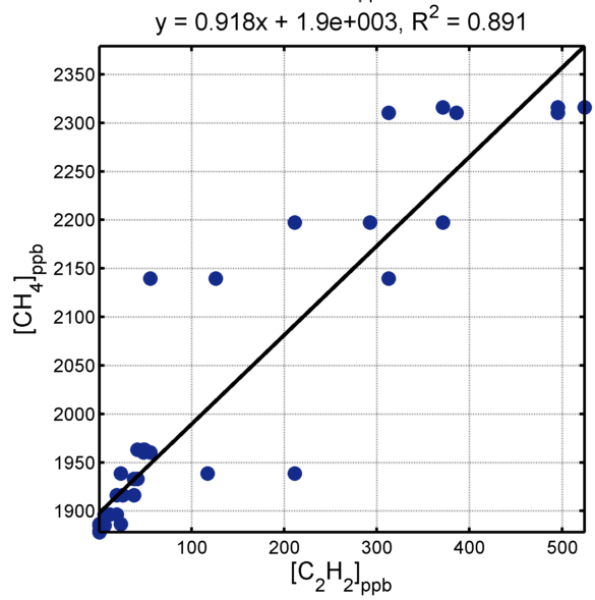

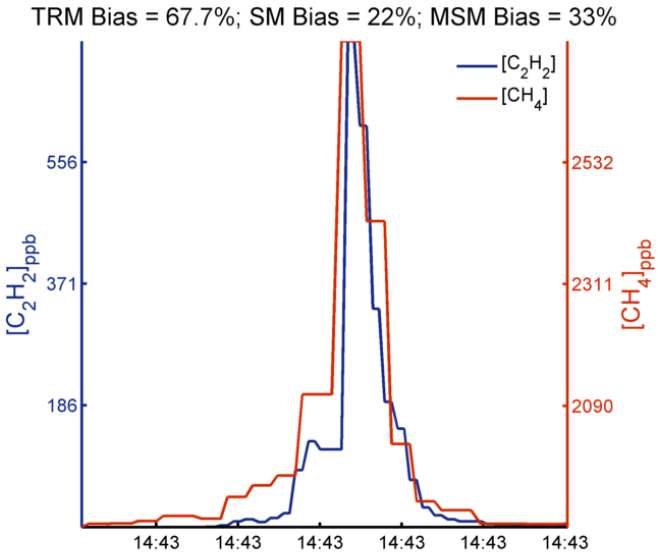
TRM Bias = 67.7%; SM Bias = 22%; MSM Bias = 33%
[C2H2]
[CH4]
556
371
186
2532
2311
2090
[C2H2]ppb
[CH4]ppb
14:43
14:43
14:43
14:43
14:43
14:43

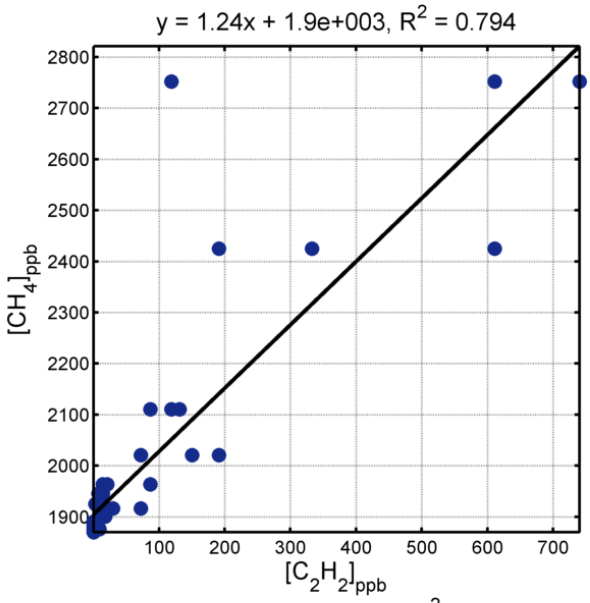
y = 1.24x + 1.9e+003, R2 = 0.794
2800
2700
2600
2500
2400
2300
2200
2100
2000
1900
100
200
300
400
500
600
700
[CH4]ppb
[C2H2]ppb

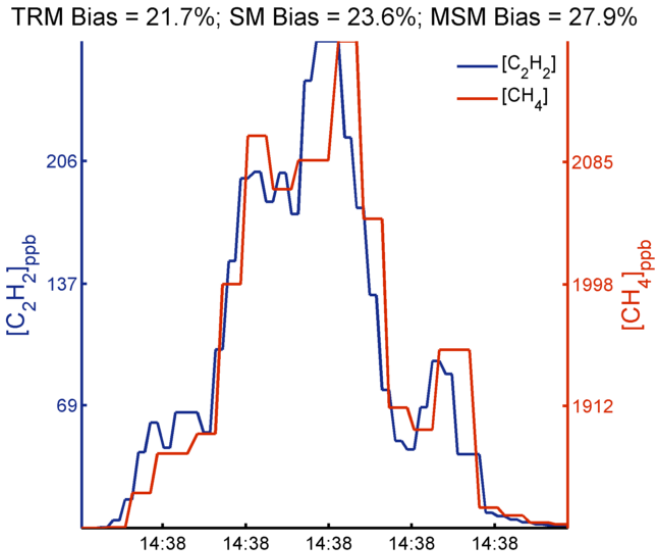
TRM Bias = 21.7%; SM Bias = 23.6%; MSM Bias = 27.9%
[C2H2]
[CH4]
206
137
69
2085
1998
1912
[C2H2]ppb
[CH4]ppb
14:38
14:38
14:38
14:38
14:38

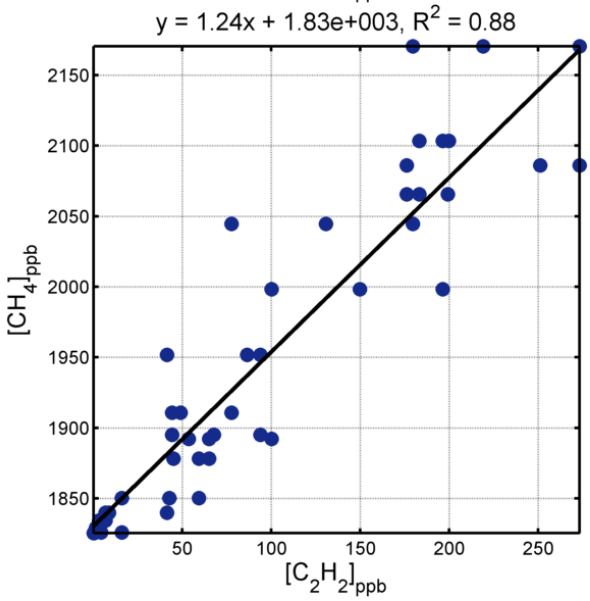
y = 1.24x + 1.83e+003, R2 = 0.88
2150
2100
2050
2000
1950
1900
1850
50
100
150
200
250
[CH4]ppb
[C2H2]ppb

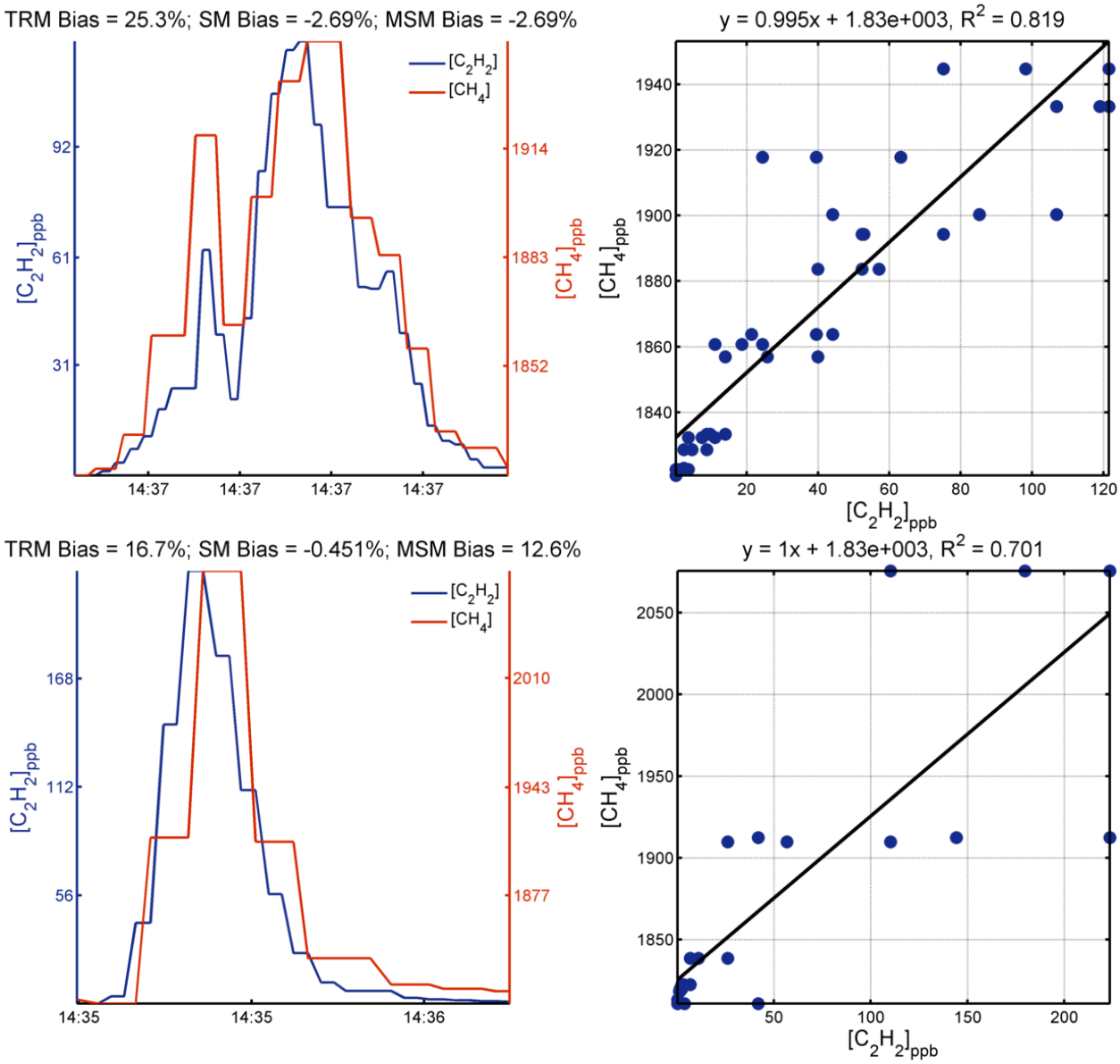
TRM Bias = 25.3%; SM Bias = -2.69%; MSM Bias = -2.69%
[C2H2]
[CH4]
92
61
31
1914
1883
1852
[C2H2]ppb
[CH4]ppb
14:37
14:37
14:37
14:37
y = 0.995x + 1.83e+003, R2 = 0.819
1940
1920
1900
1880
1860
1840
20
40
60
80
100
120
[CH4]ppb
[C2H2]ppb
TRM Bias = 16.7%; SM Bias = -0.451%; MSM Bias = 12.6%
[C2H2]
[CH4]
168
112
56
2010
1943
1877
[C2H2]ppb
[CH4]ppb
14:35
14:35
14:36
y = 1x + 1.83e+003, R2 = 0.701
2050
2000
1950
1900
1850
50
100
150
200
[CH4]ppb
[C2H2]ppb

08 April 2014

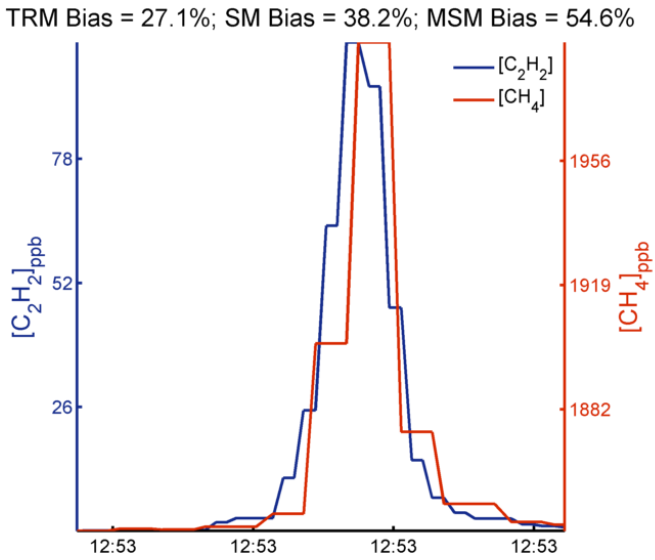

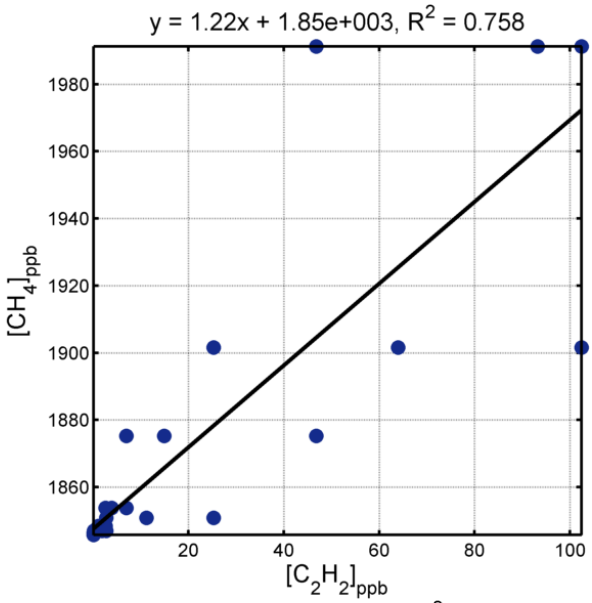

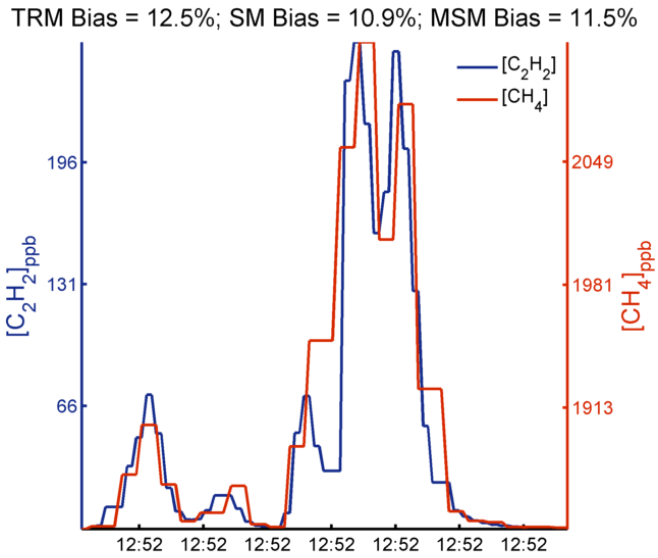

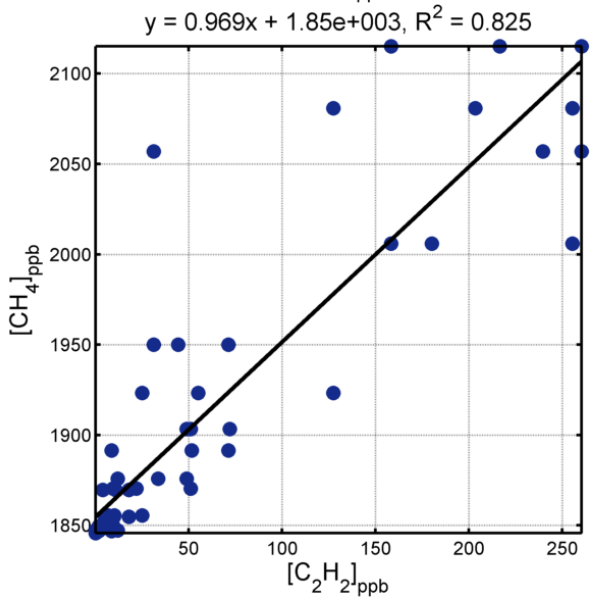

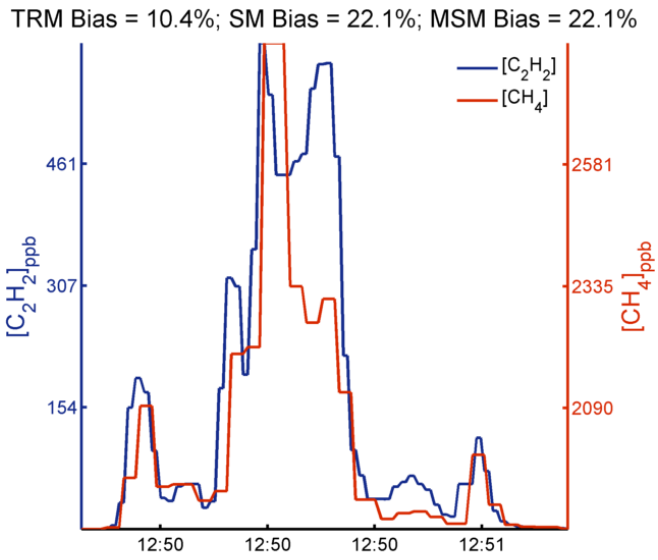
TRM Bias = 10.4%; SM Bias = 22.1%; MSM Bias = 22.1%
[C2H2]
[CH4]
461
307
154
2581
2335
2090
[C2H2]ppb
[CH4]ppb
12:50
12:50
12:50
12:51

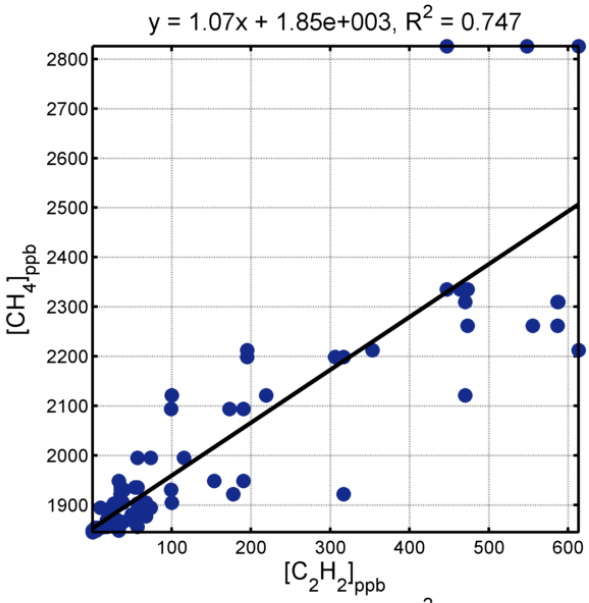
y = 1.07x + 1.85e+003, R2 = 0.747
2800
2700
2600
2500
2400
2300
2200
2100
2000
1900
100
200
300
400
500
600
[CH4]ppb
[C2H2]ppb

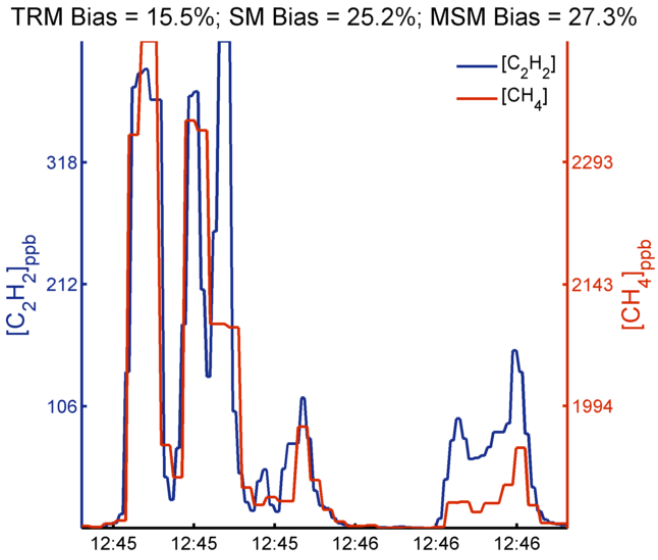
TRM Bias = 15.5%; SM Bias = 25.2%; MSM Bias = 27.3%
[C2H2]
[CH4]
318
212
106
2293
2143
1994
[C2H2]ppb
[CH4]ppb
12:45
12:45
12:45
12:46
12:46
12:46

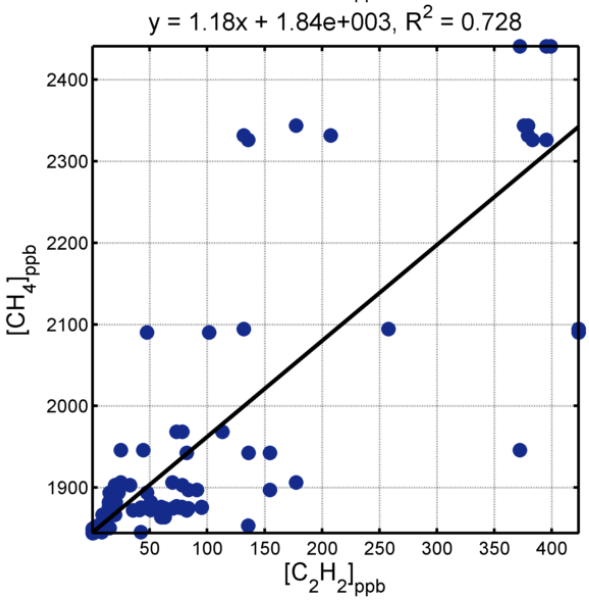
y = 1.18x + 1.84e+003, R2 = 0.728
2400
2300
2200
2100
2000
1900
50
100
150
200
250
300
350
400
[CH4]ppb
[C2H2]ppb

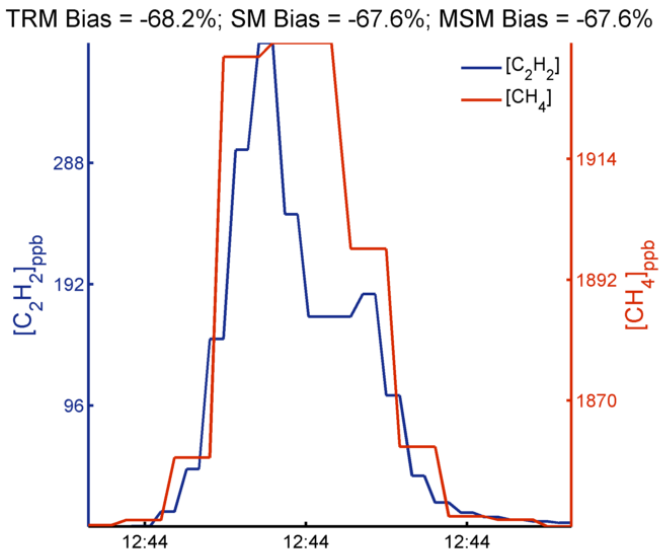
TRM Bias = -68.2%; SM Bias = -67.6%; MSM Bias = -67.6%
[C2H2]
[CH4]
288
192
96
1914
1892
1870
[C2H2]ppb
[CH4]ppb
12:44
12:44
12:44

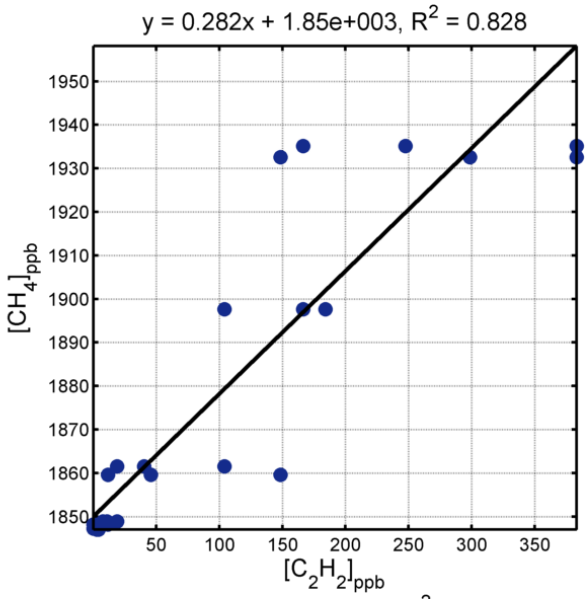
y = 0.282x + 1.85e+003, R2 = 0.828
1950
1940
1930
1920
1910
1900
1890
1880
1870
1860
1850
50
100
150
200
250
300
350
[CH4]ppb
[C2H2]ppb

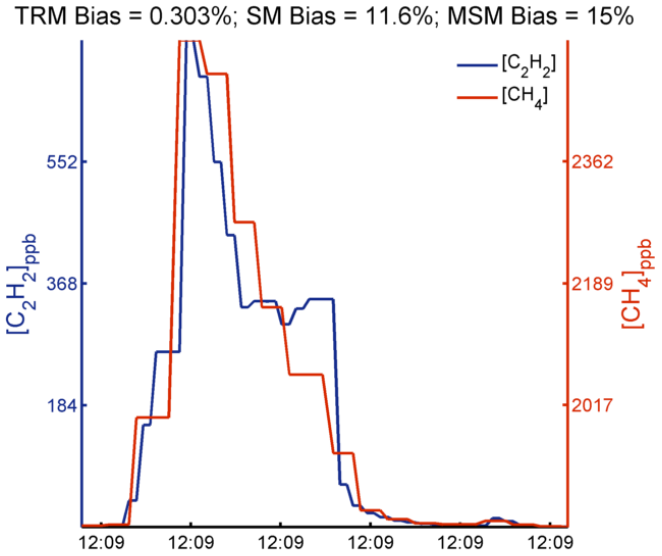
TRM Bias = 0.303%; SM Bias = 11.6%; MSM Bias = 15%
[C2H2]
[CH4]
552
368
184
2362
2189
2017
[C2H2]ppb
[CH4]ppb
12:09
12:09
12:09
12:09
12:09
12:09

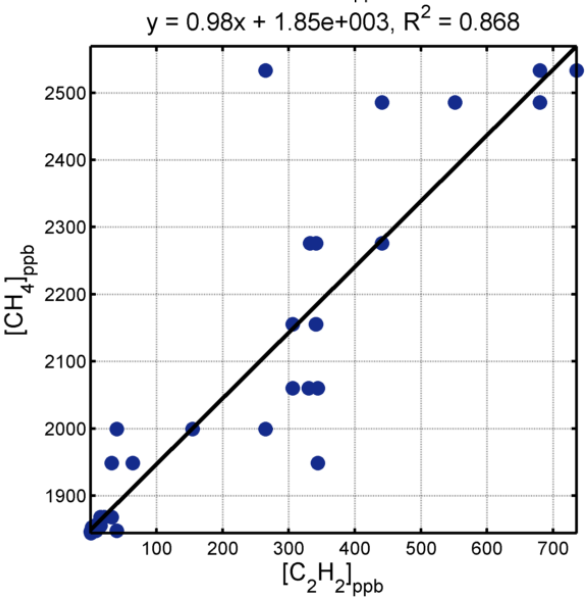
y = 0.98x + 1.85e+003, R2 = 0.868
2500
2400
2300
2200
2100
2000
1900
100
200
300
400
500
600
700
[CH4]ppb
[C2H2]ppb

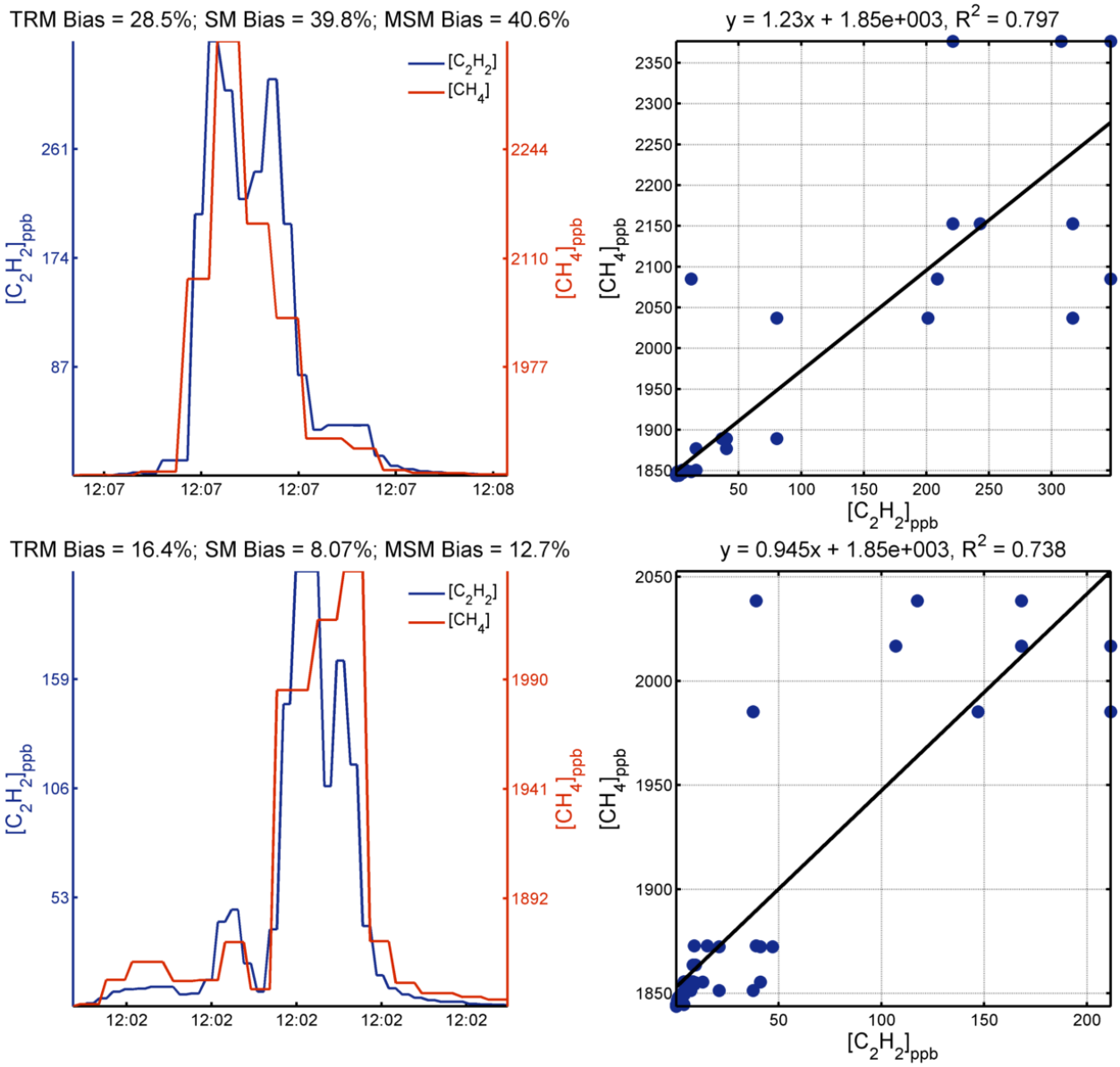
TRM Bias = 28.5%; SM Bias = 39.8%; MSM Bias = 40.6%
[C2H2]
[CH4]
261
174
87
2244
2110
1977
[C2H2]ppb
[CH4]ppb
12:07
12:07
12:07
12:07
12:08
y = 1.23x + 1.85e+003, R2 = 0.797
2350
2300
2250
2200
2150
2100
2050
2000
1950
1900
1850
50
100
150
200
250
300
[CH4]ppb
[C2H2]ppb
TRM Bias = 16.4%; SM Bias = 8.07%; MSM Bias = 12.7%
[C2H2]
[CH4]
159
106
53
1990
1941
1892
[C2H2]ppb
[CH4]ppb
12:02
12:02
12:02
12:02
12:02
y = 0.945x + 1.85e+003, R2 = 0.738
2050
2000
1950
1900
1850
50
100
150
200
[CH4]ppb
[C2H2]ppb

23 April 2014

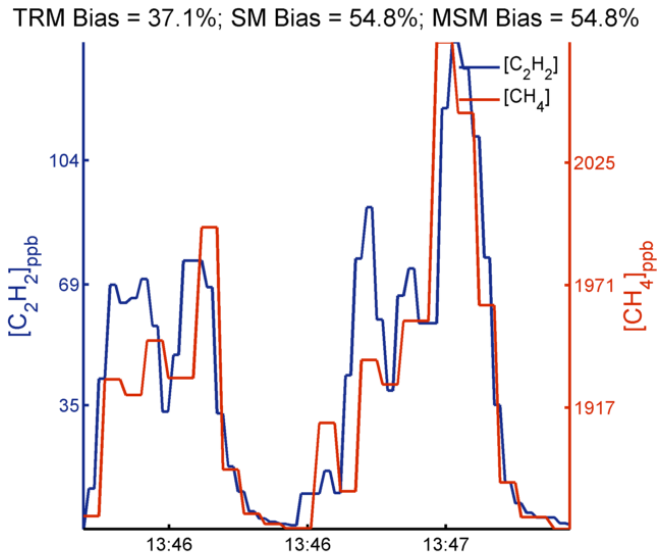

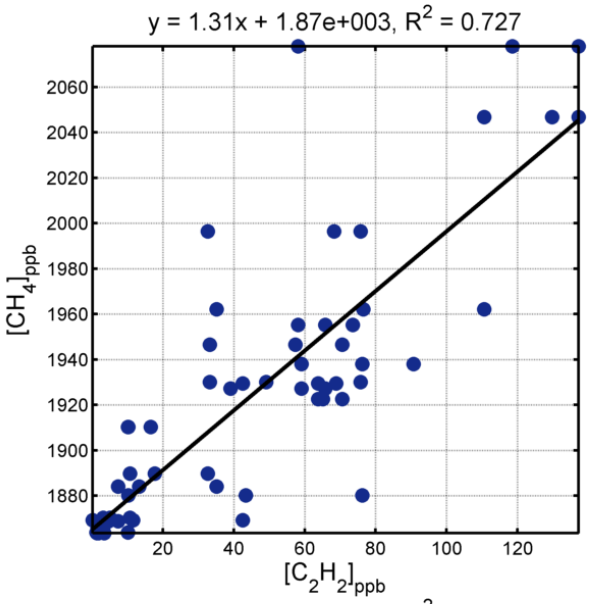

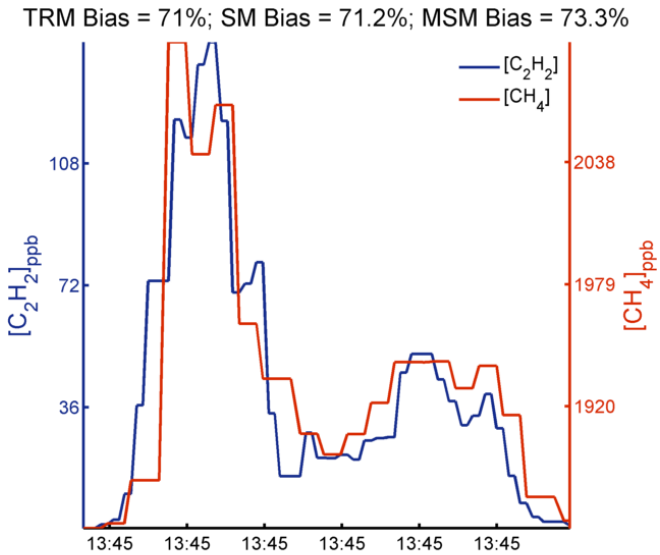

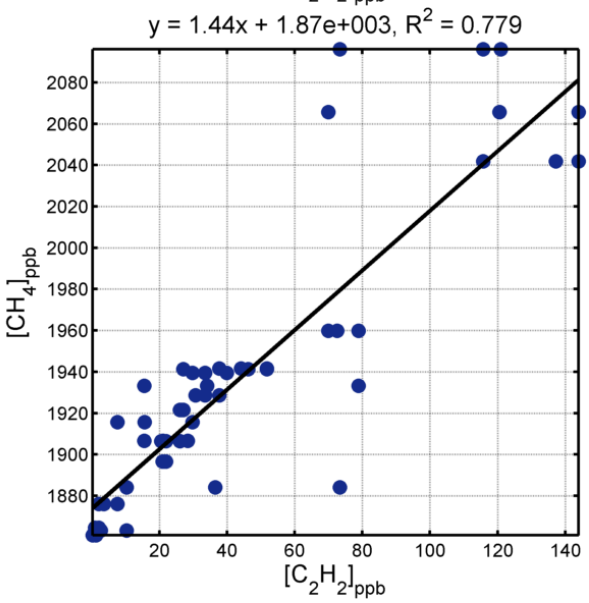

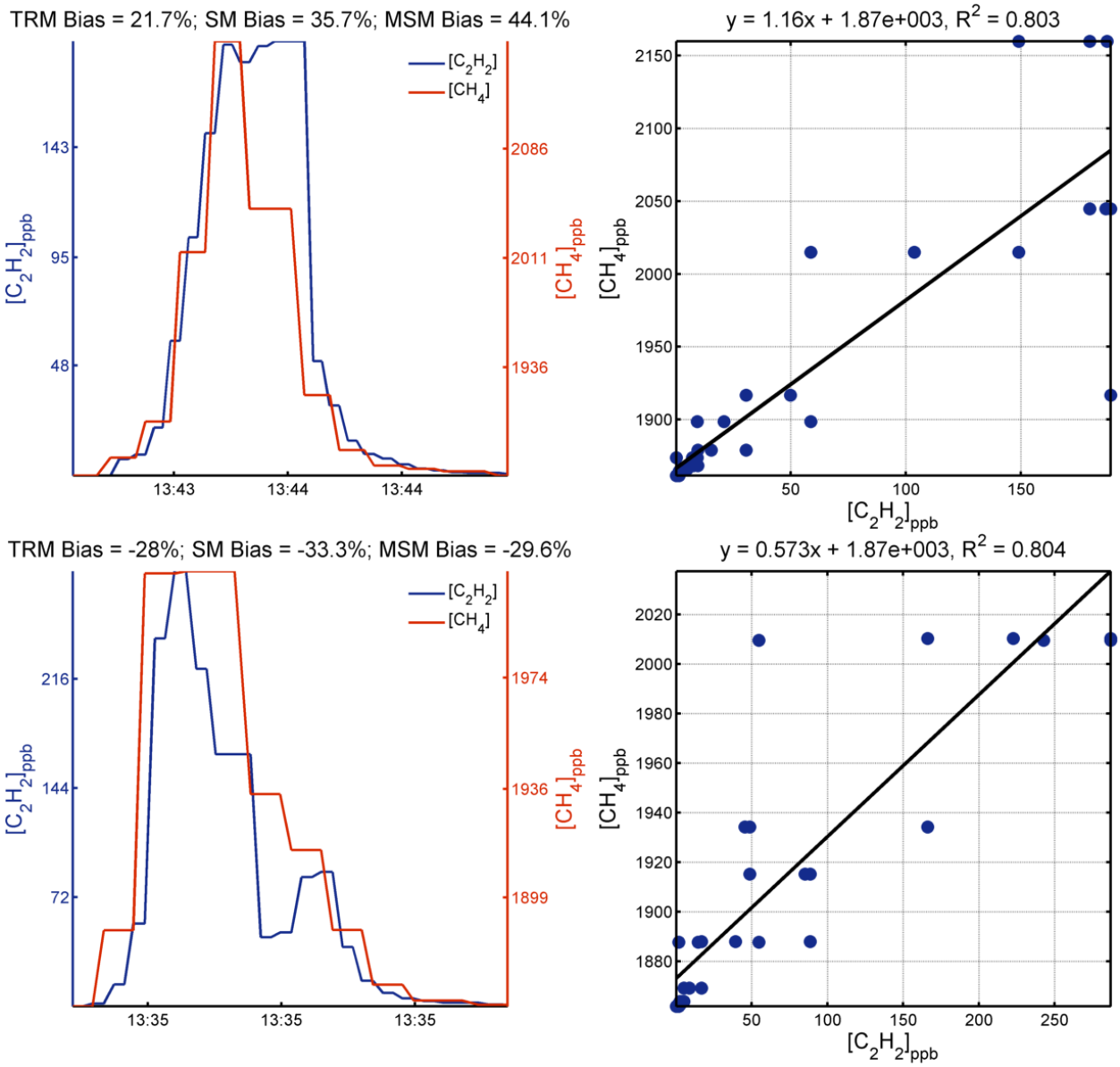
TRM Bias = 21.7%; SM Bias = 35.7%; MSM Bias = 44.1%
[C2H2]
[CH4]
143
95
48
2086
2011
1936
[C2H2]ppb
[CH4]ppb
13:43
13:44
13:44
y = 1.16x + 1.87e+003, R2 = 0.803
2150
2100
2050
2000
1950
1900
50
100
150
[CH4]ppb
[C2H2]ppb
TRM Bias = -28%; SM Bias = -33.3%; MSM Bias = -29.6%
[C2H2]
[CH4]
216
144
72
1974
1936
1899
[C2H2]ppb
[CH4]ppb
13:35
13:35
13:35
y = 0.573x + 1.87e+003, R2 = 0.804
2020
2000
1980
1960
1940
1920
1900
1880
50
100
150
200
250
[CH4]ppb
[C2H2]ppb

25 April 2014

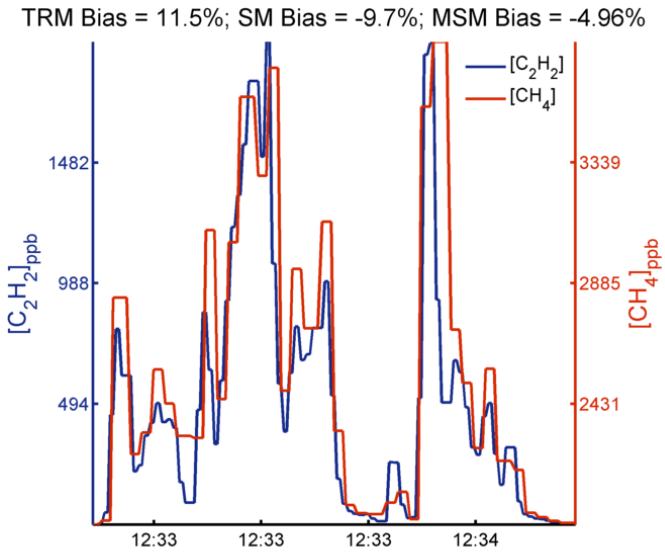

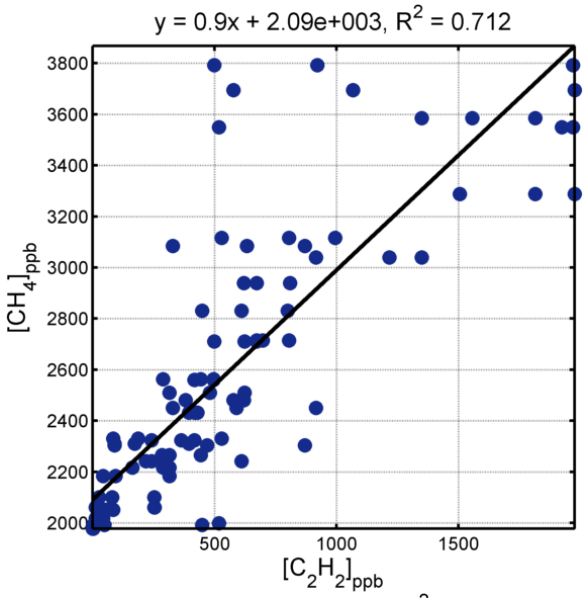

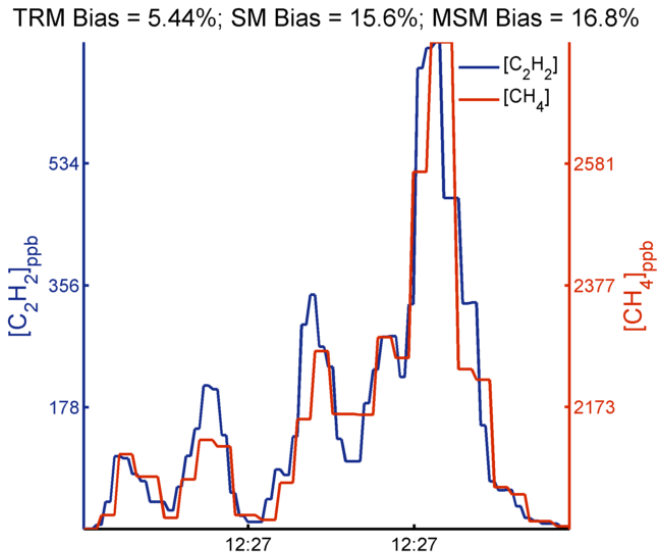

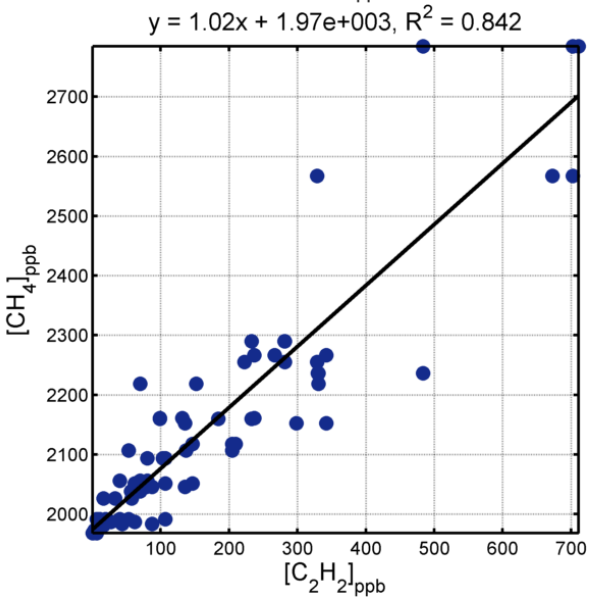

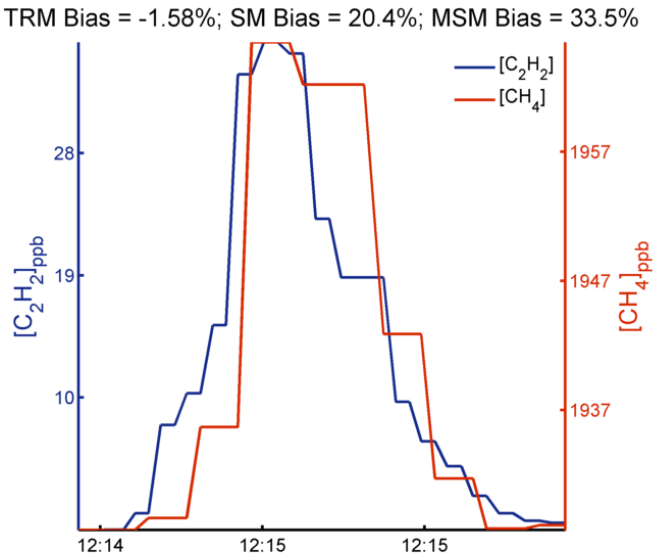
TRM Bias = -1.58%; SM Bias = 20.4%; MSM Bias = 33.5%
[C2H2]
[CH4]
28
19
10
1957
1947
1937
[C2H2]ppb
[CH4]ppb
12:14
12:15
12:15

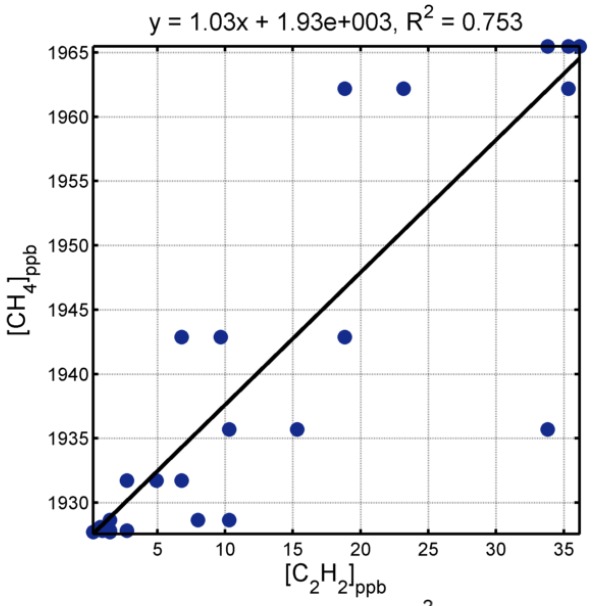
y = 1.03x + 1.93e+003, R2 = 0.753
1965
1960
1955
1950
1945
1940
1935
1930
5
10
15
20
25
30
35
[CH4]ppb
[C2H2]ppb

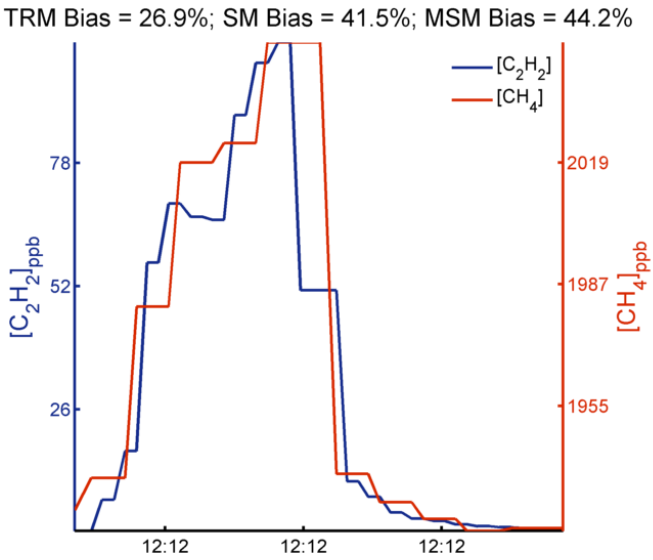
TRM Bias = 26.9%; SM Bias = 41.5%; MSM Bias = 44.2%
[C2H2]
[CH4]
78
52
26
2019
1987
1955
[C2H2]ppb
[CH4]ppb
12:12
12:12
12:12

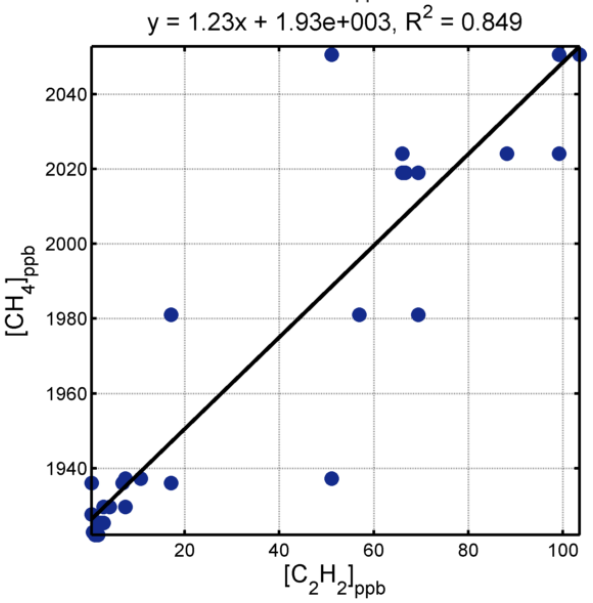
y = 1.23x + 1.93e+003, R2 = 0.849
2040
2020
2000
1980
1960
1940
20
40
60
80
100
[CH4]ppb
[C2H2]ppb

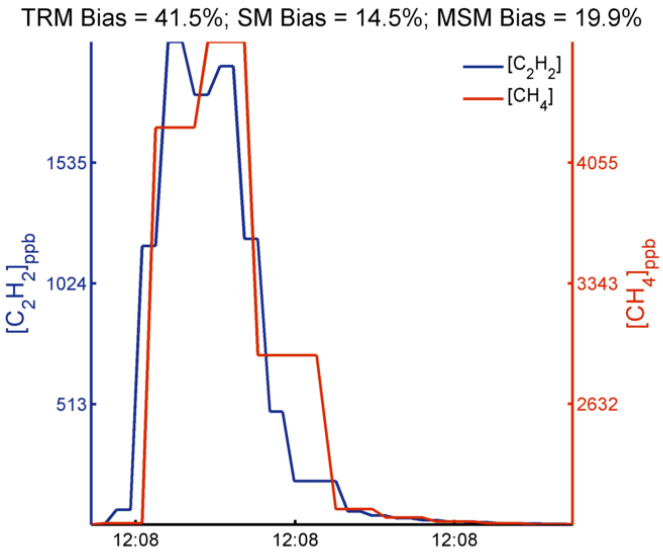
TRM Bias = 41.5%; SM Bias = 14.5%; MSM Bias = 19.9%
[C2H2]
[CH4]
1535
1024
513
4055
3343
2632
[C2H2]ppb
[CH4]ppb
12:08
12:08
12:08

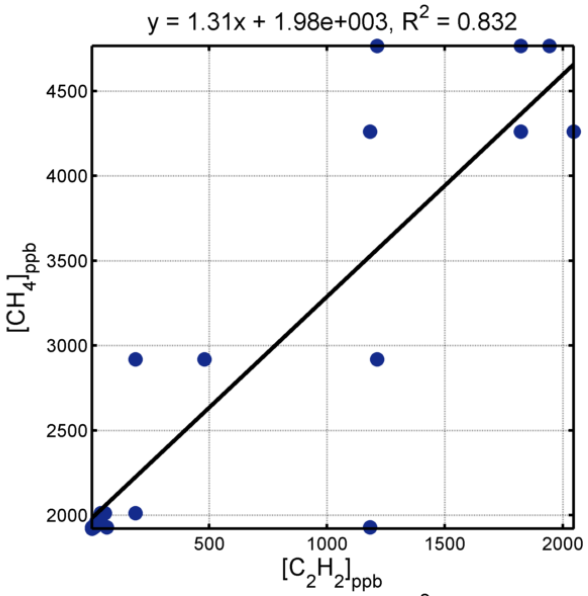
y = 1.31x + 1.98e+003, R2 = 0.832
4500
4000
3500
3000
2500
2000
500
1000
1500
2000
[CH4]ppb
[C2H2]ppb

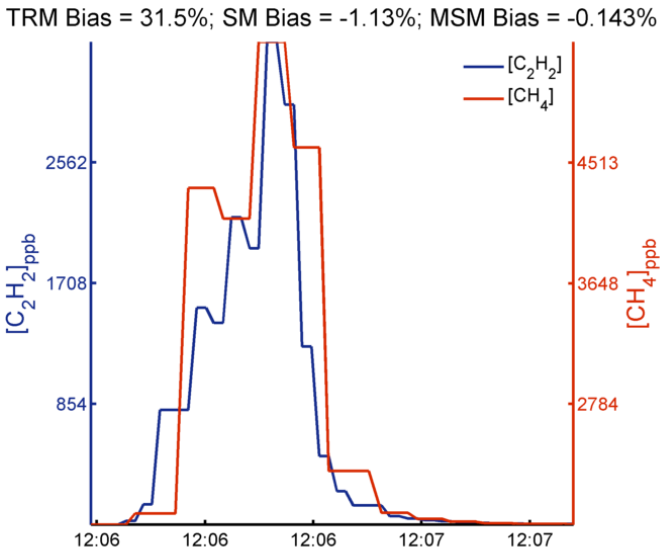
TRM Bias = 31.5%; SM Bias = -1.13%; MSM Bias = -0.143%
[C2H2]
[CH4]
2562
1708
854
4513
3648
2784
[C2H2]ppb
[CH4]ppb
12:06
12:06
12:06
12:07
12:07

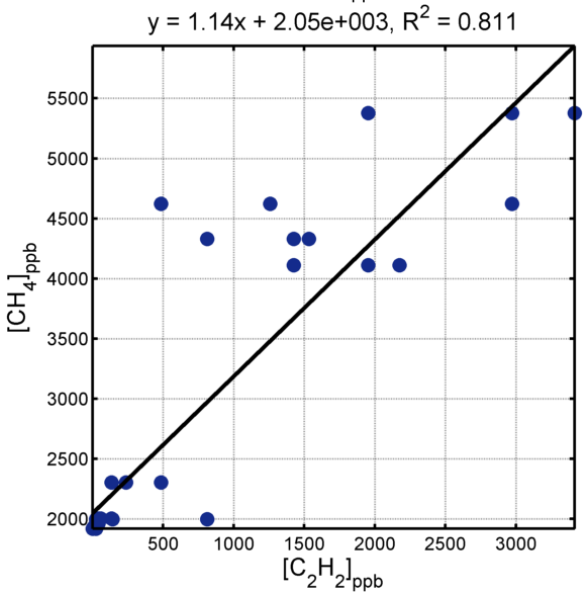
y = 1.14x + 2.05e+003, R2 = 0.811
5500
5000
4500
4000
3500
3000
2500
2000
500
1000
1500
2000
2500
3000
[CH4]ppb
[C2H2]ppb

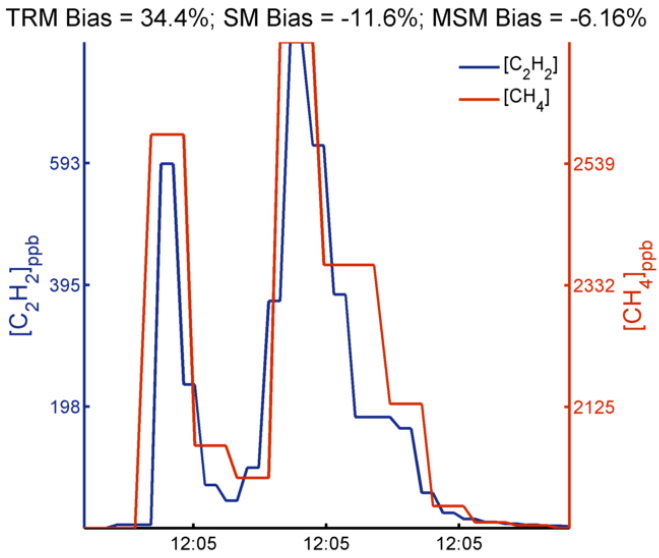
TRM Bias = 34.4%; SM Bias = -11.6%; MSM Bias = -6.16%
[C2H2]
[CH4]
593
395
198
2539
2332
2125
[C2H2]ppb
[CH4]ppb
12:05
12:05
12:05

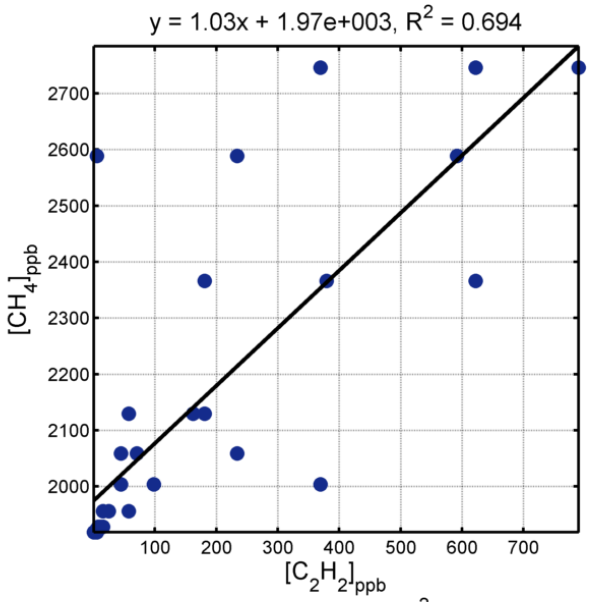
y = 1.03x + 1.97e+003, R2 = 0.694
2700
2600
2500
2400
2300
2200
2100
2000
100
200
300
400
500
600
700
[CH4]ppb
[C2H2]ppb

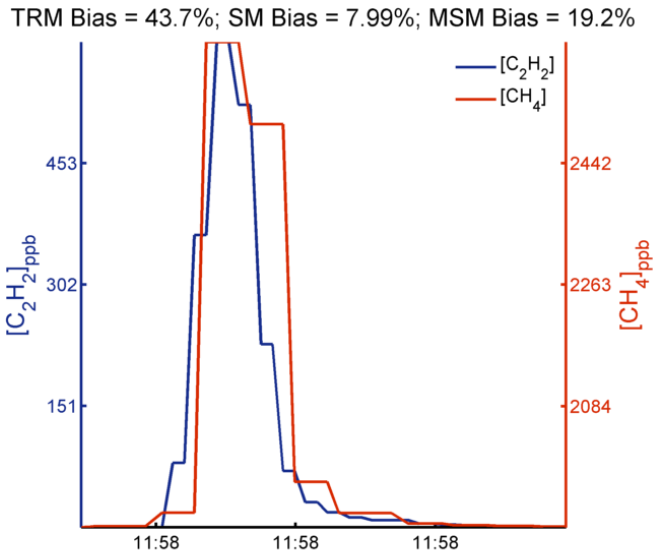
TRM Bias = 43.7%; SM Bias = 7.99%; MSM Bias = 19.2%
[C2H2]
[CH4]
453
302
151
2442
2263
2084
[C2H2]ppb
[CH4]ppb
11:58
11:58
11:58

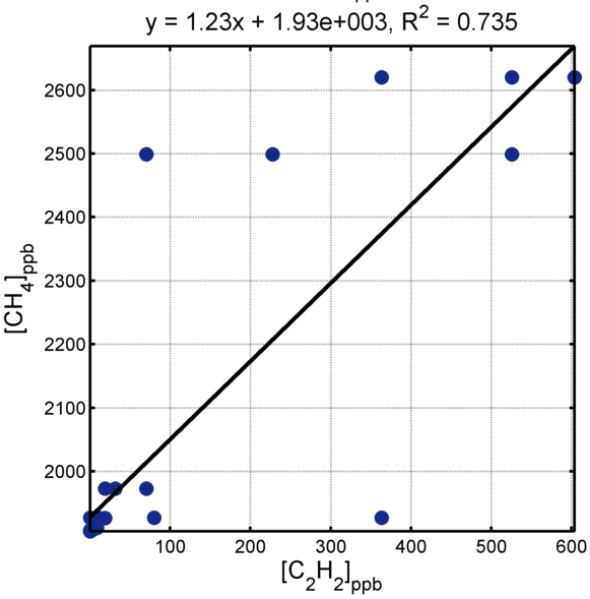
y = 1.23x + 1.93e+003, R2 = 0.735
2600
2500
2400
2300
2200
2100
2000
100
200
300
400
500
600
[CH4]ppb
[C2H2]ppb

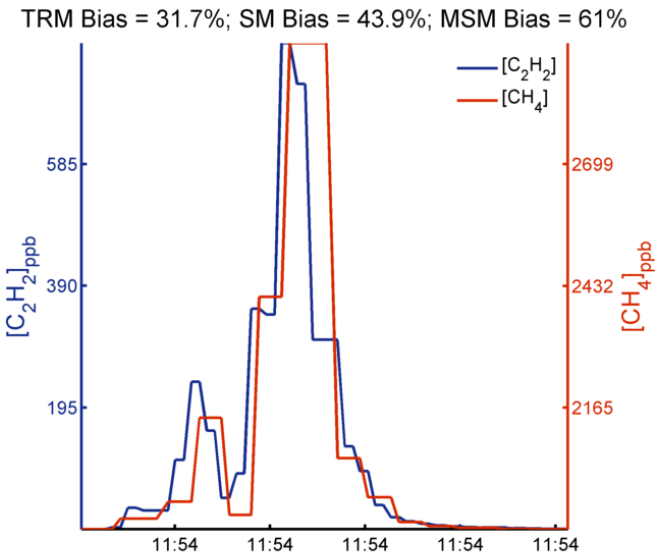
TRM Bias = 31.7%; SM Bias = 43.9%; MSM Bias = 61%
[C2H2]
[CH4]
585
390
195
2699
2432
2165
[C2H2]ppb
[CH4]ppb
11:54
11:54
11:54
11:54
11:54

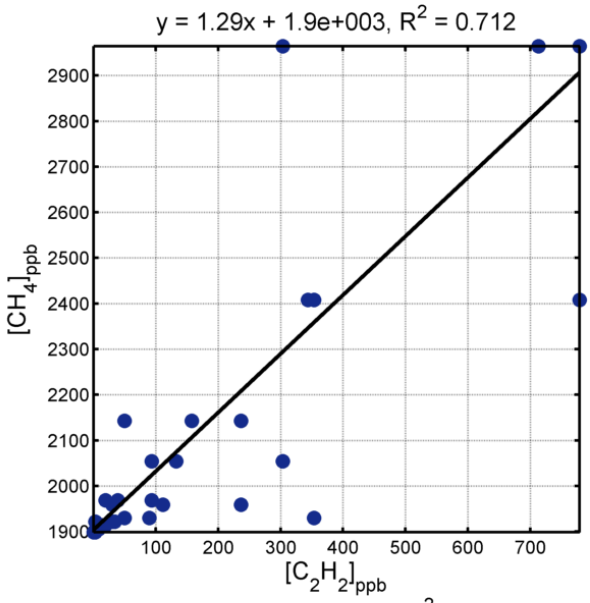
y = 1.29x + 1.9e+003, R2 = 0.712
2900
2800
2700
2600
2500
2400
2300
2200
2100
2000
1900
100
200
300
400
500
600
700
[CH4]ppb
[C2H2]ppb

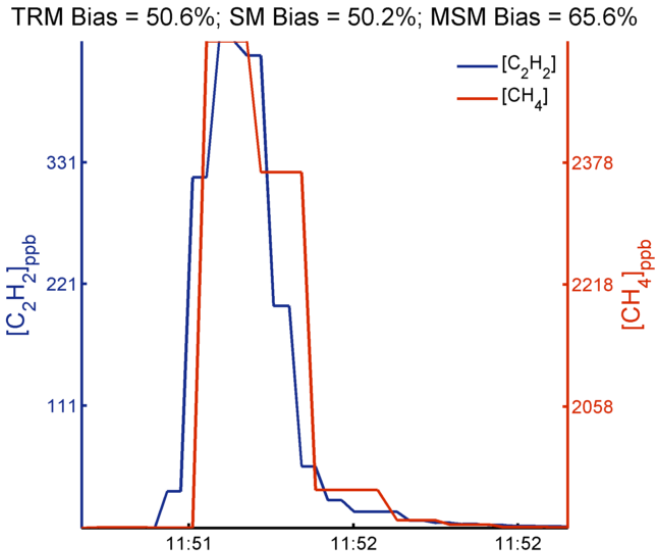
TRM Bias = 50.6%; SM Bias = 50.2%; MSM Bias = 65.6%
[C2H2]
[CH4]
331
221
111
2378
2218
2058
[C2H2]ppb
[CH4]ppb
11:51
11:52
11:52

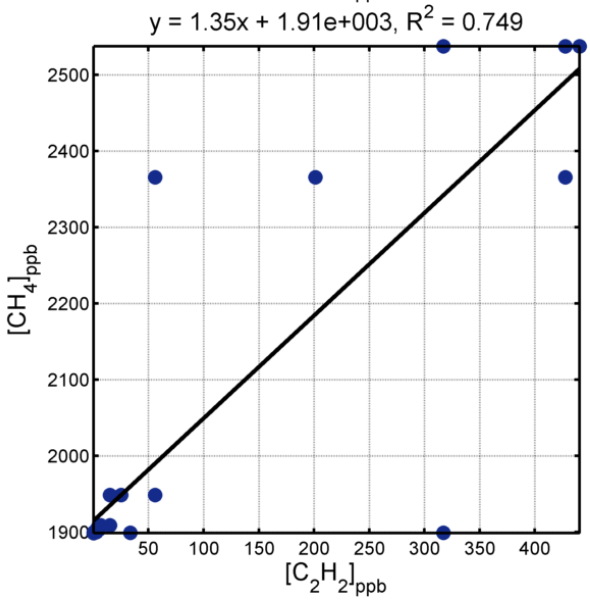
y = 1.35x + 1.91e+003, R2 = 0.749
2500
2400
2300
2200
2100
2000
1900
50
100
150
200
250
300
350
400
[CH4]ppb
[C2H2]ppb

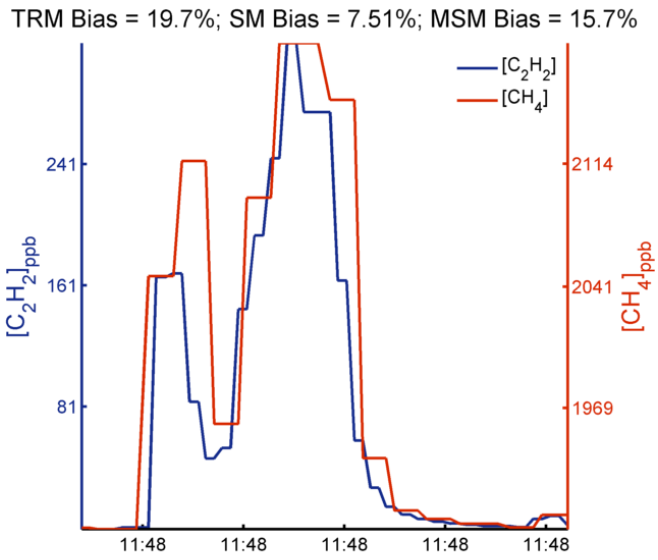
TRM Bias = 19.7%; SM Bias = 7.51%; MSM Bias = 15.7%
[C2H2]
[CH4]
241
161
81
2114
2041
1969
[C2H2]ppb
[CH4]ppb
11:48
11:48
11:48
11:48
11:48

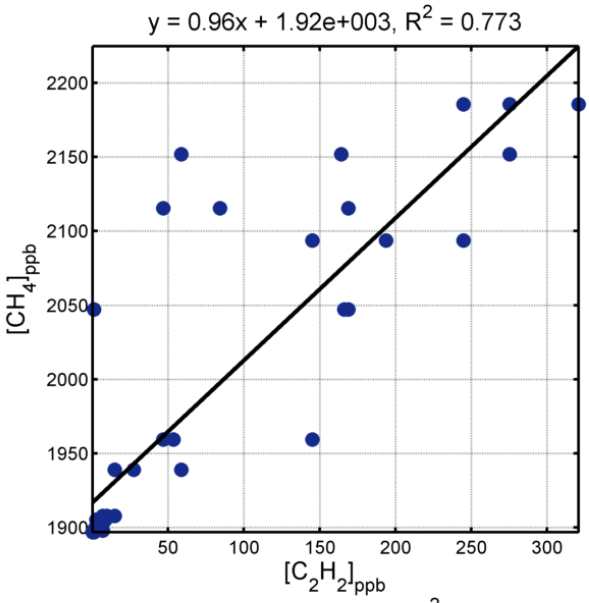
y = 0.96x + 1.92e+003, R2 = 0.773
2200
2150
2100
2050
2000
1950
1900
50
100
150
200
250
300
[CH4]ppb
[C2H2]ppb

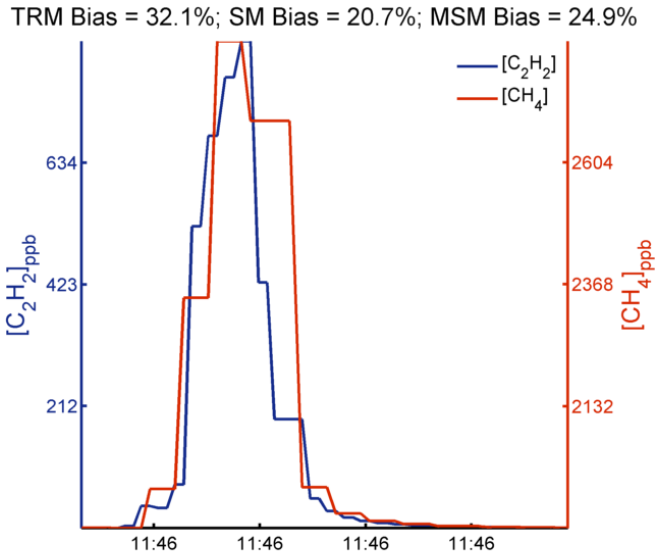
TRM Bias = 32.1%; SM Bias = 20.7%; MSM Bias = 24.9%
[C2H2]
[CH4]
634
423
212
2604
2368
2132
[C2H2]ppb
[CH4]ppb
11:46
11:46
11:46
11:46

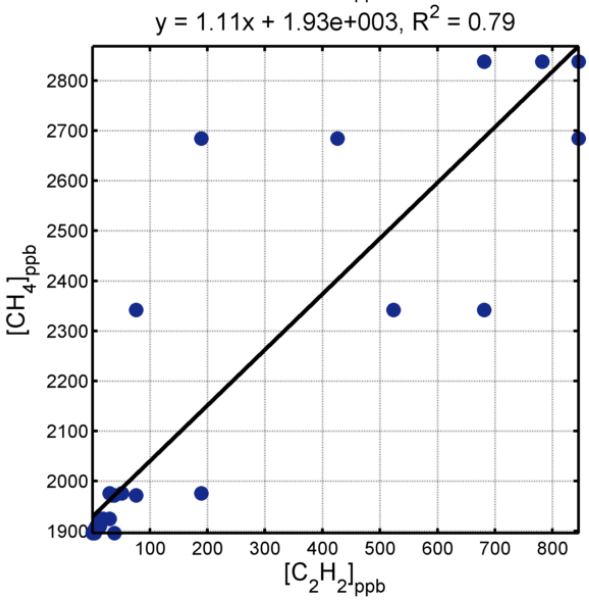
y = 1.11x + 1.93e+003, R2 = 0.79
2800
2700
2600
2500
2400
2300
2200
2100
2000
1900
100
200
300
400
500
600
700
800
[CH4]ppb
[C2H2]ppb

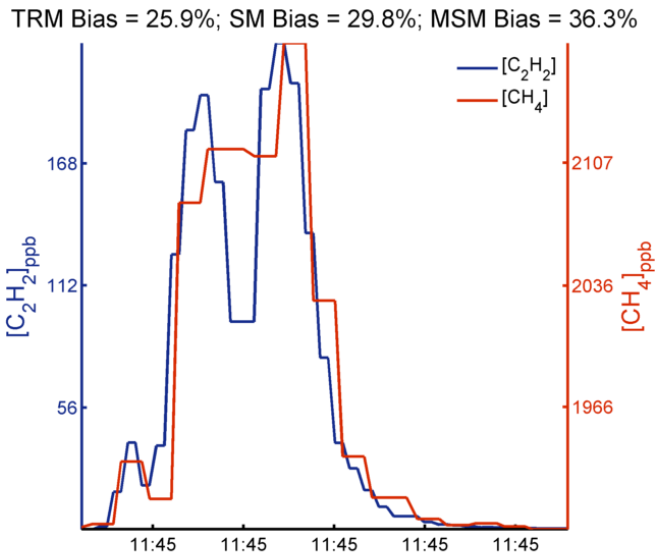
TRM Bias = 25.9%; SM Bias = 29.8%; MSM Bias = 36.3%
[C2H2]
[CH4]
168
112
56
2107
2036
1966
[C2H2]ppb
[CH4]ppb
11:45
11:45
11:45
11:45
11:45

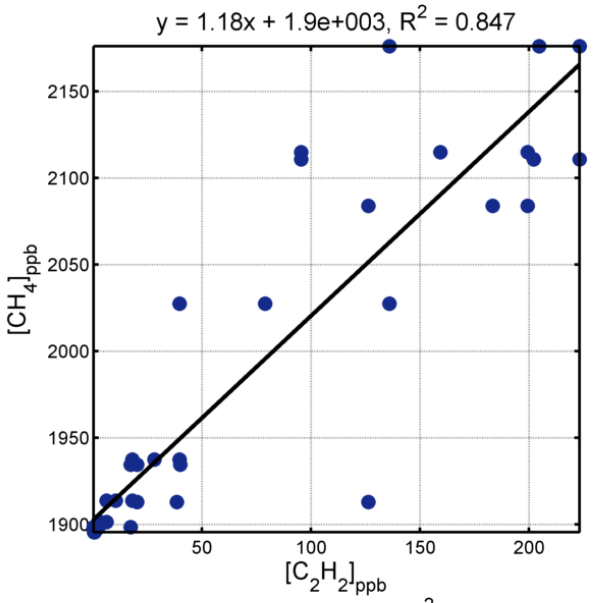
y = 1.18x + 1.9e+003, R2 = 0.847
2150
2100
2050
2000
1950
1900
50
100
150
200
[CH4]ppb
[C2H2]ppb

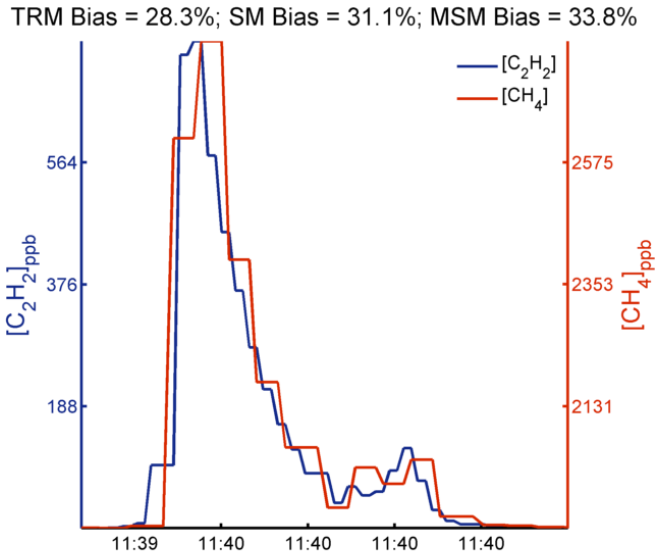
TRM Bias = 28.3%; SM Bias = 31.1%; MSM Bias = 33.8%
[C2H2]
[CH4]
564
376
188
2575
2353
2131
[C2H2]ppb
[CH4]ppb
11:39
11:40
11:40
11:40
11:40

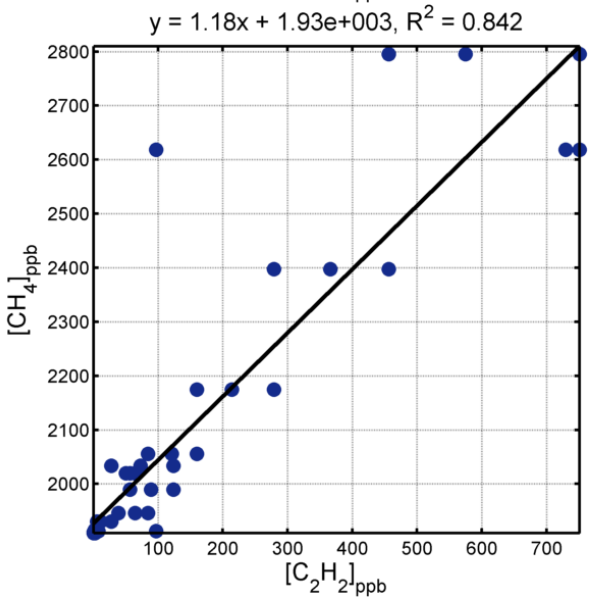
y = 1.18x + 1.93e+003, R2 = 0.842
2800
2700
2600
2500
2400
2300
2200
2100
2000
100
200
300
400
500
600
700
[CH4]ppb
[C2H2]ppb

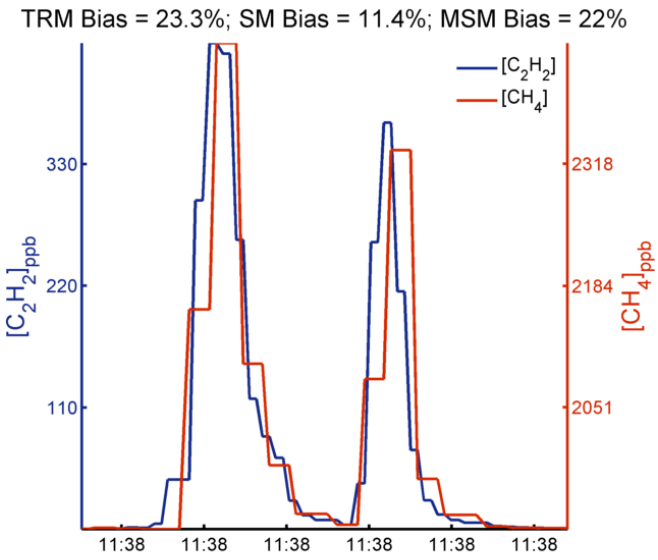
TRM Bias = 23.3%; SM Bias = 11.4%; MSM Bias = 22%
[C2H2]
[CH4]
330
220
110
2318
2184
2051
[C2H2]ppb
[CH4]ppb
11:38
11:38
11:38
11:38
11:38
11:38

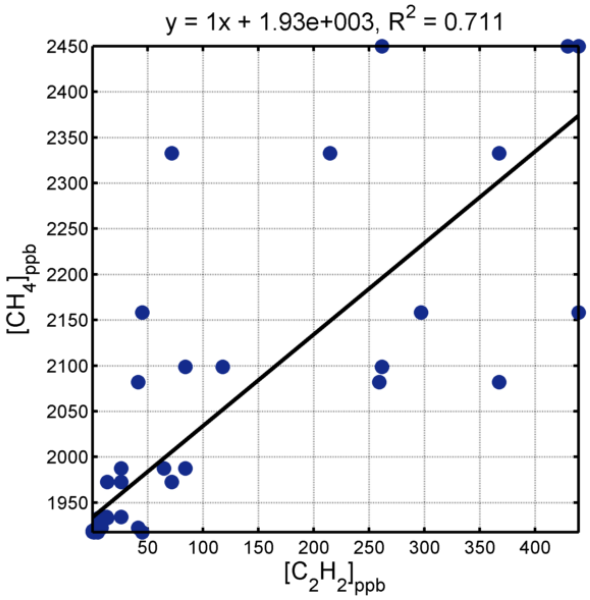
y = 1x + 1.93e+003, R2 = 0.711
2450
2400
2350
2300
2250
2200
2150
2100
2050
2000
1950
50
100
150
200
250
300
350
400
[CH4]ppb
[C2H2]ppb

Appendix B

MOBILE ANALYSIS CONCENTRATION PLOTS WITH SEPARATED SOURCES

Separated 2 meters in the crosswind direction

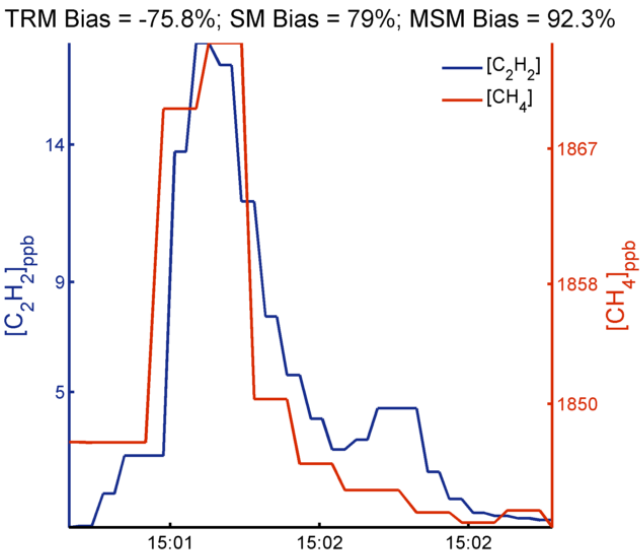

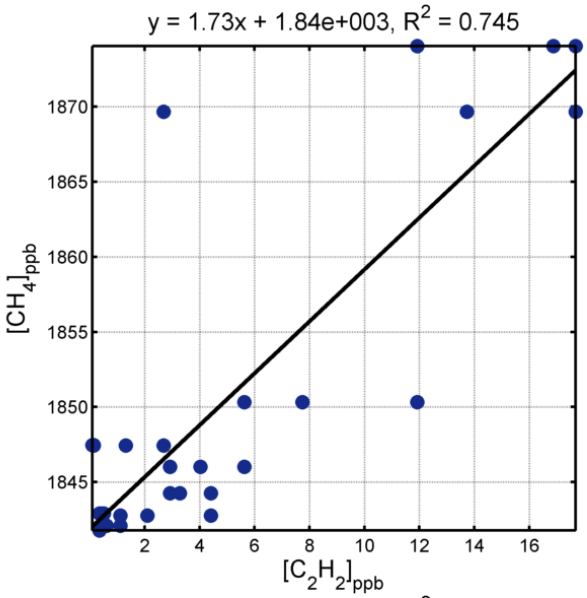

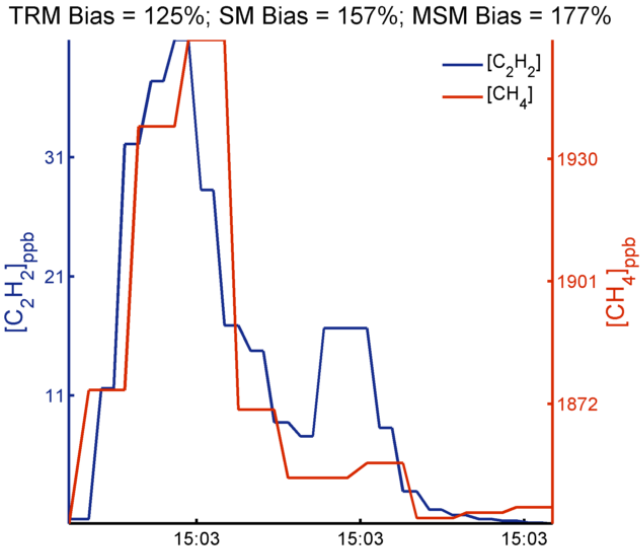

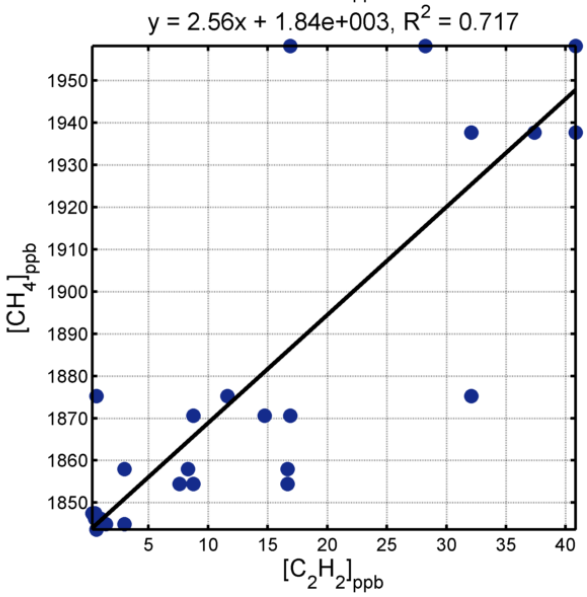

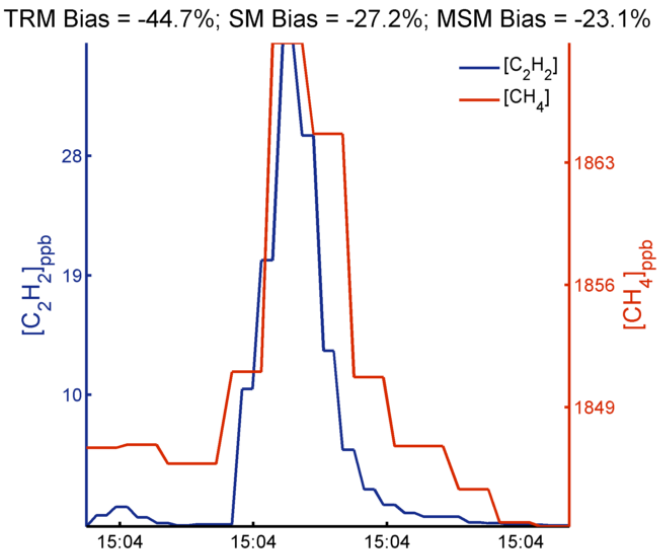
TRM Bias = -44.7%; SM Bias = -27.2%; MSM Bias = -23.1%
[C2H2]
[CH4]
[C2H2]ppb
[CH4]ppb
28
19
10
1863
1856
1849
15:04
15:04
15:04
15:04

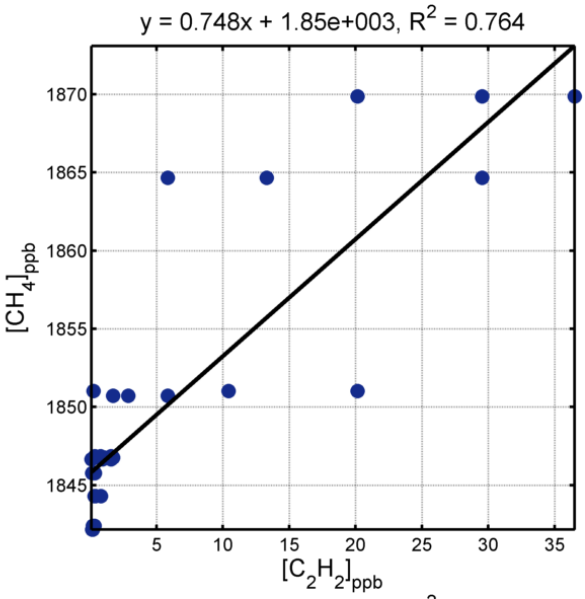
y = 0.748x + 1.85e+003, R2 = 0.764
[CH4]ppb
[C2H2]ppb
1870
1865
1860
1855
1850
1845
5
10
15
20
25
30
35

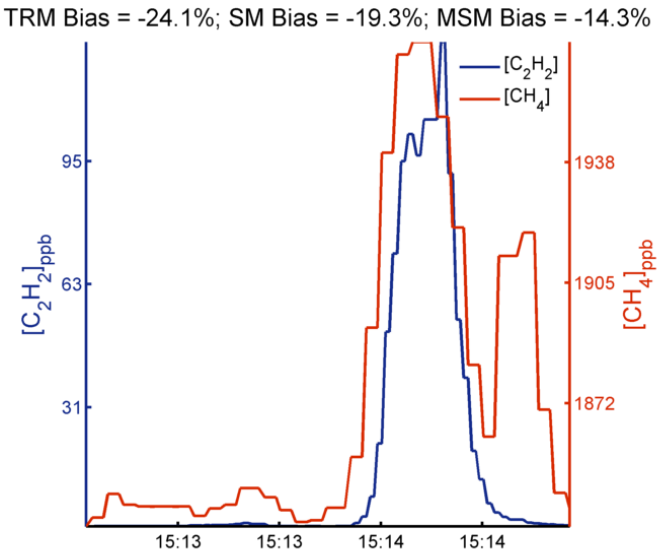
TRM Bias = -24.1%; SM Bias = -19.3%; MSM Bias = -14.3%
[C2H2]
[CH4]
[C2H2]ppb
[CH4]ppb
95
63
31
1938
1905
1872
15:13
15:13
15:14
15:14

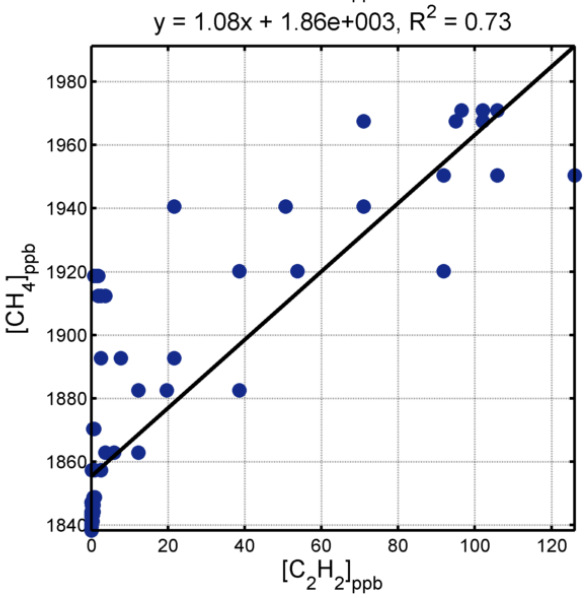
y = 1.08x + 1.86e+003, R2 = 0.73
[CH4]ppb
[C2H2]ppb
1980
1960
1940
1920
1900
1880
1860
1840
0
20
40
60
80
100
120

Acetylene separated 2 meters downwind of methane

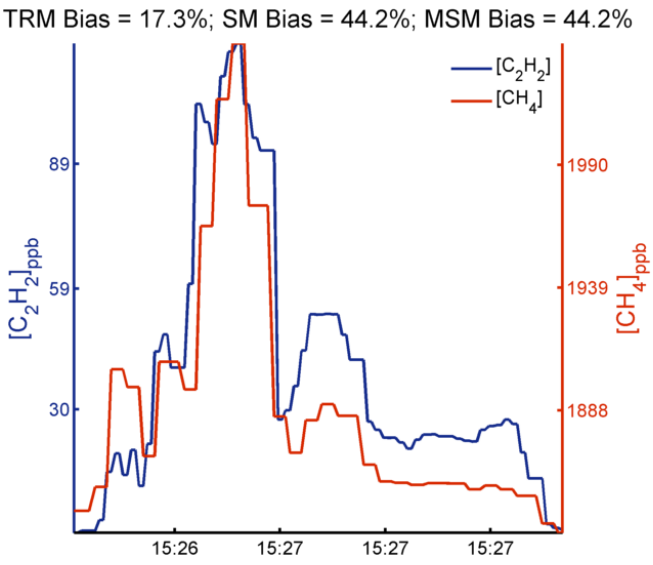

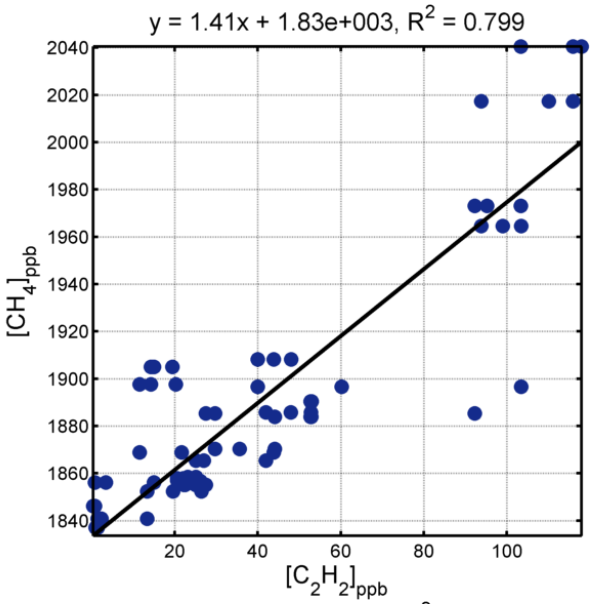

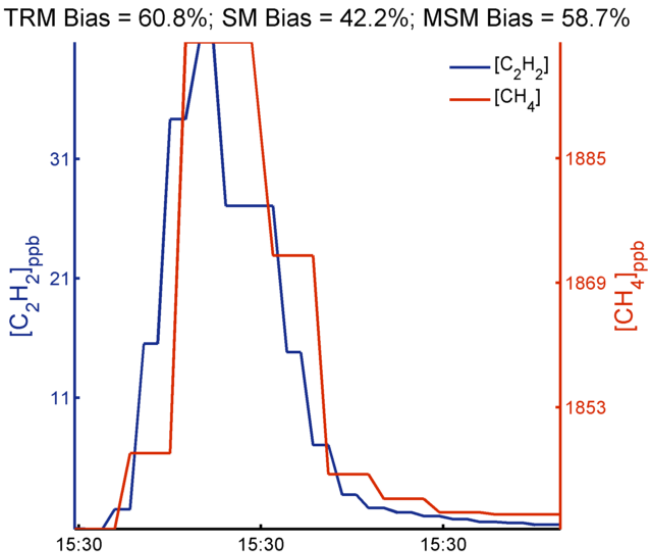

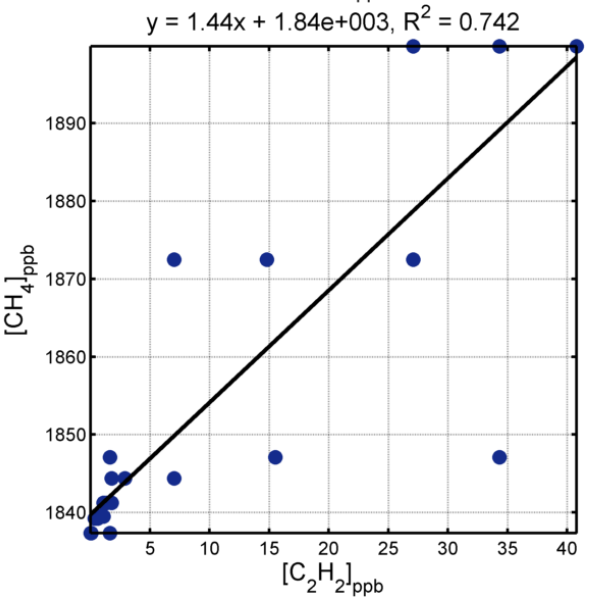

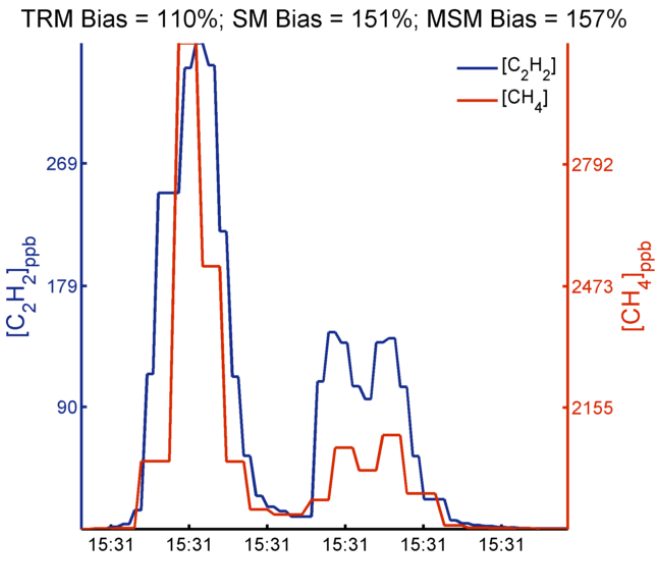
TRM Bias = 110%; SM Bias = 151%; MSM Bias = 157%
[C2H2]
[CH4]
269
179
90
2792
2473
2155
[C2H2]ppb
[CH4]ppb
15:31
15:31
15:31
15:31
15:31
15:31

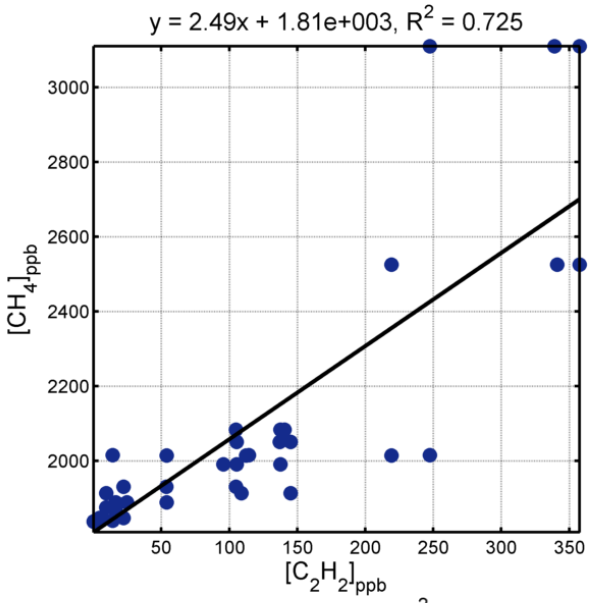
y = 2.49x + 1.81e+003, R2 = 0.725
3000
2800
2600
2400
2200
2000
50
100
150
200
250
300
350
[CH4]ppb
[C2H2]ppb

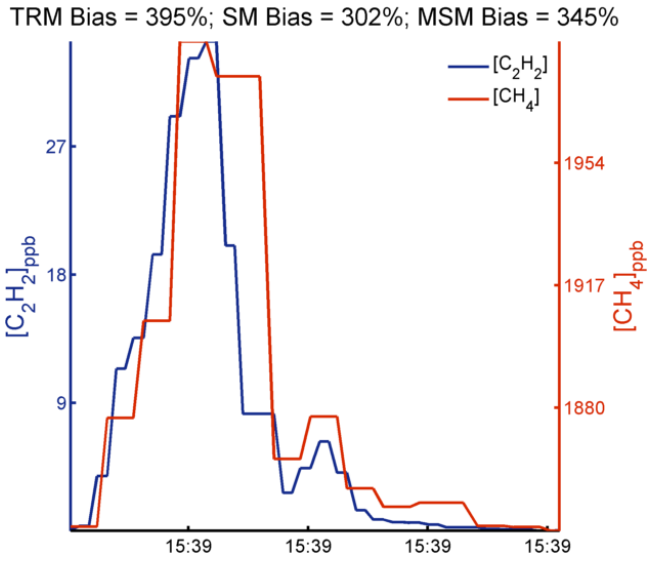
TRM Bias = 395%; SM Bias = 302%; MSM Bias = 345%
[C2H2]
[CH4]
27
18
9
1954
1917
1880
[C2H2]ppb
[CH4]ppb
15:39
15:39
15:39
15:39

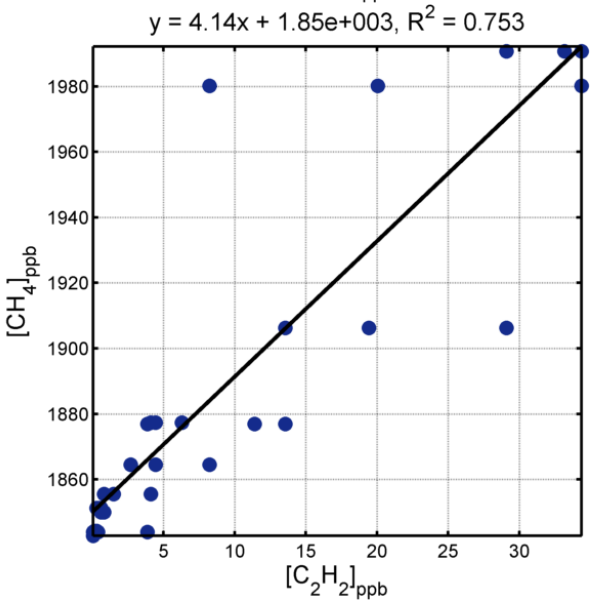
y = 4.14x + 1.85e+003, R2 = 0.753
1980
1960
1940
1920
1900
1880
1860
5
10
15
20
25
30
[CH4]ppb
[C2H2]ppb

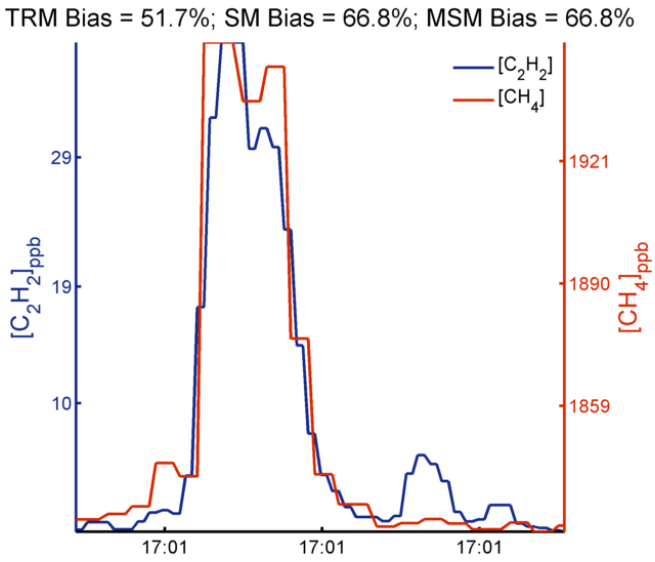
TRM Bias = 51.7%; SM Bias = 66.8%; MSM Bias = 66.8%
[C2H2]
[CH4]
29
19
10
1921
1890
1859
[C2H2]ppb
[CH4]ppb
17:01
17:01
17:01

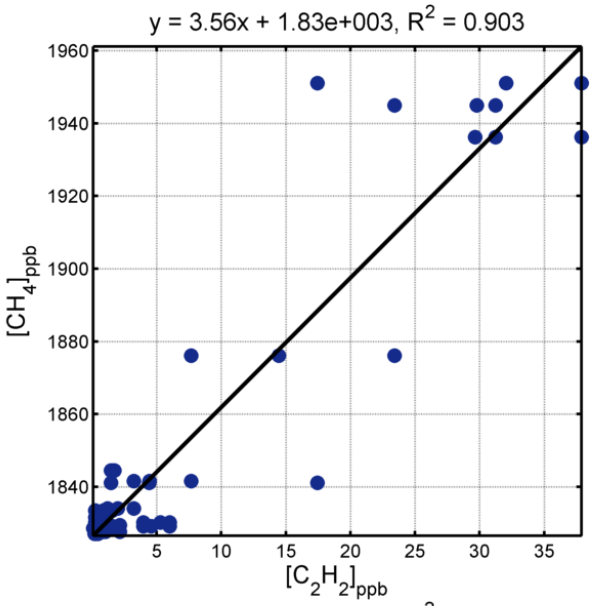
y = 3.56x + 1.83e+003, R2 = 0.903
1960
1940
1920
1900
1880
1860
1840
5
10
15
20
25
30
35
[CH4]ppb
[C2H2]ppb

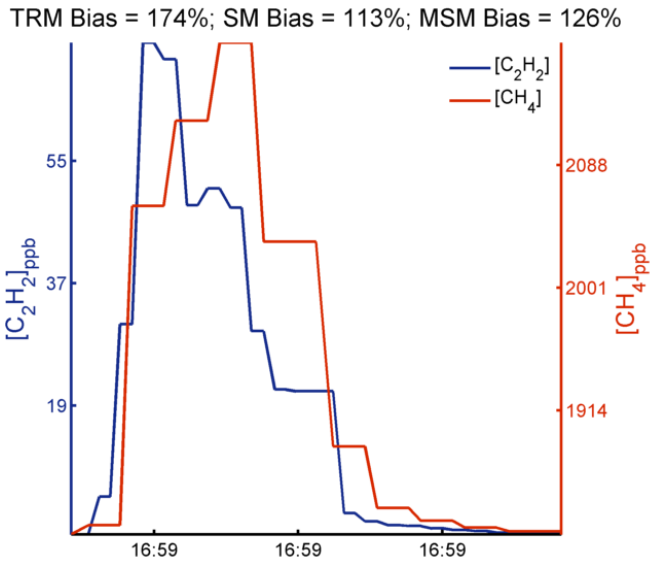
TRM Bias = 174%; SM Bias = 113%; MSM Bias = 126%
[C2H2]
[CH4]
55
37
19
2088
2001
1914
[C2H2]ppb
[CH4]ppb
16:59
16:59
16:59

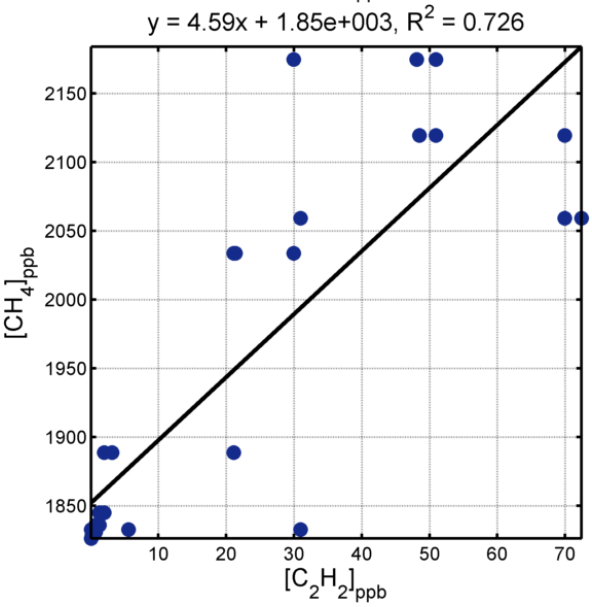
y = 4.59x + 1.85e+003, R2 = 0.726
2150
2100
2050
2000
1950
1900
1850
10
20
30
40
50
60
70
[CH4]ppb
[C2H2]ppb

Acetylene released 2 meters above-ground; methane released at ground-level

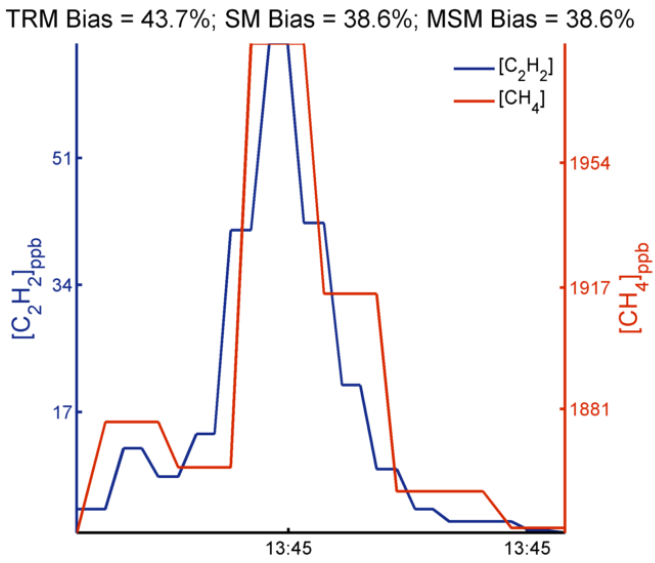

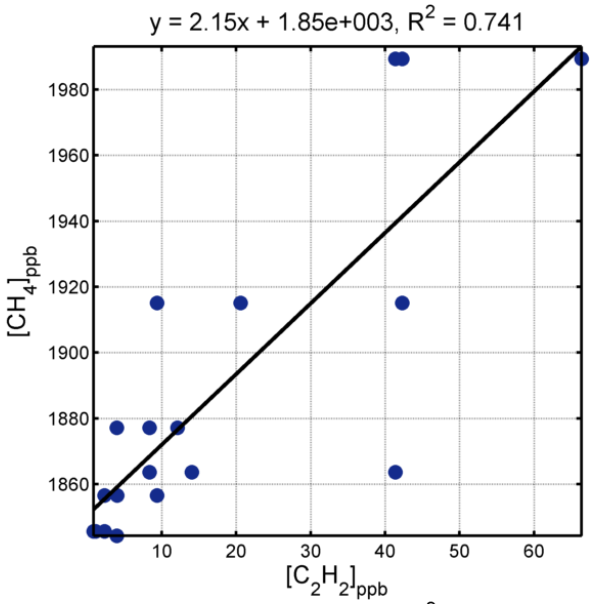

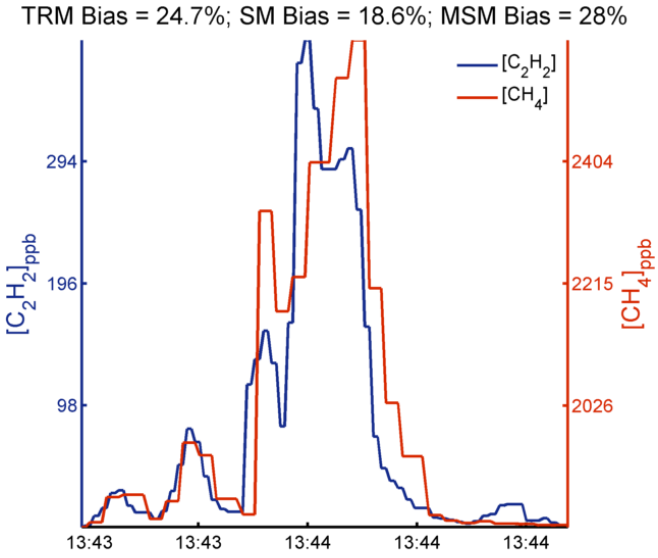

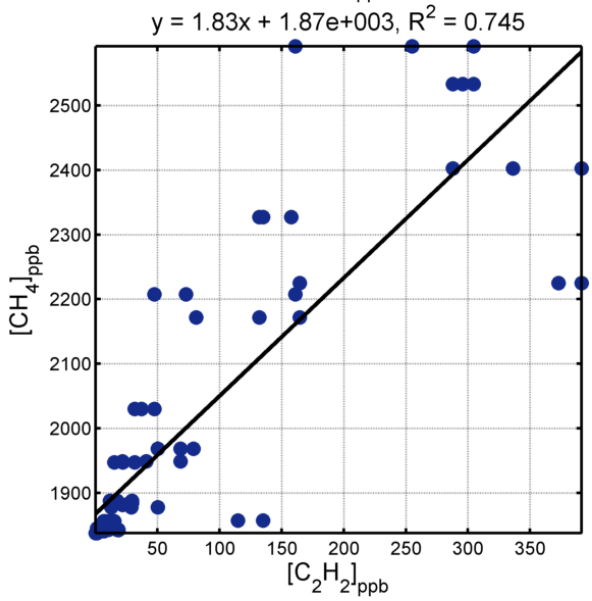

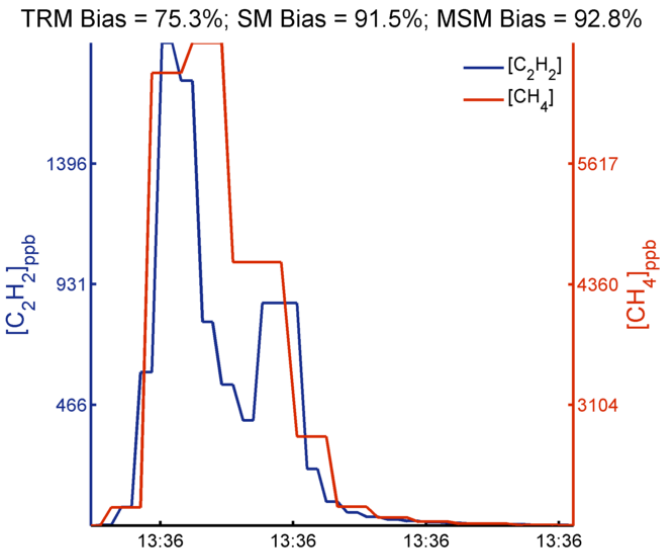
TRM Bias = 75.3%; SM Bias = 91.5%; MSM Bias = 92.8%
[C2H2]
[CH4]
1396
931
466
5617
4360
3104
[C2H2]ppb
[CH4]ppb
13:36
13:36
13:36
13:36

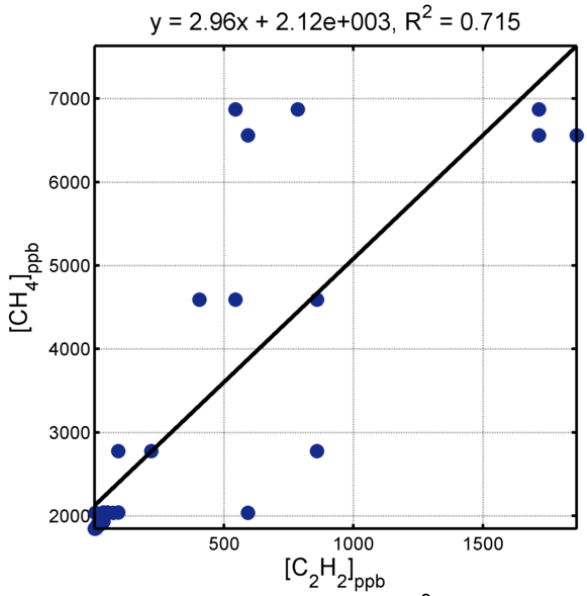
y = 2.96x + 2.12e+003, R2 = 0.715
7000
6000
5000
4000
3000
2000
500
1000
1500
[CH4]ppb
[C2H2]ppb

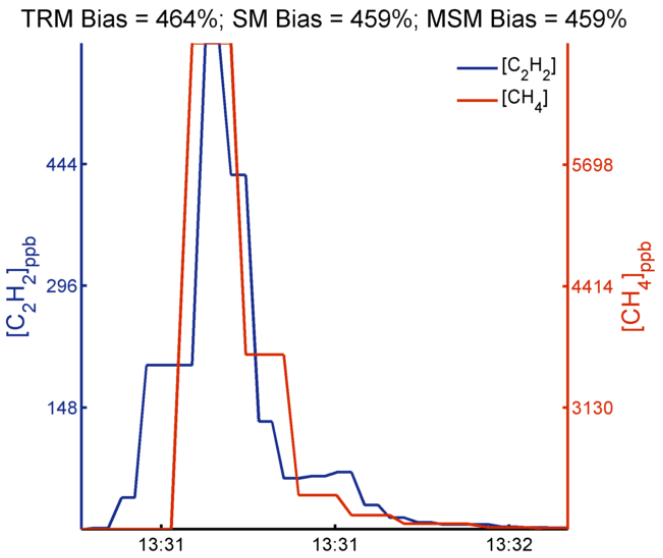
TRM Bias = 464%; SM Bias = 459%; MSM Bias = 459%
[C2H2]
[CH4]
444
296
148
5698
4414
3130
[C2H2]ppb
[CH4]ppb
13:31
13:31
13:32

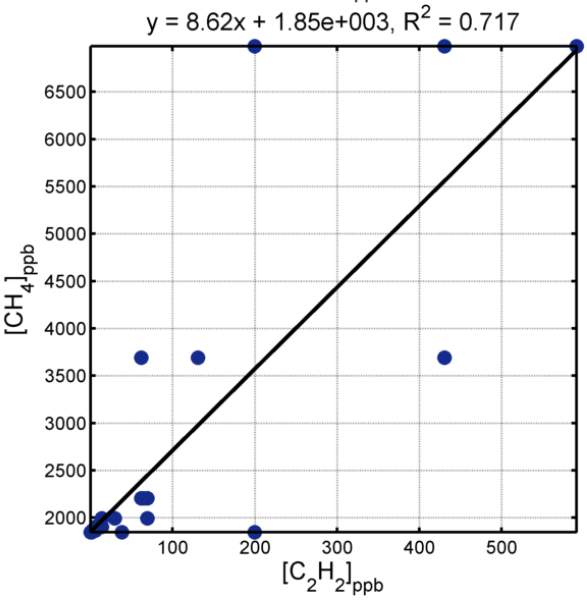
y = 8.62x + 1.85e+003, R2 = 0.717
6500
6000
5500
5000
4500
4000
3500
3000
2500
2000
100
200
300
400
500
[CH4]ppb
[C2H2]ppb

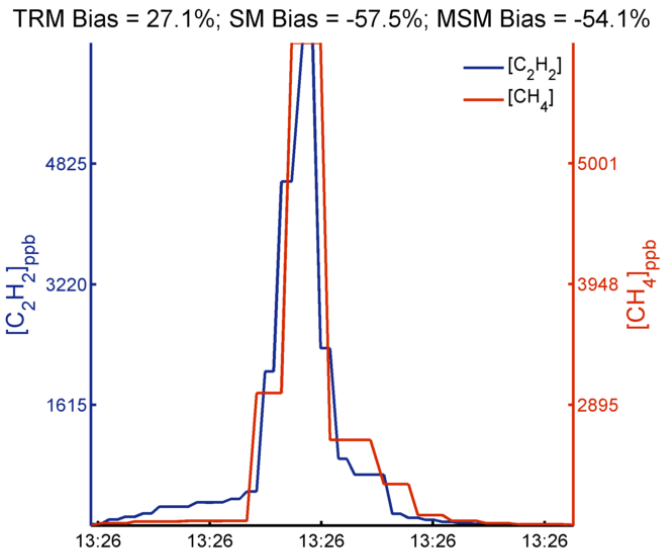
TRM Bias = 27.1%; SM Bias = -57.5%; MSM Bias = -54.1%
[C2H2]
[CH4]
4825
3220
1615
5001
3948
2895
[C2H2]ppb
[CH4]ppb
13:26
13:26
13:26
13:26
13:26

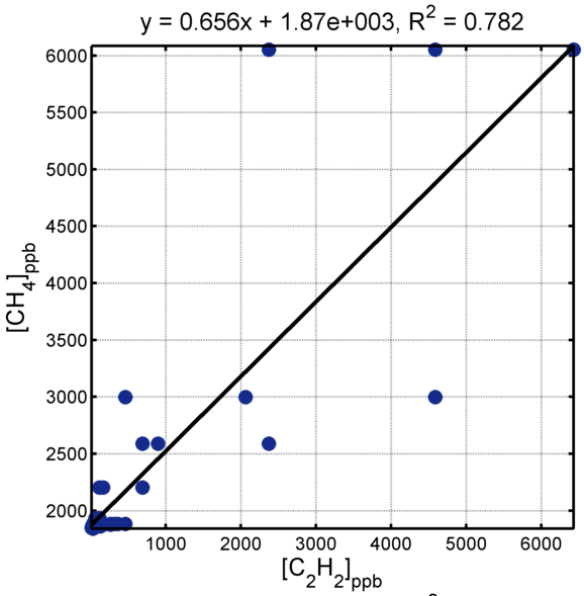
y = 0.656x + 1.87e+003, R2 = 0.782
6000
5500
5000
4500
4000
3500
3000
2500
2000
1000
2000
3000
4000
5000
6000
[CH4]ppb
[C2H2]ppb

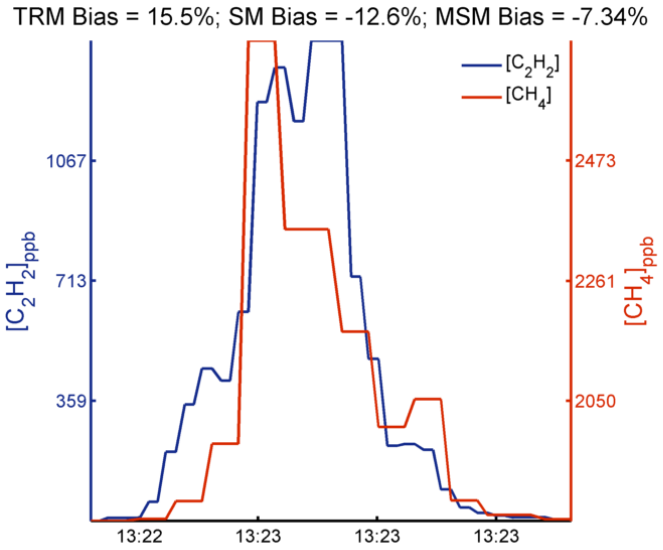
TRM Bias = 15.5%; SM Bias = -12.6%; MSM Bias = -7.34%
[C2H2]
[CH4]
1067
713
359
2473
2261
2050
[C2H2]ppb
[CH4]ppb
13:22
13:23
13:23
13:23

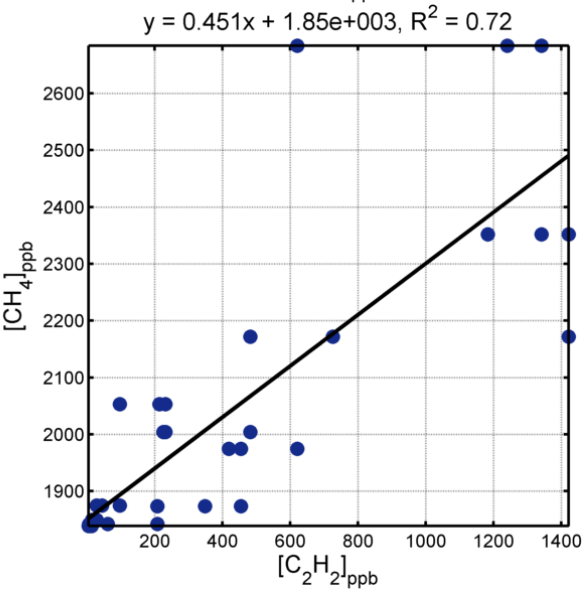
y = 0.451x + 1.85e+003, R2 = 0.72
2600
2500
2400
2300
2200
2100
2000
1900
200
400
600
800
1000
1200
1400
[CH4]ppb
[C2H2]ppb

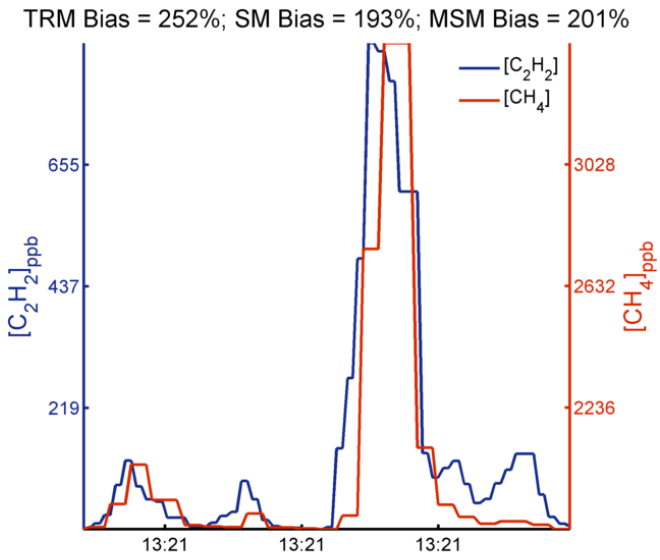
TRM Bias = 252%; SM Bias = 193%; MSM Bias = 201%
[C2H2]
[CH4]
655
437
219
3028
2632
2236
[C2H2]ppb
[CH4]ppb
13:21
13:21
13:21

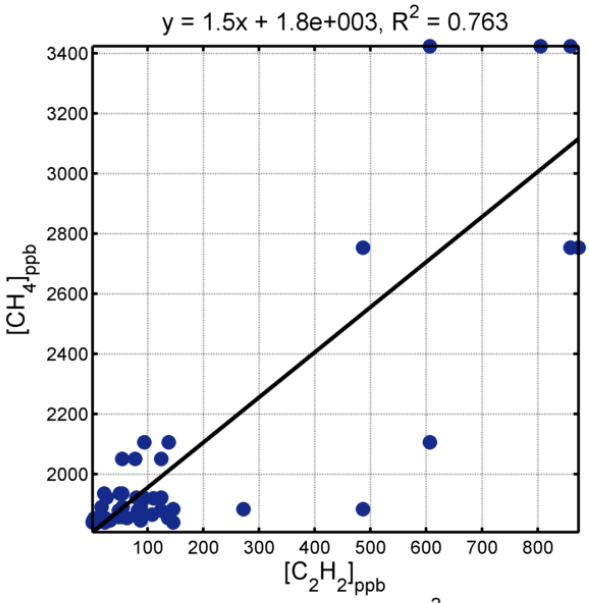
y = 1.5x + 1.8e+003, R2 = 0.763
3400
3200
3000
2800
2600
2400
2200
2000
100
200
300
400
500
600
700
800
[CH4]ppb
[C2H2]ppb

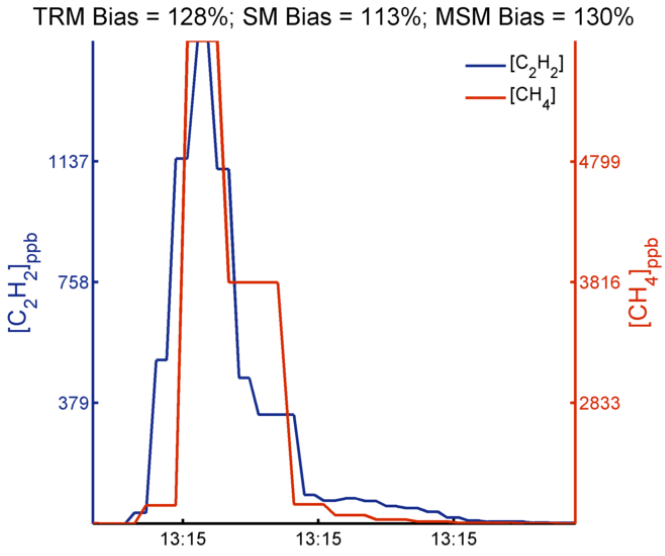
TRM Bias = 128%; SM Bias = 113%; MSM Bias = 130%
[C2H2]
[CH4]
1137
758
379
4799
3816
2833
[C2H2]ppb
[CH4]ppb
13:15
13:15
13:15

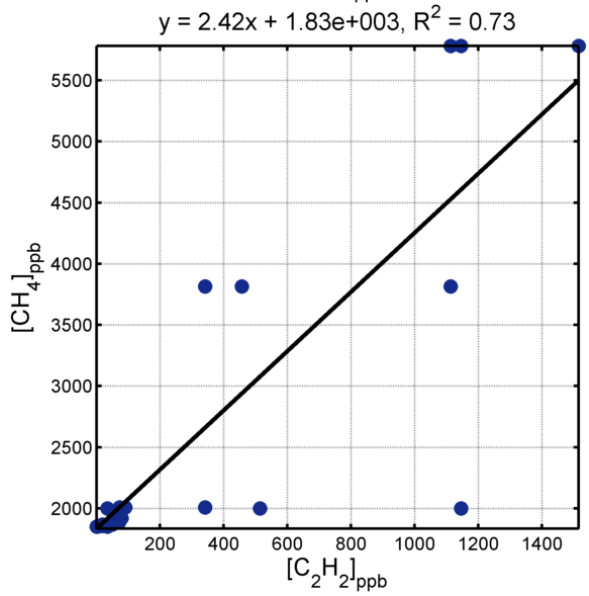
y = 2.42x + 1.83e+003, R2 = 0.73
5500
5000
4500
4000
3500
3000
2500
2000
200
400
600
800
1000
1200
1400
[CH4]ppb
[C2H2]ppb

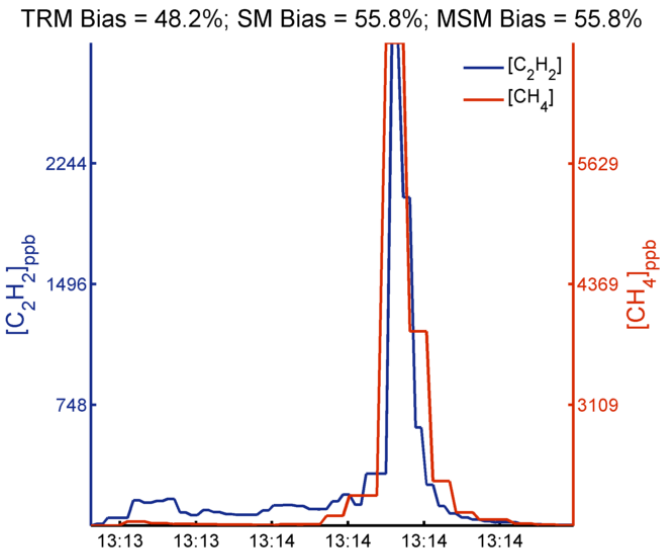
TRM Bias = 48.2%; SM Bias = 55.8%; MSM Bias = 55.8%
[C2H2]
[CH4]
2244
1496
748
5629
4369
3109
[C2H2]ppb
[CH4]ppb
13:13
13:13
13:14
13:14
13:14
13:14

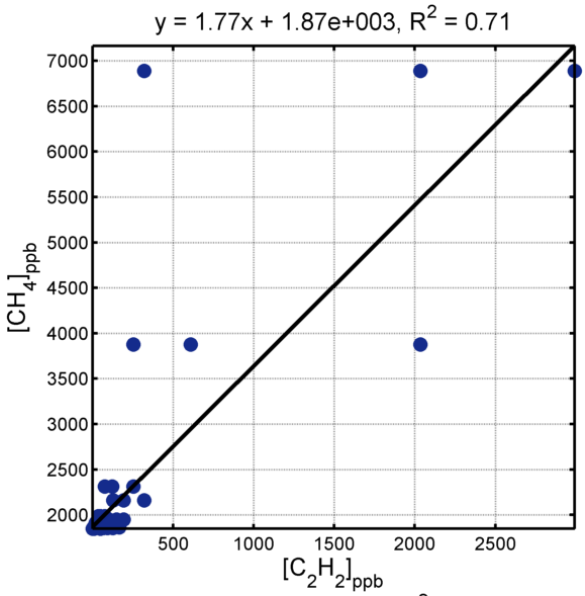
y = 1.77x + 1.87e+003, R2 = 0.71
7000
6500
6000
5500
5000
4500
4000
3500
3000
2500
2000
500
1000
1500
2000
2500
[CH4]ppb
[C2H2]ppb

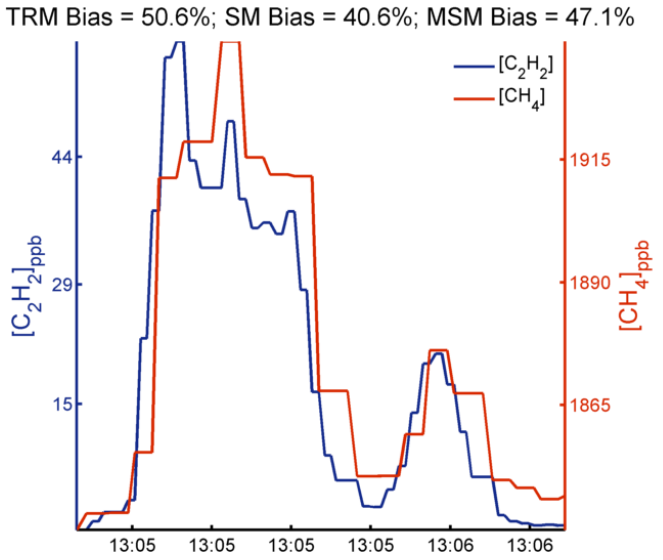
TRM Bias = 50.6%; SM Bias = 40.6%; MSM Bias = 47.1%
[C2H2]
[CH4]
44
29
15
1915
1890
1865
[C2H2]ppb
[CH4]ppb
13:05
13:05
13:05
13:05
13:06
13:06

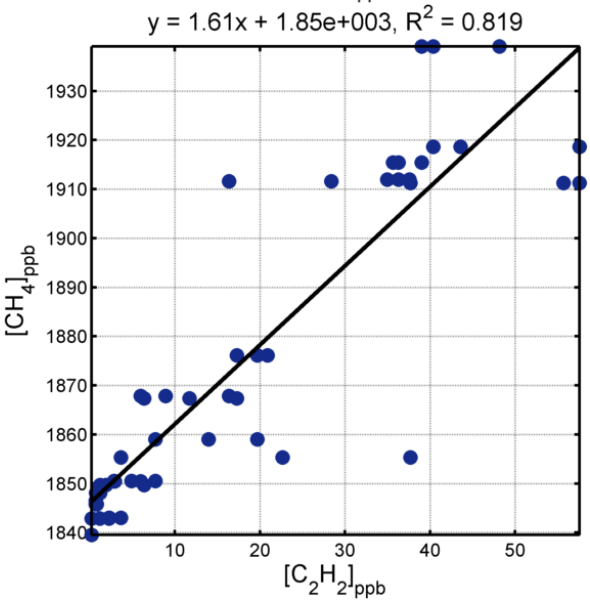
y = 1.61x + 1.85e+003, R2 = 0.819
1930
1920
1910
1900
1890
1880
1870
1860
1850
1840
10
20
30
40
50
[CH4]ppb
[C2H2]ppb

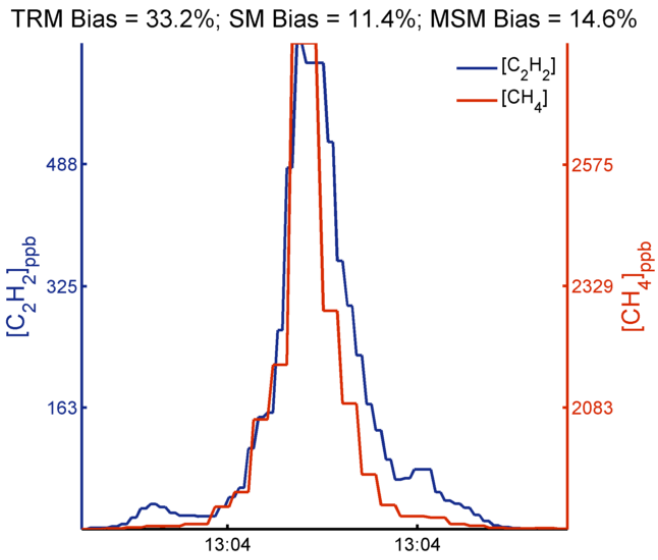
TRM Bias = 33.2%; SM Bias = 11.4%; MSM Bias = 14.6%
[C2H2]
[CH4]
488
325
163
2575
2329
2083
[C2H2]ppb
[CH4]ppb
13:04
13:04

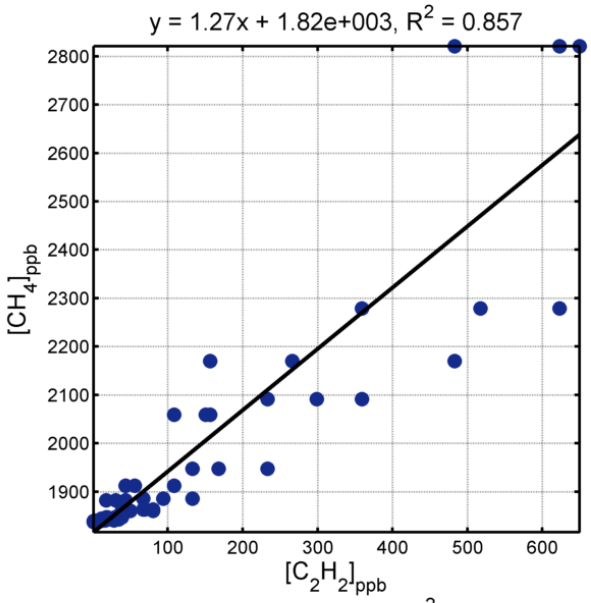
y = 1.27x + 1.82e+003, R2 = 0.857
2800
2700
2600
2500
2400
2300
2200
2100
2000
1900
100
200
300
400
500
600
[CH4]ppb
[C2H2]ppb

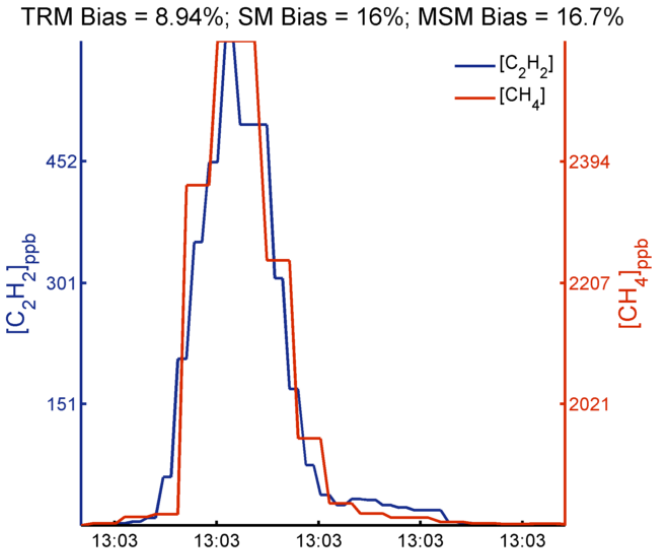
TRM Bias = 8.94%; SM Bias = 16%; MSM Bias = 16.7%
[C2H2]
[CH4]
452
301
151
2394
2207
2021
[C2H2]ppb
[CH4]ppb
13:03
13:03
13:03
13:03
13:03

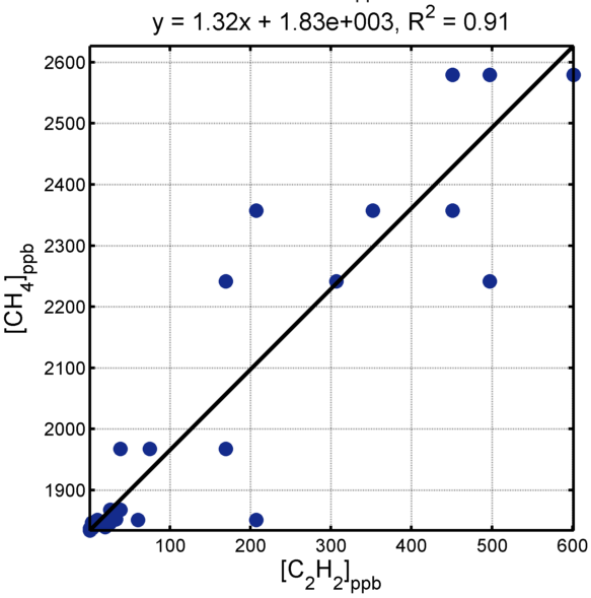
y = 1.32x + 1.83e+003, R2 = 0.91
2600
2500
2400
2300
2200
2100
2000
1900
100
200
300
400
500
600
[CH4]ppb
[C2H2]ppb

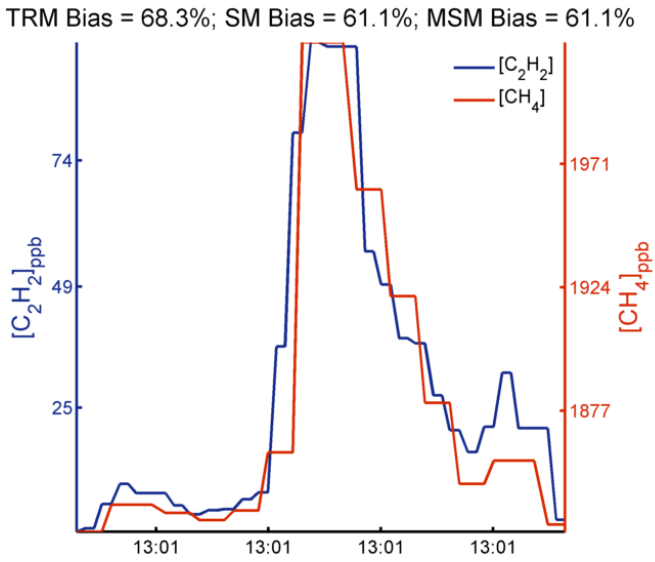
TRM Bias = 68.3%; SM Bias = 61.1%; MSM Bias = 61.1%
[C2H2]
[CH4]
74
49
25
1971
1924
1877
[C2H2]ppb
[CH4]ppb
13:01
13:01
13:01
13:01

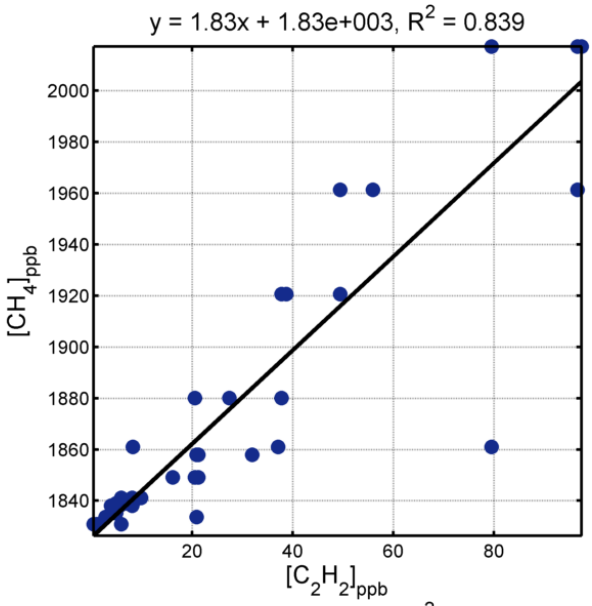
y = 1.83x + 1.83e+003, R2 = 0.839
2000
1980
1960
1940
1920
1900
1880
1860
1840
20
40
60
80
[CH4]ppb
[C2H2]ppb

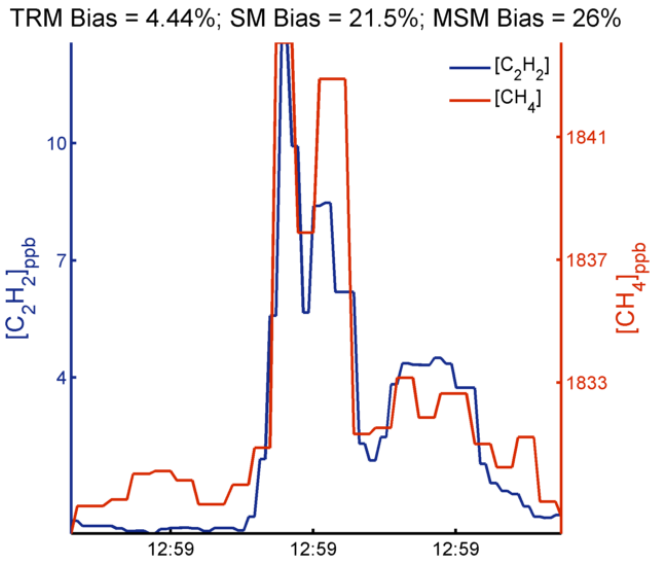
TRM Bias = 4.44%; SM Bias = 21.5%; MSM Bias = 26%
[C2H2]
[CH4]
10
7
4
1841
1837
1833
[C2H2]ppb
[CH4]ppb
12:59
12:59
12:59

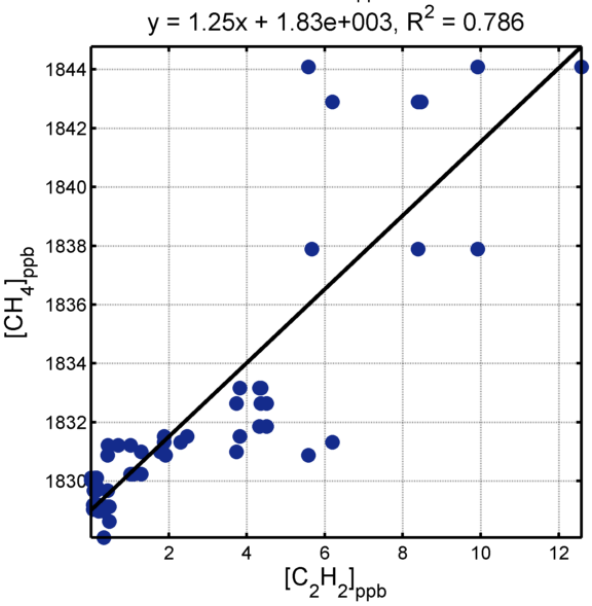
y = 1.25x + 1.83e+003, R2 = 0.786
1844
1842
1840
1838
1836
1834
1832
1830
2
4
6
8
10
12
[CH4]ppb
[C2H2]ppb

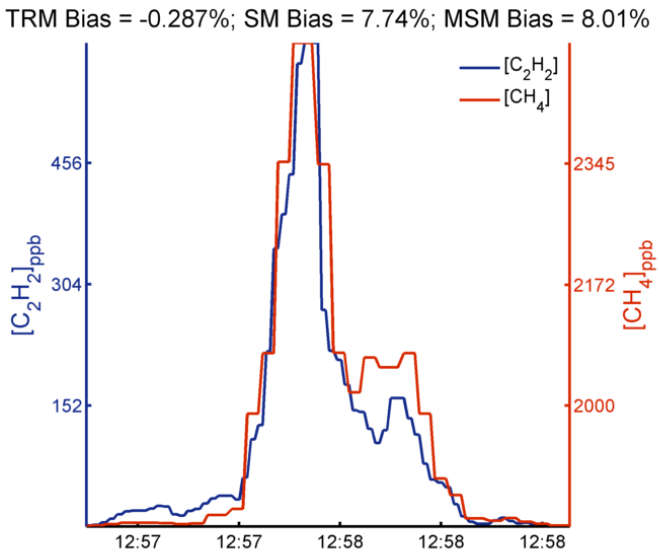
TRM Bias = -0.287%; SM Bias = 7.74%; MSM Bias = 8.01%
[C2H2]
[CH4]
456
304
152
2345
2172
2000
[C2H2]ppb
[CH4]ppb
12:57
12:57
12:58
12:58
12:58

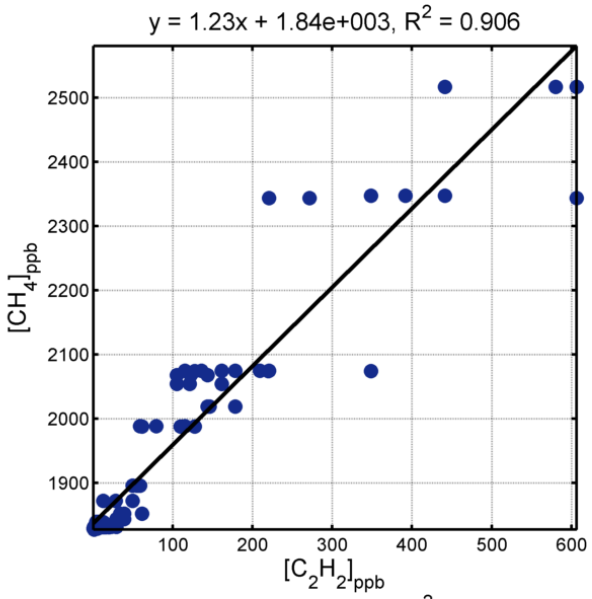
y = 1.23x + 1.84e+003, R2 = 0.906
2500
2400
2300
2200
2100
2000
1900
100
200
300
400
500
600
[CH4]ppb
[C2H2]ppb

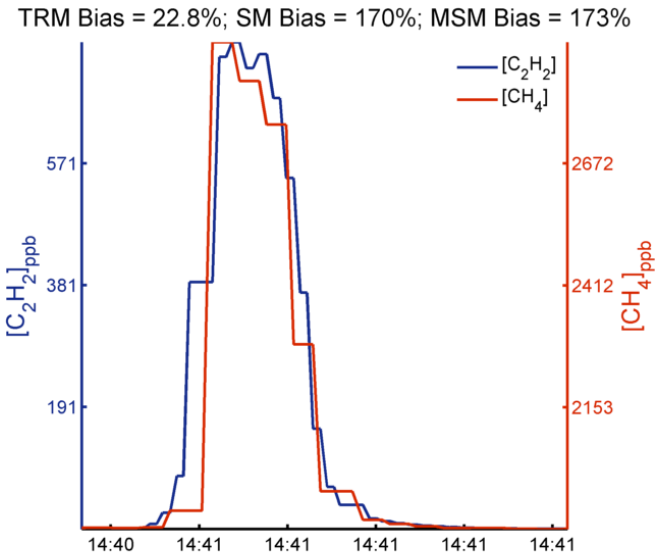
TRM Bias = 22.8%; SM Bias = 170%; MSM Bias = 173%
[C2H2]
[CH4]
571
381
191
2672
2412
2153
[C2H2]ppb
[CH4]ppb
14:40
14:41
14:41
14:41
14:41
14:41

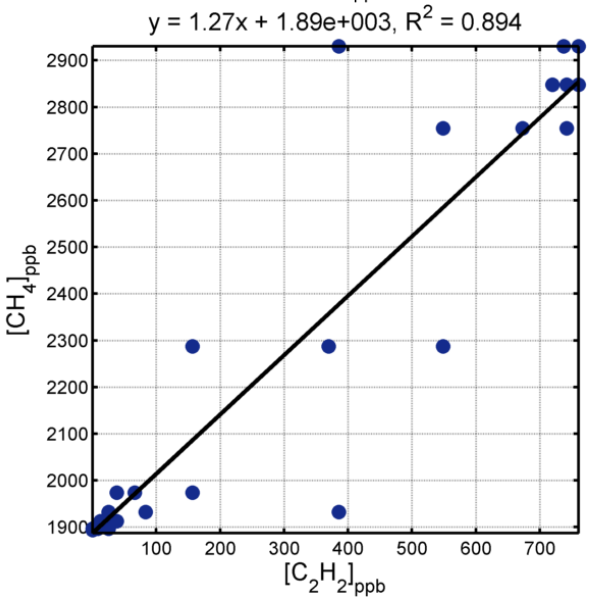
y = 1.27x + 1.89e+003, R2 = 0.894
2900
2800
2700
2600
2500
2400
2300
2200
2100
2000
1900
100
200
300
400
500
600
700
[CH4]ppb
[C2H2]ppb

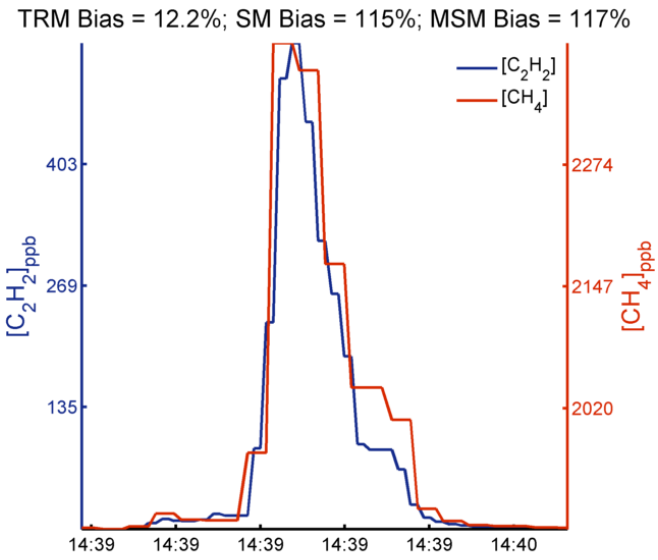
TRM Bias = 12.2%; SM Bias = 115%; MSM Bias = 117%
[C2H2]
[CH4]
403
269
135
2274
2147
2020
[C2H2]ppb
[CH4]ppb
14:39
14:39
14:39
14:39
14:39
14:40

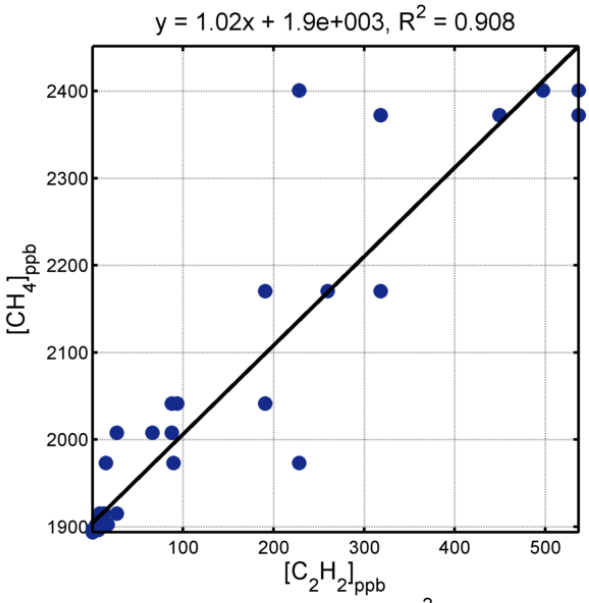
y = 1.02x + 1.9e+003, R2 = 0.908
2400
2300
2200
2100
2000
1900
100
200
300
400
500
[CH4]ppb
[C2H2]ppb

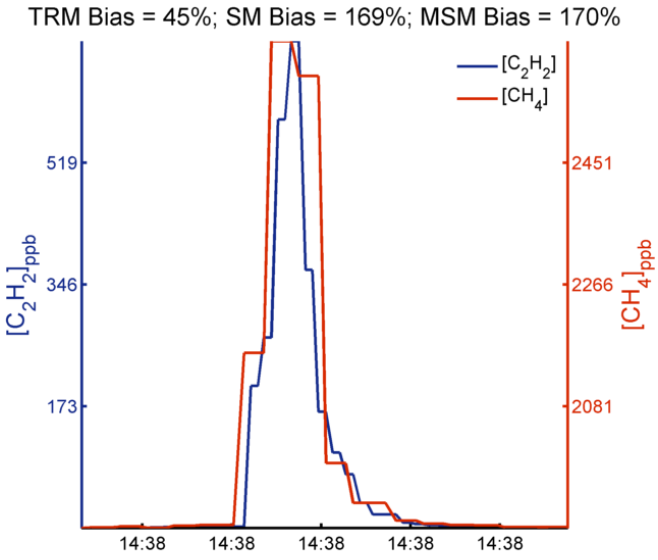
TRM Bias = 45%; SM Bias = 169%; MSM Bias = 170%
[C2H2]
[CH4]
519
346
173
2451
2266
2081
[C2H2]ppb
[CH4]ppb
14:38
14:38
14:38
14:38
14:38

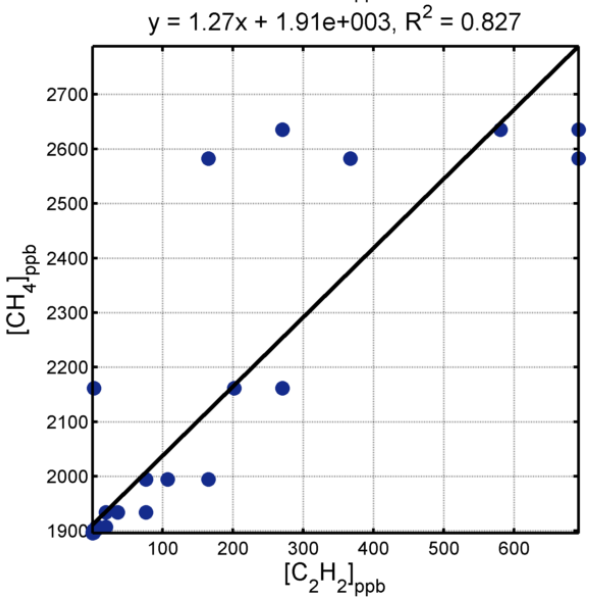
y = 1.27x + 1.91e+003, R2 = 0.827
2700
2600
2500
2400
2300
2200
2100
2000
1900
100
200
300
400
500
600
[CH4]ppb
[C2H2]ppb

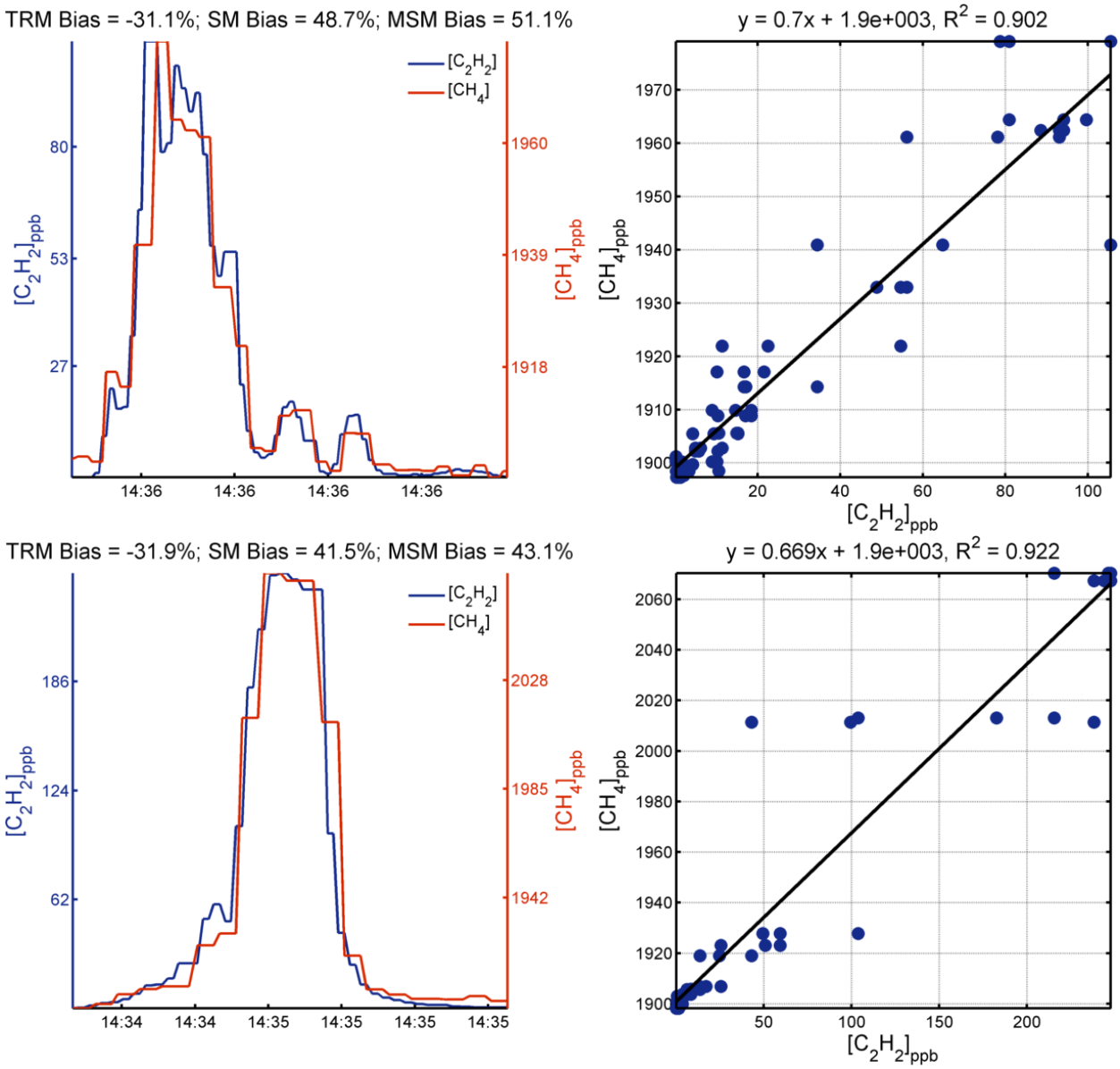
TRM Bias = -31.1%; SM Bias = 48.7%; MSM Bias = 51.1%
[C2H2]
[CH4]
80
53
27
1960
1939
1918
[C2H2]ppb
[CH4]ppb
14:36
14:36
14:36
14:36
y = 0.7x + 1.9e+003, R2 = 0.902
1970
1960
1950
1940
1930
1920
1910
1900
20
40
60
80
100
[CH4]ppb
[C2H2]ppb
TRM Bias = -31.9%; SM Bias = 41.5%; MSM Bias = 43.1%
[C2H2]
[CH4]
186
124
62
2028
1985
1942
[C2H2]ppb
[CH4]ppb
14:34
14:34
14:35
14:35
14:35
14:35
y = 0.669x + 1.9e+003, R2 = 0.922
2060
2040
2020
2000
1980
1960
1940
1920
1900
50
100
150
200
[CH4]ppb
[C2H2]ppb

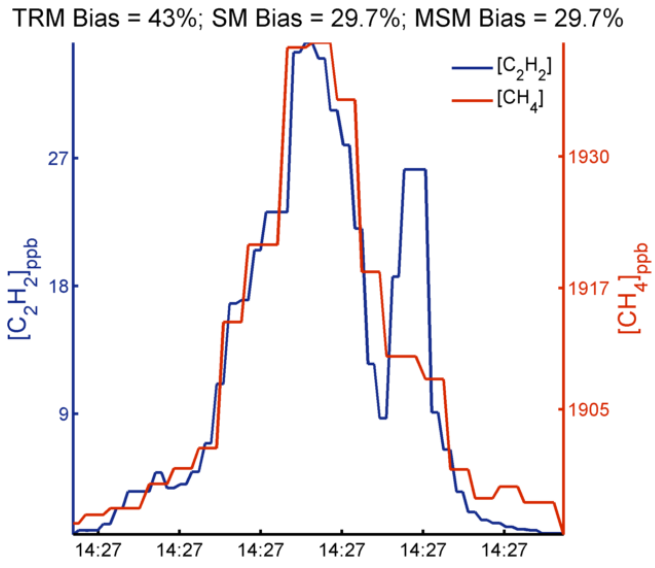
TRM Bias = 43%; SM Bias = 29.7%; MSM Bias = 29.7%
[C2H2]
[CH4]
27
18
9
1930
1917
1905
[C2H2]ppb
[CH4]ppb
14:27
14:27
14:27
14:27
14:27
14:27

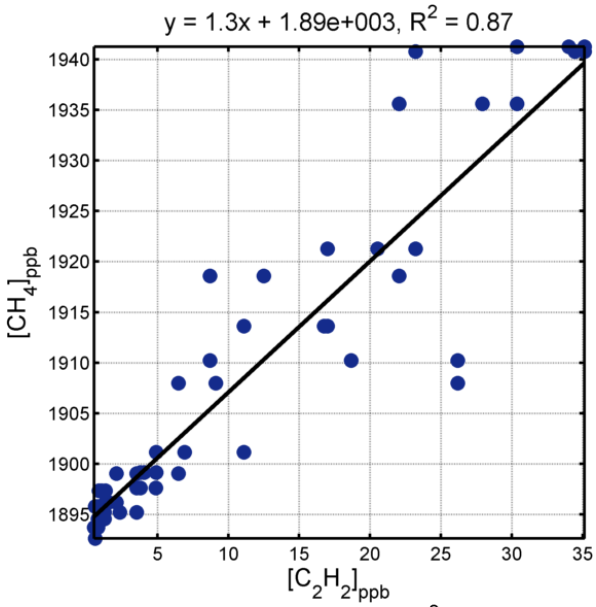
y = 1.3x + 1.89e+003, R2 = 0.87
1940
1935
1930
1925
1920
1915
1910
1905
1900
1895
5
10
15
20
25
30
35
[CH4]ppb
[C2H2]ppb

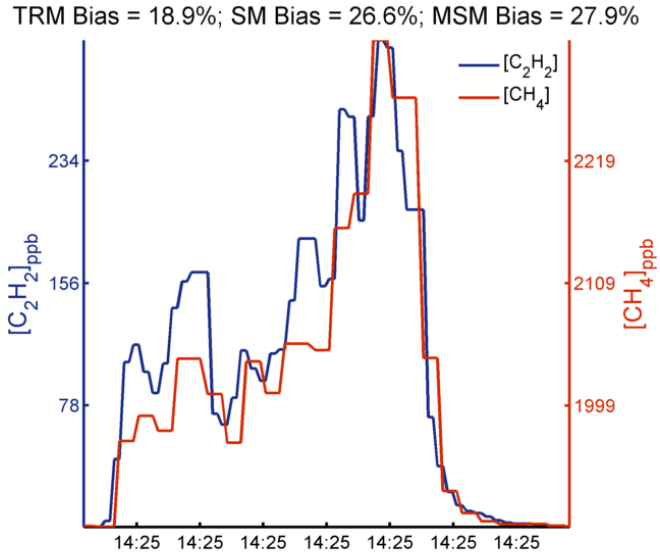
TRM Bias = 18.9%; SM Bias = 26.6%; MSM Bias = 27.9%
[C2H2]
[CH4]
234
156
78
2219
2109
1999
[C2H2]ppb
[CH4]ppb
14:25
14:25
14:25
14:25
14:25
14:25
14:25

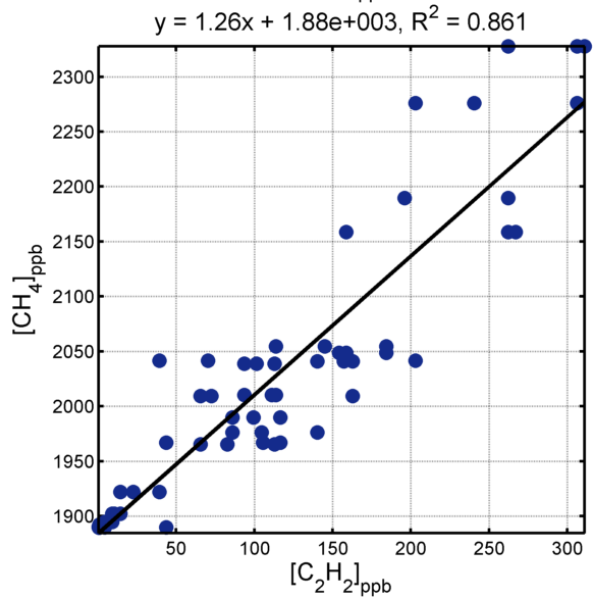
y = 1.26x + 1.88e+003, R2 = 0.861
2300
2250
2200
2150
2100
2050
2000
1950
1900
50
100
150
200
250
300
[CH4]ppb
[C2H2]ppb

Appendix C

STATIONARY ANALYSIS CONCENTRATION AND POINT SOURCE GAUSSIAN PLOTS

14 March 2014

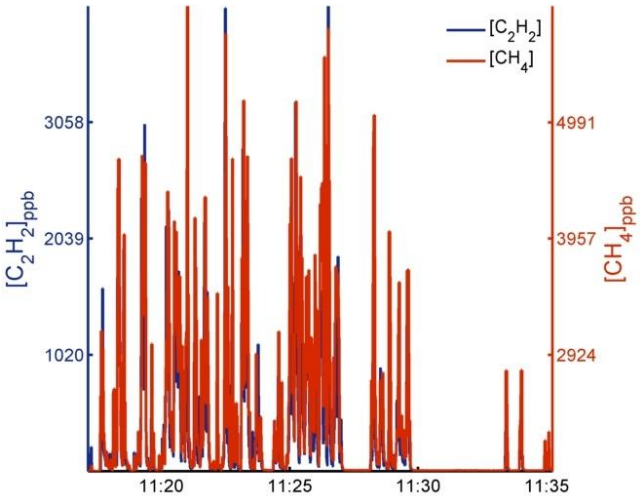

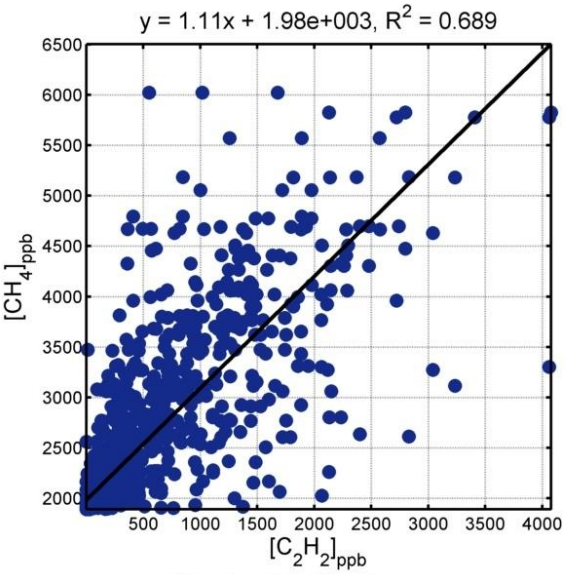

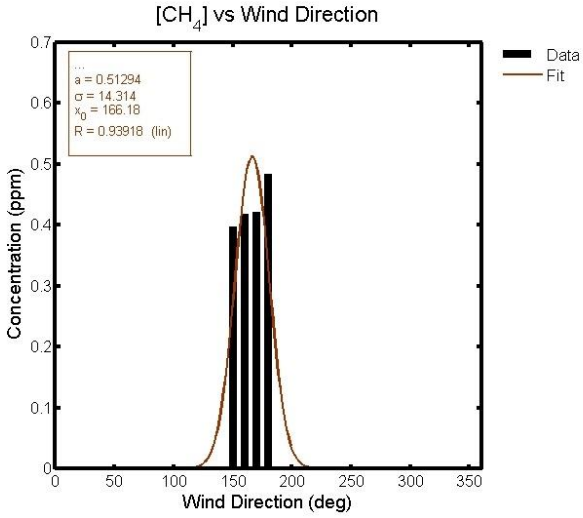

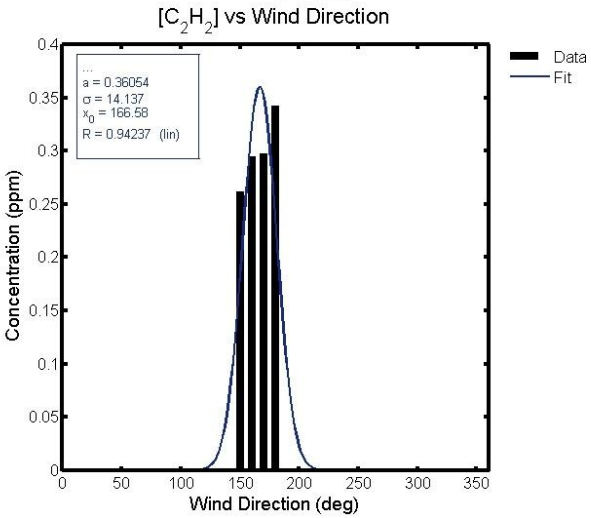

Standard Background Correction	% Bias	Interpolated Background Correction	% Bias
TRM	-28.8	**TRM**	-29.8
Slope Method	-40.4	**Slope Method**	-46.4
PSG CH_4	-16.3	**PSG CH_4**	44.4
PSG C_2H_2	-27.5		

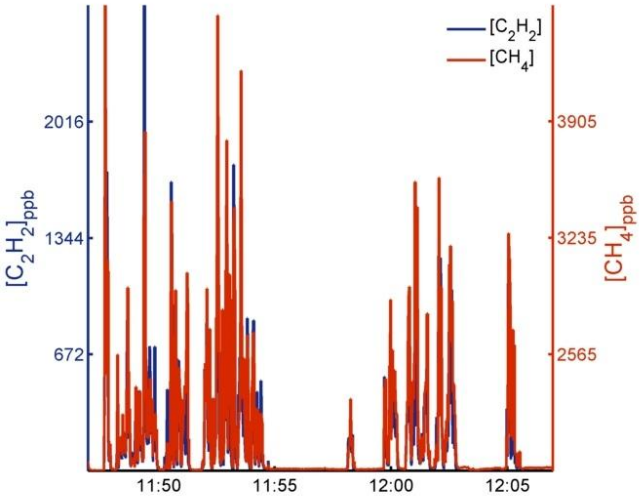

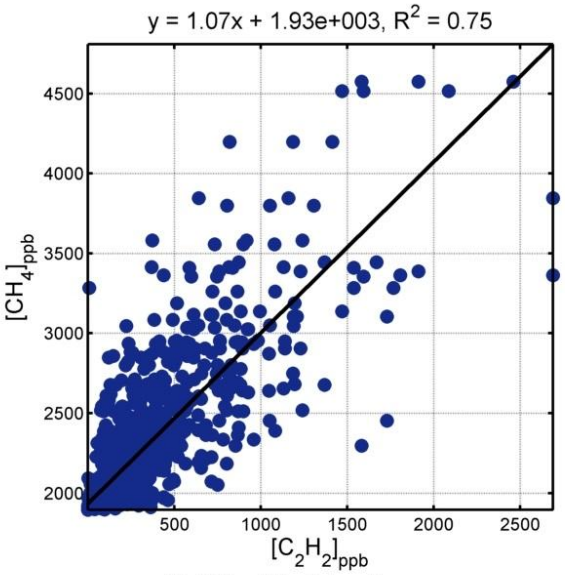

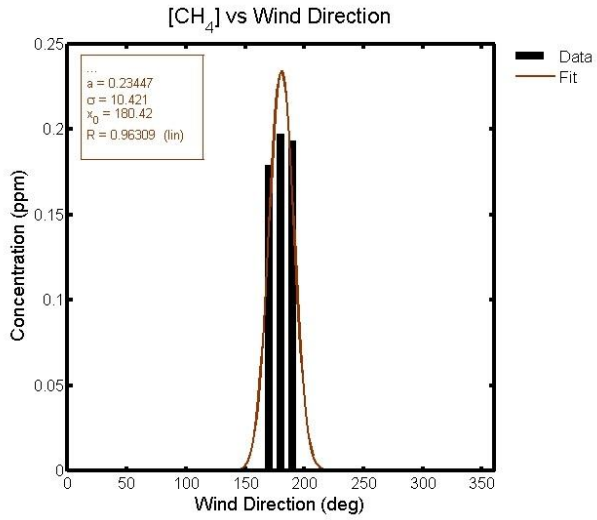

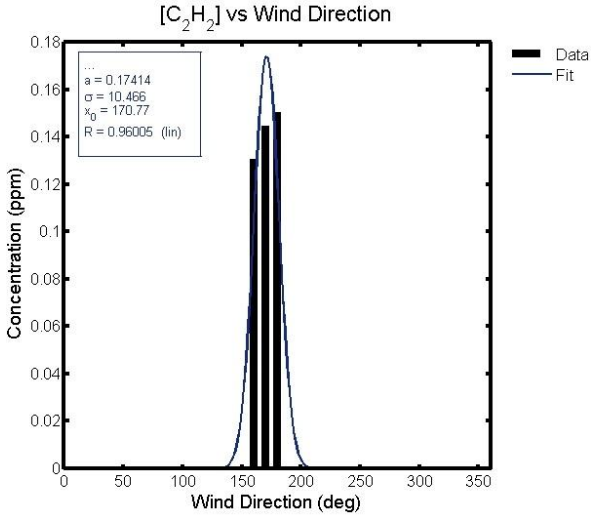

Standard Background Correction	% Bias	Interpolated Background Correction	% Bias
TRM	-34.2	**TRM**	-37.1
Slope Method	-43.1	**Slope Method**	-48.5
PSG CH_4	10.6	**PSG CH_4**	65.0
PSG C_2H_2	1.19		

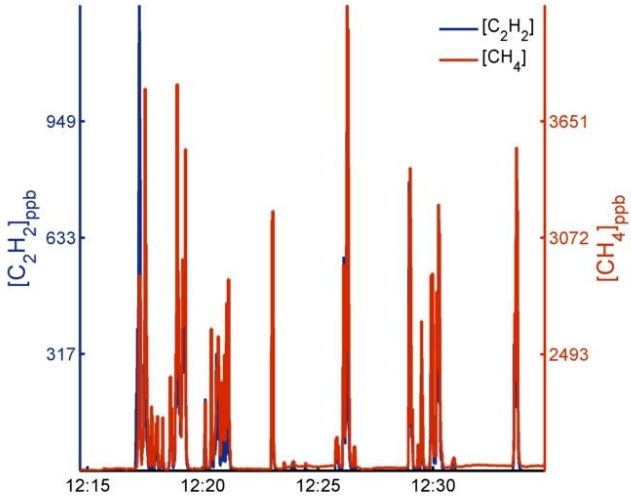

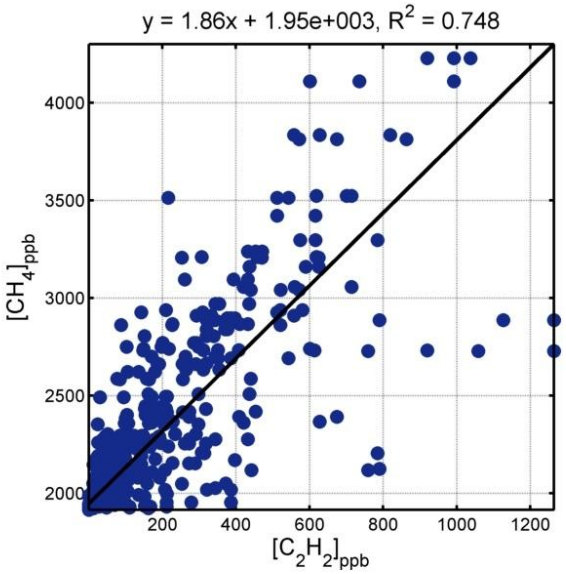

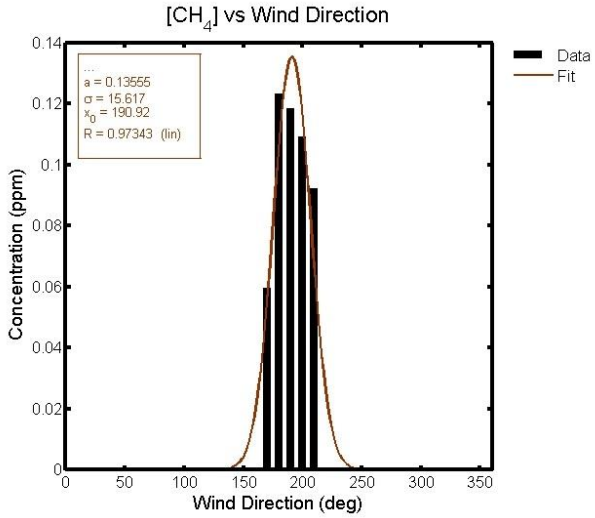

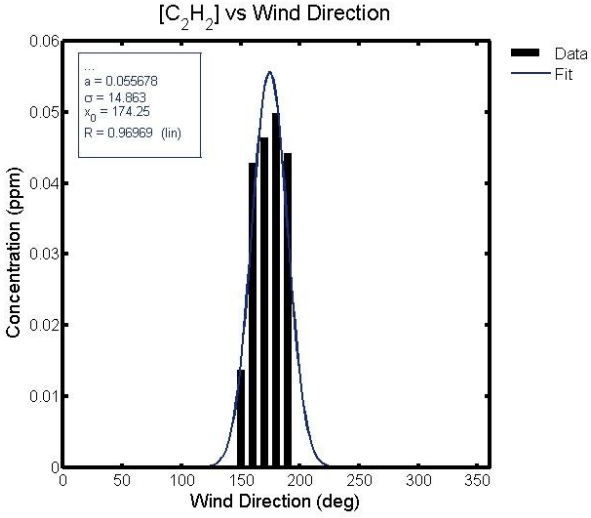

Standard Background Correction	% Bias	Interpolated Background Correction	% Bias
TRM	25.8	**TRM**	11.9
Slope Method	-3.13	**Slope Method**	-7.66
PSG CH_4	-21.9	**PSG CH_4**	47.3
PSG C_2H_2	-60.5		

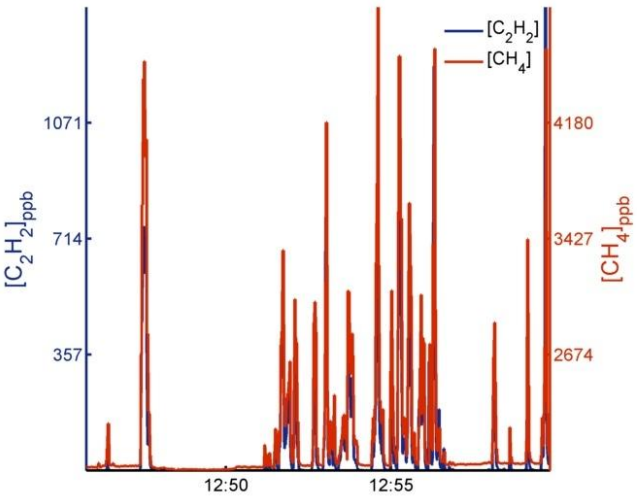

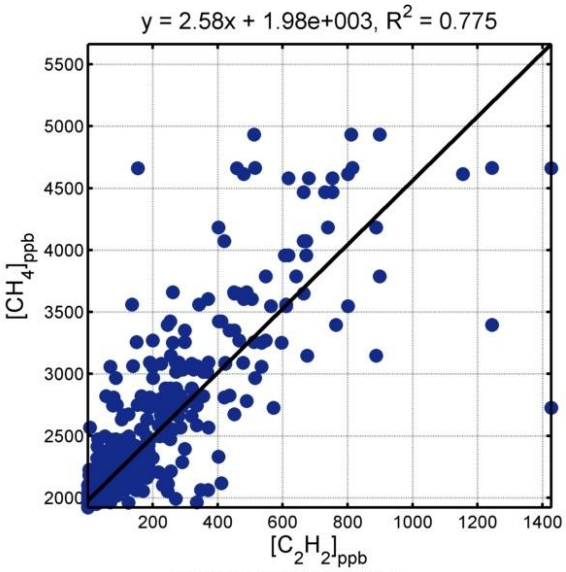

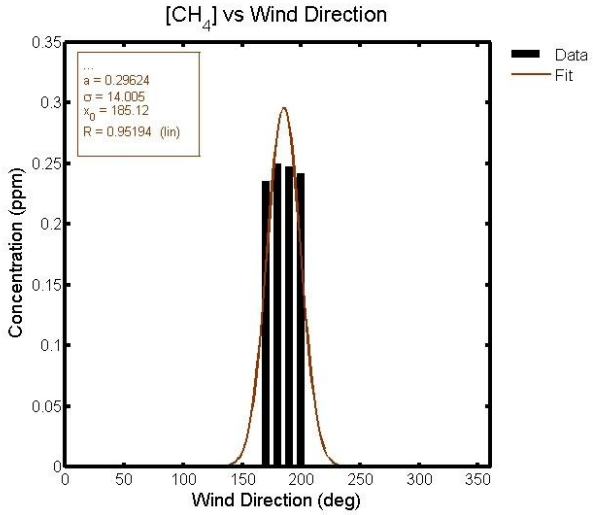

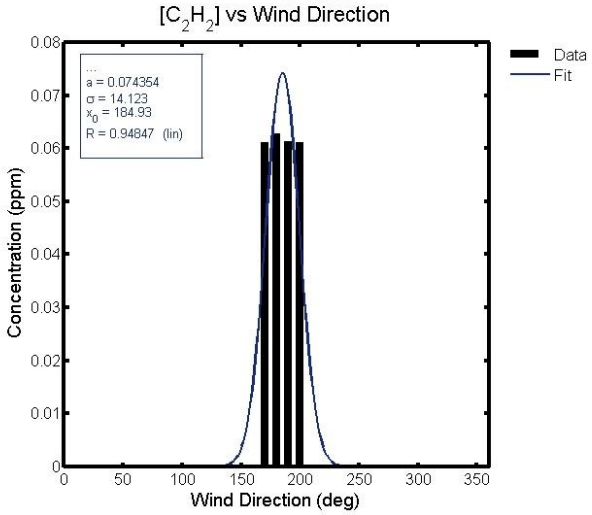

Standard Background Correction	% Bias	Interpolated Background Correction	% Bias
TRM	12.8	**TRM**	1.06
Slope Method	-8.45	**Slope Method**	-9.02
PSG CH_4	18.6	**PSG CH_4**	98.5
PSG C_2H_2	-45.0		

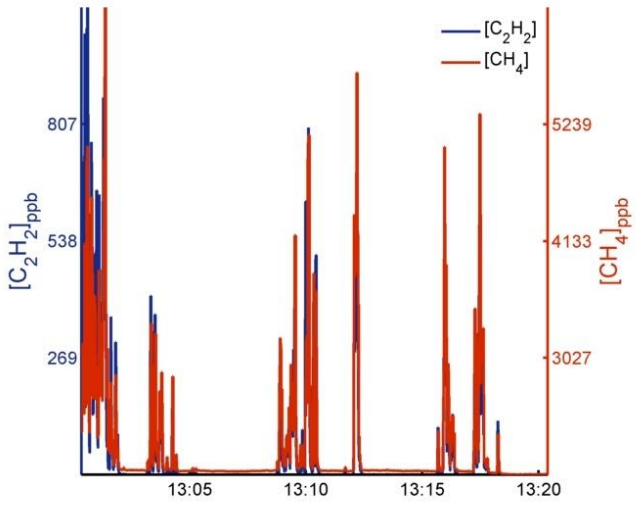

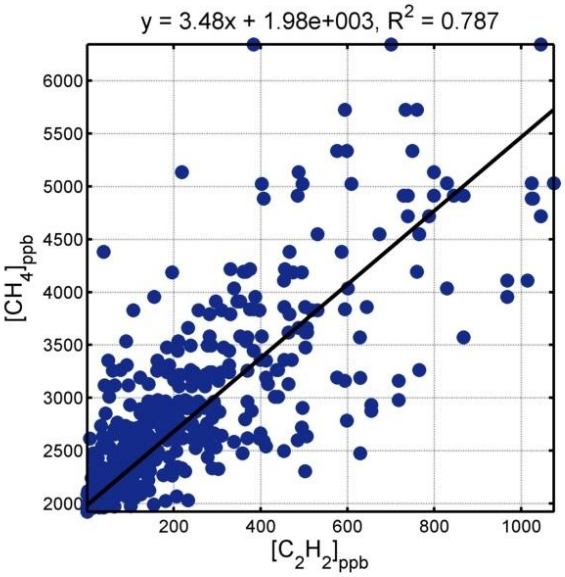

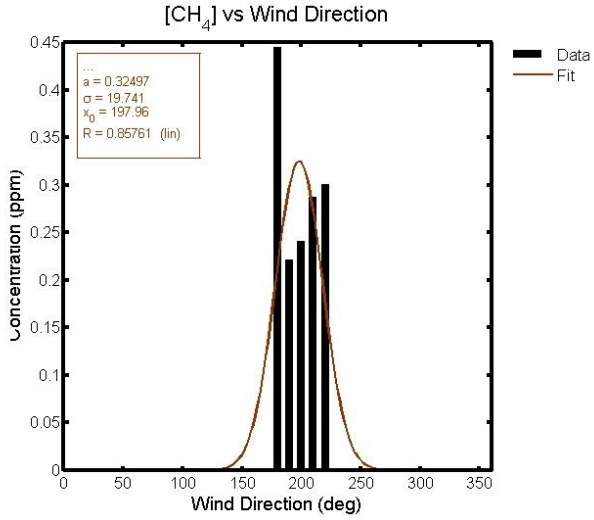

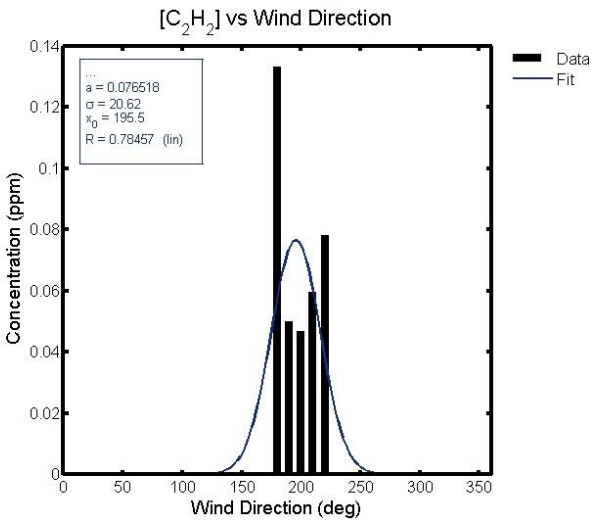

Standard Background Correction	% Bias	Interpolated Background Correction	% Bias
TRM	19.3	**TRM**	20.8
Slope Method	-5.82	**Slope Method**	8.47
PSG CH_4	-21.1	**PSG CH_4**	-14.3
PSG C_2H_2	-55.6		

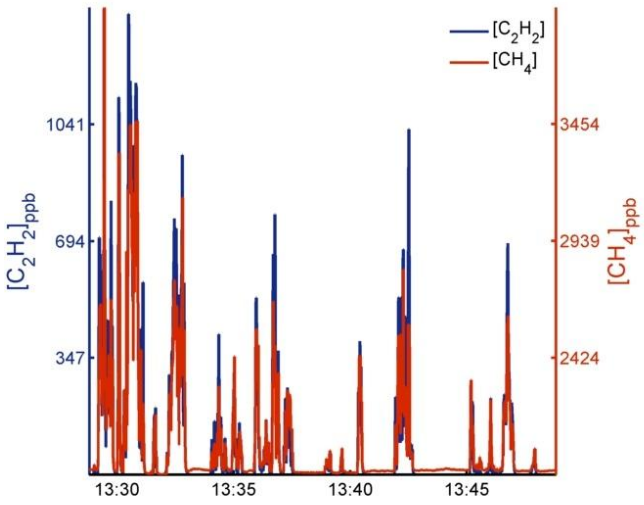

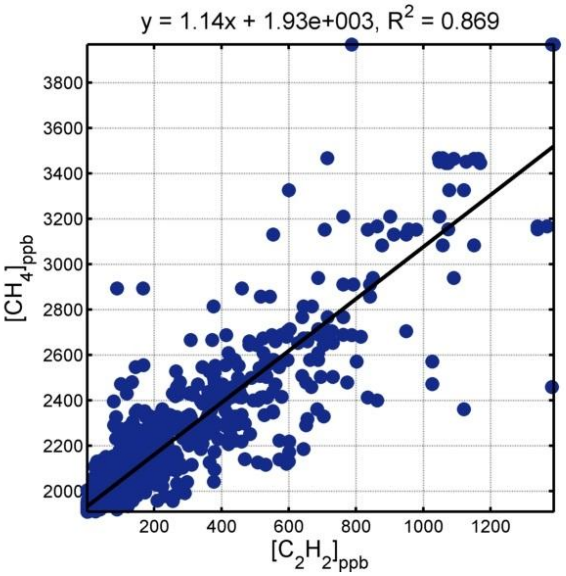

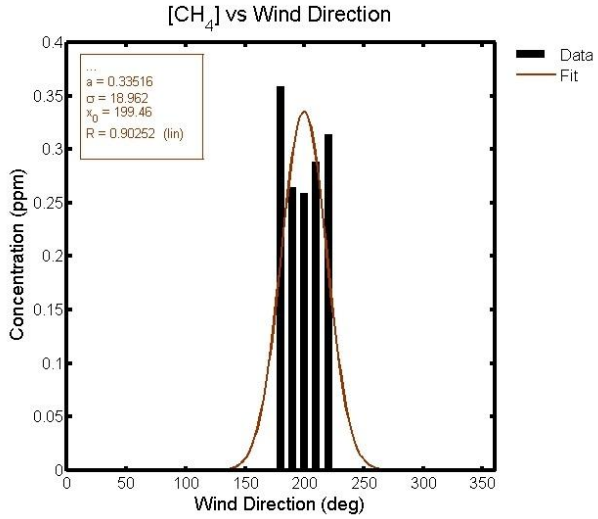

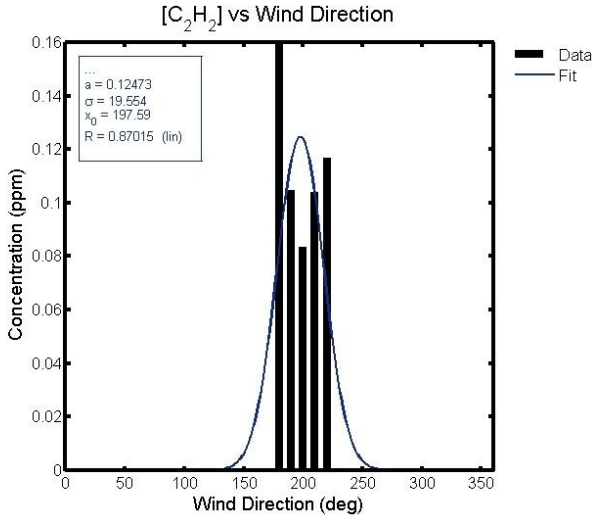

Standard Background Correction	% Bias	Interpolated Background Correction	% Bias
TRM	35.5	**TRM**	22.1
Slope Method	17.8	**Slope Method**	14.5
PSG CH_4	368	**PSG CH_4**	198
PSG C_2H_2	7.06		

23 April 2014

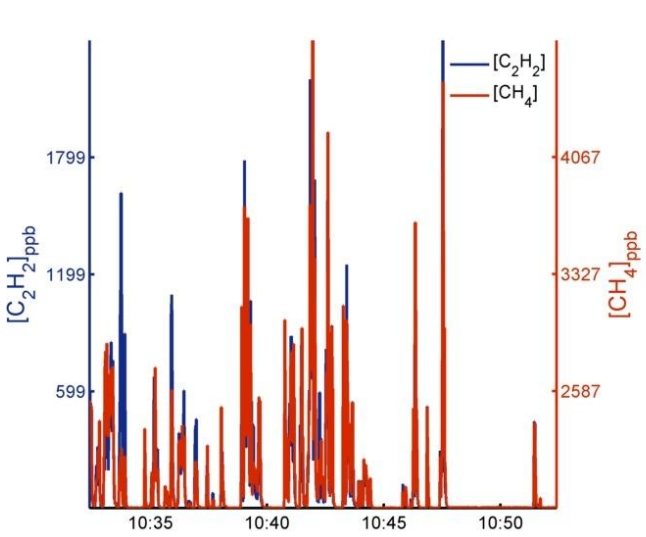

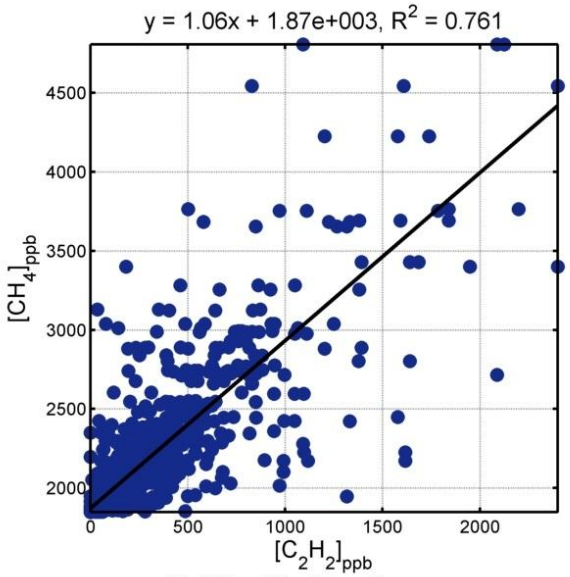

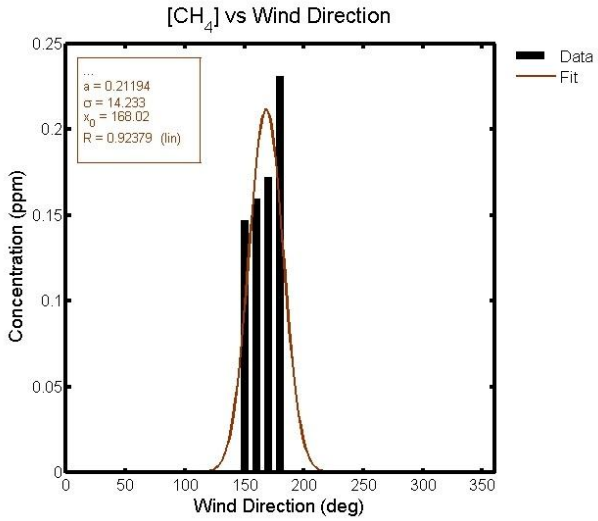

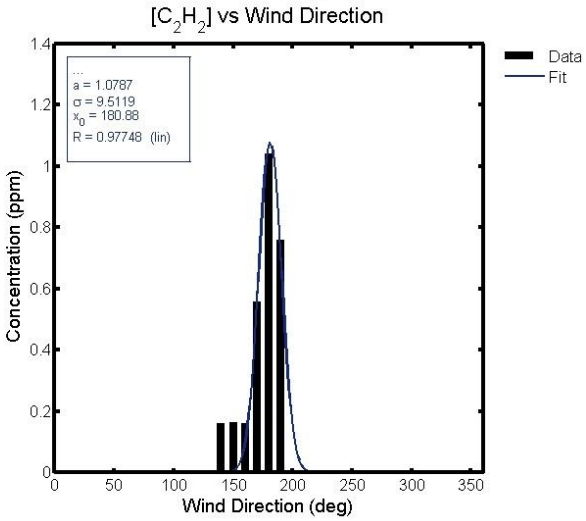

Standard Background Correction	% Bias	Interpolated Background Correction	% Bias
TRM	23.7	**TRM**	46.8
Slope Method	6.19	**Slope Method**	13.0
PSG CH_4	61.5	**PSG CH_4**	146
PSG C_2H_2	441		

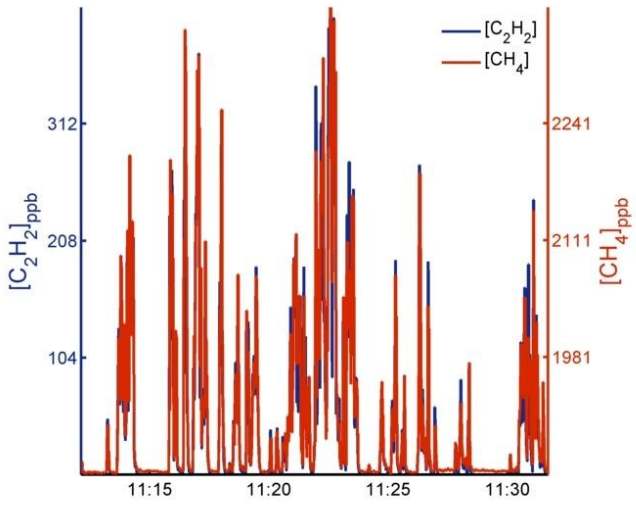

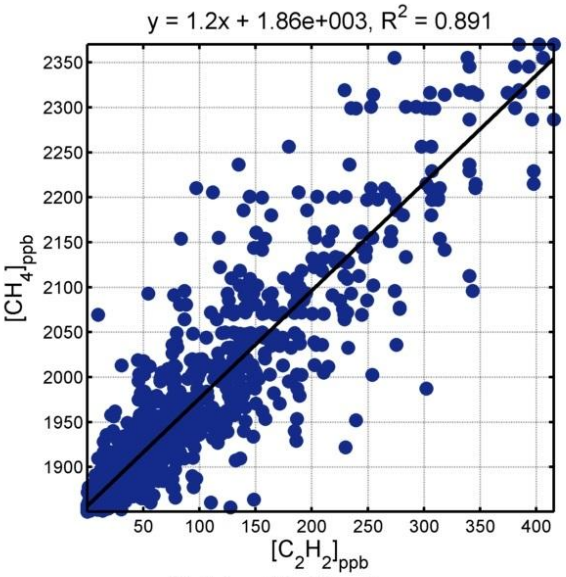

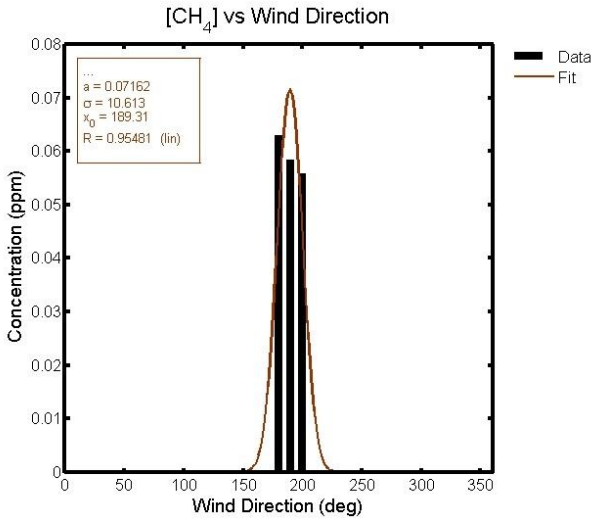

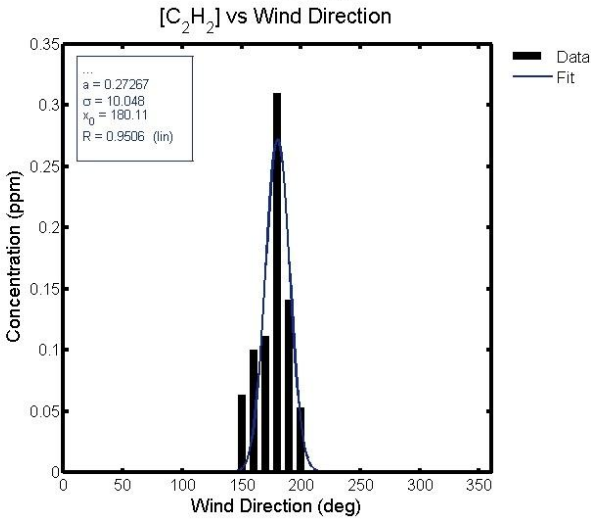

Standard Background Correction	% Bias	Interpolated Background Correction	% Bias
TRM	29.7	**TRM**	19.3
Slope Method	19.8	**Slope Method**	20.8
PSG CH_4	229	**PSG CH_4**	275
PSG C_2H_2	255		

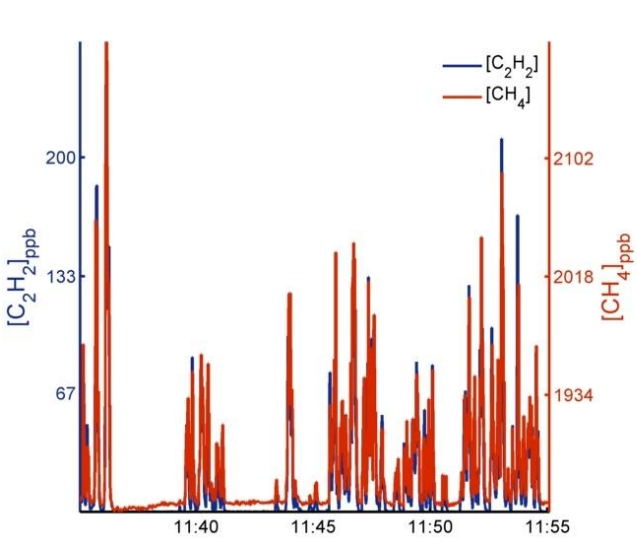

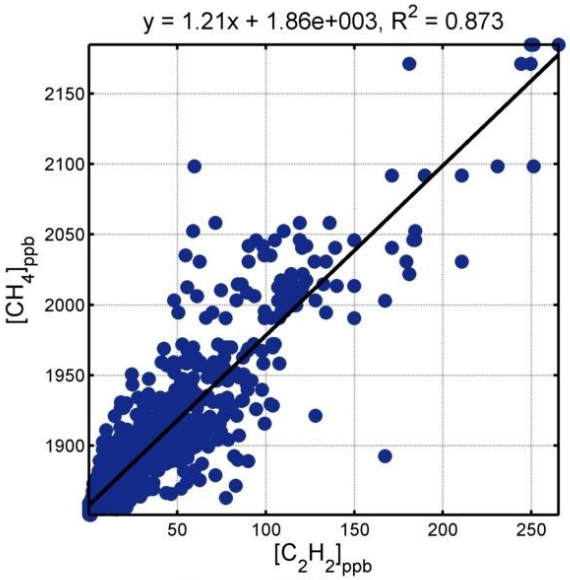

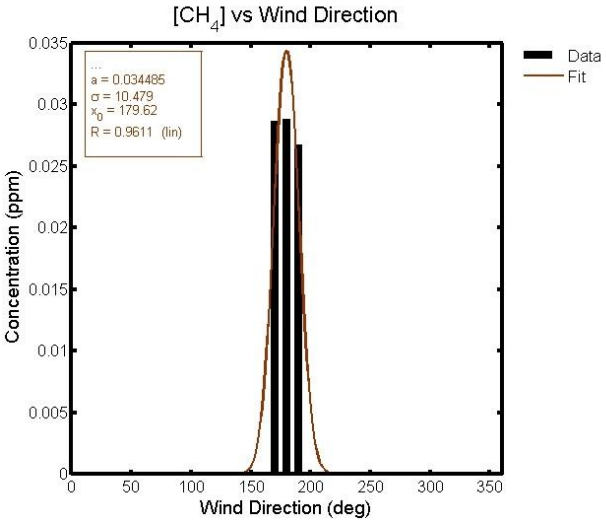

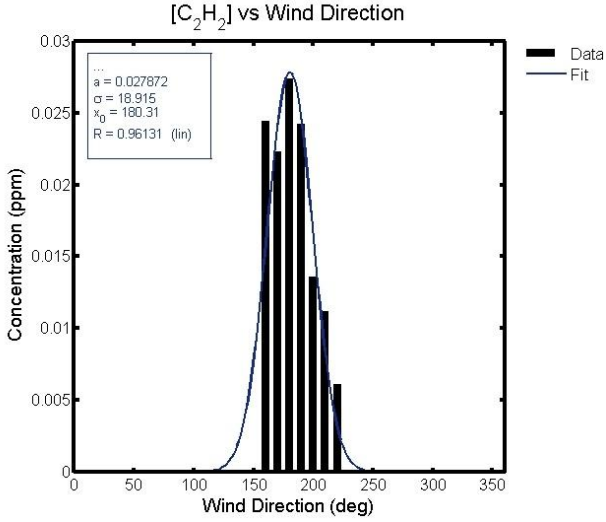

Standard Background Correction	% Bias	Interpolated Background Correction	% Bias
TRM	45.0	**TRM**	26.9
Slope Method	20.7	**Slope Method**	20.7
PSG CH_4	312	**PSG CH_4**	365
PSG C_2H_2	-36.3		

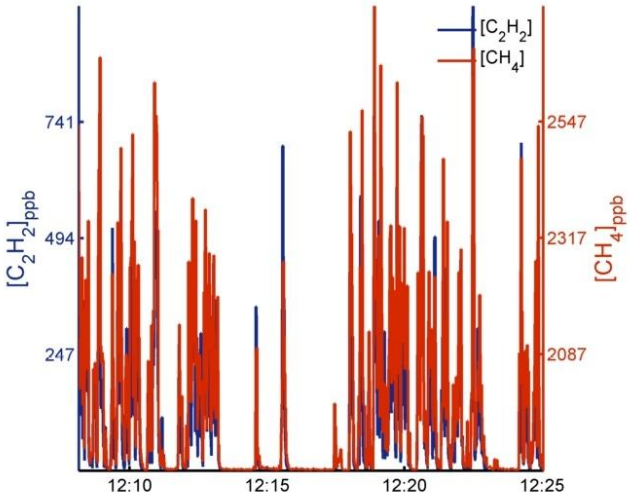

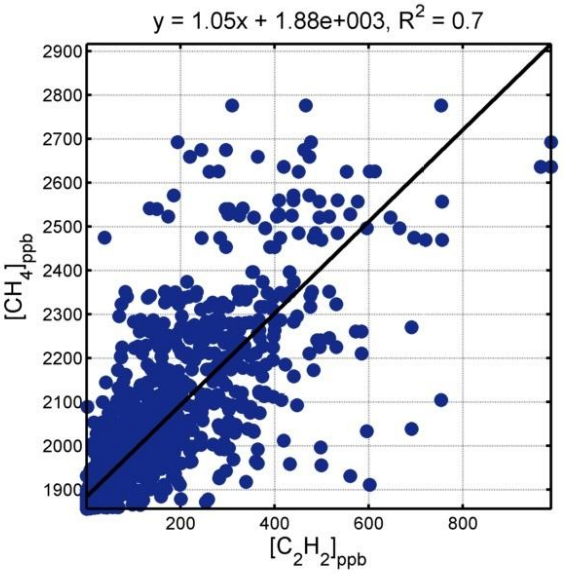

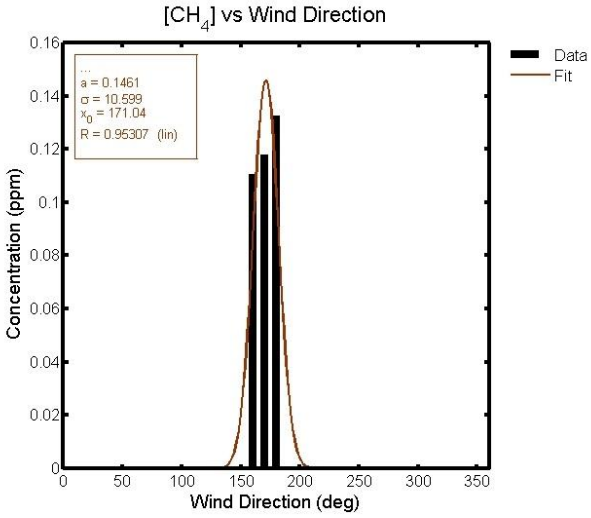

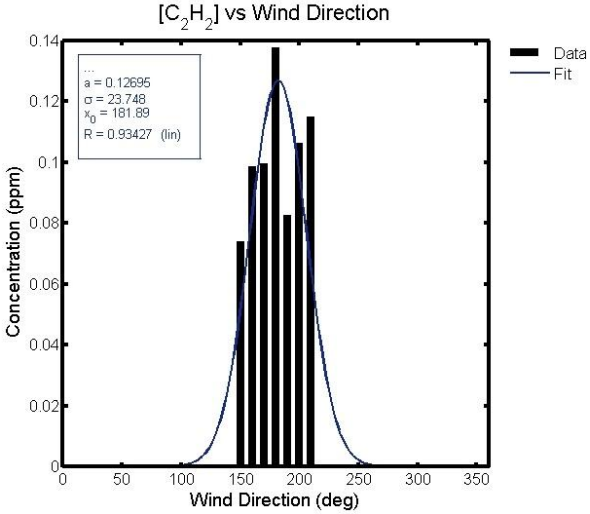

Standard Background Correction	% Bias	Interpolated Background Correction	% Bias
TRM	33.1	**TRM**	29.8
Slope Method	4.51	**Slope Method**	2.69
PSG CH_4	113	**PSG CH_4**	177
PSG C_2H_2	-62.7		

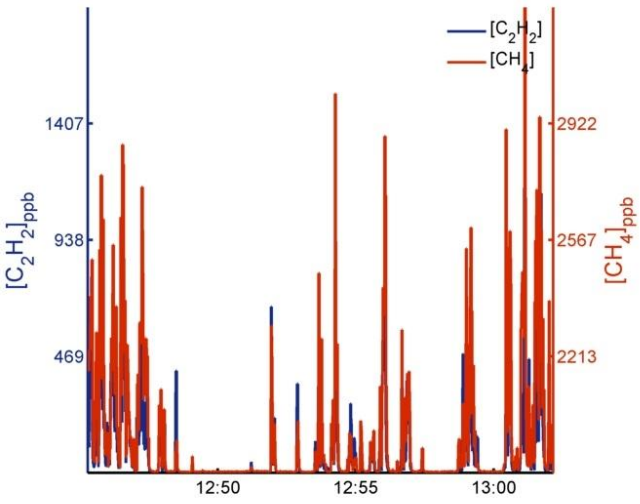

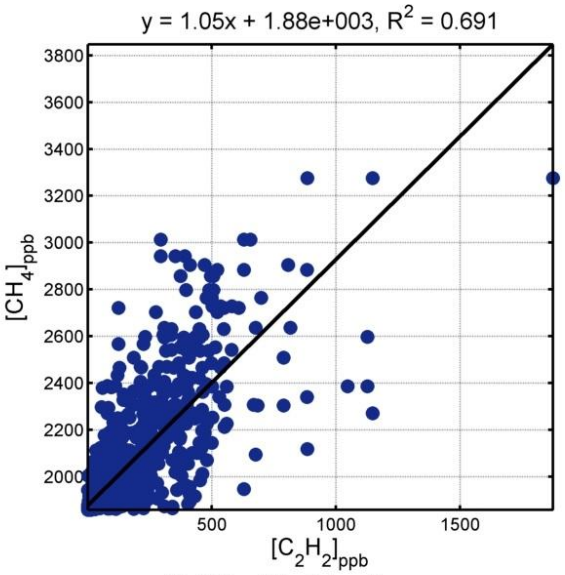

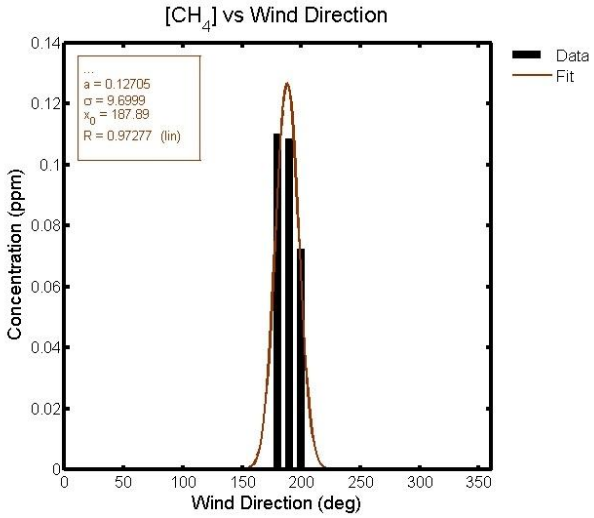

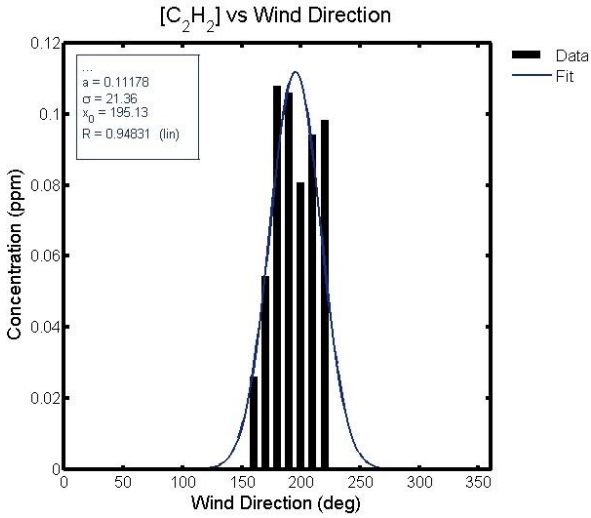

Standard Background Correction	% Bias	Interpolated Background Correction	% Bias
TRM	24.1	**TRM**	-13.8
Slope Method	5.13	**Slope Method**	-6.11
PSG CH_4	7.16	**PSG CH_4**	4.51
PSG C_2H_2	-81.3		

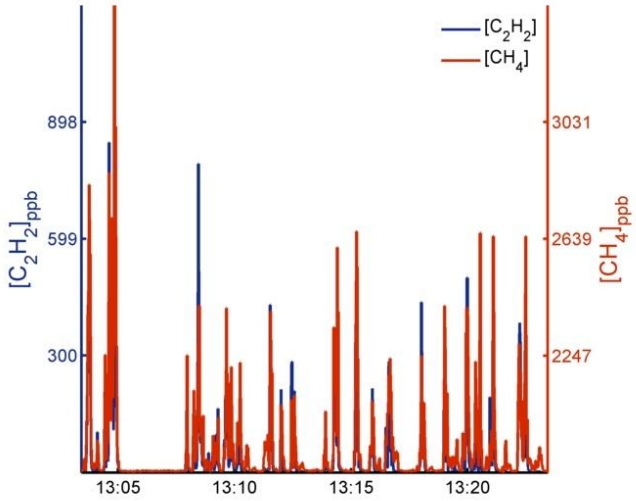

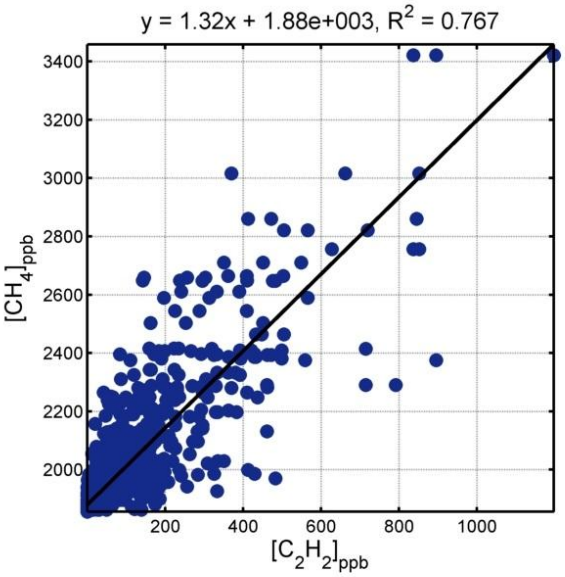

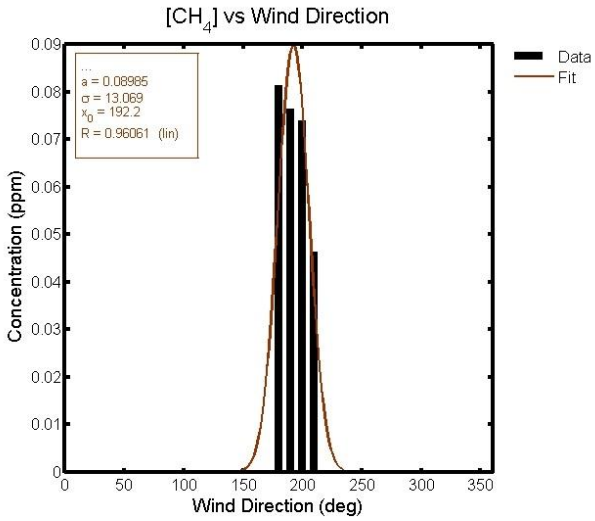

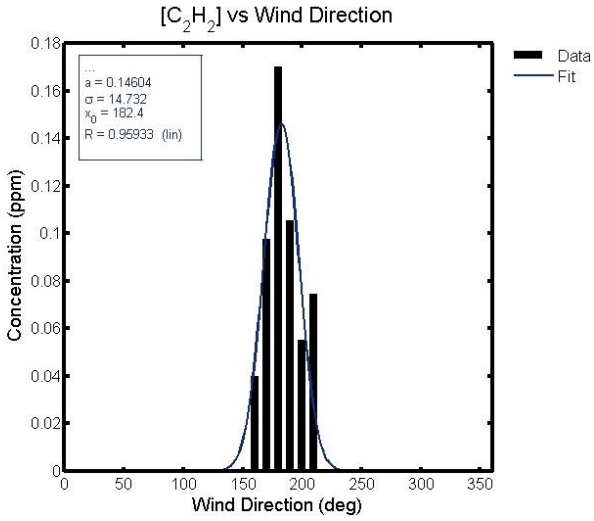

Standard Background Correction	% Bias	Interpolated Background Correction	% Bias
TRM	80.4	**TRM**	66.7
Slope Method	32.0	**Slope Method**	31.6
PSG CH_4	16.4	**PSG CH_4**	51.7
PSG C_2H_2	-63.1		

19 September 2014

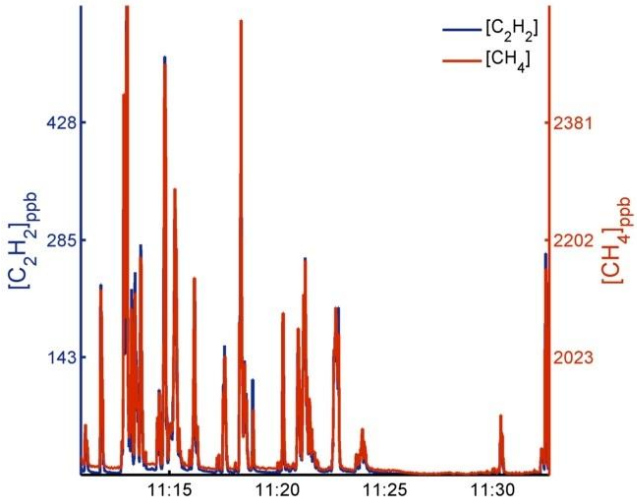

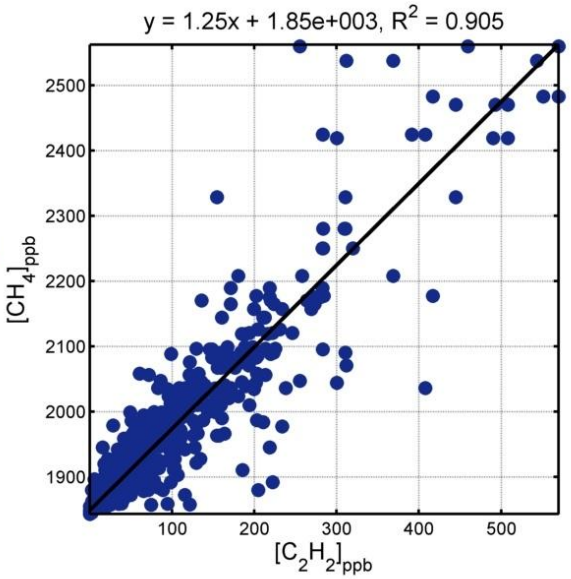

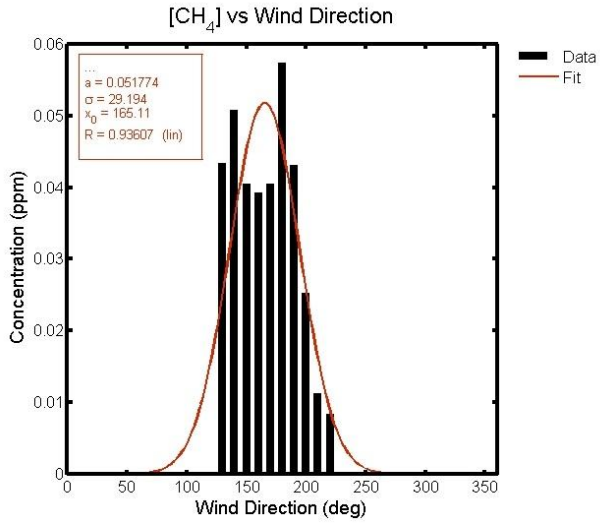

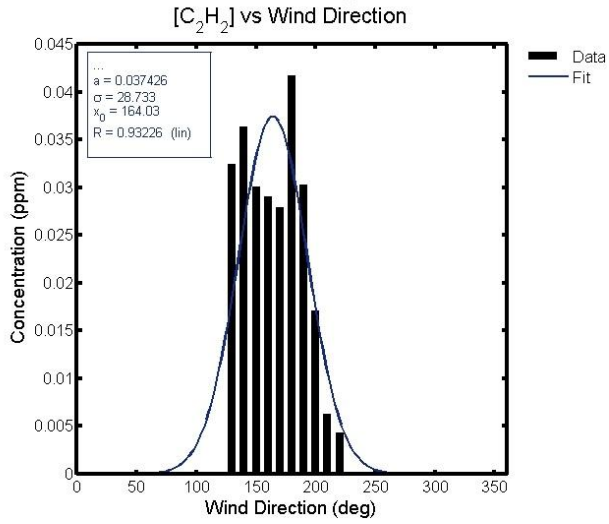

Standard Background Correction	% Bias	Interpolated Background Correction	% Bias
TRM	40.2	**TRM**	12.8
Slope Method	25.4	**Slope Method**	25.5
PSG CH_4	-67.8	**PSG CH_4**	-15.5
PSG C_2H_2	-85.7		

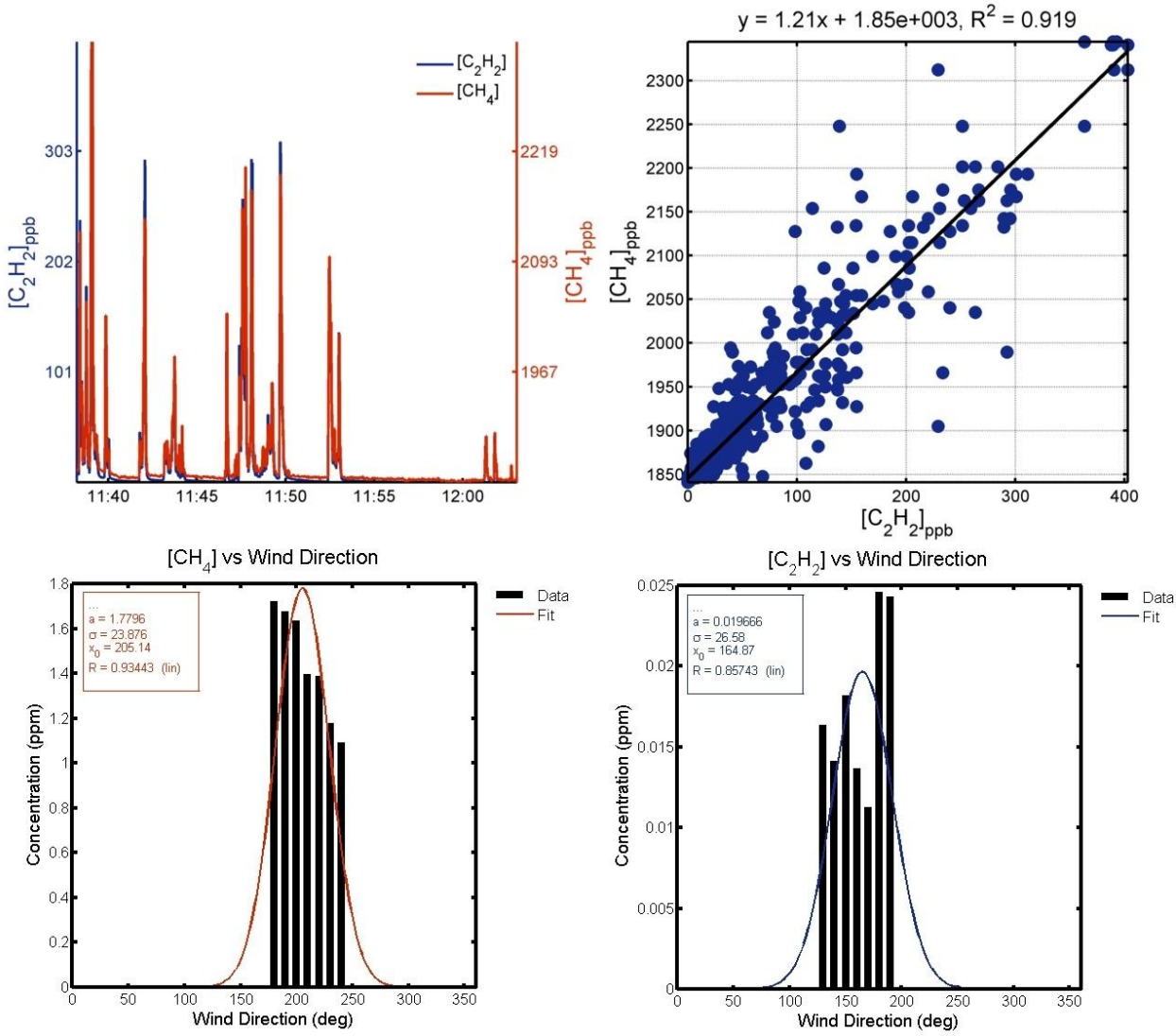

Standard Background Correction	% Bias	Interpolated Background Correction	% Bias
TRM	37.1	**TRM**	14.7
Slope Method	21.1	**Slope Method**	19.3
PSG CH_4	-80.0	**PSG CH_4**	-39.5
PSG C_2H_2	-91.6		

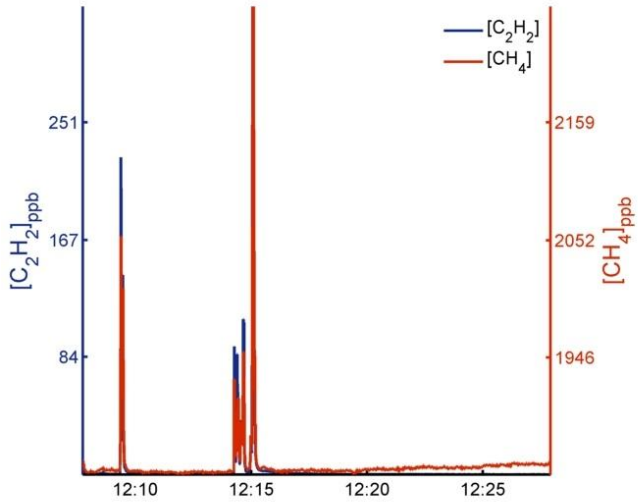

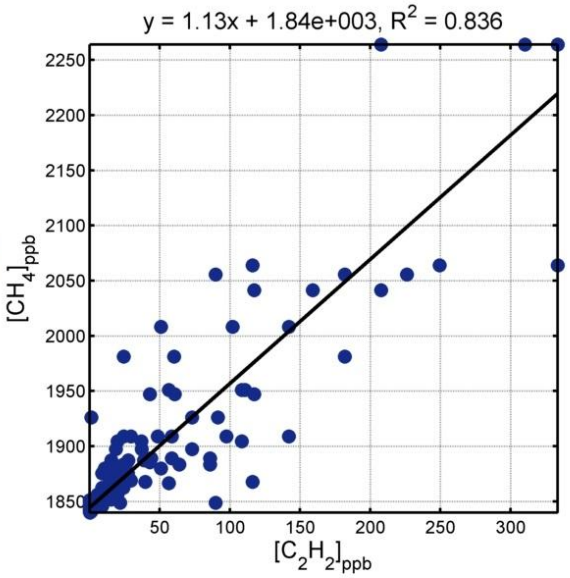

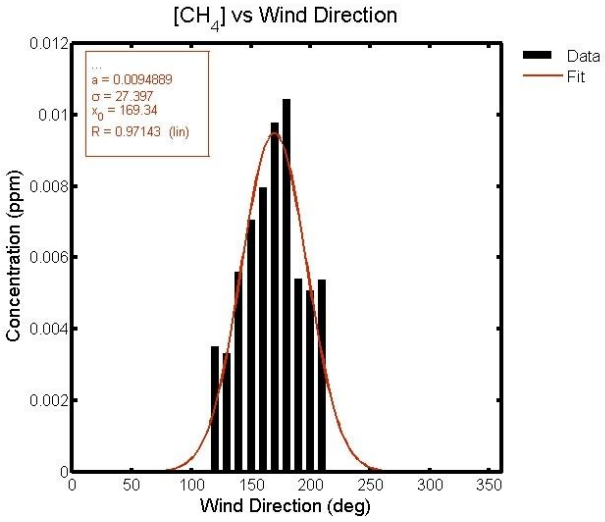

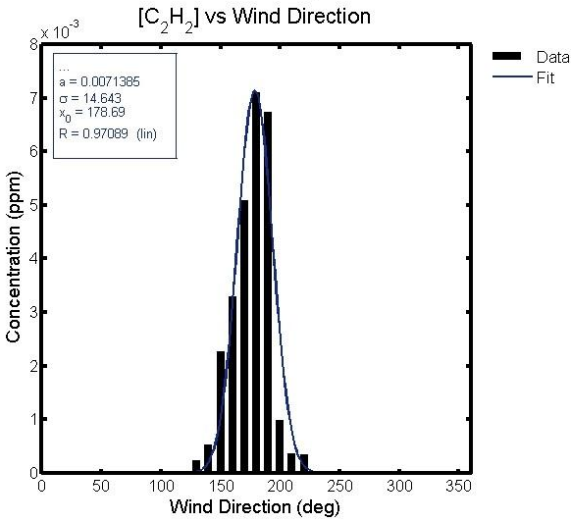

Standard Background Correction	% Bias	Interpolated Background Correction	% Bias
TRM	28.3	**TRM**	21.4
Slope Method	12.6	**Slope Method**	17.9
PSG CH_4	-93.5	**PSG CH_4**	-72.1
PSG C_2H_2	-97.0		

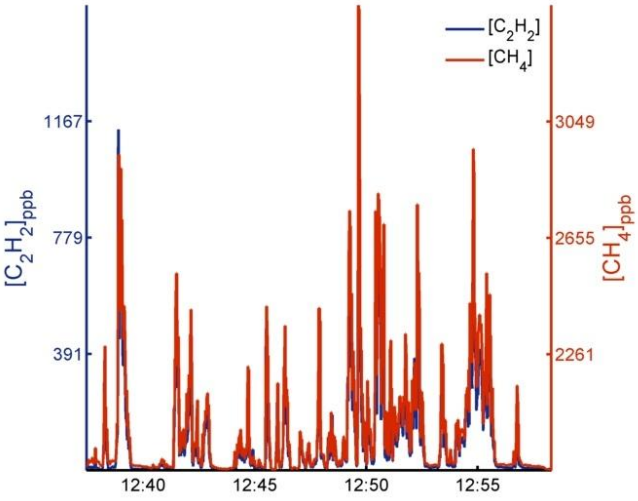

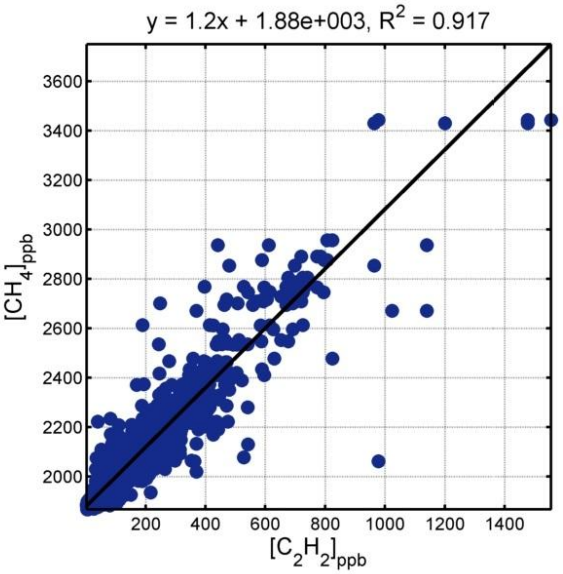

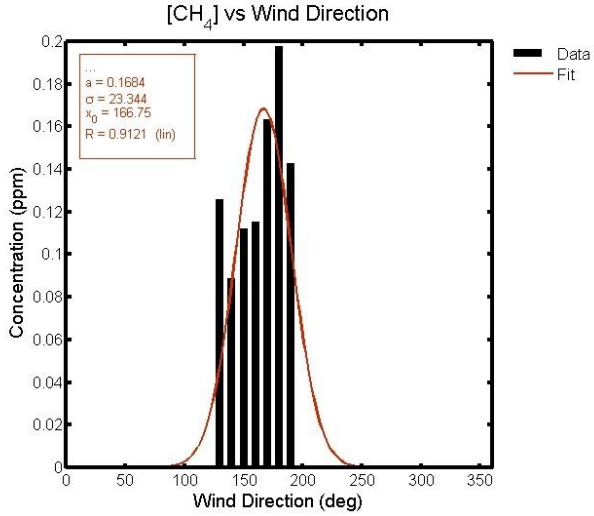

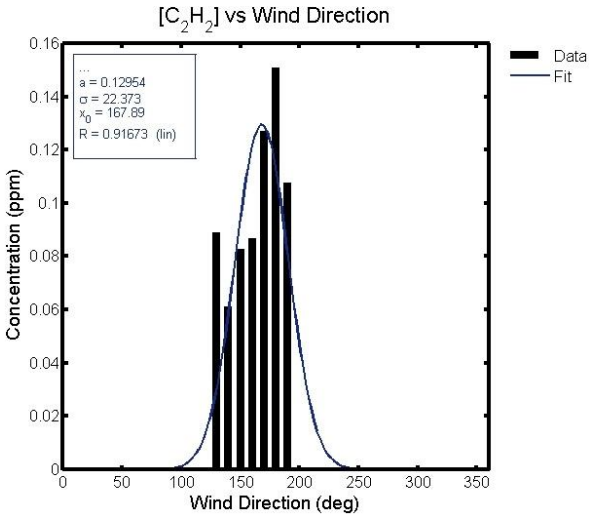

Standard Background Correction	% Bias	Interpolated Background Correction	% Bias
TRM	33.0	**TRM**	25.3
Slope Method	20.4	**Slope Method**	21.4
PSG CH_4	-21.0	**PSG CH_4**	92.7
PSG C_2H_2	-62.6		

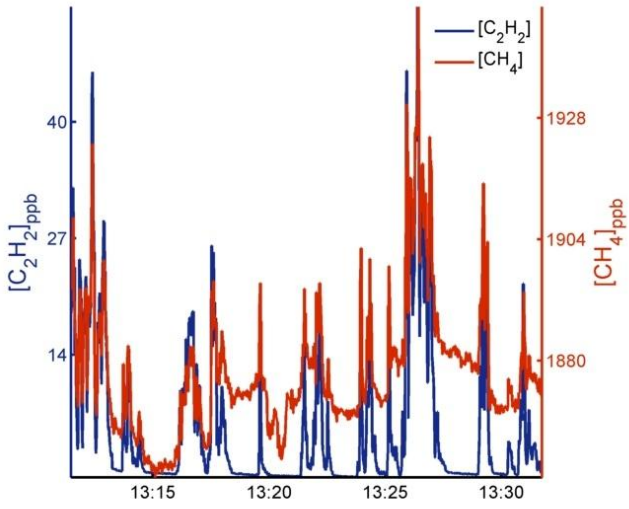

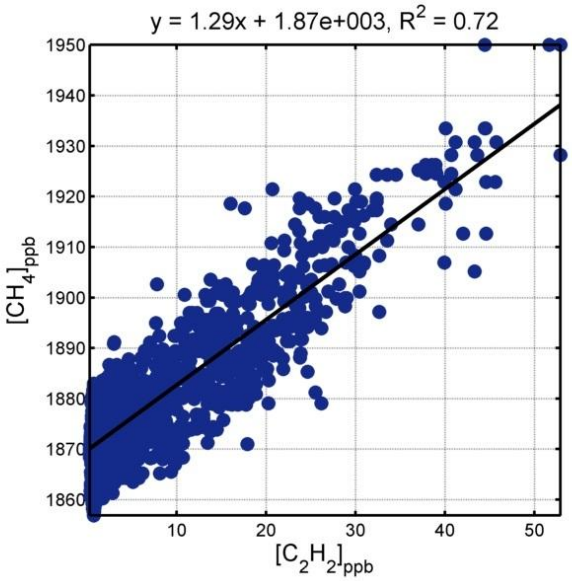

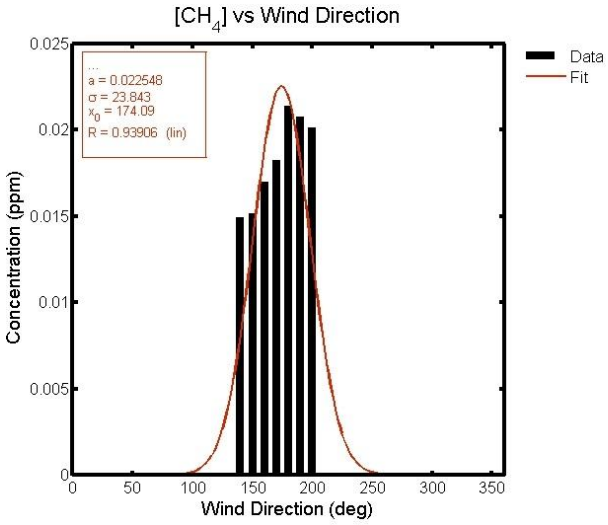

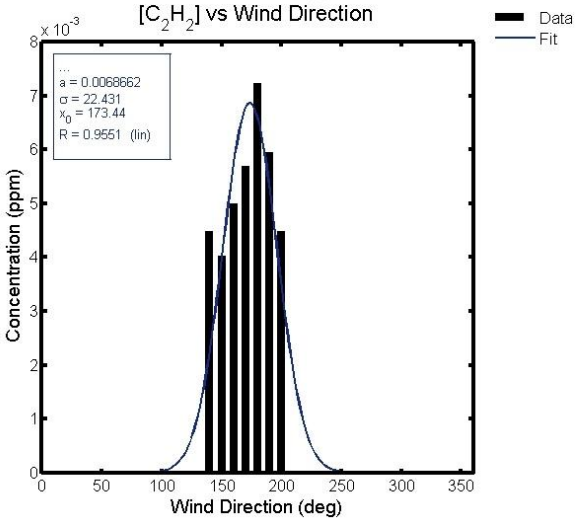

Standard Background Correction	% Bias	Interpolated Background Correction	% Bias
TRM	232	**TRM**	27.3
Slope Method	29.3	**Slope Method**	23.1
PSG CH_4	-26.9	**PSG CH_4**	47.8
PSG C_2H_2	-86.3		

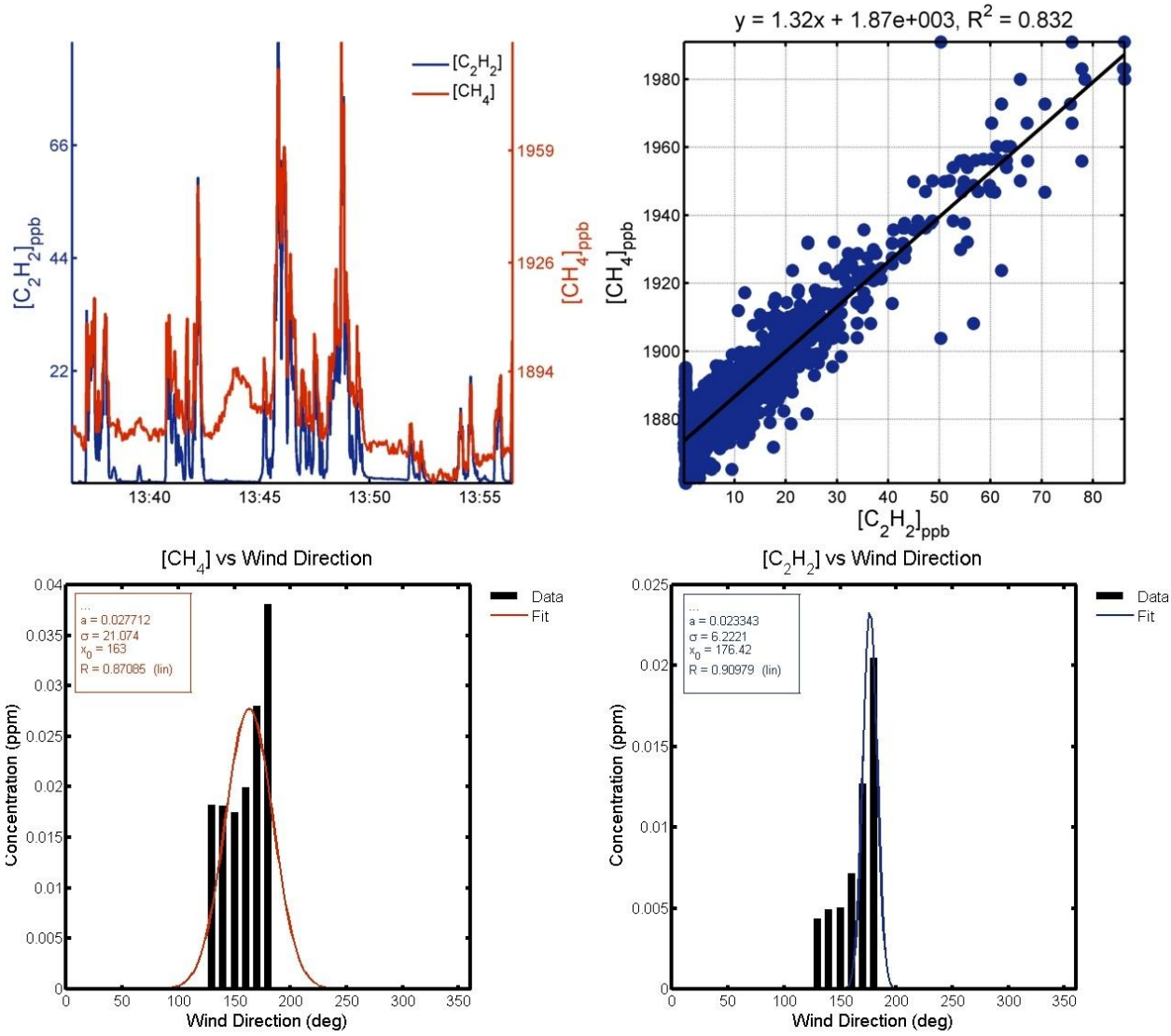

Standard Background Correction	% Bias	Interpolated Background Correction	% Bias
TRM	118	**TRM**	14.2
Slope Method	32.3	**Slope Method**	25.0
PSG CH_4	0.92	**PSG CH_4**	34.8
PSG C_2H_2	-47.6		

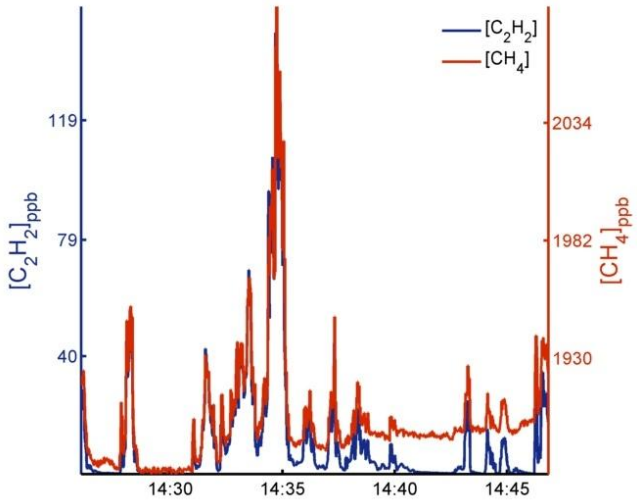

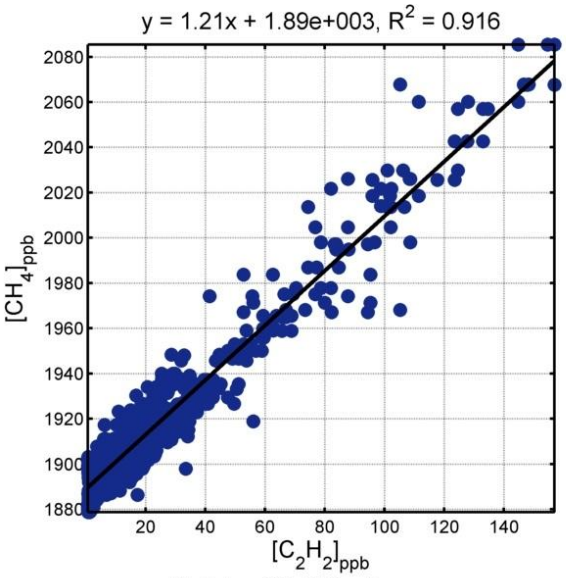

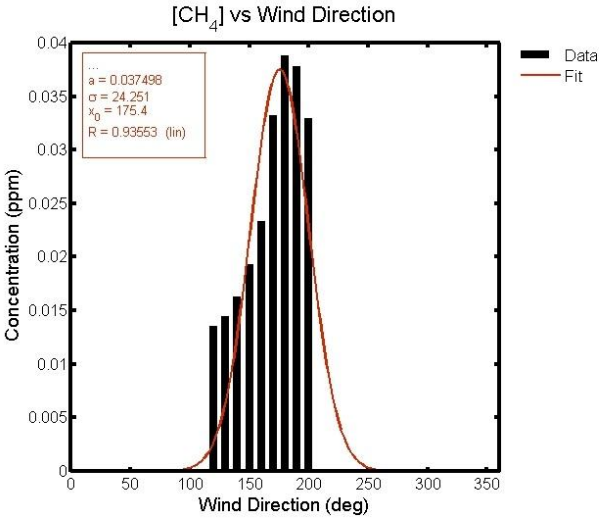

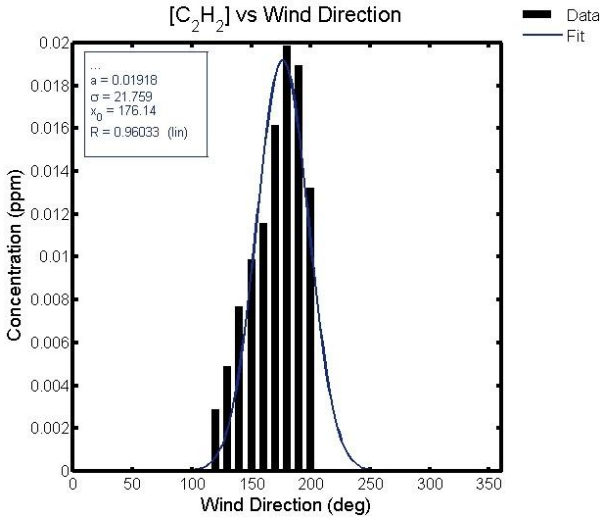

Standard Background Correction	% Bias	Interpolated Background Correction	% Bias
TRM	86.2	**TRM**	20.2
Slope Method	20.6	**Slope Method**	26.8
PSG CH_4	-4.32	**PSG CH_4**	9.16
PSG C_2H_2	-69.8		

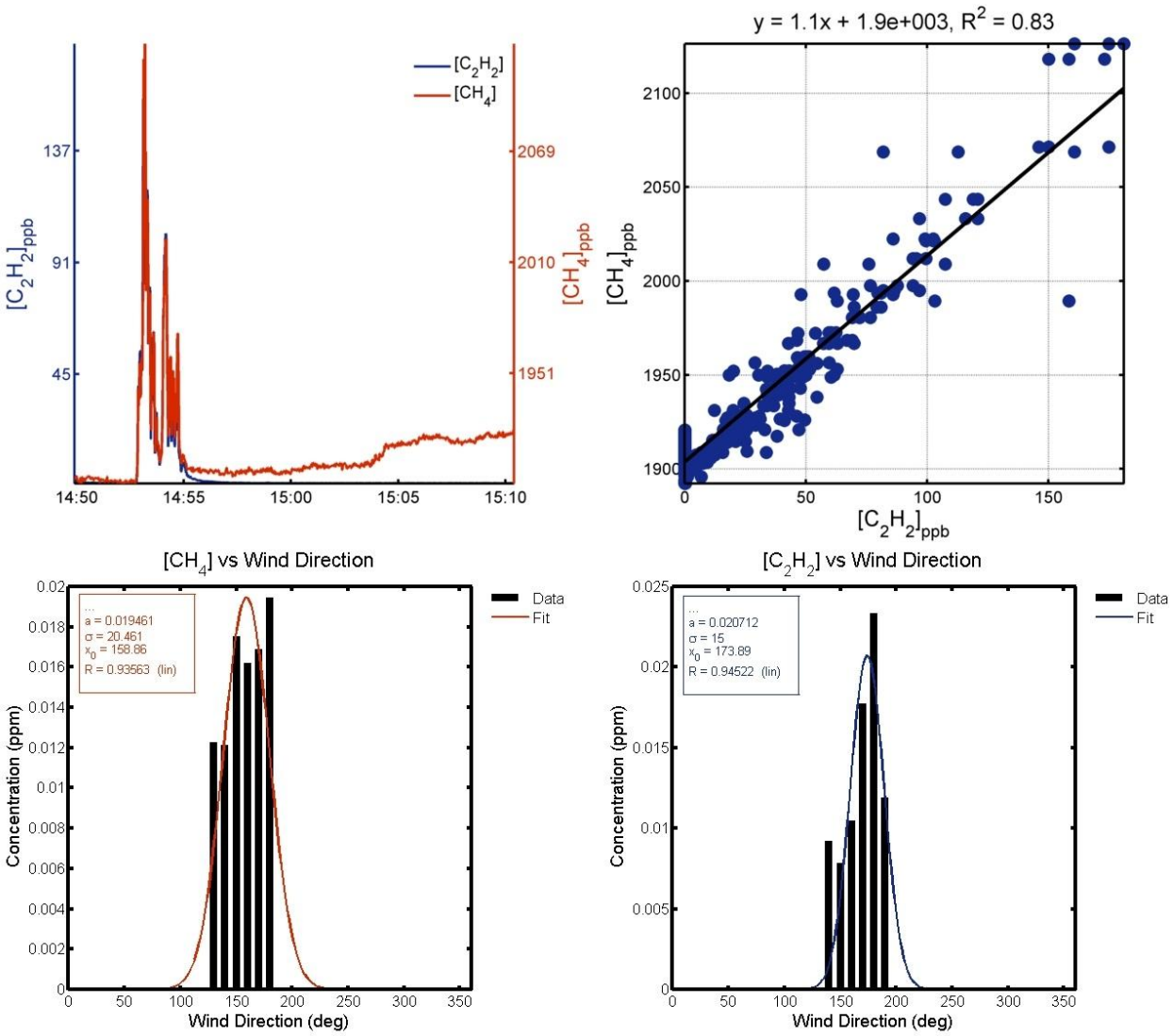

Standard Background Correction	% Bias	Interpolated Background Correction	% Bias
TRM	27.5	**TRM**	30.7
Slope Method	10.3	**Slope Method**	18.6
PSG CH_4	-64.2	**PSG CH_4**	-38.7
PSG C_2H_2	-76.5		

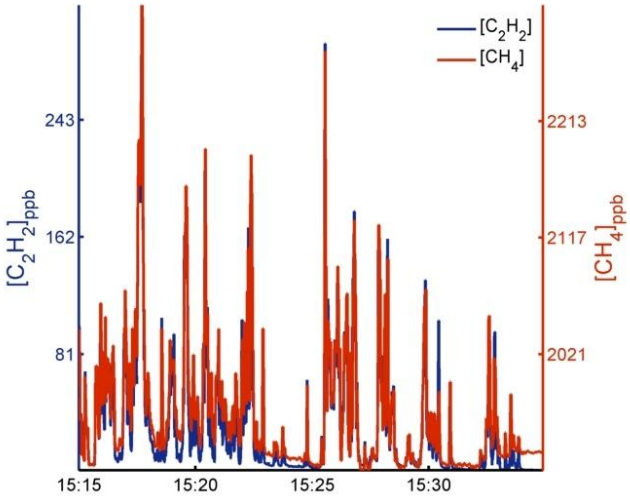

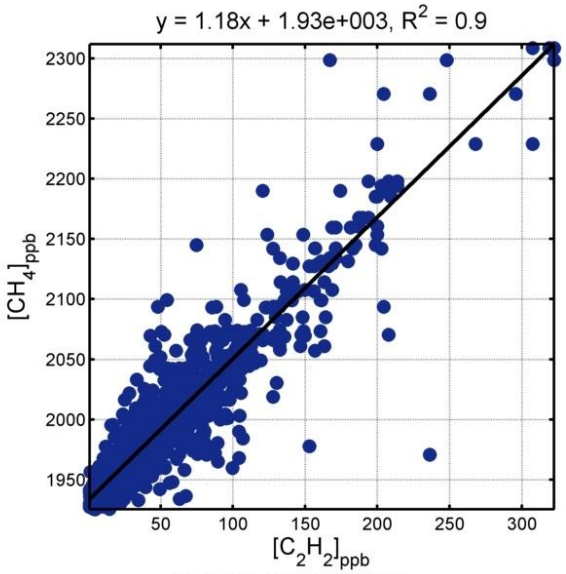

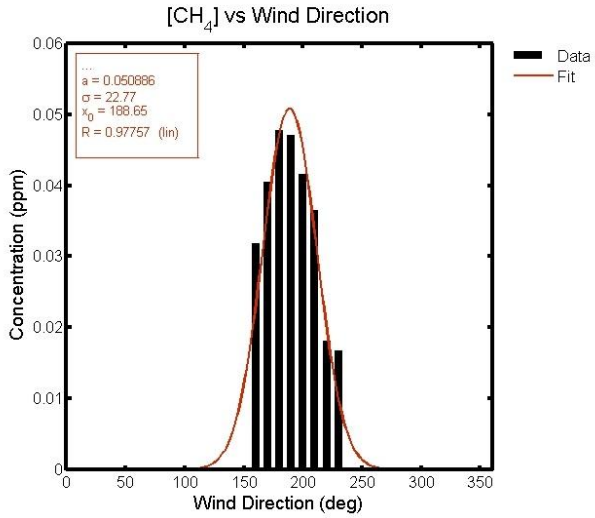

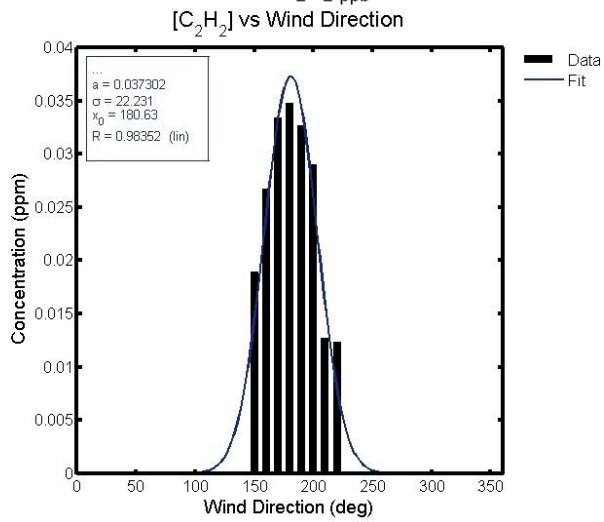

Standard Background Correction	% Bias	Interpolated Background Correction	% Bias
TRM	37.2	**TRM**	20.7
Slope Method	17.6	**Slope Method**	18.4
PSG CH_4	-0.92	**PSG CH_4**	128
PSG C_2H_2	-55.3		

Appendix D

PICARRO CALIBRATION

The Picarro A0941 mobile measurement kit with G2203 analyzer were calibrated using prepared concentration cylinders of methane and acetylene as well as Zero Air cylinders that contain <0.1 ppm of total hydrocarbons. Calibration of the Picarro kit used in this study was performed on 2 May of 2014. The range of calibrations for both gases is given below in **Table D.1** and **Table D.2**.

Table D.1 Methane Calibration. 100 ppm cylinder of methane and Zero Air cylinder each connected to separate MFCs. Flow rate for Picarro was 5 liters per minute. Excess flow was vented outside.

Methane Calibration				
Actual (ppm)	**Average Measured (ppm)**	**Stdev Measured (ppm)**	**Zero Air (LPM)**	**100ppm Methane (LPM)**
0	0	0	10	0
5	4.8	0.03	9.5	0.5
10	9.1	0.02	9	1
20	20.8	0.02	8	2
50	51.9	0.01	5	5
100	98.3	0.05	0	con

Table D.2 Acetylene Calibration. 1 ppm cylinder of acetylene and Zero Air cylinder each connected to separate MFCs. Flow rate for Picarro was 5 liters per minute. Excess flow was vented outside

Acetylene Calibration				
Actual (ppm)	**Average Measured (ppm)**	**Stdev Measured (ppm)**	**Zero Air (LPM)**	**100ppm Methane (LPM)**
0	0	0	10	0
50	48.1	0.2	9.5	0.5
100	96.2	0.5	9	1
500	498.4	0.4	5	5
800	810.3	0.5	2	8
1000	984.9	0.7	0	10

Appendix E

EDDY COVARIANCE DATA QUALITY ASSESSMENTS

In this study, data quality assessments were applied to eddy covariance data gathered from our micrometeorological station. These tests, also known as *steady state tests*, determine whether all eddy covariance variables are homogeneous in time [*Foken and Wichura*, 1996].

The first test, the instationarity test, is used to determine if eddy covariance data do not significantly vary over the course of a sample period. This is accomplished by dividing a sample period into *M* intervals. In the case of this experiment a sample period is 20 minutes in length and *M* = four 5 minute time series intervals. The covariance between *w*, the vertical wind speed, and χ, either the horizontal wind speed or a scalar, such as temperature, is computed over all *M* intervals. *N* is the number of data points within these short intervals (in this case, at 20 Hz sampling frequency, *N* = 6000 for 5 minute time series). Where *j* defines a single measurement in time, the covariance between *w* and χ within each *i* short interval is computed along with the average for all *M* segments:

$$\left(\overline{w'\chi'}\right)_i = \frac{1}{N-1}\left[\sum_j w_j \cdot \chi_j - \frac{1}{N}\left(\sum_j w_j \cdot \sum_j \chi_j\right)\right] \quad \textbf{E.1}$$

$$\left(\overline{w'\chi'}\right)_{segments} = \frac{1}{M}\sum_i \left(\overline{w'\chi'}\right)_i \quad \textbf{E.2}$$

Next, the covariance over the entire period is determined:

$$\left(\overline{w'\chi'}\right)_{entire} = \frac{1}{M \cdot N - 1}\left[\sum_i \left(\sum_j w_j \cdot \chi_j\right)_i - \frac{1}{M \cdot N}\sum_i \left(\sum_j w_j \cdot \sum_j \chi_j\right)_i\right] \quad \textbf{E.3}$$

If the results from **Eqns. E.2** and **E.3** differ by less than ~30%, the measurement is considered to be stationary. We have performed this measurement for χ = horizontal wind speed and sonic temperature. Below are the results obtained across 20 minute sample periods over the course of each stationary experiment day.

The second test determines if the boundary layer has well-developed turbulence. This test is known as the integral turbulence characteristics test and follows a general form as shown in *Thomas and Foken* [2002]:

$$\frac{\sigma_X}{X_*} = \varphi_X\left(\frac{z-d}{L}, \frac{(z-d)\cdot f}{u_*}, \ldots\right) \quad \textbf{E.4}$$

The left side of **Eqn. E.4** calculates the ratio of the standard deviation of a turbulent parameter to its flux X_*. If this ratio can be modeled as a function of boundary layer stability, a well-developed turbulence can be assumed. Modeled stability is a function of the dimensionless height $\frac{z-d}{L}$, with $z-d$ representing the effective instrument sample height and L the Obukhov Length [*Monin and Obukhov* 1954]. In cases of neutral conditions, latitude dependence given by the Coriolis parameter f is also taken into account.

The parameterization φ_X is a function of the turbulent parameter being evaluated as well as boundary layer stability. A table of parameterizations described in *Thomas and Foken* [2002] is shown in **Table E.1** for each integral turbulence characteristic (ITC).

Table E.1 Parameterizations for modeled ITC values of wind and temperature variables. Parameterizations are a function of calculated dimensionless height $\frac{z-d}{L}$.

ITC	$\frac{z-d}{L} \leq -0.2$	$-0.2 < \frac{z-d}{L} < 0.4$
σ_w/u_*	$1.3\left(1-2\frac{(z-d)}{L}\right)^{1/3}$	$0.21\ln\left(\frac{z_+ \cdot f}{u_*}\right)+3.1$
σ_u/u_*	$4.15\left(\left\|\frac{(z-d)}{L}\right\|\right)^{1/3}$	$0.44\ln\left(\frac{z_+ \cdot f}{u_*}\right)+6.3$

z_+= 1m (mathematical artifact to allow for a dimensionless calculation).

Figure E.1 and **E.2** display the ITC for *u* and *w* and the *uw* and wT_s stationarity quality assessments for 14 March and 19 September of 2014. Dotted lines at 30% in each panel represent the threshold value for eddy covariance data of exceptional quality. Combined, ITC and stationarity values can give an overall quality flag numbering system, shown below in **Table E.2**. Examining all quality assessments using this flag numbering system, all portions of the 14 March and 19 September experiments show at least good quality eddy covariance data that may be used in emission rate estimation models.

Table E.2 Overall data quality flagging system used for determining high-quality eddy covariance data.

Stationarity Test Deviation (%)	Integral Turbulence Characteristic Deviation (%)	Quality Control flag
<30	<30	0
<100	<100	1
>100	>100	2

QC flag 0: exceptional quality data.
1: good quality data.
2: data of questionable quality.

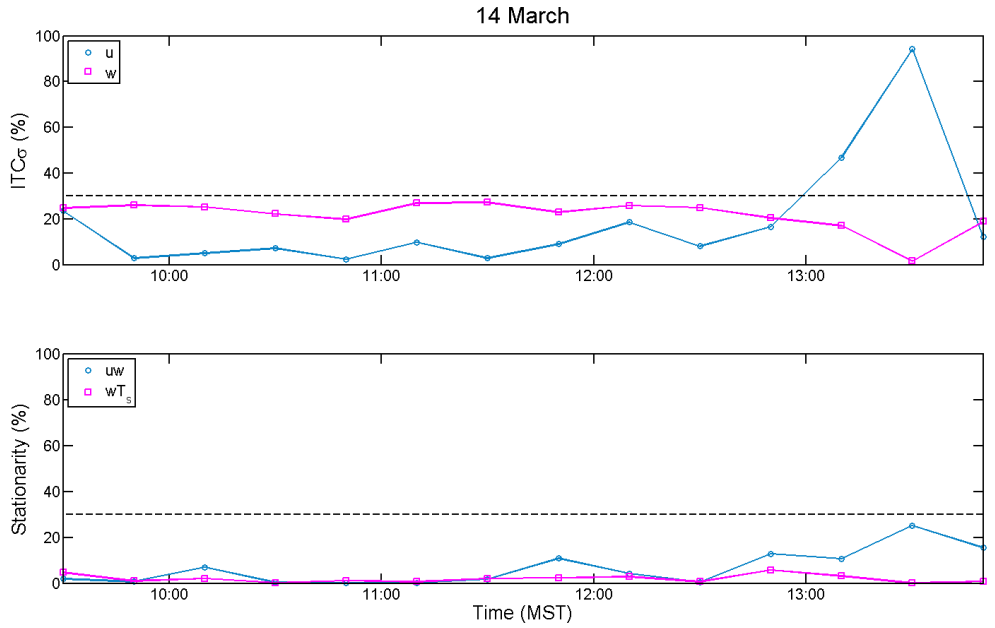

Figure E.1 Integral turbulence characteristics test for *u* and *w* (top) and tests for stationarity between *u* and *w* and *w* and T_s (bottom) for the 14 March 2014 Christman experiment. Horizontal dashed lines are present at 30% in each figure, indicating that any point below this line is of "exceptional" quality.

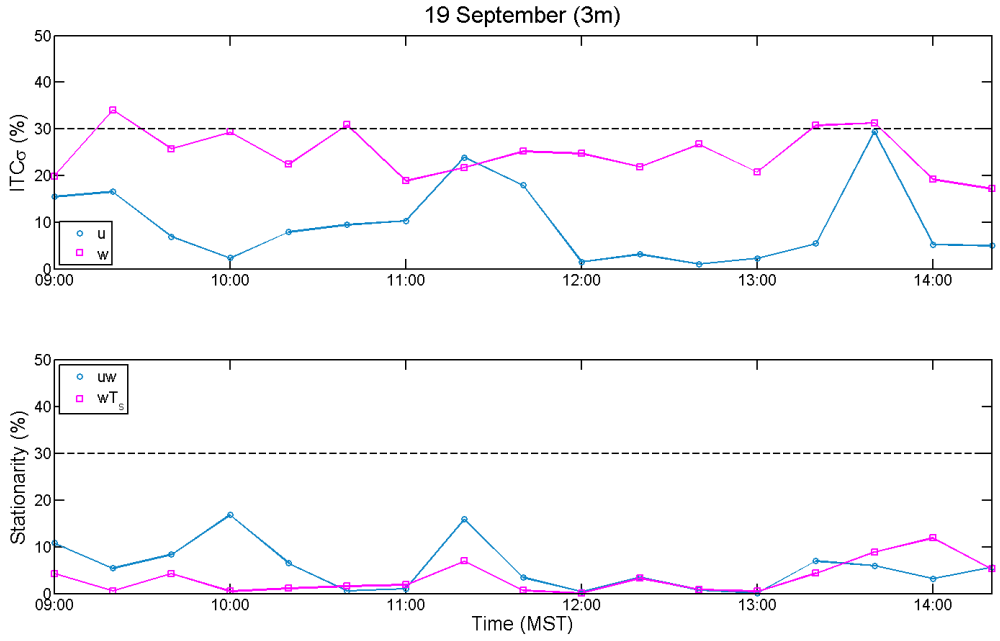

Figure E.2 Integral turbulence characteristics test for *u* and *w* (top) and tests for stationarity between *u* and *w* and *w* and T_s (bottom) for the 19 September 2014 Christman experiment. The sonic anemometer located 3 m above the surface was used in this assessment. Horizontal dashed lines are present at 30% in each figure, indicating that any point below this line is of "exceptional" quality.

Sonic anemometer data for 23 April was supplied by a team from the University of Wyoming Atmospheric Science Department who were on-site during testing as well. Their LabVIEW software [National Instruments Corporation, Austin TX, US] carries with it its own QA/QC protocols that were implemented by the experimental team.